Stability of Power Systems

An introduction

Mehrdad Ghandhari

Royal Institute of Technology (KTH)
Electric Power and Energy Systems
VT21

Contents

Chapter 1
Introduction

This compendium should be considered as an introduction to power system stability and control. A more detailed and comprehensive discussion and presentation may be found in the references given in this compendium.

The function of an electric power system is to produce electricity and to transmit it to customers. Thus, an electric power system may be divided into three parts, one concerned with generation, one with transmission, and one with consumption as shown in Figure 1.1. Electricity is produced at lower voltage at a generator. The generator then feeds its electric power into the transmission system via a step-up transformer in order to increase the voltage from the generation level (10 to 25 kV) to the transmission level (hundreds of kV). Then at the load center, it is stepped-down to lower voltages for distribution to customers.

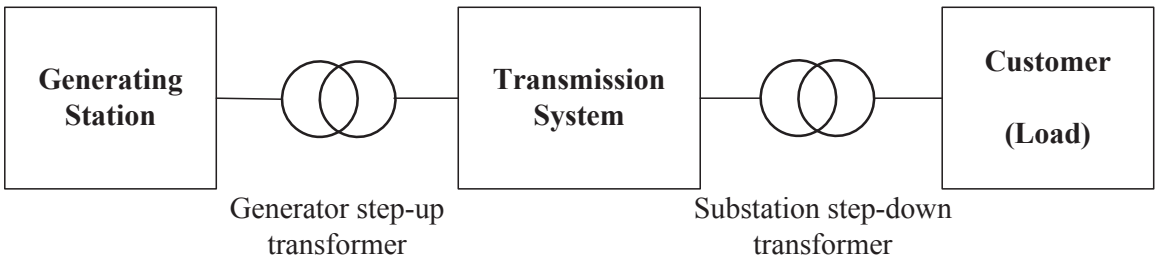

Figure 1.1. Basic structure of an electric power system.

Since modern society is strongly dependent on electricity, high reliability of supply and high level of system security are of fundamental importance. However, in an electric power system electricity cannot easily and economically be stored in large quantities. This special property implies that electricity must be produced the instant it is used that is the produced power must be in balance with the consumed power. Furthermore, power systems are frequently subjected to various types of disturbances which may be small, in the form of load changes and control actions, or large in the form of a short circuit on a transmission line or loss of a large generator. The system must however be able to adjust to the changing conditions and operate satisfactorily despite these disturbances. Thus, to keep the high reliability of supply and high level of system security will be a challenge for system operators.

By using computing and analysis tools, power system security analysis is a major activity for power system operators to determine the robustness of the power system to the occurrence of certain disturbances. This analysis normally concerns:

- **Static security analysis** which deals with operating and engineering constraints

such as overloading of transmission lines, transformers and other equipments, and also bus voltage magnitudes in a post-disturbance state.

- **Dynamic security analysis** which deals with power system dynamic response to disturbances. For instance, after a disturbance whether the system will survive the ensuing transient and move into a secure state.

Therefore, the operation of a power system must be subject to security and reliable standards developed by the system operator. A main principle underlying these standards is the so called N-1 criterion.

Definition 1.1 *The N-1 criterion states that the power system must be operated at all times such that after an unplanned loss of an important generator or transmission facility it will remain in a secure state.*

Furthermore, when a loss occurs the system must be returned to a new N-1 secure state within a specified time (normally within 15-20 minutes) to withstand a possible new loss.

The modern (interconnected) electric power systems are often considered as the most complex man-made dynamical systems for use in daily life (far away as just "two holes in the wall"). They consist of many individual elements connected together to form a large, complex system capable of generating, transmitting and distributing electrical energy over a large geographical area. Because of this interconnection of elements, a large variety of dynamic interactions are possible, some of which will only affect some of elements or parts of the system, while others may affect the system as a whole. Therefore, it is crucially necessary to have knowledge about how a power system behaves (or responds) to different disturbances, and also to understand the dynamics of the system.

Power system dynamics are mainly initiated by a disturbance, and they occur in different time scales. Based on their physical character these dynamics may be fast, relatively slow or very slow. The fast dynamics (known as electromagnetic dynamics) are those associated with fast electromagnetic changes in the electrical machines or operation of the protection system. The time frame of these fast dynamics is from milliseconds to a second. The relatively slow dynamics (known as electromechanical dynamics) are those associated with the oscillation of the rotating masses of the generators and motors. The time frame of the electromechanical dynamics is from around a second to several seconds. Finally, the very slow dynamics are those associated with the system frequency control (due to the turbine governing systems), and the thermodynamic changes (due to boiler control action in the steam power plants). In this compendium, the main focus is on the electromechanical dynamics.

In general, mathematical models are used to analyze dynamic behavior of power systems. One interesting feature of classifying the power system dynamics, as introduced above, is that it will be easier to derive an appropriate mathematical model including components relevant to the specific dynamic (particularly due to the time frame of

the specific dynamic). For instance, a disturbance may eventually excite all of the above mentioned dynamics in a power system, but for the same disturbance we may have different mathematical models to adequately describe the specific dynamic. If a mathematical model which describes the electromagnetic dynamic will also be included in the mathematical model of the electromechanical dynamic, then the model will obviously result in unnecessary high computation time, and it will not give any useful information when only the electromechanical dynamic is of concern.

Since the main focus of this compendium is on the electromechanical dynamic, only the mathematical models of this dynamic will be derived to be able to study and understand the concept of power system stability.

Power system stability is of fundamental importance concerning system security, and it has been defined in many different ways. However, in this compendium we use the definitions presented by IEEE/CIGRE Joint Task Force in [1].

Definition 1.2 *Power system stability is the ability of an electric power system, for a given initial operating condition, to regain a state of operating equilibrium after being subjected to a physical disturbance, with most system variables bounded so that practically the entire system remains intact [1].*

To facilitate analysis of stability, power system stability has been classified into different categories in [1] as follows:

- **Rotor angle stability** refers to the ability of synchronous machines of an interconnected power system to remain in synchronism after being subjected to a disturbance. Instability that may result occurs in the form of increasing angular swings of some generators leading to their loss of synchronism with other generators. Loss of synchronism can occur between one machine and the rest of the system, or between groups of machines, with synchronism maintained within each group after separating from each other.

  Rotor angle stability may be characterized as follows:

  - **Small-signal stability** which is concerned with the ability of the power system to maintain synchronism under small disturbances. The disturbances are considered to be sufficiently small that linearization of system equations is permissible for purposes of analysis.
  - **Transient stability** which is concerned with the ability of the power system to maintain synchronism when subjected to a large disturbance, such as a short–circuit on a transmission line. Transient stability depends on the initial operating conditions of the system as well as the type, severity and location of the disturbance.

- **Voltage stability** refers to the ability of a power system to maintain steady voltages at all buses in the system after being subjected to a disturbance from a

given initial operating condition. Instability that may result occurs in the form of a progressive fall or rise of voltages of some buses.

Depending on the time scale the voltage instability may be classified as fast (a couple of seconds) or slow (tens of seconds to minutes).

- **Frequency stability** refers to the ability of a power system to maintain steady frequency following a severe system upset resulting in a significant imbalance between generation and load. It depends on the ability to maintain/restore equilibrium between system generation and load, with minimum unintentional loss of load. Instability that may result occurs in the form of sustained frequency swings leading to tripping of generating units and/or loads.

Since mathematical models are used to describe power system dynamics, power system stability will also be defined based on the mathematical theory concerning stability of dynamical systems. In the evaluation of stability the concern is to the dynamic behavior of the power system when subjected to a disturbance.

Figure 1.2 shows the basic structure of a power generating unit. In this compendium, the dynamics and mathematical models of the components shown in the figure will be presented.

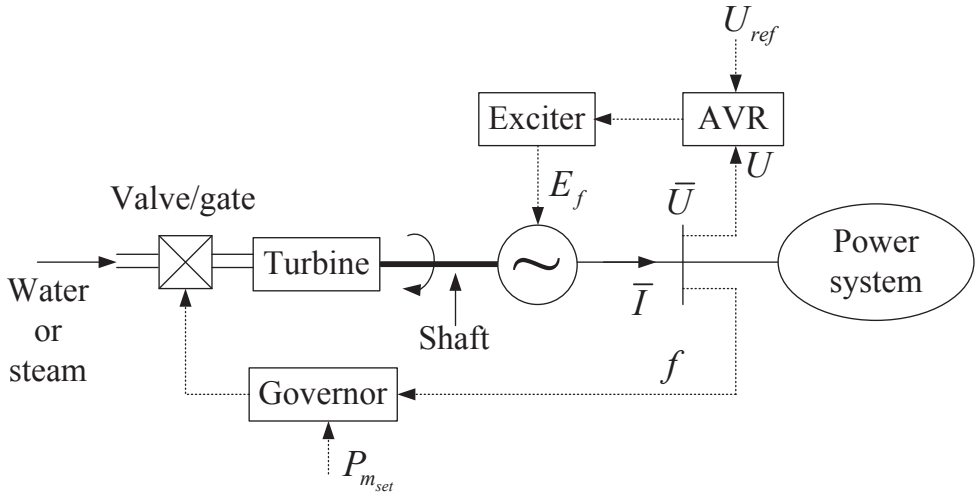

Figure 1.2. Block diagram of a power generating unit.

Three mathematical models to describe the dynamics of a synchronous generator will be presented. Those models are referred to as classical model, one-axis model and two-axis model. In the classical model, the generator is represented by a voltage source with constant magnitude behind a reactance. However, in the two other models the magnitude of the voltage is considered as a state variable and also a function of the field voltage E_f. This voltage can be controlled by the generator excitation system which consists of an exciter and an Automatic Voltage Regulator (AVR). The primary function of an exciter is to provide a dc source for field excitation of a synchronous generator, and the AVR controls the excitation voltage. A control on excitation voltage

results in controlling the field current (or E_f) which in turn controls the terminal voltage U and reactive power.

To get an insight into power system stability, the power system indicated in Figure 1.2 will be represented by an equivalent model to analyze the behavior a generator connected to an infinite bus. This system is known as Single Machine Infinite Bus (SMIB) system based on which transient stability will be discussed, and also the concept of Equal Area Criterion will be presented.

Then, power system stability analysis will be applied to a general multi-machine power system. Due to the load models (which will also be discussed) the dynamic of a multi-machine power system may be described by a set of differential-algebraic equations or only by a set of differential equations. The first model is refereed to as Structure Preserving Model (SPM), and the second one is referred to as Reduced Network Model (RNM).

For studying transient stability of a multi-machine power system, there are several methods two of which will be briefly discussed in this compendium. The first method is known as Transient Energy Function (TEF) method (termed also the direct method) which is based on Lyapunov's direct method. The second method is known as SIngle Machine Equivalent (SIME) method which transforms the trajectories of a multi-machine power system into the trajectory of a single machine equivalent system. Then, by refreshing the parameters of the single machine equivalent system at each integration time–step, the SIME method numerically assesses the transient stability of this equivalent system based on the Equal Area Criterion.

Small-signal stability analysis is also discussed in this compendium. This analysis deals with small disturbances, and it is applied to linearized system models. It provides valuable information about the inherent dynamic characteristics of the power system. Moreover, by this analysis, the excitation system can be designed to enhance the small-signal stability in a power system.

Finally, the dynamic of a hydro turbine and turbine governor will be discussed. The objective of a turbine governing system installed in a generating unit is to produce a desired power which is partly determined by the set value for the produced power and partly by a contribution originating from the frequency control.

Chapter 2
Mathematical modeling

For being able to understand and analyze dynamic of a system, normally mathematical models are derived to describe the dynamic of the system. Fortunately, for mechanical and electrical systems (such as power systems) there are laws of nature which are basis for deriving these mathematical models. For example, Kirchhoff's laws, Newton's laws, Ohm's law, induction law and etc. Applying these laws, the dynamic of the system can then be described by a set of differential equations of the form

$$\frac{d}{dt}x(t) = \dot{x} = f(x) \tag{2.1}$$

where x is the n_x–dimensional state vector belongs to the Euclidean space R^{n_x}, and f is a vector-valued function $f : \mathcal{D} \to R^{n_x}$ which is continuous and has continuous first-order partial derivatives with respect to x on a domain $\mathcal{D} \subset R^{n_x}$ into R^{n_x}. The solution to (2.1) is designated by $x(t)$ with $x(t_o)$ as an initial state at initial time $t = t_o$.

2.1 Definitions and notations

Definition 2.1 *Any x_o for which $\dot{x} = f(x_o) = 0$, is termed equilibrium point (e.p).*

Definition 2.2 *A system is in a steady-state, if the system is settled to an e.p, i.e $\dot{x} = f(x_o) = 0$.*

Definition 2.3 *A system is in a dynamic-state if $\dot{x} = f(x) \neq 0$.*

One of the important issues regarding dynamical systems is to characterize and study stability of equilibrium points since stability theory plays a central role in systems theory and engineering. Stability of equilibrium points is usually characterized in the sense of Lyapunov, a Russian mathematician and engineer (1857-1918) who laid the foundation of the stability theory which now carries his name.

Three concepts are introduced to characterize stability of an equilibrium point, namely:

- Stability in the sense of Lyapunov, (Definition 2.4).
- Lyapunov's indirect method, (Theorem 2.1).
- Lyapunov's direct method, (Theorem 2.2).

Definition 2.4 *An equilibrium point is Lyapunov stable (or stable in the sense of Lyapunov) if solutions that start near the equilibrium point remain near the equilibrium point for all time. More precisely, the equilibrium point x_o of* (2.1) *is*

- *stable if, for each* $\epsilon > 0$ *(no matter how small), there exists a* $\gamma = \gamma(\epsilon) > 0$ *such that, (see* Figure 2.1*)*

$$\|x(t_o) - x_o\| < \gamma \quad \Rightarrow \quad \|x(t) - x_o\| < \epsilon \quad , \quad \forall\, t \geq t_o$$

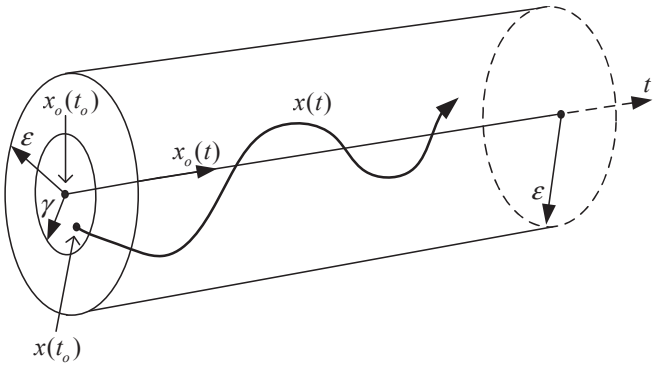

Figure 2.1. The equilibrium point x_o is stable.

- *unstable if not stable.*
- *asymptotically stable if it is stable and* γ *can be chosen such that, (see* Figure 2.2*)*

$$\|x(t) - x_o\| \to 0 \quad as \quad t \to \infty$$

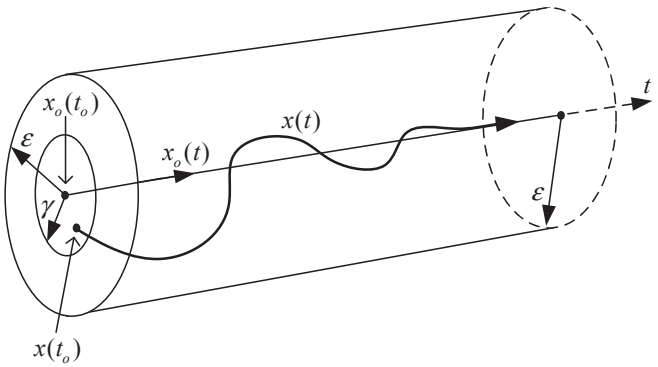

Figure 2.2. The equilibrium point x_o is asymptotically stable.

Note that in the above figures, $x_o = x_o(t)$, $\forall\, t \geq t_o$.

Example 2.1 *Consider the system shown in* Figure 2.3. *The system has two equilibrium points,* $x_o = P1$ *and* $x_o = P2$. *By applying* Definition 2.4, *characterize the stability of these points.*

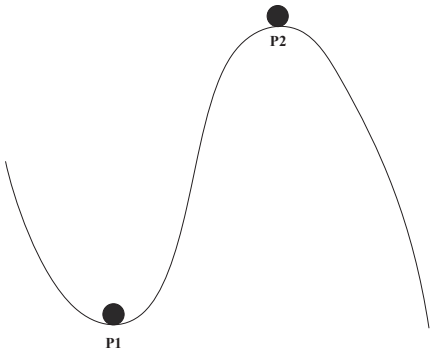

Figure 2.3. A simple system with two equilibrium points.

Assuming there is no friction in the system, and releasing the ball from any initial position $x(t_o)$ sufficiently close to $x_o = P1$ within a circle of radius γ centered at $x_o = P1$, the motion of the ball will then be limited within a circle of radius ϵ centered at $x_o = P1$, see Figure 2.4. Since there is no friction in the system, the ball will move (or oscillate) around $x_o = P1$ for ever within the circle. Therefore, $x_o = P1$ is a stable e.p, and the $\epsilon - \gamma$ requirement is satisfied. However, if there is friction in the system, the ball will eventually stay at $x_o = P1$ which is now asymptotically stable.

Next, releasing the ball from any initial position $x(t_o)$ sufficiently close to $x_o = P2$, the ball will leave the circle of radius ϵ. Therefore, $x_o = P2$ is unstable since the $\epsilon - \gamma$ requirement cannot be satisfied.

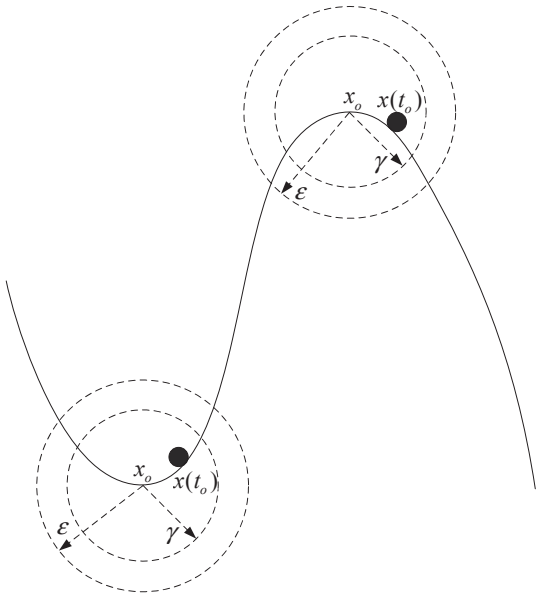

Figure 2.4. Stability of equilibrium points based on Definition 2.4.

Stability of the equilibrium point of (2.1) can also be defined by examining the linearized system. This approach is known as Lyapunov's indirect method. Linearizing the nonlinear system (2.1) around the equilibrium point x_o, we obtain

$$\Delta\dot{x} = A\Delta x \tag{2.2}$$

where

$$A = \left[\frac{\partial f(x)}{\partial x}\right]_{x=x_o} = \left[\begin{array}{ccc} \frac{\partial f_1(x)}{\partial x_1} & \cdots & \frac{\partial f_1(x)}{\partial x_{n_x}} \\ \vdots & \ddots & \vdots \\ \frac{\partial f_{n_x}(x)}{\partial x_1} & \cdots & \frac{\partial f_{n_x}(x)}{\partial x_{n_x}} \end{array}\right]_{x=x_o} \tag{2.3}$$

which is also called the Jacobian matrix at x_o. The eigenvalues of A (i.e., λ) are obtained by solving

$$\left| A - \lambda \underline{\mathbf{1}} \right| = 0 \tag{2.4}$$

where $\underline{\mathbf{1}}$ is an identity matrix.

Theorem 2.1 *Let x_o be the equilibrium point of the nonlinear system* (2.1)*. Then,*

(i) *x_o is asymptotically stable if all eigenvalues of matrix A have negative real parts.*

(ii) *x_o is unstable if any eigenvalue of matrix A has a positive real part.*

A more qualitative approach to stability analysis is Lyapunov's direct method. The method requires finding a scalar function which has some very special properties.

Theorem 2.2 *The equilibrium point x_o of* (2.1) *is stable if a continuously differentiable scalar function $\mathcal{V}(x)$ can be found satisfying the following conditions:*

(i) $\mathcal{V}(x_o) = 0$,

(ii) $\mathcal{V}(x) > 0$ *for all $x \in \mathcal{D}$, except at x_o,*

(iii) $\dot{\mathcal{V}}(x) = \frac{\partial \mathcal{V}(x)}{\partial x} \cdot f(x) \leq 0$ *for all $x \in \mathcal{D}$.*

The equilibrium point x_o is asymptotically stable if conditions (i)-(ii) *hold, and*

(iv) $\dot{\mathcal{V}}(x) < 0$ *for all $x \in \mathcal{D}$, except at x_o where $\dot{\mathcal{V}}(x_o) = 0$,*

or, alternatively

(v) $\dot{\mathcal{V}}(x) \leq 0$ *, provided that $\dot{\mathcal{V}}(x)$ is not identically zero on any solution $x(t)$ in $\mathcal{D}$, except at x_o.*

A function $\mathcal{V}(x)$ satisfying the above conditions is called Lyapunov function. The proofs of the above theorems can be found in [2].

Thus by applying Theorem 2.1, the local stability or instability of an equilibrium point of a nonlinear system (2.1) can be characterized based on the stability or instability of the linearized system (2.2). However, it should be noted that the statement (i) in Theorem 2.1 is generally not applicable if some (complex) eigenvalues have zero real parts, and for these cases Lyapunov's direct method (i.e. Theorem 2.2) can be applied to characterize the stability of the equilibrium point.

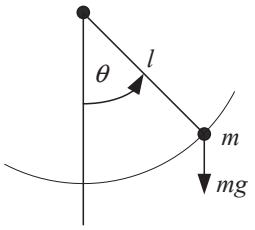

Figure 2.5. A simple pendulum system.

Example 2.2 *Consider the simple pendulum system shown in* Figure 2.5*, where a spherical mass with weight* m *is attached to a rod of negligible weight with length* l*.*

Assuming a rigid pendulum (i.e. the length l *is fixed), the mass moves along a circle of radius* l*. The position along this circle is given by* $l\,\theta$*. There is also a damping (or frictional) torque* T_D *resisting the motion which is assumed linearly proportional to the speed of the mass, i.e.* $T_D = D\,\dot{\theta}$ *where* $D \geq 0$ *is a damping constant.*

Describe mathematically the dynamic of this system. Also, find its equilibrium points, and characterize their stability.

Applying Newton's second law of motion, the following mathematical model (also termed equation of motion) can then be obtained:

$$M\,\ddot{\theta} + mgl\sin(\theta) + D\,\dot{\theta} = 0 \tag{2.5}$$

where $M = ml^2$ is moment of inertia and g is the acceleration due to gravity. Note that $\dot{\theta}$ is the angular velocity.

Let

$$C_1 = mgl \quad , \quad \omega = \dot{\theta} \quad \text{and} \quad x = [x_1 \quad x_2]^T = \begin{bmatrix} x_1 \\ \\ x_2 \end{bmatrix} \tag{2.6}$$

Taking the state variables as $x_1 = \theta$ and $x_2 = \dot{\theta} = \omega$, then (2.5) and (2.6) give

$$\dot{x} = \begin{bmatrix} \dot{x}_1 \\ \\ \dot{x}_2 \end{bmatrix} = \begin{bmatrix} \dot{\theta} \\ \\ \ddot{\theta} \end{bmatrix} = \begin{bmatrix} x_2 \\ \\ \frac{1}{M}(-C_1\sin(x_1) - Dx_2) \end{bmatrix} = \begin{bmatrix} f_1(x) \\ \\ f_2(x) \end{bmatrix} = f(x) \tag{2.7}$$

which is of the form given in (2.1) with $n_x = 2$. According to Definition 2.1, the equilibrium points of the system are given by $f(x_o) = 0$, i.e.

$$\begin{bmatrix} \dot{x}_1 \\ \\ \dot{x}_2 \end{bmatrix} = \begin{bmatrix} x_{2o} \\ \\ \frac{1}{M}(-C_1\sin(x_{1o}) - Dx_{2o}) \end{bmatrix} = \begin{bmatrix} f_1(x_o) \\ \\ f_2(x_o) \end{bmatrix} = \begin{bmatrix} 0 \\ \\ 0 \end{bmatrix} \tag{2.8}$$

Thus, $x_{2o} = 0$ and $x_{1o} = \pm k\pi$, where k is any integer. From the physical description of the pendulum, it is clear that the pendulum has only two equilibrium positions corresponding to the equilibrium points

$$x_o = [x_{10} \quad x_{2o}]^T = [0 \quad 0]^T \quad \text{and} \quad x_o = [x_{10} \quad x_{2o}]^T = [\pi \quad 0]^T$$

Other equilibrium points are repetitions of these two positions which correspond to the number of full swings the pendulum would make before it rests at one of the two equilibrium positions.

Linearizing system (2.7) around its equilibrium point x_o, the matrix A is obtained as

$$A = \left[\frac{\partial f(x)}{\partial x}\right]_{x=x_o} = \left[\begin{array}{cc} \frac{\partial f_1(x)}{\partial x_1} & \frac{\partial f_1(x)}{\partial x_2} \\ \\ \frac{\partial f_2(x)}{\partial x_1} & \frac{\partial f_2(x)}{\partial x_2} \end{array}\right]_{x=x_o} = \left[\begin{array}{cc} 0 & 1 \\ \\ -\frac{K}{M} & -\frac{D}{M} \end{array}\right] \tag{2.9}$$

where $K = C_1 \cos(x_{1o})$.

Based on (2.4), the eigenvalues of A are given by

$$\begin{aligned} \lambda_1 &= -\frac{D}{2M} - \sqrt{\left(\frac{D}{2M}\right)^2 - \frac{K}{M}} \\ \lambda_2 &= -\frac{D}{2M} + \sqrt{\left(\frac{D}{2M}\right)^2 - \frac{K}{M}} \end{aligned} \tag{2.10}$$

It is obvious that $K = C_1 > 0$ with $x_{1o} = 0$, and $K = -C_1 < 0$ with $x_{1o} = \pi$. Thus, both eigenvalues of the matrix A have negative real parts with $x_o = [0 \quad 0]^T$. However, the real part of λ_2 is positive with $x_o = [\pi \quad 0]^T$. Applying Theorem 2.1, it can be found that $x_o = [0 \quad 0]^T$ is asymptotically stable, but $x_o = [\pi \quad 0]^T$ is unstable.

By applying Theorem 2.2, it can also be shown that $x_o = [0 \quad 0]^T$ is asymptotically stable. Lyapunov's direct method is closely related to the energy of the system. In many physical systems the total energy of the system is a good candidate for a Lyapunov function, and these energy-based functions are known as energy functions in the literature. The energy function for the system in Example 2.2 is given by

$$\begin{aligned} \mathcal{V}(x) = W_K + W_P &= \frac{1}{2} M\, x_2^2 + \int_0^{x_1} C_1 \sin(y)\, dy \\ &= \frac{1}{2} M\, x_2^2 + C_1 \left(1 - \cos(x_1)\right) \end{aligned} \tag{2.11}$$

where $W_K = \frac{1}{2} M x_2^2$ is the kinetic energy and $W_P = C_1(1 - \cos(x_1))$ is the potential energy of the pendulum.

Next, it will be shown that the function $\mathcal{V}(x)$ satisfies the conditions of Theorem 2.2 for $x_o = [0 \quad 0]^T$.

- $\mathcal{V}(x_o) = 0$. Thus, condition (i) is satisfied.

- The gradient of $\mathcal{V}(x)$ is given by

$$\nabla \mathcal{V}(x) = \frac{\partial \mathcal{V}(x)}{\partial x} = \begin{bmatrix} \frac{\partial \mathcal{V}(x)}{\partial x_1} & \frac{\partial \mathcal{V}(x)}{\partial x_2} \end{bmatrix} = \begin{bmatrix} C_1 \sin(x_1) & M\, x_2 \end{bmatrix}$$

  Since $\nabla \mathcal{V}(x_o) = 0$, the function $\mathcal{V}(x)$ has a local extremum at $x_o = [0 \quad 0]^T$. It will now be shown that this extremum is a local minimum, that is $\mathcal{V}(x) > 0$.

  Obviously, this extremum is a minimum if the Hessian matrix of $\mathcal{V}(x)$ is positive definite. The Hessian matrix of $\mathcal{V}(x)$ is given by

$$\mathcal{H} = \frac{\partial^2 \mathcal{V}(x)}{\partial x^2} = \begin{bmatrix} \frac{\partial^2 \mathcal{V}(x)}{\partial x_1^2} & \frac{\partial^2 \mathcal{V}(x)}{\partial x_1 \partial x_2} \\ \\ \frac{\partial^2 \mathcal{V}(x)}{\partial x_2 \partial x_1} & \frac{\partial^2 \mathcal{V}(x)}{\partial x_2^2} \end{bmatrix} = \begin{bmatrix} C_1 \cos(x_1) & 0 \\ \\ 0 & M \end{bmatrix}$$

  which is a real symmetric matrix.

  $\mathcal{H}$ is a positive definite matrix if all its eigenvalues are positive. It can be shown that the eigenvalues of $\mathcal{H}$ are $\lambda_1 = M$ and $\lambda_2 = C_1 \cos(x_1)$. Since M is a positive constant, $\mathcal{H}$ is positive definite if $-\frac{\pi}{2} < x_1 < \frac{\pi}{2}$.

  Thus, $\mathcal{V}(x) > 0$ in a neighborhood (i.e. $\mathcal{D}$) of x_o. Therefore, condition (ii) is also satisfied.

- The time derivative of $\mathcal{V}(x)$ is given by

$$\begin{aligned} \dot{\mathcal{V}}(x) =& \frac{\partial \mathcal{V}(x)}{\partial x} \cdot \dot{x} = \nabla \mathcal{V}(x) \cdot f(x) = \\ &= [C_1\, sin(x_1) \quad M\, x_2] \cdot \begin{bmatrix} x_2 \\ \\ \frac{1}{M}(-C_1 \sin(x_1) - D x_2) \end{bmatrix} = -D\, x_2^2 \leq 0 \end{aligned} \tag{2.12}$$

  Since $\dot{x} = f(x) \neq 0$ (or more precisely $\dot{x}_2 = f_2(x) \neq 0$) on $x_2 = 0$ except at x_o, condition (v) is also satisfied. Thus, the equilibrium point $x_o = [0 \quad 0]^T$ is asymptotically stable.

Assume that $D = 0$. The eigenvalues are then given by

$$\lambda_{1,2} = \pm \sqrt{-\frac{K}{M}}$$

By virtue of Theorem 2.1, it can still be shown that $x_o = [\pi \quad 0]^T$ is unstable. But, Theorem 2.1 cannot characterize the stability of $x_o = [0 \quad 0]^T$ when $D = 0$ (why?).

By applying Theorem 2.2, we may however be able to characterize the stability of $x_o = [0 \quad 0]^T$.

It has already been shown that the energy function (2.11) satisfies conditions (i)-(ii). With $D = 0$ the time derivative of $\mathcal{V}(x)$ is then given by

$$\begin{aligned}\dot{\mathcal{V}}(x) =& \frac{\partial \mathcal{V}(x)}{\partial x} \cdot \dot{x} = \nabla \mathcal{V}(x) \cdot f(x) = \\ &= [C_1 \, sin(x_1) \quad M \, x_2] \cdot \begin{bmatrix} x_2 \\ \\ \frac{1}{M}(-C_1 \sin(x_1)) \end{bmatrix} = 0\end{aligned} \tag{2.13}$$

which satisfied condition (iii). Therefore, $x_o = [0 \quad 0]^T$ is stable (but not asymptotically). Henceforth, a stable (or an asymptotically stable) equilibrium point will be designated by x_o^s, and an unstable equilibrium point by x_o^u.

Assume that the pendulum is settled on its stable e.p $x_o^s = [0 \quad 0]^T$. At time $t = t_f$, a torque T (as a disturbance) is applied to the pendulum, and at time $t = t_c$ the applied torque (or disturbance) is removed.

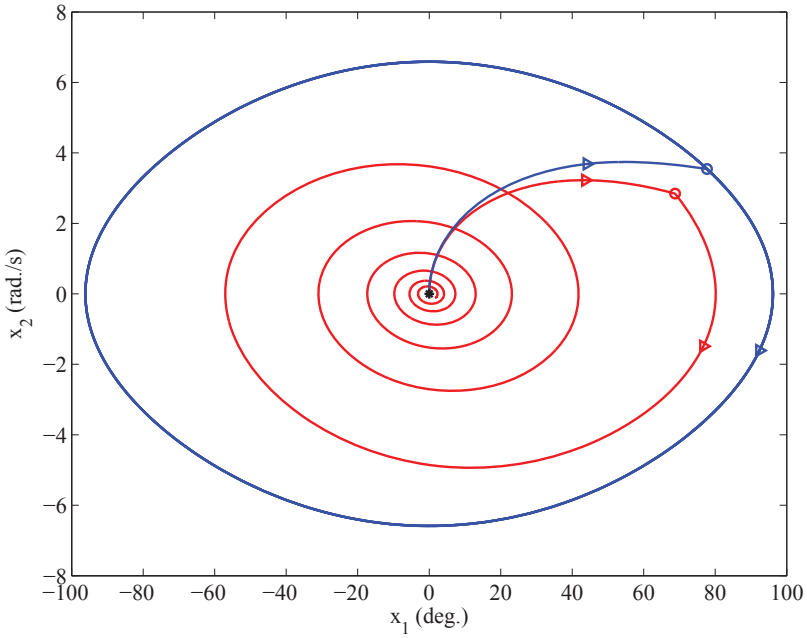

Figure 2.6. Phase portrait of the pendulum system.

Figure 2.6 illustrates phase portrait of the pendulum system due to the applied disturbance. The curve in the figure is termed the system trajectory (or motion). The stable e.p of the system is indicated by "*". During disturbance the system trajectory (i.e. the pendulum) moves from its stable e.p towards the point indicated by "o" where the disturbance is removed. This point is the initial point of the post-disturbance system. Note that in this example, the pre-disturbance system and the post-disturbance system have the same stable e.p.

When the system is frictionless (or undamped), i.e. $D = 0$, x_o^s is not asymptotically stable. Thus, the trajectory of the post-disturbance system (blue line) oscillates around x_o^s. However, when the system is damped, i.e. $D > 0$, x_o^s is asymptotically stable. Therefore, the trajectory (red line) tends to x_o^s as $t \to \infty$.

Consider now the damped pendulum system. In Figure 2.7, the initial points are indicated by "o", and x_o^s by "*". Moreover, the unstable equilibrium points $x_o^{u1} = [-180 \quad 0]^T$ and $x_o^{u2} = [180 \quad 0]^T$ are indicated by "+".

As shown in the figure, the trajectories whose initial states (or points) lie within the shaded region converge to x_o^s. However, the trajectories whose initial states (or points) lie outside the shaded region will never tend to x_o^s.

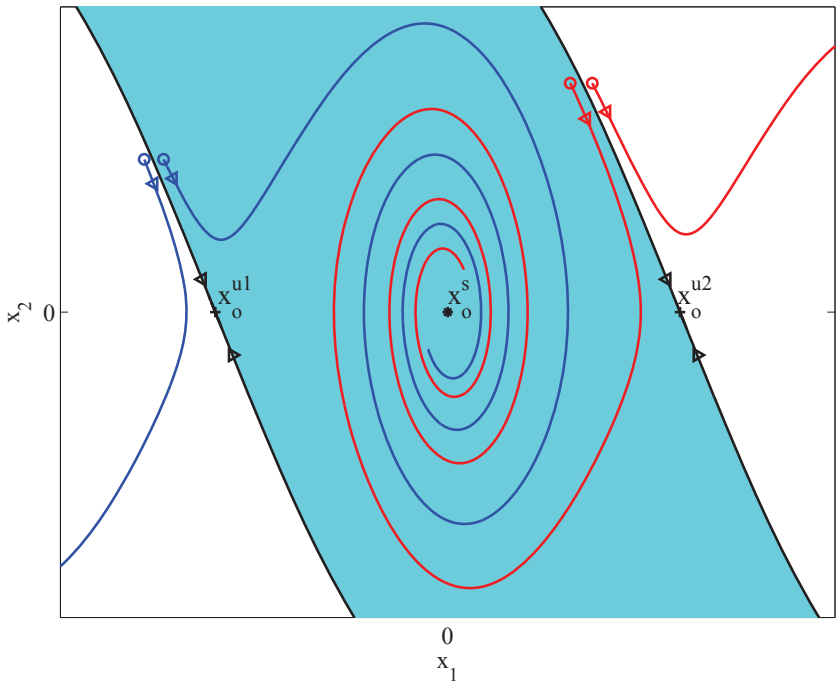

Figure 2.7. Stability region of the damped pendulum system.

The shaded region is termed the stability region of x_o^s. Boundary of the stability region is termed the stability boundary.

Definition 2.5 *The stability region of x_o^s is a region in the state space from which all trajectories converge to x_o^s. Furthermore, the trajectory whose initial point lies on the stability boundary will never leave the stability boundary and will converge to the unstable equilibrium point on the stability boundary as time goes to infinity.*

The stability region of the undamped pendulum system is illustrated in Figure 2.8. Since x_o^s is not asymptotically stable, trajectories starting within the stability region will only oscillate around x_o^s. However, trajectories starting outside the stability region will diverge that means the pendulum rotates (not oscillates).

Figure 2.9 illustrates variation of the total energy (see equation (2.11)) in the pendulum system. When the system is damped the total energy of the post-disturbance system decreases that is the system is a dissipative system (see equation (2.12)). However, when the system is undamped the total energy is constant that is the system is a conservative system (see equation (2.13)).

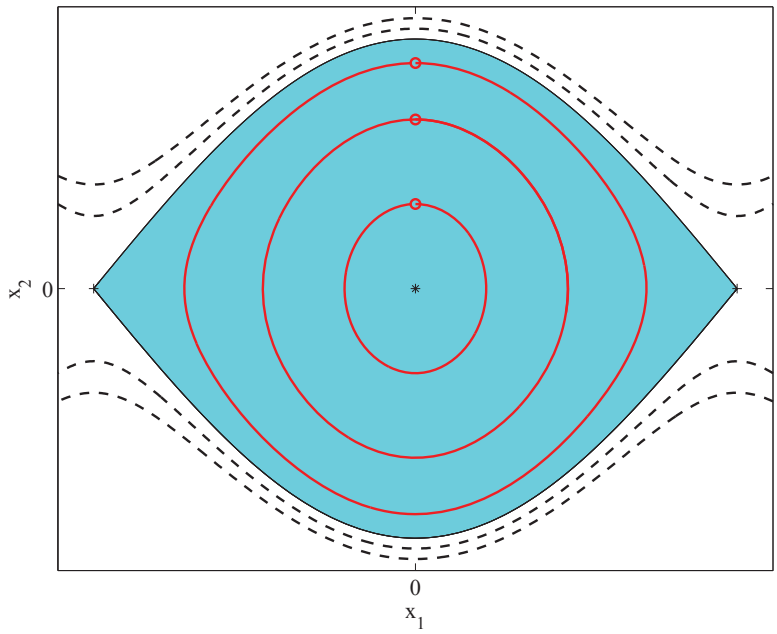

Figure 2.8. Stability region of the undamped pendulum system.

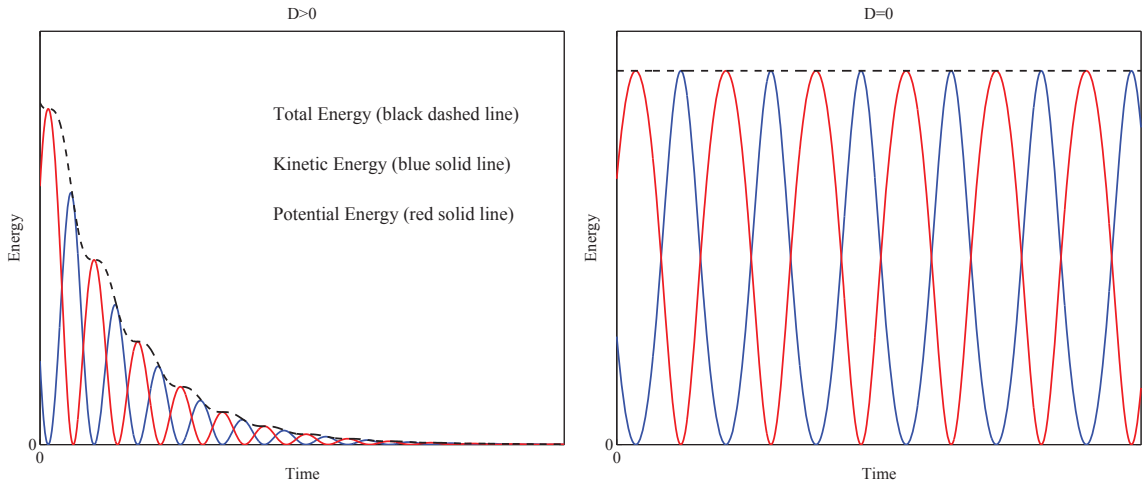

Figure 2.9. Variation of energy in the pendulum system.

Chapter 3

Synchronous machines modeling

Synchronous machines play an important roll in power systems. Nowadays almost all power generators are synchronous generators. They convert mechanical power into electrical form, and feed it into the transmission system. Many large loads are also driven by synchronous motors. Furthermore, in large sizes, synchronous condensers may be used to provide a very convenient and continuous control of reactive power and voltage. These machines can be classified as either high-speed machines with cylindrical rotors (or round-rotors) driven by steam or gas turbines, or low-speed machines with salient-pole rotors driven by hydro turbines.

Synchronous machines are the most important components in the analysis of electromechanical oscillations in power systems. Further, as discussed in Chapter 1, rotor angle stability relies on keeping interconnected synchronous machines in synchronism after a disturbance. Therefore, it is of fundamental importance to understand the behavior and dynamics of synchronous machines in power system stability study.

Figure 3.1 illustrates simply a generating unit which is an electromechanical system that can be divided into an electrical part (synchronous generator) and a mechanical part (shaft and turbine).

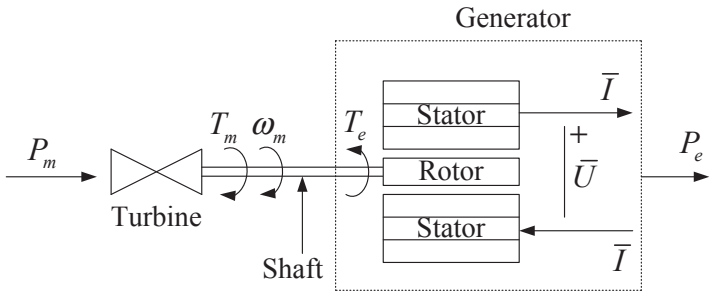

Figure 3.1. A simple illustration of a generating unit.

The synchronous generator can also be divided into two parts, one static part called the stator (or armature) and one rotating part called the rotor (or field). The stator has a distributed winding which is connected to the ac power system. The stator winding (called also the armature winding) consists of three identical phase windings which are 120 electrical degrees apart. These windings carry the load current and supply power to the system. The rotor has a winding (called the field winding) which carries a direct current (provided by an exciter) to produce a magnetic flux.

Figure 3.2 shows a simplified salient-pole synchronous generator. The ends of each of the phase windings are denoted by a and a' (phase a), b and b' (phase b) and c and c' (phase c). The stator is represented by three magnetic axes a, b and c each corresponding to one of the phase windings. However, the rotor is represented by two axes, namely: the direct axis (d-axis), which is the magnetic axis of the field winding (known as pole axis), and the quadrature axis (q-axis), which is the axis of symmetry

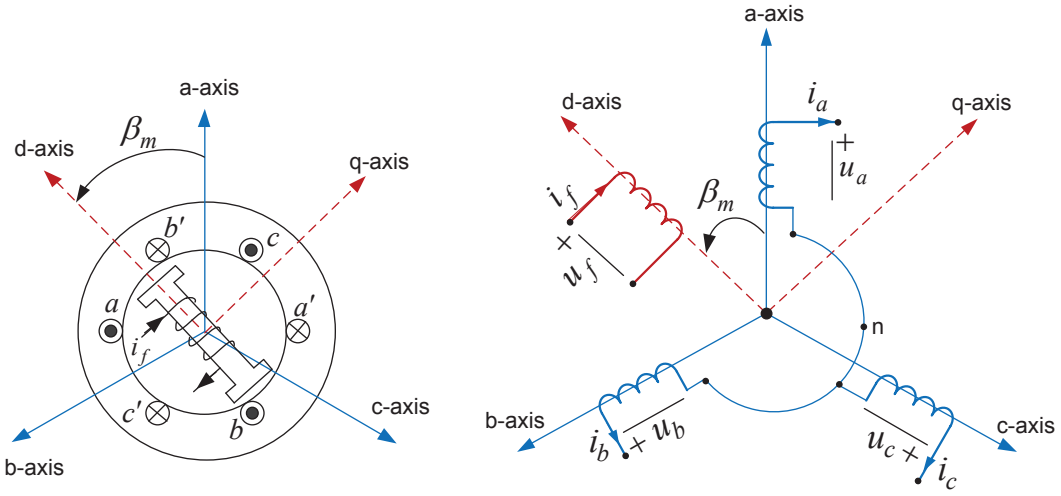

Figure 3.2. Symbolic representation of a synchronous generator.

between two poles (known as the interpole axis). In this compendium, the q-axis is located 90 electrical degrees behind the d-axis.

The rotor can also be equipped with additional short-circuited damper windings to reduce the mechanical oscillations of the rotor. Figure 3.3 shows a salient-pole synchronous generator with one damper winding on the d-axis of the rotor, and one damper winding on the q-axis of the rotor.

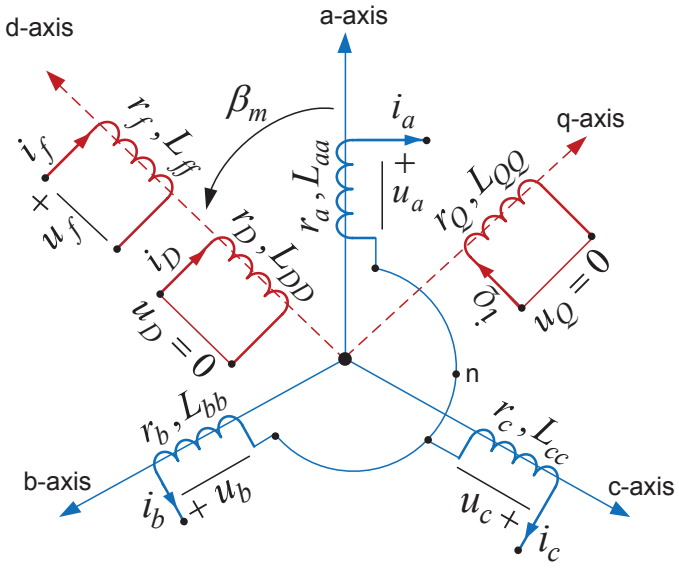

Figure 3.3. A simplified salient-pole synchronous generator with damper windings.

The mechanical rotor angle β_m (also called the mechanical angle of the shaft) defines the instantaneous position of the rotor d-axis with respect to a stationary reference. The a-axis is here chosen as the reference. Thus, this angle is defined by

$$\beta_m = \omega_m t + \beta_{mo} \tag{3.1}$$

where ω_m is the mechanical speed (or angular velocity) of the rotor (or shaft), and β_{mo} is the initial position of the rotor, i.e. at $t = t_0 = 0$ the position of the rotor is given by

$\beta_m(t_0) = \beta_{mo}$ with respect to the a-axis. The rotor angle can be expressed in electrical radians (or degrees) by

$$\beta = \frac{p}{2}\,\beta_m \tag{3.2}$$

where β is the (electrical) rotor angle measured in electrical radians (or degrees), and p is the number of the poles. Note that $\beta = \beta_m$ when $p = 2$.

Similarly, the electrical speed of the rotor (i.e. ω_g) can be obtained by

$$\omega_g = \frac{p}{2}\,\omega_m \tag{3.3}$$

where $\omega_g = \dfrac{d\beta}{dt} = 2\pi f$, and f is the electrical frequency of the system given in (Hz). Based on equations (3.2)-(3.3), the following can therefore be obtained

$$\begin{aligned} \beta = \frac{p}{2}\,\beta_m = \frac{p}{2}\,\omega_m t + \frac{p}{2}\beta_{mo} = \omega_g t + \beta_o \\ \frac{d\,\beta}{dt} = \omega_g \\ \frac{d^{\,2}\beta}{dt^2} = \frac{d\,\omega_g}{dt} \end{aligned} \tag{3.4}$$

Positive direction of rotation is counter-clockwise, and positive angle β_m (or β) is measured in the positive direction of rotation. Since β is measured with respect to a stationary reference axis on the stator, it is an absolute measure of rotor angle. Consequently, it continuously increases with time. In the steady-state, the rotor rotates with a speed corresponding to the system nominal frequency f_s (in Europe $f_s = 50\,(Hz)$, and in USA $f_s = 60\,(Hz)$) that is

$$\frac{d\beta}{dt} = \omega_g = \omega_s = 2\pi f_s$$

where $\omega_s = 2\pi f_s$ is a constant normally called (electrical) synchronous speed. Therefore, in the steady-state the rotor angle β increases uniformly with time. Due to practical issues, it is more convenient to measure the angular position from the q-axis with respect to a reference axis which rotates at synchronous speed, i.e ω_s. This new angular position is defined by

$$\begin{aligned} \delta &= (\beta - \frac{\pi}{2}) - \omega_s t = \omega_g t + \beta_o - \frac{\pi}{2} - \omega_s t = (\omega_g - \omega_s)t + (\beta_o - \frac{\pi}{2}) \\ &= (\omega_g - \omega_s)t + \delta_o \end{aligned} \tag{3.5}$$

Note that in the steady-state $\omega_g = \omega_s$, and $\delta = \delta_o$ which is a constant. Moreover,

$$\begin{aligned} \frac{d\delta}{dt} = \dot{\delta} = \ (\omega_g - \omega_s) = \omega \\ \frac{d^{\,2}\delta}{dt^2} = \ddot{\delta} = \frac{d}{dt}(\omega_g - \omega_s) = \dot{\omega}_g = \dot{\omega} \end{aligned} \tag{3.6}$$

that is, $\dot{\delta} = \omega$ represents the deviation of the rotor speed from synchronism.

The rotor mechanical synchronous speed is however given by $\omega_{ms} = 2\pi n_o$, where n_o is given in revolution per minute. Note that

$$\frac{\omega_g}{\omega_s} = \frac{\frac{p}{2}\omega_m}{\frac{p}{2}\omega_{ms}} = \frac{\omega_m}{\omega_{ms}} \tag{3.7}$$

3.1 Swing equation

Consider again Figure 3.1. When the rotor is rotated by the turbine, a rotating magnetic flux is produced in the air gap. The magnetomotive force (mmf) produced by the field current in the filed winding combines with the mmf produced by currents in the stator winding. The resultant flux across the air gap between the stator and rotor induces voltage in each phase of the armature winding. These induced voltages have the same magnitudes, but are phase-shifted by 120 electrical degrees. The resultant flux also provides the electromagnetic torque (or the electrical output torque denoted by T_e (Nm)) between the stator and rotor. This electromagnetic torque (developed in the generator when it delivers power) opposes the torque of the turbine (or the mechanical input torque denoted by T_m (Nm)).

One of the most important factors in studying electromechanical dynamics of a power system is the motion of the rotor during and after a disturbance. The dynamic of this motion is described by a set of differential equation based on Newton's second law

$$J\frac{d^2\beta_m}{dt^2} = J\frac{d\,\omega_m}{dt} = T_m - T_e \tag{3.8}$$

where J (kgm^2) is the total moment of inertia of the turbine, shaft and generator. Equation (3.8) is known as the swing equation. Multiplying the swing equation with ω_m the following can be obtained

$$\omega_m J\frac{d\,\omega_m}{dt} = P_m - P_e \tag{3.9}$$

where

$P_m = \omega_m\, T_m$ is the mechanical power input given in (W)

$P_e = \omega_m\, T_e$ is the three-phase electrical power output given in (W)

Next, the inertia constant H of the generator is defined by

$$H = \frac{W_{Ks}}{S_{ng}} = \frac{0.5J\omega_{ms}^2}{S_{ng}} \quad (s) \tag{3.10}$$

where W_{Ks} is the total kinetic energy stored in the generator in the steady-state (or stored kinetic energy in the rotating inertia at speed ω_{ms}), and S_{ng} is the generator rated three-phase VA. Typically, H ranges between 3 and 6 seconds, depending on the size and type of generator. The inertia constant states how many seconds it would take to bring the generator from synchronous speed to standstill if rated power is extracted from it while no mechanical power is supplied by the turbine.

Substituting J from equation (3.10) into the swing equation (3.9) yields

$$\omega_m \frac{2HS_{ng}}{\omega_{ms}^2} \frac{d\,\omega_m}{dt} = P_m - P_e \tag{3.11}$$

or by virtue of equations (3.3)-(3.7)

$$\frac{2HS_{ng}}{\omega_s} \frac{d\,\omega_g}{dt} = \frac{\omega_s}{\omega_g}(P_m - P_e) \tag{3.12}$$

During the electromechanical dynamics of a power system, the rotor speed is near synchronous speed, i.e. $\frac{\omega_g}{\omega_s} \approx 1$ and it has a negligible effect on the right hand side of (3.12). Therefore, the following swing equation is commonly used for analysis of the electromechanical dynamics (or transients) of a power system,

$$\frac{2HS_{ng}}{\omega_s} \frac{d\,\omega_g}{dt} = \frac{\omega_s}{\omega_g}(P_m - P_e) \approx P_m - P_e \tag{3.13}$$

Dividing both sides of (3.13) with an arbitrary three-phase base power $S_{base}^{3\phi}$ results in

$$M \frac{d\,\omega_g}{dt} = \frac{P_m - P_e}{S_{base}^{3\phi}} = P_{mpu} - P_{epu} \tag{3.14}$$

where

$$M = \frac{2H}{\omega_s} \frac{S_{ng}}{S_{base}^{3\phi}} \tag{3.15}$$

Applying equation (3.6), the motion of the rotor is then described by

$$\begin{aligned} \dot{\delta} &= (\omega_g - \omega_s) = \omega \\ \dot{\omega} &= \frac{1}{M}(P_{mpu} - P_{epu}) \end{aligned} \tag{3.16}$$

Furthermore, the contribution of mechanical friction in the bearings and/or damping power provided by damper windings may be included in the swing equation (3.16). This power is denoted by $P_D = D\,(\omega_g - \omega_s) = D\,\omega$, where $D = \frac{D'}{\omega_s}$, and D' is a small positive constant. Including the damping, (3.16) is then rewritten as

$$\begin{aligned} \dot{\delta} &= \omega \\ \dot{\omega} &= \frac{1}{M}(P_{mpu} - P_{epu} - D\omega) \end{aligned} \tag{3.17}$$

However, with ω expressed in (pu), then (3.17) is rewritten as

$$\begin{aligned} \dot{\delta} &= \omega_s\,\omega_{pu} \\ \dot{\omega}_{pu} &= \frac{1}{M'}(P_{mpu} - P_{epu} - D'\,\omega_{pu}) \end{aligned} \tag{3.18}$$

where, $M' = \omega_s\,M$ and $D' = \omega_s\,D$.

Note that since the effect of $\frac{\omega_g}{\omega_s}$ on the right hand side of (3.12) is negligible, it has been assumed that $\frac{\omega_g}{\omega_s} \approx 1$. However, the small variations of ω_g are sufficient to produce significant rotor angle deviation. Therefore, it is not justified to assume that $\dot{\delta} = (\omega_g - \omega_s) = \omega \approx 0$.

3.2 Electrical equations

Consider again the synchronous generator shown in Figure 3.3. In developing the mathematical model the following assumptions are made:

- The magnetic circuits are linear (i.e., no saturation).
- Magnetic hysteresis is negligible.
- The stator magnetomotive force (mmf) and flux are sinusoidal.

Since the windings are magnetically coupled with each other, the flux linkage of each winding is due to its own current and the currents in all the other windings. The flux linkage of each winding is therefore given by:

$$\begin{bmatrix} \psi_a \\ \psi_b \\ \psi_c \\ \hline \psi_f \\ \psi_D \\ \psi_Q \end{bmatrix} = \left[\begin{array}{ccc|ccc} L_{aa} & L_{ab} & L_{ac} & L_{af} & L_{aD} & L_{aQ} \\ L_{ba} & L_{bb} & L_{bc} & L_{bf} & L_{bD} & L_{bQ} \\ L_{ca} & L_{cb} & L_{cc} & L_{cf} & L_{cD} & L_{cQ} \\ \hline L_{fa} & L_{fb} & L_{fc} & L_{ff} & L_{fD} & L_{fQ} \\ L_{Da} & L_{Db} & L_{Dc} & L_{Df} & L_{DD} & L_{DQ} \\ L_{Qa} & L_{Qb} & L_{Qc} & L_{Qf} & L_{QD} & L_{QQ} \end{array}\right] \begin{bmatrix} i_a \\ i_b \\ i_c \\ \hline i_f \\ i_D \\ i_Q \end{bmatrix} \begin{matrix} \\ \\ \text{stator} \\ \\ \\ \text{rotor} \end{matrix} \tag{3.19}$$

or

$$\begin{bmatrix} \psi_{abc} \\ \psi_{fDQ} \end{bmatrix} = \begin{bmatrix} L_{abc,abc} & L_{abc,fDQ} \\ L_{fDQ,abc} & L_{fDQ,fDQ} \end{bmatrix} \begin{bmatrix} i_{abc} \\ i_{fDQ} \end{bmatrix} \tag{3.20}$$

or in more compact form

$$\psi_{srf} = L_{srf}\, i_{srf} \tag{3.21}$$

where *srf* stands for stator reference frame that is the flux linkage equations are given in the stator reference frame.

In (3.19), L_{aa}, L_{bb} and L_{cc} represent the self-inductances of the stator three phase windings, and L_{ff}, L_{DD} and L_{QQ} represent the self-inductances of the rotor field and damper windings. The mutual inductance between two windings m and n is given by L_{mn}. It should be noted that L_{mn}=L_{nm}, and $L_{abc,fDQ} = L^T_{fDQ,abc}$.

It can be shown that all the elements of $L_{abc,abc}$, $L_{abc,fDQ}$ and $L_{fDQ,abc}$ vary as functions of the rotor angular displacement β (i.e., they are functions of time). However, all the elements of $L_{fDQ,fDQ}$ are constants. Also, $L_{fQ} = L_{DQ} = 0$, [3]-[6].

Using the voltage polarities and current directions of Figure 3.3, and also applying Kirchhoff's voltage law, the voltage equations for the stator and rotor windings are

$$\frac{d}{dt}\left[\begin{array}{c}\psi_a\\ \psi_b\\ \psi_c\\ \hline \psi_f\\ \psi_D\\ \psi_Q\end{array}\right] = -\left[\begin{array}{ccc|ccc}r_a & 0 & 0 & 0 & 0 & 0\\ 0 & r_b & 0 & 0 & 0 & 0\\ 0 & 0 & r_c & 0 & 0 & 0\\ \hline 0 & 0 & 0 & r_f & 0 & 0\\ 0 & 0 & 0 & 0 & r_D & 0\\ 0 & 0 & 0 & 0 & 0 & r_Q\end{array}\right]\left[\begin{array}{c}i_a\\ i_b\\ i_c\\ \hline i_f\\ i_D\\ i_Q\end{array}\right] - \left[\begin{array}{c}u_a\\ u_b\\ u_c\\ \hline -u_f\\ 0\\ 0\end{array}\right]\begin{array}{l}\text{stator}\\ \\ \\ \\ \text{rotor}\\ \\ \end{array} \tag{3.22}$$

or

$$\frac{d}{dt}\begin{bmatrix}\psi_{abc}\\ \psi_{fDQ}\end{bmatrix} = -\begin{bmatrix}R_{abc} & 0\\ 0 & R_{fDQ}\end{bmatrix}\begin{bmatrix}i_{abc}\\ i_{fDQ}\end{bmatrix} - \begin{bmatrix}u_{abc}\\ u_{fDQ}\end{bmatrix} \tag{3.23}$$

or in more compact form

$$\frac{d\psi_{srf}}{dt} = \dot{\psi}_{srf} = -\left(R_{srf}\, i_{srf} + u_{srf}\right) \tag{3.24}$$

which is a set of differential equations describing the electrical behavior (or dynamic) of a synchronous generator. However, (having replaced ψ_{srf} in (3.24) with (3.21)) this set of differential equations will be containing time-varying coefficients (since most of the elements of L_{srf} are functions of time) which make the analysis of the generator dynamics more difficult.

Fortunately, this problem can be overcome by the so called Park's transformation. This transformation consists in transforming the phase quantities of the stator (for instance, u_{abc}, i_{abc} and ψ_{abc}) into three new quantities called *dqo*-components (i.e., u_{dqo}, i_{dqo} and ψ_{dqo}). The *d*- and *q*-components rotate together with the rotor, with the *d*-component laying along the *d*-axis of the rotor, and the *q*-component laying along the *q*-axis of the rotor. The *o*-component vanishes under balanced operation. Thus, by Park's transformation the quantities in the stator reference frame (*srf*) are transformed to the rotor reference frame (*rrf*). This transformation is made by the matrix P, where

$$P = \sqrt{\frac{2}{3}}\begin{bmatrix}\cos(\beta) & \cos\left(\beta - \frac{2\pi}{3}\right) & \cos\left(\beta + \frac{2\pi}{3}\right)\\ \sin(\beta) & \sin\left(\beta - \frac{2\pi}{3}\right) & \sin\left(\beta + \frac{2\pi}{3}\right)\\ \frac{1}{\sqrt{2}} & \frac{1}{\sqrt{2}} & \frac{1}{\sqrt{2}}\end{bmatrix} \tag{3.25}$$

It should be noted that $P^{-1} = P^T$, i.e. P is orthogonal.

The voltages, currents and flux linkages in the rotor reference frame are obtained by

$$\begin{aligned} u_{dqo} &= P\, u_{abc}\\ i_{dqo} &= P\, i_{abc}\\ \psi_{dqo} &= P\, \psi_{abc} \end{aligned} \tag{3.26}$$

The quantities in the rotor reference frame can also be transformed to the stator reference frame by the inverse transformation as follows

$$\begin{aligned} u_{abc} =& P^{-1}\, u_{dqo} = P^{T}\, u_{dqo} \\ i_{abc} =& P^{-1}\, i_{dqo} = P^{T}\, i_{dqo} \\ \psi_{abc} =& P^{-1}\, \psi_{dqo} = P^{T}\, \psi_{dqo} \end{aligned} \tag{3.27}$$

Applying (3.27) to (3.20), the following are obtained

$$\begin{aligned} \begin{bmatrix} P^T\,\psi_{dqo} \\ \psi_{fDQ} \end{bmatrix} &= \begin{bmatrix} L_{abc,abc} & L_{abc,fDQ} \\ L_{fDQ,abc} & L_{fDQ,fDQ} \end{bmatrix} \begin{bmatrix} P^T\, i_{dqo} \\ i_{fDQ} \end{bmatrix} \quad \Rightarrow \\ \begin{bmatrix} P^T & 0 \\ 0 & \underline{\mathbf{1}} \end{bmatrix} \begin{bmatrix} \psi_{dqo} \\ \psi_{fDQ} \end{bmatrix} &= \begin{bmatrix} L_{abc,abc} & L_{abc,fDQ} \\ L_{fDQ,abc} & L_{fDQ,fDQ} \end{bmatrix} \begin{bmatrix} P^T & 0 \\ 0 & \underline{\mathbf{1}} \end{bmatrix} \begin{bmatrix} i_{dqo} \\ i_{fDQ} \end{bmatrix} \end{aligned} \tag{3.28}$$

Let

$$P_{ex} = \begin{bmatrix} P & 0 \\ 0 & \underline{\mathbf{1}} \end{bmatrix}$$

Then,

$$\begin{bmatrix} \psi_{dqo} \\ \psi_{fDQ} \end{bmatrix} = P_{ex} \begin{bmatrix} L_{abc,abc} & L_{abc,fDQ} \\ L_{fDQ,abc} & L_{fDQ,fDQ} \end{bmatrix} P_{ex}^{-1} \begin{bmatrix} i_{dqo} \\ i_{fDQ} \end{bmatrix} \tag{3.29}$$

or in more compact form

$$\psi_{rrf} = P_{ex}\, L_{srf}\, P_{ex}^{-1}\, i_{rrf} = L_{rrf}\, i_{rrf} \tag{3.30}$$

where

$$L_{rrf} = \begin{bmatrix} L_{dqo,dqo} & L_{dqo,fDQ} \\ L_{fDQ,dqo} & L_{fDQ,fDQ} \end{bmatrix} = \left[\begin{array}{ccc|ccc} L_d & 0 & 0 & k\,M_f & k\,M_D & 0 \\ 0 & L_q & 0 & 0 & 0 & k\,M_Q \\ 0 & 0 & L_o & 0 & 0 & 0 \\ \hline k\,M_f & 0 & 0 & L_{ff} & L_{fD} & 0 \\ k\,M_D & 0 & 0 & L_{Df} & L_{DD} & 0 \\ 0 & k\,M_Q & 0 & 0 & 0 & L_{QQ} \end{array}\right]$$

with $k = \sqrt{\frac{3}{2}}$. Note that the inductance matrix L_{rrf} is symmetrical, and all the elements of this matrix are constants (i.e., independent of time) which is the main advantage of Park's transformation.

Equation (3.29) (or (3.30)) may be written in detail to give

$$\begin{bmatrix} \psi_d \\ \psi_f \\ \psi_D \end{bmatrix} = \begin{bmatrix} L_d & k\,M_f & k\,M_D \\ k\,M_f & L_{ff} & L_{fD} \\ k\,M_D & L_{fD} & L_{DD} \end{bmatrix} \begin{bmatrix} i_d \\ i_f \\ i_D \end{bmatrix} \tag{3.31}$$

$$\begin{bmatrix} \psi_q \\ \psi_Q \end{bmatrix} = \begin{bmatrix} L_q & k\,M_Q \\ k\,M_Q & L_{QQ} \end{bmatrix} \begin{bmatrix} i_q \\ i_Q \end{bmatrix} \tag{3.32}$$

$$\psi_o = L_o\, i_o \tag{3.33}$$

These equations describe three magnetically decoupled winding sets. Under balanced operation i_o is zero. Since we are dealing with symmetrical three-phase systems in this compendium, the winding set (3.33) is omitted.

Figure 3.4 shows a pictorial representation of Park's transformation. The winding set (3.31) is laying on the d-axis of the rotor. The windings f and D (in red) are the physical field and damper windings of the rotor shown in Figure 3.3, while the winding d (in blue) is a fictitious winding representing the effect of the stator windings on the d-axis, and it rotates with the field winding. The winding set (3.32) is laying on the q-axis of the rotor. The winding Q (in red) is the physical damper winding of the rotor shown in Figure 3.3, while the winding q (in blue) is also a fictitious winding representing the effect of the stator windings on the q-axis. Note that these two winding sets are magnetically decoupled (as shown in Figure 3.4) which is another advantage of Park's transformation.

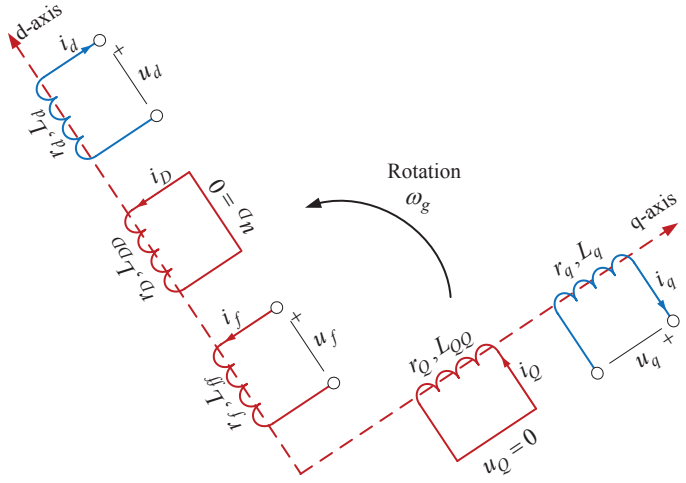

Figure 3.4. Representation of the salient-pole synchronous generator based on Park's transformation.

Equation (3.24) can also be transformed to the rotor reference frame by applying

$$\psi_{srf} = P_{ex}^{-1}\,\psi_{rrf} \quad , \quad i_{srf} = P_{ex}^{-1}\,i_{rrf} \quad \text{and} \quad u_{srf} = P_{ex}^{-1}\,u_{rrf}$$

Then, the following can be obtained

$$\dot{\psi}_{rrf} = -\left(R_{rrf}\,i_{rrf} + u_{rrf} + P_{ex}\left[\frac{d}{dt}P_{ex}^{-1}\right]\psi_{rrf}\right) \tag{3.34}$$

Note that $\frac{d}{dt}P_{ex}^{-1} \neq 0$, since P_{ex}^{-1} is a function of β (i.e. a function of time).

Assuming $r_a = r_b = r_c = r$ (which in most cases is true), it can be shown that

$$R_{rrf} = P_{ex}\,R_{srf}\,P_{ex}^{-1} = R_{srf} \quad \text{with} \quad R_{abc} = R_{dqo} = r\underline{\mathbf{1}}$$

Having determined $P_{ex}\left[\frac{d}{dt}P_{ex}^{-1}\right]$, it can be shown that (by expanding equation (3.34))

$$\begin{aligned}\dot{\psi}_d &= -\left(u_d + r\, i_d + \omega_g\, \psi_q\right)\\ \dot{\psi}_q &= -\left(u_q + r\, i_q - \omega_g\, \psi_d\right)\\ \dot{\psi}_o &= -\left(u_o + r\, i_o\right)\end{aligned} \tag{3.35}$$

and

$$\begin{aligned}\dot{\psi}_f &= u_f - r_f\, i_f\\ \dot{\psi}_D &= -\, r_D\, i_D\\ \dot{\psi}_Q &= -\, r_Q\, i_Q\end{aligned} \tag{3.36}$$

Equation (3.35) is known as *stator transients*, since only stator quantities are involved in this equation. Note that u_d, u_q, i_d, i_q, ψ_d and ψ_q are the rotor-equivalents of the stator voltages, currents and flux linkages. Once again, dealing with symmetrical three-phase systems, then $u_o = i_o = 0$. Therefore, $\dot{\psi}_o$ can be omitted. Equation (3.36) is known as *rotor transients*, since only rotor quantities are involved in this equation.

Equations (3.35)-(3.36) (i.e., equation (3.34) in compact form) together with equations (3.31)-(3.33) (i.e., equation (3.30) in compact form) describe the electrical dynamic of a synchronous generator in the rotor reference frame. These equations together with equation (3.13) determine the behavior of the synchronous generator during different disturbances in a power system.

In order to make a qualitative analysis of the behavior of a synchronous generator, it is often meaningful to use models that comprise more simplifications and approximations than those detailed model given by (3.35)-(3.36) and (3.31)-(3.33). Therefore, the following assumptions are made:

1. Only balanced operation is considered that is the third equation in (3.35) is removed, and also only positive-sequence quantities are considered.

2. The stator transients are neglected that is $\dot{\psi}_d = \dot{\psi}_q = 0$ in (3.35). This assumption is justified since they are numerically small compared to $\omega_g\, \psi_d$ and $\omega_g\, \psi_q$ [3].

3. All the stator resistances are neglected that is $r = 0$ in (3.35). This assumption is justified since they are very small.

4. During the transient-state the rotor speed is near synchronous speed, i.e. $\dfrac{\omega_g}{\omega_s} \approx 1$ (note however that these variations are sufficient to produce significant rotor angle deviation).

5. The rotor transient saliency is neglected that is $x'_q \approx x'_d$. It should be noted that if there is no rotor winding on the q-axis of the rotor, then $x'_q = x_q$.

6. There are no damper windings on the rotor that is $i_D = i_Q = 0$.

Based on the above assumptions, equations (3.31)-(3.32) may be rewritten as

$$\begin{aligned} \psi_d &= L_d\, i_d + k\, M_f\, i_f \\ \psi_f &= k\, M_f\, i_d + L_{ff}\, i_f \\ \psi_q &= L_q\, i_q \end{aligned} \tag{3.37}$$

and equations (3.35)-(3.36) may be rewritten as

$$\begin{aligned} u_d &= -\omega_s\, \psi_q = -\omega_s\, L_q\, i_q \\ u_q &= \omega_s\, \psi_d = \omega_s\, (L_d\, i_d + k\, M_f\, i_f) \\ \dot{\psi}_f &= u_f - r_f\, i_f \end{aligned} \tag{3.38}$$

Figure 3.5 (a) shows a synchronous generator connected to a transmission network via its terminal bus. The voltage at the terminal bus is $\bar{U}$ and the current injected to this bus is $\bar{I}$. Note that $\bar{U}$ is the generator **line-to-neutral** terminal voltage.

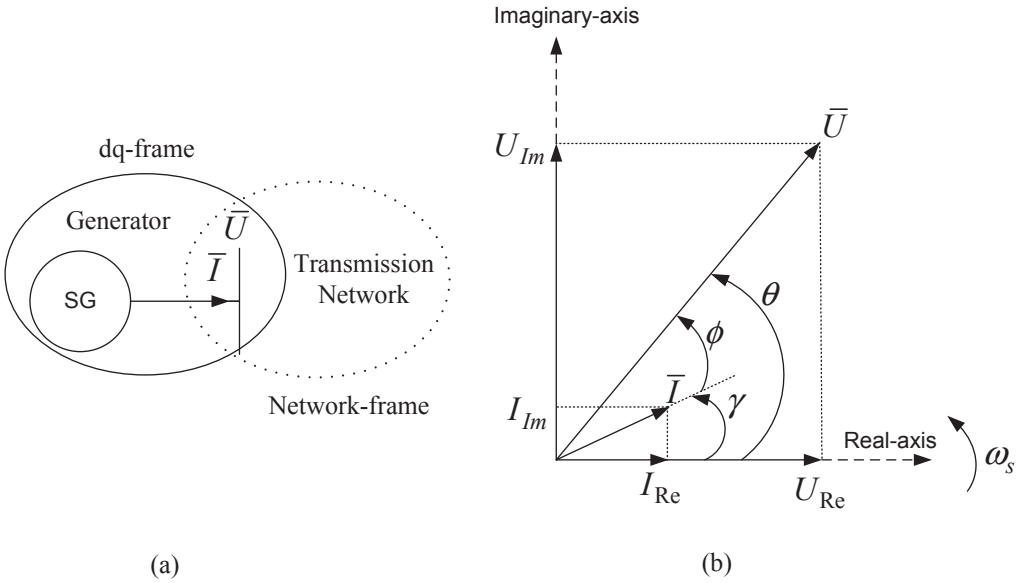

Figure 3.5. Single-line diagram of an SG connected to a transmission network, and the phasor diagram of $\bar{U}$ and $\bar{I}$ in the network reference frame.

In the transmission network, the voltages and currents are obtained and defined in the network reference frame which rotates at synchronous speed ω_s (see Figure 3.5 (b)). However, as seen from the generator, the stator equivalent quantities are defined in the rotor reference frame (dq-frame) based on Park's transformation which rotates at the rotor electrical speed ω_g.

Using the Real-axis as the reference, the following can be obtained in the network reference frame.

$$\begin{aligned} \bar{U} &= U e^{j\theta} = U\cos(\theta) + jU\sin(\theta) = U_{Re} + jU_{Im} \\ \bar{I} &= I e^{j\gamma} = I\cos(\gamma) + jI\sin(\gamma) = I_{Re} + jI_{Im} \\ \phi &= \theta - \gamma \end{aligned} \tag{3.39}$$

Under balanced operation, the instantaneous phase voltages and currents at the terminal bus in the network reference frame are given by

$$\begin{aligned} u_a &= \sqrt{2}\,U\cos(\omega_s t+\theta) \quad &,\quad i_a &= \sqrt{2}\,I\cos(\omega_s t+\gamma) \\ u_b &= \sqrt{2}\,U\cos(\omega_s t+\theta-120) \quad &,\quad i_b &= \sqrt{2}\,I\cos(\omega_s t+\gamma-120) \\ u_c &= \sqrt{2}\,U\cos(\omega_s t+\theta+120) \quad &,\quad i_c &= \sqrt{2}\,I\cos(\omega_s t+\gamma+120) \end{aligned} \tag{3.40}$$

Next, an interface (or a relationship) between the components of $\bar{U}$ and $\bar{I}$ in the rotor reference frame and the network reference frame is derived.

3.3 Steady-state model

In equation (3.38), u_d and u_q may be rewritten as

$$\begin{aligned} u_d &= -\,\omega_s\,L_q\,i_q = -x_q\,i_q \\ u_q &= \omega_s L_d i_d + k\omega_s M_f i_f = x_d i_d + \frac{\sqrt{3}}{\sqrt{2}}\,e_q \end{aligned} \tag{3.41}$$

where $e_q = \omega_s M_f i_f$ is the stator equivalent electromotive force (emf) corresponding to i_f, $x_d = \omega_s L_d$ is the d-axis synchronous reactance, and $x_q = \omega_s L_q$ is the q-axis synchronous reactance. For the round-rotor generator $x_d = x_q$, and for the salient-pole generator $x_d > x_q$. However, it may be assumed that $x_d \approx x_q$ if saliency is neglected. Furthermore, note that u_d, u_q, i_d and i_q in equation (3.41) are interpreted as the instantaneous quantities of the fictitious windings in d- and q-axis due to Park's transformation.

Applying equation (3.26) (i.e. Park's transformation) to equation (3.40), and measuring the rotor position from the q-axis by the new angle δ, then by setting $\beta = \frac{\pi}{2} + \delta$ the following can be obtained

$$\begin{aligned} u_q &= \;\sqrt{3}\,U\cos((\omega_g-\omega_s)t+\delta-\theta) \quad &,\quad i_q &= \;\sqrt{3}\,I\cos((\omega_g-\omega_s)t+\delta-\gamma) \\ u_d &= -\sqrt{3}\,U\sin((\omega_g-\omega_s)t+\delta-\theta) \quad &,\quad i_d &= -\sqrt{3}\,I\sin((\omega_g-\omega_s)t+\delta-\gamma) \end{aligned} \tag{3.42}$$

In the steady-state $\omega_g = \omega_s$, and equation (3.42) may be rewritten as

$$\begin{aligned} u_q &= \;\sqrt{3}\,U\cos(\delta-\theta) \quad &,\quad i_q &= \;\sqrt{3}\,I\cos(\delta-\gamma) \\ u_d &= -\sqrt{3}\,U\sin(\delta-\theta) \quad &,\quad i_d &= -\sqrt{3}\,I\sin(\delta-\gamma) \end{aligned} \tag{3.43}$$

Next, consider the following complex quantities

$$\begin{aligned} u_q + j\,u_d &= \sqrt{3}\,U\,[\cos(\delta-\theta) - j\,\sin(\delta-\theta)] \\ &= \sqrt{3}\,U\,e^{-j(\delta-\theta)} = \sqrt{3}\,\bar{U}\,e^{-j\delta} \end{aligned} \tag{3.44}$$

and

$$\begin{aligned} i_q + j\,i_d &= \sqrt{3}\,I\,[\cos(\delta-\gamma) - j\,\sin(\delta-\gamma)] \\ &= \sqrt{3}\,I\,e^{-j(\delta-\gamma)} = \sqrt{3}\,\bar{I}\,e^{-j\delta} \end{aligned} \tag{3.45}$$

It can be shown that [4]-[5]

$$U_d = \frac{u_d}{\sqrt{3}} \quad , \quad U_q = \frac{u_q}{\sqrt{3}} \quad , \quad I_d = \frac{i_d}{\sqrt{3}} \quad , \quad I_q = \frac{i_q}{\sqrt{3}} \quad \text{and} \quad E_q = \frac{e_q}{\sqrt{2}} \tag{3.46}$$

where U_d, U_q, I_d are I_q the components of $\bar{U}$ and $\bar{I}$ along the dq-axes. These components and E_q are also referred to the per-phase rms stator equivalent of the rotor referenced magnitudes u_d, u_q, i_d, i_q and e_q. Furthermore, E_q is also known as field excitation. Note that, U_d, U_q, I_d are I_q are different from u_d, u_q, i_d and i_q.

Based on (3.46), the following is obtained from equation (3.41)

$$\begin{aligned} U_d &= -x_q\, I_q \qquad \Rightarrow \qquad I_q = -\frac{U_d}{x_q} \\ U_q &= x_d\, I_d + E_q \qquad \Rightarrow \qquad I_d = \frac{U_q - E_q}{x_d} \end{aligned} \tag{3.47}$$

and from equations (3.44)-(3.45)

$$\begin{aligned} \bar{U} &= U_{Re} + jU_{Im} = (U_q + j\, U_d)\, e^{j\delta} = U_q\, e^{j\delta} + j\, U_d\, e^{j\delta} = \bar{U}_q + \bar{U}_d \\ \bar{I} &= I_{Re} + jI_{Im} = (I_q + j\, I_d)\, e^{j\delta} = I_q\, e^{j\delta} + j\, I_d\, e^{j\delta} = \bar{I}_q + \bar{I}_d \end{aligned} \tag{3.48}$$

Equation (3.48) gives the relationship (or interface) between the components of $\bar{U}$ and $\bar{I}$ in the dq-axes reference frame (based on Park's transformation) which is rotating at speed ω_g and in the network reference frame which is rotating at synchronous speed ω_s. This interface is also shown in Figure 3.6. The position of the q-axis with respect to the synchronous reference frame is given by $\delta = (\omega_g - \omega_s)t + \delta_0$, see equation (3.5). Note that in steady-state $\omega_g = \omega_s$, and $\delta = \delta_0$.

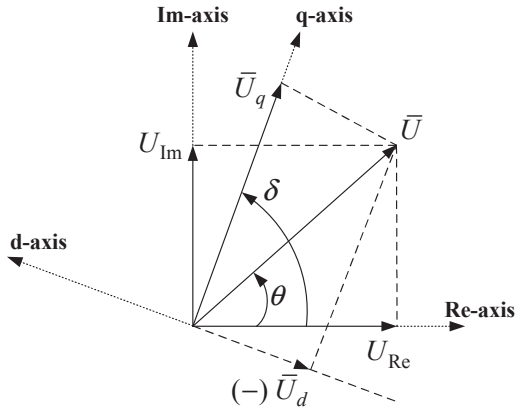

Figure 3.6. Generator-network interface.

The interface between the generator reference frame and the network reference frame may be given in matrix form as

$$\begin{bmatrix} U_q \\ U_d \end{bmatrix} = \begin{bmatrix} \cos(\delta) & \sin(\delta) \\ -\sin(\delta) & \cos(\delta) \end{bmatrix} \begin{bmatrix} U_{Re} \\ U_{Im} \end{bmatrix} = \begin{bmatrix} U\,\cos(\theta - \delta) \\ U\,\sin(\theta - \delta) \end{bmatrix} \tag{3.49}$$

The inverse relation is given by

$$\begin{bmatrix} U_{Re} \\ U_{Im} \end{bmatrix} = \begin{bmatrix} \cos(\delta) & -\sin(\delta) \\ \sin(\delta) & \cos(\delta) \end{bmatrix} \begin{bmatrix} U_q \\ U_d \end{bmatrix} \tag{3.50}$$

By virtue of (3.49), equation (3.47) can then be rewritten as

$$\begin{aligned} I_q &= -\frac{U\,\sin(\theta-\delta)}{x_q} \\ I_d &= \frac{U\,\cos(\theta-\delta)-E_q}{x_d} \end{aligned} \tag{3.51}$$

From equations (3.47)-(3.48), we have

$$\begin{aligned} \bar{U} &= (U_q + j\,U_d)\,e^{j\delta} = x_d\,I_d\,e^{j\delta} + E_q\,e^{j\delta} - j\;x_q\,I_q\,e^{j\delta} \\ &= -\,j\,x_d\,j\,I_d\,e^{j\delta} + E_q\,e^{j\delta} - j\,x_q\,I_q\,e^{j\delta} \\ &= -\,j\,x_d\,\bar{I}_d + \bar{E}_q - j\,x_q\,\bar{I}_q \qquad \text{(V)} \end{aligned} \tag{3.52}$$

or

$$\bar{E}_q = \bar{U} + j\,x_d\,\bar{I}_d + j\,x_q\,\bar{I}_q \qquad \text{(V)} \tag{3.53}$$

Usually, the position of the q-axis is not known (i.e. δ is not known). However (based on the load flow calculation), $\bar{U}$ and $\bar{I}$ are known. Therefore, the position of the q-axis with respect to the network reference frame can be obtained by some mathematical manipulation in equation (3.53) as follows

$$\begin{aligned} \bar{E}_q &= \bar{U} + j\,x_d\,\bar{I}_d + j\,x_q\,(\bar{I}-\bar{I}_d) \\ &= \bar{U} + j\,x_q\,\bar{I} + j\,(x_d - x_q)\bar{I}_d \\ &= \bar{E}_Q + j\,(x_d - x_q)\bar{I}_d \qquad \text{(V)} \end{aligned} \tag{3.54}$$

The phasor diagram of equations (3.53) and (3.54) is shown in Figure 3.7.

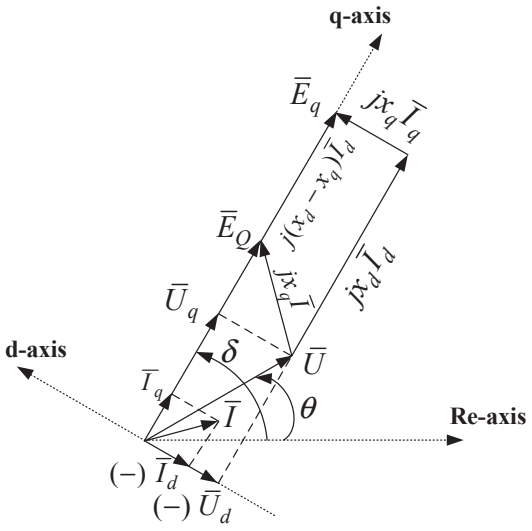

Figure 3.7. Phasor diagram representing equations (3.53) and (3.54).

In equation (3.54), $\bar{E}_Q = \bar{U} + j\, x_q\, \bar{I}$ can be easily calculated since $\bar{U}$ and $\bar{I}$ are known. Subsequently, $\bar{E}_q$ can be easily calculated. Note that $\bar{E}_Q$ and $\bar{E}_q$ both have the phase angle δ. Another mathematical manipulation in equation (3.53) gives

$$\begin{aligned} \bar{E}_q &= \bar{U} + j\, x_d\, (\bar{I} - \bar{I}_q) + j\, x_q\, \bar{I}_q \\ &= \bar{U} + j\, x_d\, \bar{I} - j\, (x_d - x_q)\bar{I}_q \qquad \text{(V)} \end{aligned} \tag{3.55}$$

or

$$\bar{E} = \bar{E}_q + j\, (x_d - x_q)\bar{I}_q = \bar{U} + j\, x_d\, \bar{I} \qquad \text{(V)} \tag{3.56}$$

where $\bar{E}$ is termed the generator internal voltage behind the d-axis synchronous reactance. The circuit representation of equation (3.56) is shown in Figure 3.8.

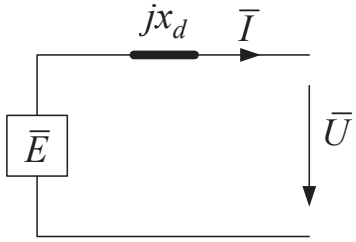

Figure 3.8. Per-phase equivalent circuit of a synchronous generator in steady-state.

By virtue of equations (3.47)-(3.51), the three-phase (complex) electrical power output of the generator is given by

$$\begin{aligned} \bar{S}_e &= 3\, \bar{U}\, \bar{I}^* = 3\, (U_q + j\, U_d)\, (I_q - j\, I_d) = 3\, (U_q\, I_q + U_d\, I_d) + j3\, (U_d\, I_q - U_q\, I_d) \\ &= P_e + j\, Q_e \qquad \text{(VA)} \end{aligned} \tag{3.57}$$

where

$$\begin{aligned} P_e &= 3\, (U_q\, I_q + U_d\, I_d) \\ &= 3\, \frac{U^2 \sin(\delta - \theta)\, \cos(\delta - \theta)}{x_q} + 3\, \frac{E_q\, U \sin(\delta - \theta) - U^2 \sin(\delta - \theta)\, \cos(\delta - \theta)}{x_d} \\ &= 3\, \frac{E_q\, U \sin(\delta - \theta)}{x_d} + 3\, \frac{U^2 \sin(2(\delta - \theta))}{2} \left(\frac{1}{x_q} - \frac{1}{x_d} \right) \qquad \text{(W)} \end{aligned} \tag{3.58}$$

and

$$\begin{aligned} Q_e &= 3\, (U_d\, I_q - U_q\, I_d) \\ &= 3\, \frac{-U^2 \sin^2(\delta - \theta)}{x_q} + 3\, \frac{E_q\, U \cos(\delta - \theta) - U^2 \cos^2(\delta - \theta)}{x_d} \\ &= -\, 3\, U^2 \left(\frac{\sin^2(\delta - \theta)}{x_q} + \frac{\cos^2(\delta - \theta)}{x_d} \right) + 3\, \frac{E_q\, U \cos(\delta - \theta)}{x_d} \qquad \text{(VAr)} \end{aligned} \tag{3.59}$$

Since $r = 0$, the generator three-phase active power (P_e) can also be obtained by

$$\begin{aligned} P_e &= \text{Real}\, [3\, \bar{E}\, \bar{I}^*] \\ &= 3\, \frac{E_q\, U \sin(\delta - \theta)}{x_d} + 3\, \frac{U^2 \sin(2(\delta - \theta))}{2} \left(\frac{1}{x_q} - \frac{1}{x_d} \right) \qquad \text{(W)} \end{aligned} \tag{3.60}$$

If saliency is neglected, i.e. $x_d \approx x_q$, then $\bar{E}_q = \bar{E}_Q = \bar{E}$, and

$$\begin{aligned} P_e &= 3\,\frac{E_q\,U\sin(\delta-\theta)}{x_d} \\ Q_e &= -3\,\frac{U^2 - E_q\,U\cos(\delta-\theta)}{x_d} \end{aligned} \tag{3.61}$$

3.4 Transient-state model

3.4.1 Classical model

From (3.37), the following can be obtained

$$i_f = \frac{\psi_f - k\,M_f\,i_d}{L_{ff}} \tag{3.62}$$

Substituting i_f from (3.62) into u_q in (3.38), the following is obtained

$$u_q = \omega_s\left(L_d - \frac{k^2\,M_f^2}{L_{ff}}\right)i_d + k\,\frac{\omega_s\,M_f}{L_{ff}}\,\psi_f = x'_d\,i_d + \frac{\sqrt{3}}{\sqrt{2}}\,e'_q \tag{3.63}$$

where, $e'_q = \dfrac{\omega_s\,M_f}{L_{ff}}\,\psi_f$ is termed the q-axis transient emf which is proportional to the field flux linkage ψ_f, and $x'_d = \omega_s\,L_d - \dfrac{\omega_s\,k^2\,M_f^2}{L_{ff}} = x_d - \dfrac{\omega_s\,k^2\,M_f^2}{L_{ff}}$ is termed the d-axis transient reactance.

Note that $x'_d < x_d$, and $x'_q = x_q$ since there is no rotor winding on the q-axis. Then, for the classical model we have

$$\begin{aligned} u_d &= -\,x_q\,i_q \\ u_q &= x'_d\,i_d + \frac{\sqrt{3}}{\sqrt{2}}\,e'_q \end{aligned} \tag{3.64}$$

where, e'_q is constant since ψ_f is assumed constant in the classical model. This implies that in the classical model there is no electrical dynamic since the only dynamic in equation (3.38) will be set to zero, $\dot{\psi}_f = 0$.

Based on the assumption 4 above, equations (3.43)-(3.53) will be also valid for the classical model with the exception that E_q and x_d will be replaced by E'_q and x'_d, respectively. Thus, for the classical model

- Equation (3.51) is modified to

$$\begin{aligned} I_q &= -\,\frac{U\,\sin(\theta-\delta)}{x_q} \\ I_d &= \frac{U\,\cos(\theta-\delta) - E'_q}{x'_d} \end{aligned} \tag{3.65}$$

- Equation (3.53) is modified to

$$\bar{E}'_q = \bar{U} + j\, x'_d\, \bar{I}_d + j\, x_q\, \bar{I}_q \qquad \text{(V)} \tag{3.66}$$

The phasor diagram of equations (3.53) and (3.66) is shown in Figure 3.9.

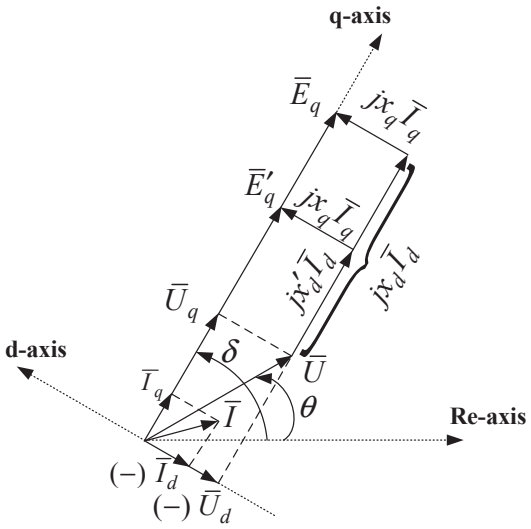

Figure 3.9. Phasor diagram representing equations (3.53) and (3.66).

Note that from the figure the following can be obtained

$$E_q = E'_q - (x_d - x'_d)\, I_d \tag{3.67}$$

- Equation (3.56) is modified to

$$\bar{E}' = \bar{E}'_q - j\,(x_q - x'_d)\bar{I}_q = \bar{U} + j\, x'_d\, \bar{I} \qquad \text{(V)} \tag{3.68}$$

where $\bar{E}'$ is termed the generator transient internal voltage behind the d-axis transient reactance. The phasor diagram of equation (3.68) is shown in Figure 3.10, where δ' is the phase angle of $\bar{E}'$. Note that $\delta = \delta' + \alpha'$.

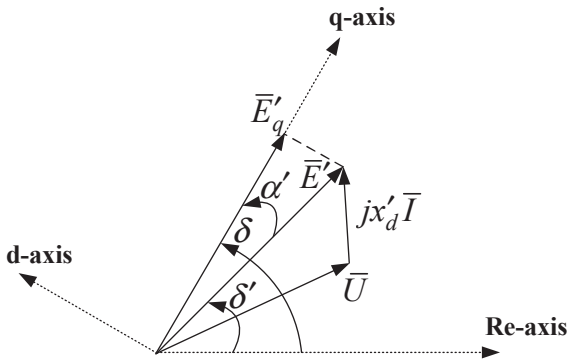

Figure 3.10. Phasor diagram representing equation (3.68)

Since ψ_f is assumed constant, E' and α' are also constant with respect to the rotor axes [5], and in the classical model the generator is represented by a voltage source with a constant magnitude E' behind its d-axis transient reactance x'_d as shown in Figure 3.11 (a).

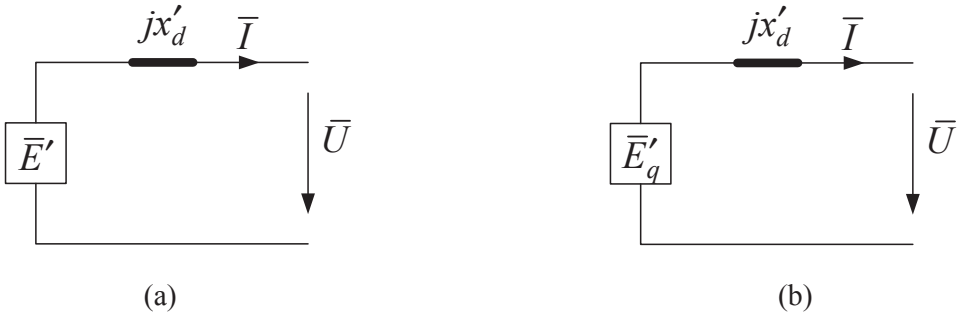

Figure 3.11. Equivalent circuit of a synchronous generator for transient-state studies.

The generator three-phase active power is then given by

$$\begin{aligned} P_e &= \text{Real}\,[3\,\bar{E}'\,\bar{I}^*] = 3\,(U_q I_q + U_d I_d) = 3(E'_q\,I_q + (x'_d - x_q) I_d\,I_q) \\ &= 3\,\frac{E'_q\,U\sin(\delta-\theta)}{x'_d} + 3\,\frac{U^2\sin(2(\delta-\theta))}{2}\left(\frac{1}{x_q} - \frac{1}{x'_d}\right) \qquad \text{(W)} \end{aligned} \tag{3.69}$$

Based on the assumption 5, $x'_d \approx x_q$. This assumption results in $\bar{E}'_q = \bar{E}'$ (i.e. $\delta = \delta'$ and $\alpha' = 0$), and in Figure 3.11 (a) the voltage source ($\bar{E}'$) is replaced by $\bar{E}'_q = E'_q\,e^{j\delta}$ as shown in Figure 3.11 (b) based on which

$$\bar{E}'_q = \bar{U} + j\,x'_d\,\bar{I} \qquad \text{(V)} \tag{3.70}$$

and (since $r = 0$)

$$P_e = \text{ Real }\left[3\bar{E}'_q\,\bar{I}^*\right] = \,3\,E'_q\,I_q = \,3\frac{E'_q\,U}{x'_d}\sin(\delta-\theta) \qquad \text{(W)} \tag{3.71}$$

The dynamic of a synchronous generator represented by the classical model is then described only by the swing equation (3.17), i.e.

$$\begin{aligned} \dot{\delta} &= \omega \\ \dot{\omega} &= \frac{1}{M}(P_{mpu} - P_{epu} - D\omega) \end{aligned} \tag{3.72}$$

where, P_{mpu} is assumed to be constant and P_{epu} is the per unit value of P_e in equation (3.71) which is defined in Section 3.5.

3.4.2 One-axis model

In the classical model, ψ_f is assumed constant which implies that e'_q (or E'_q) is also constant. This assumption is justified if the generator is located long away from the disturbance point.

In the one-axis model (also known as flux-decay model), the variation of ψ_f is however considered (although it changes slowly). This change can be determined by differentiating $e'_q = \dfrac{\omega_s M_f}{L_{ff}} \psi_f$ (, and substituting $\dot{\psi}_f$ from (3.38)) as follows:

$$\dot{e'_q} = \frac{\omega_s M_f}{L_{ff}} \dot{\psi}_f = \frac{\omega_s M_f}{L_{ff}} (u_f - r_f i_f) \tag{3.73}$$

which can be rewritten as

$$\frac{L_{ff}}{r_f} \dot{e'_q} = \frac{\omega_s M_f}{r_f} u_f - \omega_s M_f i_f \tag{3.74}$$

Let

$$T'_{do} = \frac{L_{ff}}{r_f} \quad , \quad e_f = \frac{\omega_s M_f}{r_f} u_f \quad \text{and from (3.41)} \quad e_q = \omega_s M_f i_f$$

where, T'_{do} is termed the d-axis transient open-circuit time constant, and e_f is an emf proportional to the field voltage u_f. Then, equation (3.74) is rewritten as

$$T'_{do} \dot{e'_q} = e_f - e_q \tag{3.75}$$

Let also

$$E'_q = \frac{e'_q}{\sqrt{2}} \quad , \quad E_f = \frac{e_f}{\sqrt{2}} \quad \text{and} \quad E_q = \frac{e_q}{\sqrt{2}} \tag{3.76}$$

where, E'_q, E_f and E_q are the rms values of e'_q, e_f and e_q.

Substituting equations (3.76) and (3.67) into (3.75) and using (3.65), the dynamic of E'_q (with rms quantities) is obtained as follows

$$\begin{aligned} T'_{do} \dot{E'_q} &= E_f - E_q = E_f - E'_q + (x_d - x'_d) I_d \\ &= E_f - \frac{x_d}{x'_d} E'_q + \frac{x_d - x'_d}{x'_d} U \cos(\delta - \theta) \end{aligned} \tag{3.77}$$

The dynamic of the generator using the one-axis model is then given by (in (pu))

$$\begin{aligned} \dot{\delta} &= \omega \\ \dot{\omega} &= \frac{1}{M}(P_{mpu} - P_{epu} - D\omega) \\ \dot{E'}_{qpu} &= \frac{1}{T'_{do}} \left(E_{fpu} - \frac{x_{dpu}}{x'_{dpu}} E'_{qpu} + \frac{x_{dpu} - x'_{dpu}}{x'_{dpu}} U_{pu} \cos(\delta - \theta) \right) \end{aligned} \tag{3.78}$$

where, P_{epu} is the per unit value of P_e in equation (3.71), and E_{fpu} is constant. The per unit variables are defined in Section 3.5.

The one-axis model is widely used in voltage stability analysis, and also small-signal analysis for designing Power System Stabilizer (PSS). The impact of PSS on damping of electromechanical oscillation will be discussed further in this compendium.

3.4.3 Two-axis model

In the two-axis model, it is assumed that the q-axis of the rotor is equipped with a short-circuited damper winding. This winding may also represent the effect of the rotors of the high-speed generators which are driven by steam or gas turbines, and have cylindrical (or round) rotors made up of solid steel forging. A high-speed generator often does not have special damper windings. However, the solid steel rotor body acts as a damper winding in the q-axis by offering paths for eddy currents [5]-[6].

Having a short-circuited damper winding in the q-axis of the rotor then $i_Q \neq 0$ in the assumption 6, and equations (3.37) and (3.38) are rewritten as

$$\begin{aligned}
\psi_d &= L_d\, i_d + k\, M_f\, i_f \\
\psi_f &= k\, M_f\, i_d + L_{ff}\, i_f \\
\psi_q &= L_q\, i_q + k\, M_Q\, i_Q \\
\psi_Q &= k\, M_Q\, i_q + L_{QQ}\, i_Q \quad \Rightarrow \quad i_Q = \frac{\psi_Q - k\, M_Q\, i_q}{L_{QQ}}
\end{aligned} \tag{3.79}$$

and

$$\begin{aligned}
u_d &= -\,\omega_s\, \psi_q = -\omega_s\, (L_q\, i_q + k\, M_Q\, i_Q) \\
u_q &= \omega_s\, \psi_d \\
\dot{\psi}_f &= u_f - r_f\, i_f \\
\dot{\psi}_Q &= -\,r_Q\, i_Q
\end{aligned} \tag{3.80}$$

Substituting i_Q from equation (3.79) into u_d in (3.80), the following is obtained

$$u_d = -\left(\omega_s\, L_q - \frac{\omega_s\, k^2\, M_Q^2}{L_{QQ}}\right) i_q - k\, \frac{\omega_s\, M_Q}{L_{QQ}}\, \psi_Q = -x'_q\, i_q + \frac{\sqrt{3}}{\sqrt{2}}\, e'_d \tag{3.81}$$

where, $e'_d = -\dfrac{\omega_s\, M_Q}{L_{QQ}}\, \psi_Q$, and $x'_q = \omega_s\, L_q - \dfrac{\omega_s\, k^2\, M_Q^2}{L_{QQ}} = x_q - \dfrac{\omega_s\, k^2\, M_Q^2}{L_{QQ}}$. This reactance is termed the q-axis transient reactance. Note that $x'_q < x_q$.

Equation (3.64) is then modified as

$$\begin{aligned}
u_d &= -x'_q\, i_q + \frac{\sqrt{3}}{\sqrt{2}}\, e'_d = -x'_q\, i_q + \sqrt{3}\, E'_d \\
u_q &= x'_d\, i_d + \frac{\sqrt{3}}{\sqrt{2}}\, e'_q = x'_d\, i_d + \sqrt{3}\, E'_q
\end{aligned} \tag{3.82}$$

or

$$\begin{aligned}
U_d &= -x'_q\, I_q + E'_d \quad \Rightarrow \quad I_q = -\frac{U_d - E'_d}{x'_q} \\
U_q &= x'_d\, I_d + E'_q \quad \Rightarrow \quad I_d = \frac{U_q - E'_q}{x'_d}
\end{aligned} \tag{3.83}$$

where, $E'_d = \dfrac{e'_d}{\sqrt{2}}$.

Following a procedure similar to that for the one-axis model, the dynamic of E'_d (with rms quantities) is obtained as follows

$$T'_{qo}\dot{E}'_d = -E'_d - (x_q - x'_q)I_q = -\frac{x_q}{x'_q}E'_d - \frac{x_q - x'_q}{x'_q}U\sin(\delta - \theta)$$

where, $T'_{qo} = \dfrac{L_{QQ}}{r_Q}$ is termed the q-axis transient open-circuit time constant.

Thus, the dynamic of the generator using the two-axis model is given in (pu) by

$$\begin{aligned}
\dot{\delta} &= \omega \\
\dot{\omega} &= \frac{1}{M}(P_{mpu} - P_{epu} - D\omega) \\
\dot{E}'_{qpu} &= \frac{1}{T'_{do}}\left(E_{fpu} - \frac{x_{dpu}}{x'_{dpu}}E'_{qpu} + \frac{x_{dpu} - x'_{dpu}}{x'_{dpu}}U_{pu}\cos(\delta - \theta)\right) \\
\dot{E}'_{dpu} &= \frac{1}{T'_{qo}}\left(-\frac{x_{qpu}}{x'_{qpu}}E'_{dpu} - \frac{x_{qpu} - x'_{qpu}}{x'_{qpu}}U_{pu}\sin(\delta - \theta)\right)
\end{aligned} \tag{3.84}$$

where, P_{epu} is the per unit value of

$$\begin{aligned}
P_e &= 3(U_q\, I_q + U_d\, I_d) = 3(E'_q\, I_q + E'_d\, I_d + (x'_d - x'_q)I_d\, I_q) = 3(E'_q\, I_q + E'_d\, I_d) \\
&= 3\,\frac{E'_q U\ \sin(\delta - \theta) + E'_d U\ \cos(\delta - \theta)}{x'_d}
\end{aligned} \tag{3.85}$$

since $x'_q = x'_d$ based on the assumption 5. The two-axis model is widely used in transient stability analysis especially for modeling generators with round rotors.

Table 3.1 gives the typical values of generator parameters (depending upon the size of generator). Reactances are expressed in (pu) based on the generator rated values, H is given in (s) based on the generator rated three-phase MVA, and time constants are given in (s).

Parameter	Round Rotor	Salient-Pole Rotor
x_d	1.0 – 2.3	0.6 – 1.5
x_q	1.0 – 2.3	0.4 – 1.0
x'_d	0.15 – 0.4	0.2 – 0.5
x'_q	0.3 – 1.0	—
T'_{do}	3.0 – 10.0	1.5 – 9.0
T'_{qo}	0.5 – 2.0	–
H	2.5 – 10	2.0 – 4.0

Table 3.1. Typical values of generator parameters [6].

3.5 Per unit conversion

As described in [3]-[4], it is more convenient to normalize the generator quantities based on the following base values.

$$\begin{aligned} S_{base}^{1\phi} &= \text{the generator rated per-phase VA} \\ U_{base}^{LN} &= \text{the generator rated } \textbf{line-to-neutral} \text{ rms terminal voltage} \\ I_{base} &= \frac{S_{base}^{1\phi}}{U_{base}^{LN}} \qquad \text{and} \qquad Z_{base} = \frac{U_{base}^{LN}}{I_{base}} \quad \Rightarrow \\ S_{base}^{1\phi} &= U_{base}^{LN}\, I_{base} \quad \text{and} \qquad U_{base}^{LN} = Z_{base}\, I_{base} \end{aligned} \tag{3.86}$$

Applying the above base values to equation (3.70), then

$$\frac{\bar{E}'_q}{U_{base}^{LN}} = \frac{\bar{U}}{U_{base}^{LN}} + j\frac{x'_d\,\bar{I}}{Z_{base}\,I_{base}} \quad \Rightarrow \quad \bar{E}'_{qpu} = \bar{U}_{pu} + j\,x'_{dpu}\,\bar{I}_{pu} \tag{3.87}$$

where

$$\bar{E}'_{qpu} = \frac{\bar{E}'_q}{U_{base}^{LN}} \quad , \quad \bar{U}_{pu} = \frac{\bar{U}}{U_{base}^{LN}} \quad , \quad \bar{I}_{pu} = \frac{\bar{I}}{I_{base}} \quad \text{and} \quad x'_{dpu} = \frac{x'_d}{Z_{base}} \tag{3.88}$$

Also, (3.71) can be converted to (pu) as follows

$$\begin{aligned} \frac{P_e}{S_{base}^{1\phi}} &= 3\,\frac{E'_q\,U}{x'_d\,U_{base}^{LN}\,I_{base}}\,\sin(\delta-\theta) = 3\,\frac{E'_q}{U_{base}^{LN}}\,\frac{U}{U_{base}^{LN}}\,\frac{Z_{base}}{x'_d}\,\sin(\delta-\theta) \;\Rightarrow \\ P_{epu_{1\phi}} &= 3\,\frac{E'_{qpu}\,U_{pu}}{x'_{dpu}}\,\sin(\delta-\theta) \end{aligned} \tag{3.89}$$

If the generator rated three-phase VA ($S_{base}^{3\phi} = 3\,S_{base}^{1\phi}$) is used as the base power, and the generator rated **line-to-line** rms terminal voltage ($U_{base}^{LL} = \sqrt{3}\,U_{base}^{LN}$) is used as the base voltage, then

$$\begin{aligned} S_{base}^{3\phi} &= \sqrt{3}\,U_{base}^{LL}\,I_{base} \\ I_{base} &= \frac{S_{base}^{3\phi}}{\sqrt{3}U_{base}^{LL}} = \frac{3S_{base}^{1\phi}}{3U_{base}^{LN}} \quad \text{(i.e., the same numerical value as in (3.86))} \\ Z_{base} &= \frac{(U_{base}^{LL})^2}{S_{base}^{3\phi}} = \frac{U_{base}^{LN}}{I_{base}} \quad \text{(i.e., the same numerical value as in (3.86))} \end{aligned} \tag{3.90}$$

Also, if the **line-to-line** rms voltage ($\bar{U}^{LL} = \sqrt{3}\,\bar{U}$) of the terminal bus is considered in Figure 3.11 (b), then the equation (3.70) is written as

$$\bar{E}'_q = \frac{U^{LL}}{\sqrt{3}} + j\,x'_d\,\bar{I} \quad \Rightarrow \quad \sqrt{3}\,\bar{E}'_q = U^{LL} + j\,x'_d\,\sqrt{3}\,\bar{I} \tag{3.91}$$

Applying the base values given in (3.90) to equation (3.91), then

$$\frac{\sqrt{3}\,\bar{E}'_q}{U_{base}^{LL}} = \frac{\bar{U}^{LL}}{U_{base}^{LL}} + j\frac{x'_d\,\sqrt{3}\,\bar{I}}{Z_{base}\,\sqrt{3}\,I_{base}} \quad \Rightarrow \quad \bar{E}'_{qpu} = \bar{U}_{pu} + j\,x'_{dpu}\,\bar{I}_{pu} \tag{3.92}$$

where

$$\begin{aligned}
\bar{E}'_{qpu} &= \frac{\sqrt{3}\,\bar{E}'_q}{U^{LL}_{base}} = \frac{\bar{E}'_q}{U^{LN}_{base}} \quad \text{(i.e., the same numerical value as in (3.88))} \\
\bar{U}_{pu} &= \frac{\bar{U}^{LL}}{U^{LL}_{base}} = \frac{\bar{U}}{U^{LN}_{base}} \quad \text{(i.e., the same numerical value as in (3.88))} \\
\bar{I}_{pu} &= \frac{\bar{I}}{I_{base}} \quad \text{and} \quad x'_{dpu} = \frac{x'_d}{Z_{base}} \quad \text{(i.e., the same numerical values as in (3.88))}
\end{aligned}$$

However, for the active power the following is obtained

$$\begin{aligned}
\frac{P_e}{S^{3\phi}_{base}} &= \frac{\sqrt{3}\,E'_q\,\sqrt{3}\,U}{x'_d\,\sqrt{3}\,U^{LL}_{base}\,I_{base}}\,\sin(\delta-\theta) = \frac{\sqrt{3}\,E'_q}{U^{LL}_{base}}\,\frac{U^{LL}}{U^{LL}_{base}}\,\frac{Z_{base}}{x'_d}\,\sin(\delta-\theta) \;\Rightarrow \\
P_{epu_{3\phi}} &= \frac{E'_{qpu}\,U_{pu}}{x'_{dpu}}\,\sin(\delta-\theta) = \frac{1}{3}\,P_{epu_{1\phi}}
\end{aligned} \tag{3.93}$$

Henceforward, the three-phase power and the line-to-line voltage at each bus will be considered, and the superscripts "3ϕ" and "LL" will therefore be omitted. Moreover, the normalization of the quantities will be based on

$$\begin{aligned}
S_{base} &= \text{an arbitrary three-phase base power} \\
U_{base} &= \text{a line-to-line base voltage} \\
I_{base} &= \frac{S_{base}}{\sqrt{3}\,U_{base}} \quad \text{and} \quad Z_{base} = \frac{(U_{base})^2}{S_{base}}
\end{aligned} \tag{3.94}$$

Thus,

$$\begin{aligned}
E_{qpu} &= \frac{\sqrt{3}E_q}{U_{base}} \quad , \quad E'_{qpu} = \frac{\sqrt{3}E'_q}{U_{base}} \quad , \quad E'_{dpu} = \frac{\sqrt{3}E'_d}{U_{base}} \quad , \quad E_{fpu} = \frac{\sqrt{3}E_f}{U_{base}} \\
x_{dpu} &= \frac{x_d}{Z_{base}} \quad , \quad x'_{dpu} = \frac{x'_d}{Z_{base}} \quad , \quad x_{qpu} = \frac{x_q}{Z_{base}} \quad , \quad x'_{qpu} = \frac{x'_q}{Z_{base}} \\
U_{pu} &= \frac{U}{U_{base}} \quad , \quad I_{pu} = \frac{I}{I_{base}} \quad , \quad P_{epu} = \frac{P_e}{S_{base}} = \frac{P_e}{\sqrt{3}\,U_{base}\,I_{base}}
\end{aligned} \tag{3.95}$$

Here-onward, if not otherwise explicitly stated, all used quantities in the compendium (apart from ω) are expressed in (pu), and the subscript "pu" will therefore be omitted.

Next, based on the above base values and considering the terminal voltage $\bar{U}$ as **line-to-line** voltage, the electric power in (pu) for the classical model and the one-axis model is given by

$$P_e = \text{ Real } \left[\bar{E}'_q\,\bar{I}^*\right] = E'_q\,I_q = \frac{E'_q\,U}{x'_d}\,\sin(\delta-\theta) \quad \text{(pu)} \tag{3.96}$$

since $x'_d = x_q$. Furthermore, the equivalent circuit of a generator represented by one of those two models is shown in Figure 3.11 (b), where

$$\bar{E}'_q = E'_q\,e^{j\,\delta} = \bar{U} + j\,x'_d\,\bar{I} \quad \text{(pu)} \tag{3.97}$$

For the two-axis mode, the electric power in (pu) is given by

$$P_e = \text{ Real } \left[\bar{E}'\,\bar{I}^*\right] = E'_q\,I_q + E'_d\,I_d = \frac{E'_q\,U\,\sin(\delta-\theta) + E'_d\,U\,\cos(\delta-\theta)}{x'_d} \quad \text{(pu)} \quad (3.98)$$

since $x'_d = x'_q$. The equivalent circuit of a generator represented by the two-axis model is similar to that shown in Figure 3.11 (a), but with

$$\bar{E}' = (E'_q + j\,E'_d)\,e^{j\,\delta} = \bar{U} + j\,x'_d\,\bar{I} \quad \text{(pu)} \quad (3.99)$$

3.6 Excitation systems

The generator excitation system consists of an exciter and an Automatic Voltage Regulator (AVR). The primary function of an exciter is to provide a dc source for field excitation of a synchronous generator, and the AVR controls the excitation voltage. A control on excitation voltage results in controlling the field current (i.e. i_f in Figure 3.3, or E_f in equation (3.78)) which in turn controls the generated voltage and reactive power. This action contributes to the enhancement of system stability.

In general, there are two types of exciters, namely rotating and static exciters. The rotating exciters make use of either dc generators or ac generators with rectifiers as sources to provide dc current to the field winding of the generator. Figure 3.12 illustrates basic structure of the excitation systems with rotating exciters.

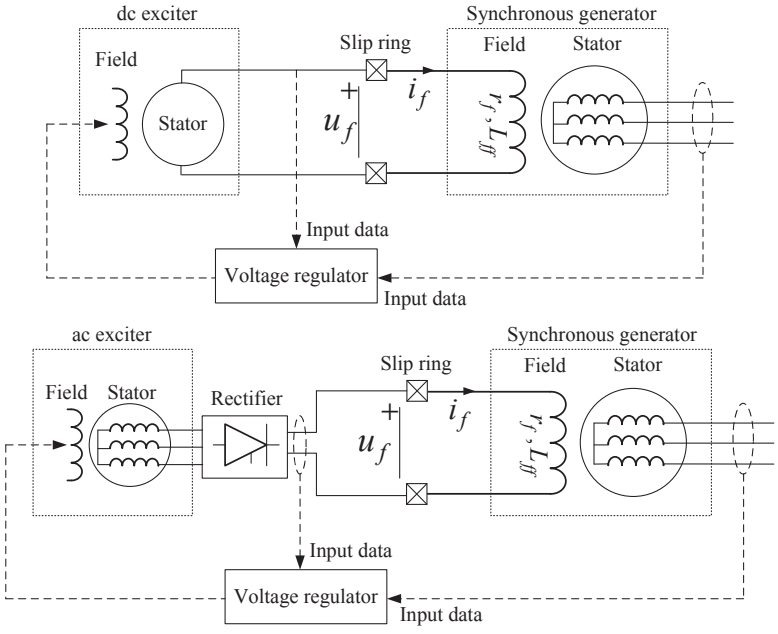

Figure 3.12. Basic structure of the excitation systems with rotating exciters.

A dc exciter may be driven by a motor or the shaft of the generator. It supplies dc current to the field winding of the synchronous generator through slip rings (a slip ring is a rotary continuity electromechanical device to transfer electrical power and

electrical signals from a stationary to a rotating structure). These excitation systems belong to early systems. Due to their obsolescence, and also the needs of today's power systems to high speed excitation systems on all grid connected generating units with high-field forcing capability, many older dc exciters are being replaced by ac or static type systems. In an ac excitation system, the ac output is rectified to provide the dc current required by the field winding of the synchronous generator. If the rectifier is stationary slip rings will be needed. With rotating rectifiers, the need for slip rings is however eliminated.

Figure 3.13 shows the basic structure of static excitation systems. The rectifiers are directly fed from the generator terminals (or the station auxiliary bus) via a step-down transformer to provide the dc current required by the field winding of the synchronous generator. In these excitation systems, slip rings are needed, and the rectifiers are controlled directly by a voltage regulator. By far, most excitation systems installed nowadays are of this type.

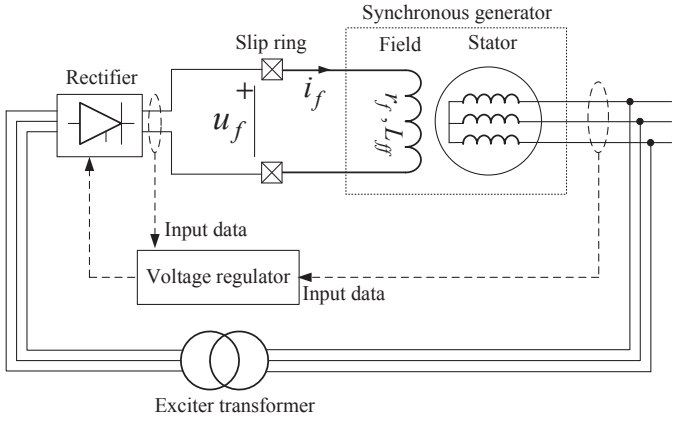

Figure 3.13. Basic structure of static excitation systems.

As mentioned before, the above figures only illustrate the basic structure of these different types of excitation systems. Each type has however different configurations which are comprehensively described in [3]-[6], and related references therein. Figure 3.14 shows the block diagram of a simple excitation system which will be used in this compendium (especially for small signal analysis).

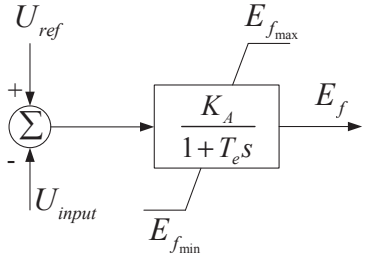

Figure 3.14. Block diagram of a simple excitation system.

In the figure, K_A and T_e represent the gain of an amplifier and the time constant of exciter, respectively. Further, U_{ref} is the set value and U_{input} is the voltage which

will be controlled. U_{input} is indeed the output of the block diagram shown in Figure 3.15, where $\bar{U}$ is the generator terminal voltage, $\bar{I}$ is the current flowing out from the generator, and $U = |\bar{U}|$.

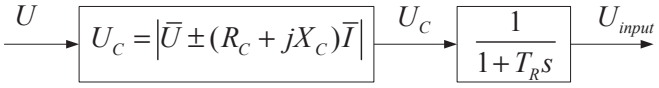

Figure 3.15. Block diagram of load compensation and transducer.

The first block is known as load compensator, and $\bar{Z}_C = R_C + jX_C \approx jX_C$ is known as the compensation impedance. If the voltage at the generator terminal will be controlled, then $\bar{Z}_C = 0$ that is $U_C = U$. However, if the voltage at a point beyond the generator terminal will be controlled, then $\bar{Z}_C \neq 0$ which represents the electrical distance between that point and the generator terminal. The negative sign means that the point at which the voltage will be controlled is closer to (or within) the transmission system. The positive sign is however used if several parallel generators (equipped with AVR) are connected to the same terminal bus via a common step-up transformer. By this compensation, the voltage at an (artificial) point within each generator will be controlled which results in an adequate and stable reactive power productions between the generators. The second block is known as transducer which represents the delay due to measuring, rectifying and filtering of the signal. T_R is usually very small, and this block can therefore be omitted. In this compendium, the load compensation is also omitted since the control of the terminal voltage is of concern that is $U_{iput} = U$.

It will be shown that excitation system with high gain will introduce very poor or negative damping in electromechanical oscillations which can lead to angular instability. To eliminate this effect and to improve the system damping in general, a supplementary damping device known as Power System Stabilizer (PSS) is added in the excitation system. This device provides an additional supplementary signal to the voltage regulator at the summing junction as shown in Figure 3.16

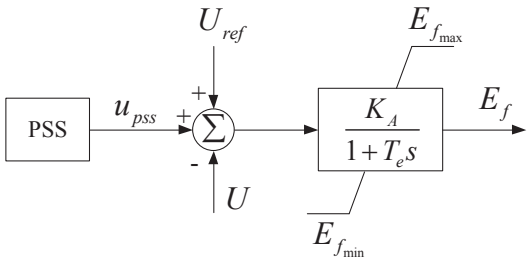

Figure 3.16. Block diagram of a simple excitation system with PSS.

Figure 3.17 shows the block diagram of a PSS.

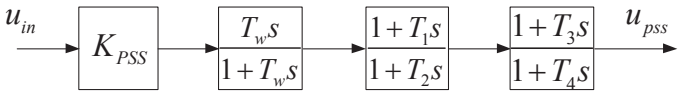

Figure 3.17. Block diagram of a PSS.

u_{in} is the input signal. The generator speed deviation (i.e ω) or the generator real power (i.e. P_e) is the most commonly used input signal. K_{PSS} is the stabilizer gain which determines the magnitude of damping provided by PSS. The first block in the figure represents a high-pass filter (known as washout block). The purpose of this filter is to stop contribution from a steady-state deviation of the input signal. The second and third blocks are known as phase compensation blocks which are indeed lead-lag type transfer functions. The purpose of these blocks are to shift the phase by setting T_1-T_4 at values so that a positive contribution to damping is obtained. Normally, the second phase compensation block will be used if the phase angle of the first phase compensation block is greater than a given maximum value. Then, $T_1 = T_3$ and $T_2 = T_4$. However, if the phase angle of the first phase compensation block is less than the given maximum value, then the second phase compensation block will not be used (i.e. $T_3 = T_4$). The tuning of a PSS is discussed in Chapter 6.

3.6.1 One-axis model with AVR and PSS

It has already been shown that the dynamic of the generator k represented by the one-axis model is given by

$$\begin{aligned}
\dot{\delta}_k &= \omega_k \\
\dot{\omega}_k &= \frac{1}{M_k}(P_{mk} - P_{ek} - D_k\omega_k) = \frac{1}{M_k}(P_{mk} - \frac{E'_{qk}\,U_k}{x'_{dk}}\sin(\delta_k - \theta_k) - D_k\omega_k) \\
\dot{E}'_{qk} &= \frac{1}{T'_{dok}}\left(E_{fk} - \frac{x_{dk}}{x'_{dk}}\,E'_{qk} + \frac{x_{dk} - x'_{dk}}{x'_{dk}}\,U_k\cos(\delta_k - \theta_k)\right)
\end{aligned} \tag{3.100}$$

where E_{fk} is constant.

Using the AVR shown in figure 3.16, then E_{fk} is not longer constant and its dynamic is given by

$$\dot{E}_{fk} = \frac{1}{T_{ek}}\,(-E_{fk} + K_{Ak}\,(U_{kref} + u_{pssk} - U_k)) \tag{3.101}$$

If no PSS is utilized then $u_{pssk} = 0$.

Using the PSS shown in figure 3.17, if the washout block and the second phase compensation block are omitted, and also the generator speed deviation (i.e ω_k) is used as the input signal, then the output signal u_{pss} can be considered as a state variable whose dynamic is given by

$$\begin{aligned}
\dot{u}_{pssk} =& \frac{1}{T_{2k}}\,(-u_{pssk} + K_{PSSk}\,\omega_k + T_{1k}\,K_{PSSk}\,\dot{\omega}_k) \\
=& \frac{1}{T_{2k}}\,\left(-u_{pssk} + K_{PSSk}\,\omega_k + T_{1k}\,K_{PSSk}\,\frac{P_{mk} - P_{ek} - D_k\omega_k}{M_k}\right)
\end{aligned} \tag{3.102}$$

In general, by using the following equivalent block diagram shown in Figure 3.17 for a PSS,

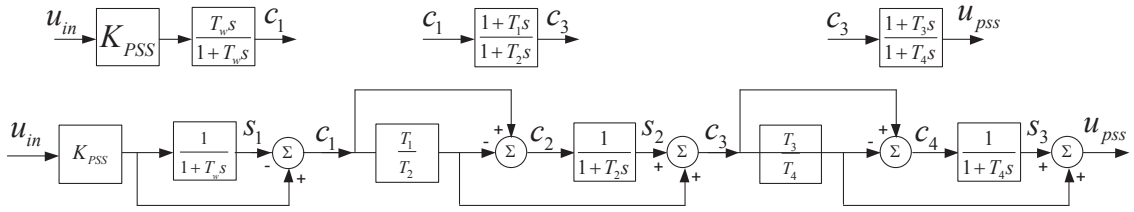

Figure 3.18. The equivalent block diagram of the PSS.

the following differential equations can be obtained and added to the dynamic model of the generator k,

$$\begin{aligned}
\dot{S}_{1k} =& \frac{1}{T_{wk}} \left(u_{ink} K_{PSSk} - S_{1k} \right) \\
\dot{S}_{2k} =& \frac{1}{T_{2k}} \left(c_{2k} - S_{2k} \right) \\
\dot{S}_{3k} =& \frac{1}{T_{4k}} \left(c_{4k} - S_{3k} \right)
\end{aligned} \tag{3.103}$$

where,

$$\begin{aligned}
c_{1k} =& u_{ink} K_{PSSk} - S_{1k} \\
c_{2k} =& c_{1k} (1 - \frac{T_{1k}}{T_{2k}}) \\
c_{3k} =& c_{1k} \frac{T_{1k}}{T_{2k}} + S_{2k} \\
c_{4k} =& c_{3k} (1 - \frac{T_{3k}}{T_{4k}})
\end{aligned} \tag{3.104}$$

and finally

$$u_{pssk} = c_{3k} \frac{T_{3k}}{T_{4k}} + S_{3k} \tag{3.105}$$

Thus, the dynamic of the generator k with the one-axis model and the proposed AVR and PSS models is given by equations (3.100)-(3.105).

Next, using (3.104) in (3.103) the following is obtained

$$\begin{aligned}
\dot{S}_{1k} &= s_{1_{uink}} u_{ink} - s_{1_{s1k}} S_{1k} \\
\dot{S}_{2k} &= s_{2_{uink}} u_{ink} - s_{2_{s1k}} S_{1k} - s_{2_{s2k}} S_{2k} \\
\dot{S}_{3k} &= s_{3_{uink}} u_{ink} - s_{3_{s1k}} S_{1k} + s_{3_{s2k}} S_{2k} - s_{3_{s3k}} S_{3k}
\end{aligned} \tag{3.106}$$

where,

$$\begin{aligned}
s_{1_{s1k}} &= \frac{1}{T_{wk}} \,,\; s_{1_{uink}} = s_{1_{s1k}} K_{PSSk} \\
s_{2_{s2k}} &= \frac{1}{T_{2k}} \,,\; s_{2_{s1k}} = s_{2_{s2k}} \left(1 - \frac{T_{1k}}{T_{2k}} \right) \,,\; s_{2_{uink}} = s_{2_{s1k}} K_{PSSk} \\
s_{3_{s3k}} &= \frac{1}{T_{4k}} \,,\; s_{3_{s2k}} = s_{3_{s3k}} \left(1 - \frac{T_{3k}}{T_{4k}} \right) \,,\; s_{3_{s1k}} = s_{3_{s2k}} \left(\frac{T_{1k}}{T_{2k}} \right) \,,\; s_{3_{uink}} = s_{3_{s1k}} K_{PSSk}
\end{aligned} \tag{3.107}$$

Furthermore, (3.105) is rewritten as

$$u_{pssk} = \frac{T_{1k}T_{3k}}{T_{2k}T_{4k}}K_{PSSk}u_{ink} - \frac{T_{1k}T_{3k}}{T_{2k}T_{4k}}S_{1k} + \frac{T_{3k}}{T_{4k}}S_{2k} + S_{3k} \tag{3.108}$$

Substituting (3.108) in (3.101) gives

$$\dot{E}_{fk} = -\frac{1}{T_{ek}}E_{fk} + \frac{K_{Ak}}{T_{ek}}U_{kref} - \frac{K_{Ak}}{T_{ek}}U_k + e_{f_{uink}}u_{ink} - e_{f_{s1k}}S_{1k} + e_{f_{s2k}}S_{2k} + e_{f_{s3k}}S_{3k} \tag{3.109}$$

where,

$$e_{f_{s3k}} = \frac{K_{Ak}}{T_{ek}}\,,\; e_{f_{s2k}} = e_{f_{s3k}}\frac{T_{3k}}{T_{4k}}\,,\; e_{f_{s1k}} = e_{f_{s2k}}\frac{T_{1k}}{T_{2k}}\,,\; e_{f_{uink}} = e_{f_{s1k}}K_{PSSk} \tag{3.110}$$

Note that, if the first lead-lag filter is only used (i.e. $T_{3k} = T_{4k}$), then the third equation in (3.106) is removed, and also (3.108) is modified as follows

$$u_{pssk} = \frac{T_{1k}}{T_{2k}}K_{PSSk}u_{ink} - \frac{T_{1k}}{T_{2k}}S_{1k} + S_{2k} \tag{3.111}$$

To summarize, the dynamic of a generator k represented by the one-axis model, and equipped with an AVR and a PSS with 2 lead-lag filters is given by

$$\begin{aligned}
\dot{\delta}_k &= \omega_k \\
\dot{\omega}_k &= \frac{1}{M_k}(P_{mk} - \frac{E'_{qk}\,U_k}{x'_{dk}}\sin(\delta_k - \theta_k) - D_k\omega_k) \\
\dot{E'}_{qk} &= \frac{1}{T'_{dok}}\left(E_{fk} - \frac{x_{dk}}{x'_{dk}}\,E'_{qk} + \frac{x_{dk} - x'_{dk}}{x'_{dk}}\,U_k\cos(\delta_k - \theta_k)\right) \\
\dot{E}_{fk} &= -\frac{1}{T_{ek}}E_{fk} + \frac{K_{Ak}}{T_{ek}}U_{kref} - \frac{K_{Ak}}{T_{ek}}U_k + e_{f_{uink}}u_{ink} - e_{f_{s1k}}S_{1k} + e_{f_{s2k}}S_{2k} + e_{f_{s3k}}S_{3k} \\
\dot{S}_{1k} &= s_{1_{uink}}u_{ink} - s_{1_{s1k}}S_{1k} \\
\dot{S}_{2k} &= s_{2_{uink}}u_{ink} - s_{2_{s1k}}S_{1k} - s_{2_{s2k}}S_{2k} \\
\dot{S}_{3k} &= s_{3_{uink}}u_{ink} - s_{3_{s1k}}S_{1k} + s_{3_{s2k}}S_{2k} - s_{3_{s3k}}S_{3k}
\end{aligned} \tag{3.112}$$

Chapter 4

Transient stability of an SMIB system

Transient stability analysis of a power system is an extensive and complicated task. However, it turns out that many of the most important phenomena and mechanisms can be captured by simple systems. In large and complicated systems it is often hard to distinguish the fundamental and decisive phenomena from the more irrelevant ones. It is therefore of importance to study simple systems to get an insight into and understanding of the basics, that can be used in the analysis of more complex systems. Therefore, this chapter focuses on transient stability of an SMIB system.

Consider the Single-Machine-Infinite-Bus (SMIB) system shown in Figure 4.1.

Figure 4.1. SMIB system.

For the above SMIB system, the following assumptions are made:

1. The classical model is applied to the synchronous generator, i.e. the synchronous generator is modeled as a constant emf (E'_q) behind its transient reactance x'_d.
2. The system is lossless and the transmission line is modeled by a series reactance.
3. Voltages and currents are symmetrical.
4. The mechanical power P_m is constant.
5. The voltage at bus N is given by $\bar{U}_N = U_N \angle \theta_N$ where both U_N and θ_N are fixed.

Based on the above assumptions, we redraw the SMIB system in Figure 4.1 as shown in Figure 4.2, where x_{tot} is the sum of the reactances of the transmission line and the two transformers.

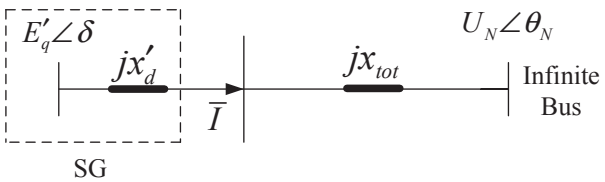

Figure 4.2. Proposed SMIB system for transient stability study.

The dynamic of this system is given by the swing equation

$$\begin{aligned} \dot{\delta} &= \omega \\ \dot{\omega} &= \frac{1}{M}(P_m - P_e - D\omega) \end{aligned} \tag{4.1}$$

where

$$P_e = \frac{E'_q\, U_N}{x'_d + x_{tot}} \sin(\delta - \theta_N) = P_{emax}\, \sin(\delta - \theta_N)$$

4.1 Analysis of the swing equation

In order to make a qualitative analysis of the swing equation, some simplifications and notations will be made as follows. Let

$$\theta_N = 0 \quad \text{and} \quad x = \begin{bmatrix} x_1 \\ x_2 \end{bmatrix} = \begin{bmatrix} \delta \\ \omega \end{bmatrix}$$

Then, the swing equation (4.1) is rewritten as

$$\begin{aligned} \dot{x} &= \begin{bmatrix} \dot{x}_1 \\ \dot{x}_2 \end{bmatrix} = \begin{bmatrix} \dot{\delta} \\ \dot{\omega} \end{bmatrix} = \begin{bmatrix} \omega \\ \frac{1}{M}(P_m - P_{emax}\sin(\delta) - D\omega) \end{bmatrix} \\ &= \begin{bmatrix} x_2 \\ \frac{1}{M}(P_m - P_{emax}\sin(x_1) - D\,x_2) \end{bmatrix} = \begin{bmatrix} f_1(x) \\ f_2(x) \end{bmatrix} = f(x) \end{aligned} \tag{4.2}$$

Thus, we are dealing with a nonlinear system of the form $\dot{x} = f(x)$ defined in equation (2.1) with $n_x = 2$. Based on Definition 2.1, the equilibrium points (e.p) of equation (4.2) are given by

$$f(x_o) = \begin{bmatrix} f_1(x_o) \\ f_2(x_o) \end{bmatrix} = \begin{bmatrix} x_{2,o} \\ \frac{1}{M}(P_m - P_{emax}\sin(x_{1,o}) - D\,x_{2,o}) \end{bmatrix} = \begin{bmatrix} 0 \\ 0 \end{bmatrix} \tag{4.3}$$

Obviously, $x_{2,o} = 0$ and $x_{1,o}$ is given by $P_m = P_e(x_{1,o}) = P_{emax}\sin(x_{1,o})$.

In the steady-state (see Definition 2.2), the generator rotates with a speed that corresponds to the system frequency (i.e. $\omega = 0 \;\Rightarrow\; \omega_g = \omega_s$), and also the mechanical power is equal to the electrical power (i.e. $P_m = P_e$).

Figure 4.3 shows variations of $P_e(\delta)$ versus the rotor angle δ. Due to practical issues, the interval of interest is $0 \leq \delta \leq \pi$.

Obviously, for

1. $P_m > P_{emax}$, there is no value of $x_{1,o}$.

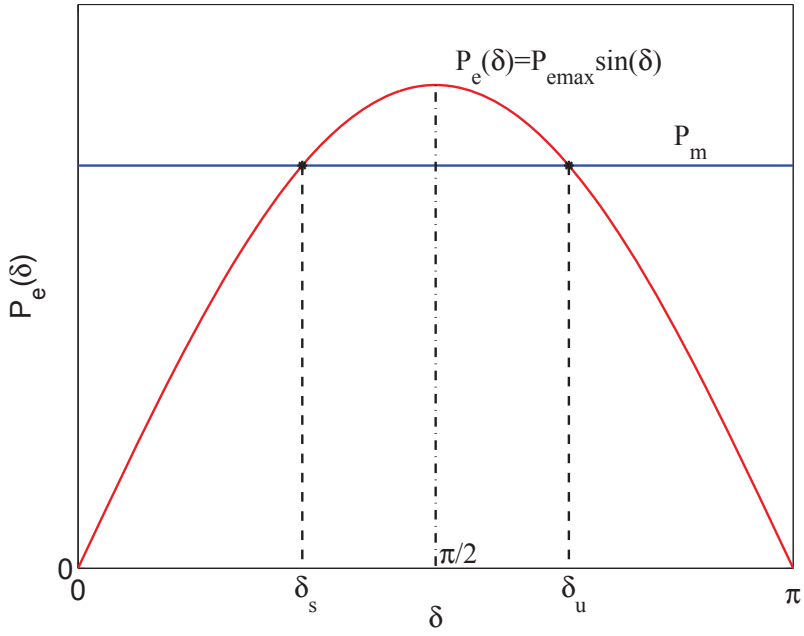

Figure 4.3. Variations of the electrical power versus the rotor angle.

2. $P_m = P_{emax}$, there is only one value of $x_{1,o}$, that is $x_{1,o} = \dfrac{\pi}{2}$.

3. $P_m < P_{emax}$, there are two values of $x_{1,o}$ as shown in Figure 4.3, i.e. $x_{1,o} = \delta_s$ and $x_{1,o} = \delta_u = \pi - \delta_s$.

Since point (3) is dealing with a normal operation it is of interest for the following analysis. As was mentioned, for point (3) there are two equilibrium points, that is

$$x_o = x_s = \begin{bmatrix} x_{1,0} \\ x_{2,o} \end{bmatrix} = \begin{bmatrix} \delta_s \\ 0 \end{bmatrix} \quad \text{and} \quad x_o = x_u = \begin{bmatrix} x_{1,0} \\ x_{2,o} \end{bmatrix} = \begin{bmatrix} \delta_u \\ 0 \end{bmatrix} \tag{4.4}$$

The question remained to be answered is which one is a stable equilibrium point (s.e.p).

4.1.1 Stability of the equilibrium points of the SMIB system

Stability of the equilibrium points (4.4) may be characterized by a similar argumentation as was given in Example 2.1. It may also be characterized by applying Theorem 2.1 as follows, see also Example 2.2.

The Jacobian of (4.2) at $x = x_o$ is given by

$$A = \begin{bmatrix} \frac{\partial f_1(x)}{\partial x_1} & \frac{\partial f_1(x)}{\partial x_2} \\ \frac{\partial f_2(x)}{\partial x_1} & \frac{\partial f_2(x)}{\partial x_2} \end{bmatrix}_{x=x_o} = \begin{bmatrix} 0 & 1 \\ -\frac{K}{M} & -\frac{D}{M} \end{bmatrix} \tag{4.5}$$

where $K = P_{emax}\cos(x_{1,o})$. The eigenvalues of (4.5) are given by

$$\lambda_{1,2} = -\frac{D}{2M} \pm \sqrt{\left(\frac{D}{2M}\right)^2 - \frac{K}{M}} \tag{4.6}$$

By analogy with the solution of Example 2.2, it can be shown that x_o is asymptotically stable if $0 < x_{1,o} < \frac{\pi}{2}$. Therefore, $x_o = x_s$ is asymptotically stable and $x_o = x_u$ is unstable. Note that D is a positive small constant.

If there is no damping in the system (i.e. $D = 0$), then the eigenvalues are given by

$$\lambda_{1,2} = \pm\sqrt{-\frac{K}{M}} \tag{4.7}$$

By virtue of Theorem 2.1, it can be shown that $x_o = x_u$ is unstable (show that). However, Theorem 2.1 cannot characterize the stability of $x_o = x_s$ when $D = 0$ (why?). Therefore, Theorem 2.2 should be applied to characterize the stability of $x_o = x_s$.

Using the following energy function [7]

$$\begin{aligned}\mathcal{V}(x) &= W_K + W_P = \frac{1}{2}M\,\omega^2 + \int_{\delta_s}^{\delta} (P_{emax}\sin(x_1) - P_m)\,dx_1 \\ &= \frac{1}{2}M\,\omega^2 - P_m(\delta - \delta_s) - P_{emax}(\cos(\delta) - \cos(\delta_s)) \\ &= \frac{1}{2}M\,\omega^2 - P_m\delta - P_{emax}\cos(\delta) + C_o\end{aligned} \tag{4.8}$$

it can be shown that $x_o = x_s$ is stable if $D = 0$. It can also be shown that $x_o = x_s$ is asymptotically stable if $D \neq 0$ (see Example 2.2). Note that in equation (4.8), $C_o = P_m\delta_s + P_{emax}\cos(\delta_s)$ is a constant such that $\mathcal{V}(x_s) = 0$.

Stability of δ_s and δ_u may also be characterized as follows. Starting with δ_s (see Figure 4.4), assume that due to some disturbance δ moves from δ_s to δ_1 at which P_e is greater than P_m (and therefore $\dot{\omega} < 0$). This causes the generator to decelerate, and therefore the rotor angle δ starts to decrease and moves back to δ_s. Furthermore, the electric power P_e as a function of δ moves back to P_m. Next, assume that due to some disturbance δ moves from δ_s to δ_2 at which P_e is less than P_m (and therefore $\dot{\omega} > 0$). This causes the generator to accelerate, and therefore the rotor angle δ starts to increase and moves back to δ_s. Also, P_e as a function of δ moves back to P_m. To summarize, when $\delta = \delta_1$, P_e is greater than P_m. Then the generator decelerates, and the rotor angle δ decreases and moves back to δ_s. As δ passes δ_s, P_e becomes less than P_m. Then the generator accelerates. However, due to the generator inertia (M or H) δ continues decreasing and after a while it swings and moves back to δ_s. As δ passes δ_s again, P_e becomes greater than P_m. Then the generator decelerates. However, due to the generator inertia (M or H) δ continues increasing and after a while it swings and moves back to δ_s. If there is no damping in the system, δ oscillates around δ_s. Therefore, δ_s is a stable e.p (but not asymptotically stable). If there is

damping in the system, then δ will eventually be settled at δ_s. Therefore, the e.p. will be asymptotically stable.

Next consider δ_u. Assume that δ moves from this e.p to δ_3 at which $\dot{\omega} > 0$ (why?). This causes the generator to accelerate, and the rotor angle δ increases and moves away from δ_u. At $\delta = \delta_4$, the rotor angle δ decreases and moves away from δ_u (why?). Therefore, this e.p is unstable (see also Example 2.1).

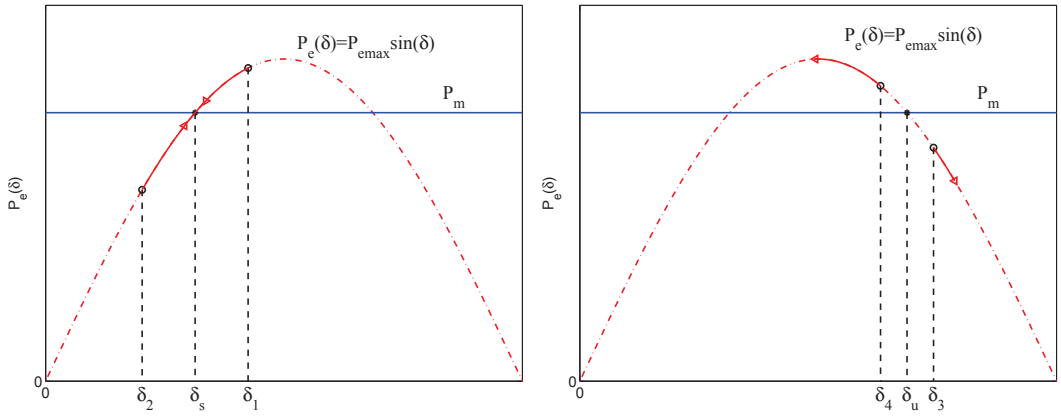

Figure 4.4. Stable and unstable equilibrium points.

Up to now, the stability of the equilibrium points of the SMIB system was discussed. Next, the transient stability of the SMIB system will be discussed.

Due to the dynamic and structure of the swing equation (4.2), only transient stability (or first swing stability) is feasible in the SMIB system, and a physically based definition of its stability may be given as follows:

Definition 4.1 *The SMIB system is transiently stable if the generator remains in synchronism with the infinite bus after being subjected to a large disturbance. Instability that may result occurs in the form of increasing rotor angle (or speed) of the generator leading to its loss of synchronism.*

However, a mathematically based definition may be given as follows:

Definition 4.2 *The SMIB system is transiently stable if the initial point of the post-disturbance system lies within the stability region of the stable e.p of the post-disturbance system.*

Example 4.1 *Consider the SMIB system shown in Figure 4.5. At time $t = t_f$ a three-phase fault occurs at point* **F** *very close to BUS 2 (i.e. it can be assumed that the fault occurs at Bus 2). At time $t = t_f + t_c$ the fault is cleared by opening the faulted line. The system data is given as follows ($S_{base} = S_{ng}$):*

Generator: $x'_d = 0.15$ *(pu),* $H = 4$ *(s),* $D = 0$, *and* $f_s = 50$ *(Hz)*

Transformer: $x_{T1} = x_{T2} = 0.10$ *(pu)*

Line: $x_L = 0.50$ *(pu) and* **BUS N:** $\bar{U}_N = U_N \angle \theta_N = 1 \angle 0$ *(pu)*

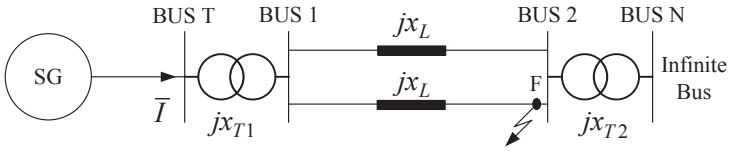

Figure 4.5. The SMIB system of Example 4.1.

Prior to the fault, the voltage at BUS 1 was $\bar{U}_1 = U_1 \angle \theta_1 = 1 \angle 20.4873^o$ *(pu). Examine transient stability of the system for the clearing times* $t_c = 70$ *(ms),* $t_c = 100$ *(ms) and* $t_c = 120$ *(ms), respectively.*

Obviously, the system goes through three states, namely a pre-fault state ($t < t_f$), a during-fault state ($t_f \leq t < t_f + t_c$), and a post-fault state ($t \geq t_f + t_c$). The pre-fault system is usually in a steady-state. Dynamic of the system in each state is given by

Pre-fault state:

$$\dot{x} = f^{pre}(x) = f^{pre}(x_o^s) = 0 \quad \Rightarrow \quad x^{pre}(t) = x_o^s + \int f^{pre}(x)\, dt = x_o^s \tag{4.9}$$

During-fault state:

$$\dot{x} = f^{f}(x) \quad \Rightarrow \quad x^{f}(t) = x(t_f) + \int f^{f}(x)\, dt \tag{4.10}$$

Post-fault state:

$$\dot{x} = f^{post}(x) \quad \Rightarrow \quad x^{post}(t) = x(t_f + t_c) + \int f^{post}(x)\, dt \tag{4.11}$$

where $x(t)$ is the solution of the system. The question is if the post-fault system with initial point $x(t_f + t_c)$ is transiently stable. To answer this question we must first identify $f^{pre}(x)$, $f^{f}(x)$, $f^{post}(x)$, and x_o^s based on the given system data.

Pre-fault state:

In this state, the system is in a steady-state. Since $\bar{U}_1$ is known prior to the fault, the following can be obtained.

$$\begin{aligned}
\bar{I} &= \frac{\bar{U}_1 - \bar{U}_N}{j(0.5 * x_L + x_{T2})} = 1.0162 \angle 10.2437^o \quad \text{(pu)} \\
\bar{E}'_q &= E'_q \angle \delta_s^{pre} = j\,(x'_d + x_{T1})\,\bar{I} + \bar{U}_1 = 1.0747 \angle 33.9393^o \quad \text{(pu)} \\
P_m &= \text{Real}\,[\bar{E}'_q\,\bar{I}^*] = 1 \quad \text{(pu)} \quad \text{or} \\
P_m &= P_e^{pre}(\delta_s^{pre}) = \text{Real}\left[\bar{E}'_q \left(\frac{\bar{E}'_q - \bar{U}_N}{j x_{tot}^{pre}}\right)^*\right] \\
&= \frac{E'_q\, U_N}{x_{tot}^{pre}} \sin(\delta_s^{pre}) = P_{emax}^{pre} \sin(\delta_s^{pre}) \\
&= 1.7911 \sin(33.9393^o) = 1 \quad \text{(pu)}
\end{aligned}$$

In this state, $\dot{x} = f^{pre}(x)$ is given by (in $f(x)$, the angle is given in radian)

$$\begin{bmatrix} \dot{\delta} \\ \dot{\omega} \end{bmatrix} = \begin{bmatrix} \omega \\ \frac{1}{M}(P_m - P_e^{pre}) \end{bmatrix} = \begin{bmatrix} \omega \\ \frac{1}{M}(P_m - P_{emax}^{pre} \sin(\delta_s^{pre})) \end{bmatrix} = \begin{bmatrix} 0 \\ 0 \end{bmatrix}$$

where

$$x_{tot}^{pre} = x'_d + x_{T1} + 0.5 * x_L + x_{T2} \quad \text{and} \quad M = \frac{2H}{\omega_s}$$

The stable e.p of the pre-fault system is given by $x_o^s = [\delta_s^{pre}\ 0]^T$

During-fault state:

In this state, because of the fault the voltage at BUS 2 is zero. Thus,

$$\begin{aligned} \bar{I}_f &= \frac{\bar{E}'_q - 0}{j(x'_d + x_{T1} + 0.5 * x_L)} = \frac{\bar{E}'_q}{jx_{tot}^f} \\ P_e^f &= \text{Real}\,[\bar{E}'_q\, \bar{I}_f^*] = \text{Real}\left[\bar{E}'_q \left(\frac{\bar{E}'_q}{jx_{tot}^f}\right)^*\right] = \text{Real}\left[\frac{(E'_q)^2}{-jx_{tot}^f}\right] = 0 \end{aligned}$$

and $\dot{x} = f^f(x)$ is given by

$$\begin{bmatrix} \dot{\delta} \\ \dot{\omega} \end{bmatrix} = \begin{bmatrix} \omega \\ \frac{1}{M}(P_m - P_e^f) \end{bmatrix} = \begin{bmatrix} \omega \\ \frac{P_m}{M} \end{bmatrix} \tag{4.12}$$

Post-fault state:

In this state, since the faulted line is removed, there is only one transmission line. We have then

$$\begin{aligned} \bar{I}_{post} &= \frac{\bar{E}'_q - \bar{U}_N}{j(x'_d + x_{T1} + x_L + x_{T2})} = \frac{\bar{E}'_q - \bar{U}_N}{jx_{tot}^{post}} \\ P_e^{post} &= \text{Real}\,[\bar{E}'_q\, \bar{I}_{post}^*] = \text{Real}\left[\bar{E}'_q \left(\frac{\bar{E}'_q - \bar{U}_N}{jx_{tot}^{post}}\right)^*\right] = \frac{E'_q\, U_N}{x_{tot}^{post}} \sin(\delta) \\ &= P_{emax}^{post} \sin(\delta) = 1.2643 \sin(\delta) \\ P_m &= P_{emax}^{post} \sin(\delta_s^{post}) \quad \Rightarrow \quad \delta_s^{post} = \arcsin\left(\frac{P_m}{P_{emax}^{post}}\right) = 52.2740^o \\ \delta_u^{post} &= 180 - \delta_s^{post},\ \text{since}\ \theta_N = 0 \end{aligned}$$

and $\dot{x} = f^{post}(x)$ is given by (in $f(x)$, the angle is given in radian)

$$\begin{bmatrix} \dot{\delta} \\ \dot{\omega} \end{bmatrix} = \begin{bmatrix} \omega \\ \frac{1}{M}(P_m - P_e^{post}) \end{bmatrix} = \begin{bmatrix} \omega \\ \frac{1}{M}(P_m - P_{emax}^{post} \sin(\delta)) \end{bmatrix} \tag{4.13}$$

The stable e.p of the post-fault system is given by $x_o^s = [\delta_s^{post}\ 0]^T$, and the unstable e.p of the post-fault system is given by $x_o^u = [\delta_u^{post}\ 0]^T$.

Figure 4.6 illustrates variations of $P_e^{pre}(\delta)$ and $P_e^{post}(\delta)$ as functions of δ. As shown in the figure, the e.p of the system is the point at which the electric power $P_e(\delta)$ intersects the mechanical power. Obviously, the pre-fault system and the post-fault system have different equilibrium points. The reason is that the post-fault system has only one transmission line which results in a higher total reactance than the pre-fault system.

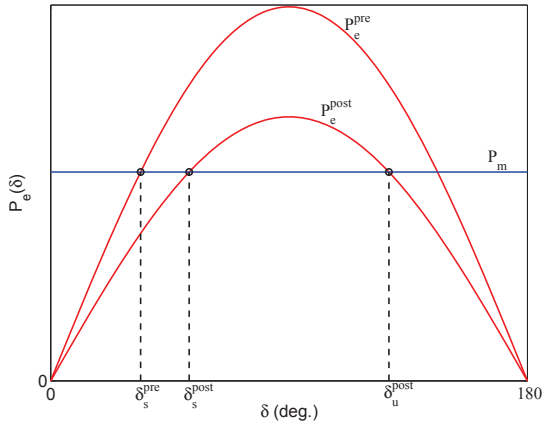

Figure 4.6. Variations of P_e^{pre} and P_e^{post} versus rotor angle δ.

Next, by using some simulation tool (like MATLAB) we are able to study the stability of the system for the given clearing time t_c. Figure 4.7 illustrates phase portrait of the SMIB system , and variations of the rotor angle δ versus time for $t_c = 70$, $t_c = 100$, and $t_c = 120$ (ms). The stability region of the stable e.p of the post-fault system is also shown in the figure (the shaded region).

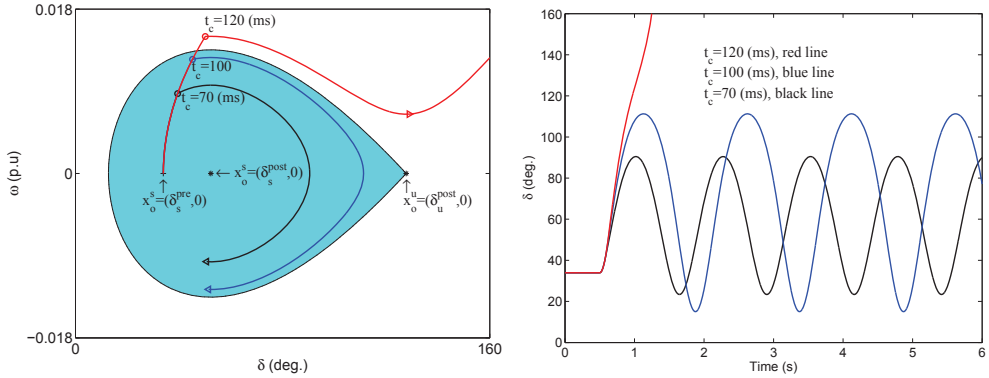

Figure 4.7. Phase portrait, and variations of the rotor angle δ versus time.

Based on Definition 4.2, the SMIB system is transiently stable for this fault with $t_c = 70$ and $t_c = 100$ (ms) since the initial point of the post-fault system lies within the stability region of the δ_s^{post}. However, the system is unstable for this fault with $t_c = 120$ (ms) (why?). Next, in order to study the dynamic performance of the system for the given fault the case $t_c = 70$ (ms) is discussed below in details.

Figure 4.8 shows variations of $P_e(\delta)$ as a function of δ (the $P_e - \delta$ figure), and the phase portrait of the system (the $\omega - \delta$ figure) during the fault. The shaded region indicates the stability region of the stable e.p of the post-fault system. In pre-fault state (i.e. in the steady-state), the system is at $x_o^s = [\delta_s^{pre} \;\; 0]^T$ where $P_e(\delta) = P_e^{pre}(\delta_s^{pre}) = P_m$. When the fault occurs the electric power (as determined above) becomes zero (i.e. $P_e(\delta) = P_e^f = 0$), and the dynamic of the system is given by equation (4.12). Therefore, the generator starts accelerating (i.e. ω is increasing) since $\dot{\omega} = \frac{P_m}{M} > 0$, and so does the rotor angle δ since $\omega > 0$ as shown in the $\omega - \delta$ figure.

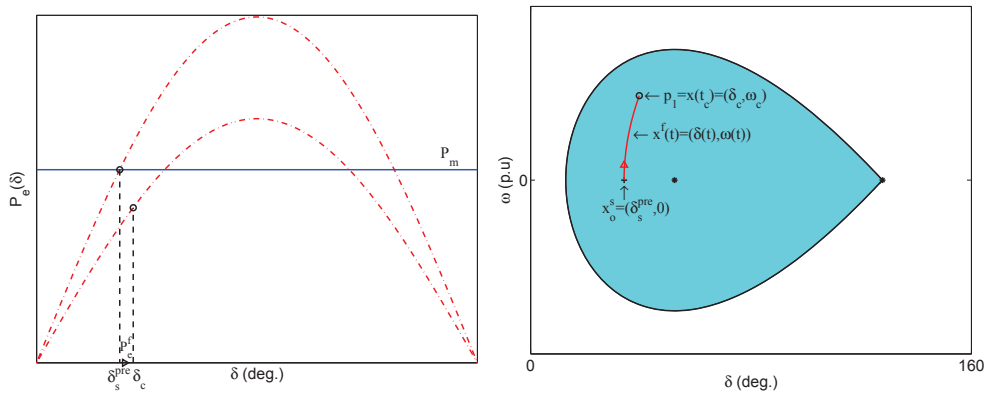

Figure 4.8. $P_e - \delta$ curve and phase portrait of the system during fault.

The fault is cleared at clearing time $t = t_c = 70$ (ms) which corresponds to point p_1 in the $\omega - \delta$ figure, and also $\delta = \delta_c$ in the $P_e - \delta$ figure. The angle δ_c is termed the clearing angle which is the corresponding rotor angle to the clearing time t_c.

The dynamic of the post-fault system is given by equation (4.13) with the initial point p_1 at which $P_m > P_e^{post}$ as shown in the $P_e - \delta$ figure of Figure 4.9. Thus, the generator continues accelerating since $\dot{\omega} = P_m - P_e^{post} > 0$, and so does the rotor angle δ since $\omega > 0$ as shown in the $\omega - \delta$ figure of Figure 4.9.

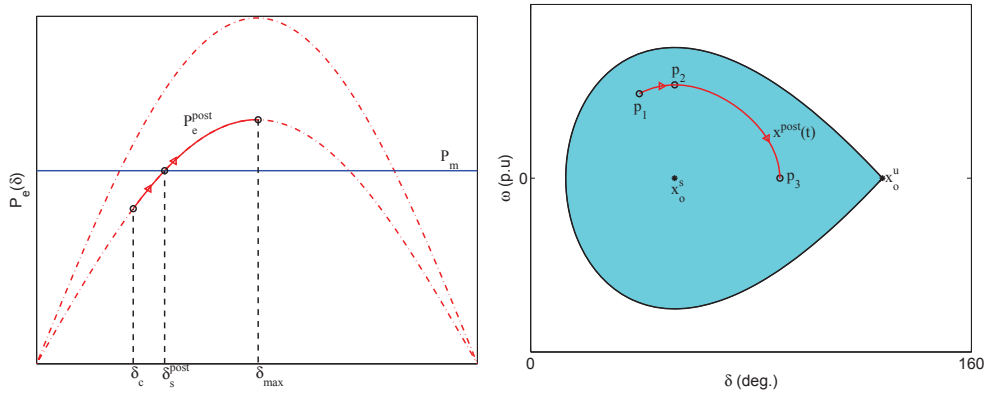

Figure 4.9. $P_e - \delta$ curve and phase portrait of the post-fault system ($\delta_c \rightarrow \delta_{max}$).

When δ reaches δ_s^{post} (i.e. when $\delta = \delta_s^{post}$), then $P_m = P_e^{post}$ which corresponds to point p_2 in the $\omega - \delta$ figure at which $\omega > 0$. Therefore, the rotor angle δ continues to increase, and P_e^{post} as a function of δ follows the direction indicated in the figure. When

δ passes δ_s^{post}, then $P_m < P_e^{post}$ (i.e. $\dot{\omega} < 0$). Thus, the generator starts decelerating, and ω decreases until it becomes zero which corresponds to point p_3 in the $\omega - \delta$ figure. However, since ω is positive between points p_2 and p_3 the rotor angle δ continues to increase. Note that $\dot{\delta} = \omega$. Since $\omega = 0$ at point p_3, then $\dot{\delta}$ is also zero at this point which means the rotor angle δ has reached its maximum (indicated as δ_{max} in Figure 4.9, see also the $\delta-$time figure of Figure 4.7).

Since $P_m < P_e^{post}$ at $\delta = \delta_{max}$, the generator continues to decelerate which results in decreasing of ω. When ω decreases and passes zero the rotor angle δ starts decreasing (or swings back), and P_e^{post} follows the direction indicated in Figure 4.10. When δ reaches δ_s^{post}, then $P_m = P_e^{post}$ which corresponds to point p_4 at which $\omega < 0$. Therefore, the rotor angle δ and P_e^{post} continue to decrease. When δ passes δ_s^{post}, then $P_m > P_e^{post}$ (i.e. $\dot{\omega} > 0$). Thus, the generator starts accelerating, and ω increases until it becomes zero which corresponds to point p_5. However, since ω is negative between points p_4 and p_5 the rotor angle δ continues to decrease until it reaches its minimum (indicated as δ_{min} in Figure 4.10 which corresponds to point p_5, see also the $\delta-$time figure of Figure 4.7).

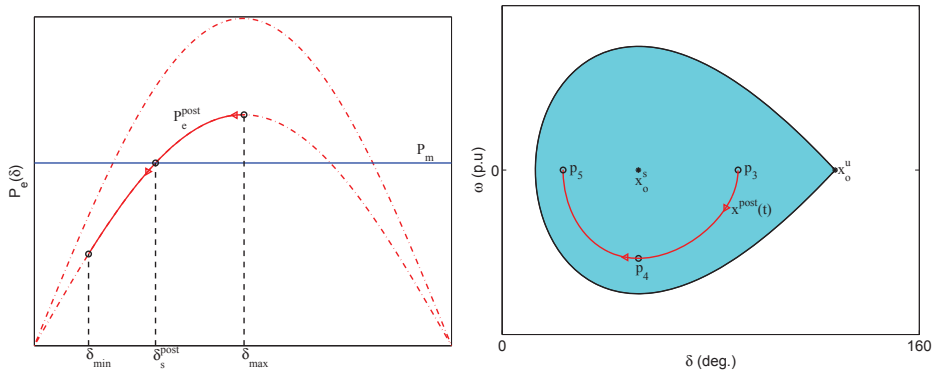

Figure 4.10. $P_e - \delta$ curve and phase portrait of the post-fault system ($\delta_{max} \rightarrow \delta_{min}$).

As shown in Figure 4.11, $P_m > P_e^{post}$ at $\delta = \delta_{min}$. Therefore, the generator continues to accelerate which results in increasing of ω, and the system will have a similar behavior as described based on Figure 4.9.

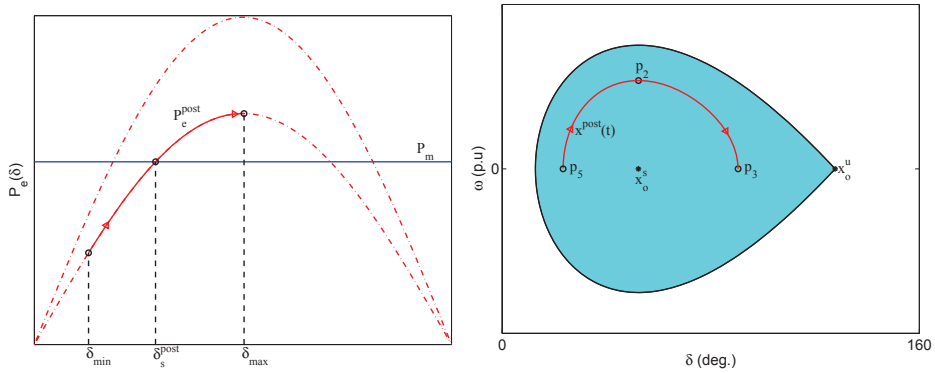

Figure 4.11. $P_e - \delta$ curve and phase portrait of the post-fault system ($\delta_{min} \rightarrow \delta_{max}$).

Since there is no damping in the system (i.e. $D = 0$) the system trajectory will oscillate

around the stable e.p of the post-fault system as shown in Figure 4.12. Therefore, the system is transiently stable (or first-swing stable) for this fault with $t_c = 70$ (ms). A similar behavior can be found in case $t_c = 100$ (ms).

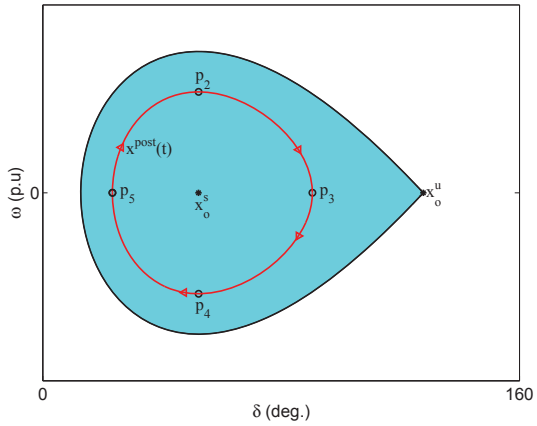

Figure 4.12. The dynamic behavior of the SMIB system for the given fault with $t_c = 70$ (ms).

Figure 4.13 shows the dynamic behavior of the SMIB system for the given fault with $t_c = 120$ (ms). The fault is cleared at point p_1 where $\delta = \delta_c$. Since $P_m > P_e^{post}$ at this point the generator accelerates which results in increasing of ω, and also the rotor angle δ (since $\omega > 0$). When δ passes δ_s^{post}, then $P_m < P_e^{post}$. Thus, the generator starts decelerating, and ω decreases. However, since ω is still positive the rotor angle increases, and P_e^{post} follows the direction indicated in the figure until it reaches the intersection point between P_e^{post} and P_m which corresponds to point p_2 at which $\delta = \delta_u^{post}$ and $\omega > 0$. Therefore, the rotor angle δ continues to increase, and P_e^{post} follows the direction indicated in the figure. When δ passes δ_u^{post}, then $P_m > P_e^{post}$. Thus, the generator starts accelerating which results in increasing of ω. Since $\omega > 0$ the rotor angle δ also continues to increase which leads to transient instability (or first-swing instability). In power system literature, it is often said that the generator falls out of step or loses synchronism (see also Definition 4.1).

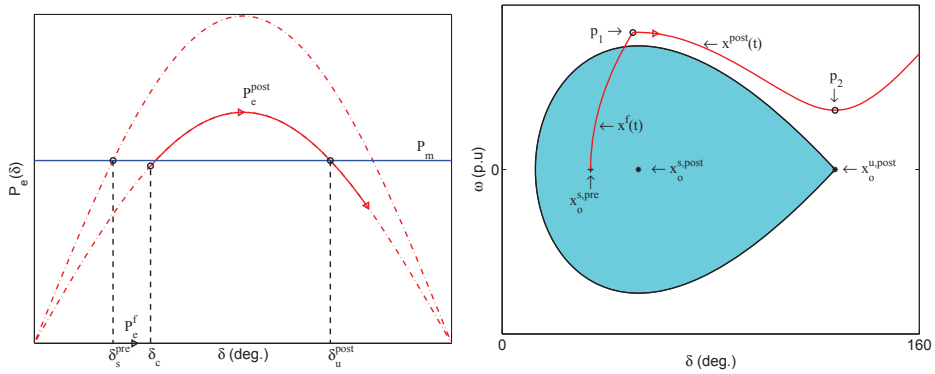

Figure 4.13. The dynamic behavior of the SMIB system for the given fault with $t_c = 120$ (ms).

Next, assume that the fault is cleared at time $t_c = t_{cc}$ at which the trajectory of the

during-fault system intersects the stability boundary of the stable e.p of the post-fault system as shown in Figure 4.14.

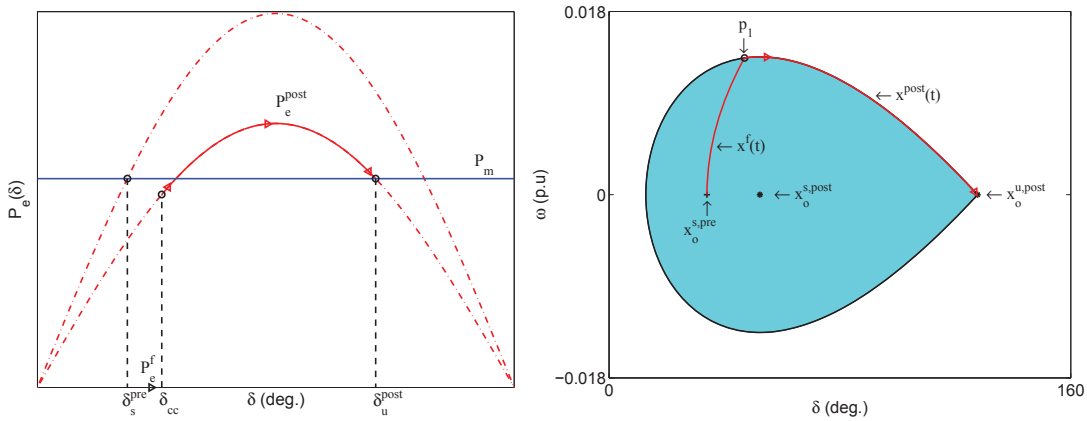

Figure 4.14. The dynamic behavior of the SMIB system for the given fault with $t_c = t_{cc}$.

In the figure, the intersection point is indicated as p_1 at which $\delta = \delta_{cc}$. Since p_1 (which is the initial point of the post-fault system) lies on the stability boundary, the trajectory of the post-fault system converges to $x_o^{u,post}$ as time goes to infinity (see Definition 2.5).

Time t_{cc} is termed critical clearing time, and δ_{cc} is termed critical clearing angle corresponding to t_{cc}.

Obviously, for any clearing time t_c which is less than the critical clearing time (i.e. $t_c < t_{cc}$) the system will be transiently stable (or first-swing stable) since the initial point (p_1) of the post-fault system will lie within the stability region of the stable e.p of the post-fault system. Consequently, if $t_c \geq t_{cc}$ the system will be transiently unstable (or first-swing unstable). Thus, the transient stability of the SMIB system can be stated for a given clearing time t_c without any numerical simulation if the critical clearing time t_{cc} is known.

For an SMIB system, the critical clearing angle δ_{cc} can analytically be determined by applying Equal Area Criterion (EAC). When the critical clearing angle δ_{cc} is known, the critical clearing time t_{cc} can also analytically be determined if the electric power during fault is constant. However, if the electric power during fault is a function of the rotor angle δ, the critical clearing time t_{cc} can be determined only by numerical integration.

4.2 Equal Area Criterion (EAC)

From Figure 4.7 (the δ-time figure) it may be concluded that the SMIB system is transiently stable (or first swing stable) if ω becomes zero. Since $\dot{\delta} = \omega$, the condition $\omega = 0$ implies that the rotor angle reaches a maximum, and then swings back (hence the name first-swing stability) as shown in Figure 4.15 for the cases $t_c = 70$ and $t_c = 100$ (ms). This observation may be expressed as

A necessary condition for transient stability (or first-swing stability) of the SMIB system is that at some time (t_m), $\dfrac{d\delta}{dt} = \omega(t_m) = 0$.

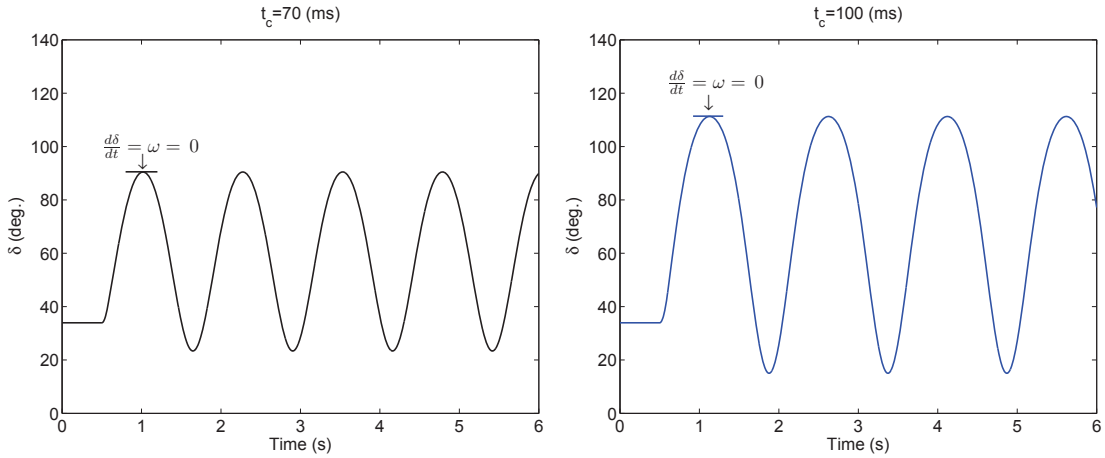

Figure 4.15. Variations of δ versus time.

Now, consider the swing equation

$$\frac{d\omega}{dt} = \frac{1}{M}(P_m - P_e(\delta))$$

Multiplying both sides of the swing equation by $\dfrac{d\delta}{dt} = \omega$, the following is obtained

$$\omega \frac{d\omega}{dt} = \frac{1}{M}(P_m - P_e(\delta)) \frac{d\delta}{dt} \tag{4.14}$$

Integration of the (4.14) gives

$$\begin{aligned}
\int_0^{\omega(t_m)} \omega \, d\omega &= \frac{1}{M} \int_{\delta_s^{pre}}^{\delta_{max}} (P_m - P_e(\delta)) \, d\delta \quad \Rightarrow \\
\frac{1}{2} (\omega(t_m))^2 &= \frac{1}{M} \int_{\delta_s^{pre}}^{\delta_{max}} (P_m - P_e(\delta)) \, d\delta \quad \Rightarrow \\
\omega(t_m) &= \sqrt{\frac{2}{M} \int_{\delta_s^{pre}}^{\delta_{max}} (P_m - P_e(\delta)) \, d\delta}
\end{aligned}$$

The stability condition is that $\omega(t_m) = 0$ which leads to

$$\int_{\delta_s^{pre}}^{\delta_{max}} (P_m - P_e(\delta)) \, d\delta = 0 \tag{4.15}$$

The SMIB system is transiently stable (or first-swing stable) if there exists an angle $\delta = \delta_{max}$ such that equation (4.15) holds.

Let $\delta = \delta_c$ be clearing angle which corresponds to clearing time t_c. Then, equation (4.15) can be rewritten as

$$\begin{aligned} \int_{\delta_s^{pre}}^{\delta_c} (P_m - P_e^f)\, d\delta \;+\; \int_{\delta_c}^{\delta_{max}} (P_m - P_e^{post})\, d\delta = 0 \quad \Rightarrow \\ \int_{\delta_s^{pre}}^{\delta_c} (P_m - P_e^f)\, d\delta \;=\; \int_{\delta_c}^{\delta_{max}} (P_e^{post} - P_m)\, d\delta \quad \Rightarrow \\ A_a \;=\; A_d \end{aligned} \tag{4.16}$$

where

$$A_a = \int_{\delta_s^{pre}}^{\delta_c} (P_m - P_e^f)\, d\delta \quad \text{and} \quad A_d = \int_{\delta_c}^{\delta_{max}} (P_e^{post} - P_m)\, d\delta \tag{4.17}$$

Thus, the SMIB system is transiently stable (or first-swing stable) if there exists an angle $\delta = \delta_{max}$ such that $A_a = A_d$ (hence the name equal area criterion) as illustrated in Figure 4.16, (P_e^f is assumed zero).

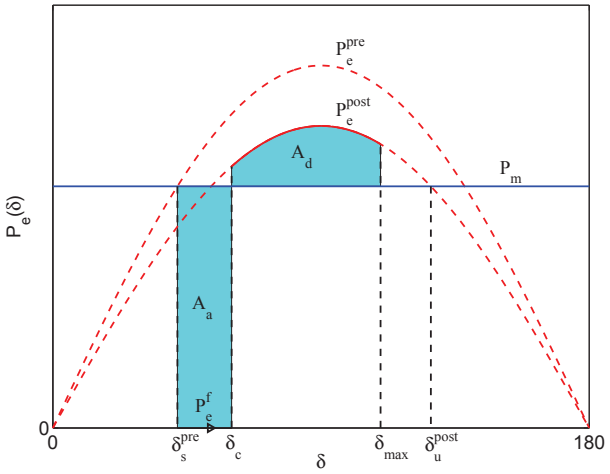

Figure 4.16. The equal area criterion (clearing angle, δ_c).

But, what are A_a and A_d? (or what do they represent?)

Consider again equation (4.14) which is rewritten as

$$M\,\omega\,\frac{d\omega}{dt} = (P_m - P_e(\delta))\,\frac{d\delta}{dt}$$

Integrating the above equation, the following is obtained

$$\int M\omega\frac{d\omega}{dt}dt = \int (P_m - P_e)\frac{d\delta}{dt}dt$$

where

$$L.H.S = \int_{\omega_1}^{\omega_2} M\omega\frac{d\omega}{dt}dt = \int_{\omega_1}^{\omega_2} M\omega\, d\omega = \frac{1}{2}M[\omega^2]_{\omega_1}^{\omega_2}$$

and

$$R.H.S \;=\; \int_{\delta_1}^{\delta_2} (P_m - P_e)\frac{d\delta}{dt}dt = \int_{\delta_1}^{\delta_2} (P_m - P_e)d\delta$$

For $\delta_1 = \delta_s^{pre}$, $\delta_2 = \delta_c$, $\omega_1 = 0$ and $\omega_2 = \omega_c$, i.e. during the fault, we have

$$\begin{aligned} L.H.S &= \frac{1}{2}M(\omega_2^2 - \omega_1^2) = \frac{1}{2}M\omega_c^2 \\ R.H.S &= \int_{\delta_1}^{\delta_2}(P_m - P_e^f)d\delta = \int_{\delta_1}^{\delta_2} P_m d\delta = P_m(\delta_c - \delta_s^{pre}) = A_a \\ A_a &= \frac{1}{2}M\omega_c^2 \end{aligned}$$

that is

- A_a represents the kinetic energy injected into the system during the fault. It is also called accelerating area.

In a similar way with $\delta_1 = \delta_c$, $\delta_2 = \delta_{max}$, $\omega_1 = \omega_c$, $\omega_2 = \omega(t_m) = 0$ and $P_e = P_e^{post}$, it can be shown that

- A_d represents the ability of the post-fault system to absorb energy, i.e. potential energy. It is also called decelerating area.

Setting $\delta_{max} = \delta_u^{post}$, the maximum value of A_d is obtained which is denoted by A_{dmax} as shown in Figure 4.17. Then, $A_a = A_{dmax}$ gives the critical angle δ_{cc}, and the SMIB system is transiently stable if $A_a < A_{dmax}$ (or $\delta_c < \delta_{cc}$).

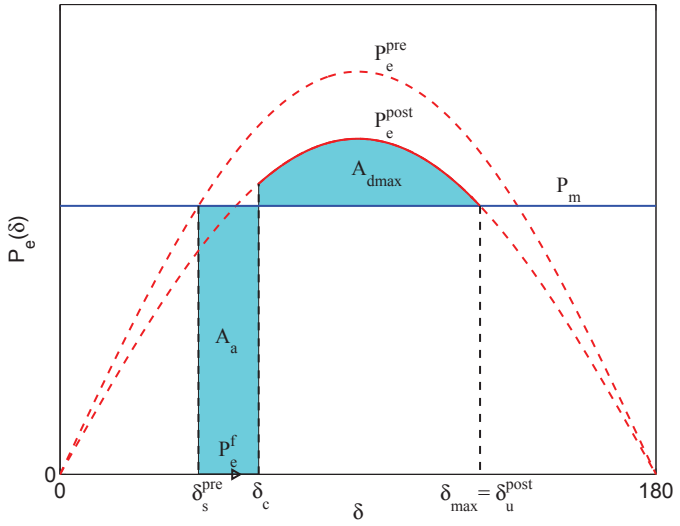

Figure 4.17. The equal area criterion (critical clearing angle, δ_{cc}).

In general, an SMIB system is transiently stable if $A_1 < A_2$ (or $\delta_c < \delta_{cc}$) where

$$\begin{aligned} A_1 &= \int_{\delta_s^{pre}}^{\delta_c}(P_m - P_e^f)\,d\delta \\ A_2 &= \int_{\delta_c}^{\delta_{max}}(P_e^{post} - P_m)\,d\delta \end{aligned} \tag{4.18}$$

with $\delta_{max} = \delta_u^{post}$. Furthermore, $A_1 = A_2$ gives δ_{cc}.

Example 4.2 *Consider the system and the case in* Example 4.1. *Determine the critical clearing angle (δ_{cc}), the critical clearing time (t_{cc}).*

The critical clearing angle δ_{cc} is given by $A_1 = A_2$ where

$$A_1 = \int_{\delta_s^{\text{pre}}}^{\delta_{cc}} (P_m - P_e^f) d\delta = P_m[\delta]_{\delta_s^{pre}}^{\delta_{cc}} = P_m(\delta_{cc} - \delta_s^{pre})$$

$$A_2 = \int_{\delta_{cc}}^{\delta_{max}} (P_e^{post} - P_m) d\delta = -P_{emax}^{post} [\cos(\delta_{max}) - \cos(\delta_{cc})] - P_m(\delta_{max} - \delta_{cc})$$

$$A_1 = A_2 \;\Rightarrow\; \delta_{cc} = \arccos[\cos(\delta_{max}) + \frac{P_m}{P_{emax}^{post}}(\delta_{max} - \delta_s^{pre})] = 0.8192(rad.) = 46.9370(deg.)$$

Since the electric power during the fault is constant ($P_e^f = 0$), the critical clearing time t_{cc} can be obtained as follows. During the fault, the dynamic of the system is given by

$$\ddot{\delta} = \frac{d\omega}{dt} = \frac{1}{M}(P_m - P_e^f) = \frac{P_m}{M}$$

Since P_m/M is a positive constant, the system has a constant acceleration during the fault. The critical clearing time t_{cc} can be obtained by integrating the above equation twice. The first integration gives:

$$d\,\omega = \frac{P_m}{M}\,dt \quad \Rightarrow \quad \int d\,\omega = \int \frac{P_m}{M}\,dt \quad \Rightarrow \quad \omega = \frac{d\delta}{dt} = \frac{P_m}{M}\,t$$

The second integration gives:

$$\int_{\delta_s^{pre}}^{\delta_{cc}} d\delta = \int_{t=0}^{t=tcc} \frac{P_m}{M}\,t\,dt \Rightarrow\; \delta_{cc} - \delta_s^{pre} = \frac{P_m}{2M}\,t_{cc}^2 \Rightarrow t_{cc} = \sqrt{\frac{2M}{P_m}(\delta_{cc} - \delta_s^{pre})} \approx 107.49(\text{ms})$$

The system is stable for this fault if $t_c < t_{cc}$ as shown in Fig. 4.18.

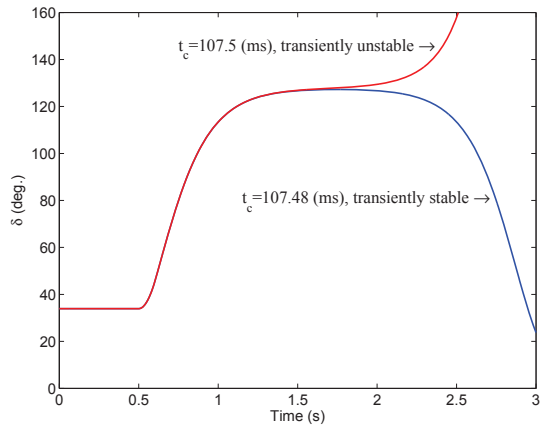

Figure 4.18. Critical clearing time, $t_{cc} = 107.49$ (ms).

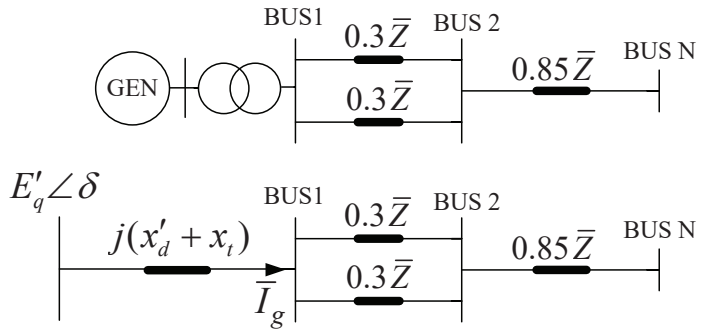

Figure 4.19. The test system.

Example 4.3 *Consider the test system shown in Figure 4.19 where BUS N is an infinite bus and* $\bar{U}_N = 0.9476\angle -44.6127$, $\bar{Z} = R + jX = 0.0673 + j0.6906$, $x'_d = x_t = 0.1$, $H = 5$, $D = 0$ *and* $\bar{E}'_q = E'_q\angle\delta = E'_q\angle\delta^{pre}_s = 1.0932\angle 10.5414$.

Consider the cases below.

Case 1: A three-phase fault occurs at BUS 1, and the fault is cleared by opening one of the lines between BUS 1 and BUS 2.

Case 2: A three-phase fault occurs at BUS 2, and the fault is cleared by opening one of the lines between BUS 1 and BUS 2.

Case 3: A three-phase fault occurs in the middle of one of the lines between BUS 1 and BUS 2, and the fault is cleared by opening the faulted line.

For each case, find the critical clearing angle and time (correct to four decimal places). Also, plot variations of δ *for* $t_c = t_{cc} - 0.0001$ *(stable case) and* $t_c = t_{cc} + 0.0001$ *(unstable case). Furthermore, plot variations of* P^{pre}_e, P^f_e *and* P^{post}_e *as a function of* δ, *and identify* A_a *and* A_{dmax} *in the figure.*

As shown in Exercise 1 and Exercise 3 (see the file "Exercise_EG2110.pdf"), the electric power can be expressed by

$$P_e = K_1 + K_2 \sin(\delta - K_3)$$

where, K_1, K_2, and K_3 can be easily determined based on the known data. For all three cases, the following are obtained (see Exercise 17)

$$\begin{aligned}
\bar{I}_g &= \left(\frac{\bar{E}'_q - \bar{U}_N}{j(x'_d + x_t) + \bar{Z}}\right) = 1.0676\angle -20.4928 \\
P_m &= P^{pre}_e = Real\left(\bar{E}'_q\,\bar{I}^*_g\right) = 1.0000 \\
K^{pre}_1 &= 0.1008 \quad ; \quad K^{pre}_2 = 1.1598 \quad ; \quad K^{pre}_3 = -0.7032 \\
K^{post}_1 &= 0.0930 \quad ; \quad K^{post}_2 = 1.0388 \quad ; \quad K^{post}_3 = -0.7010 \\
\delta^{pre}_s &= \delta^{pre}_{1s} = 10.5414 \quad \text{(deg.)} \\
\delta^{post}_s &= 20.6665 \quad \text{(deg.)} \\
\delta_{max} &= 79.0081 \quad \text{(deg.)}
\end{aligned}$$

Furthermore, δ_{cc} can be found by

$$\begin{aligned} A_1 &= \int_{\delta_s^{pre}}^{\delta_{cc}} (P_m - P_e^f)\, d\delta \\ A_2 &= \int_{\delta_c}^{\delta_{max}} (P_e^{post} - P_m)\, d\delta \\ g(\delta_{cc}) &= A_1 - A_2 = 0 \end{aligned}$$

where $g(\delta_{cc}) = 0$ is solved for δ_{cc} by applying numerical methods such as Newton-Raphson method.

In Case 1, we have $K_1^f = K_2^f = 0$. Thus,

$$\begin{aligned} A_1 &= P_m(\delta_{cc} - \delta_s^{pre}) \\ A_2 &= (K_1^{post} - P_m)(\delta_{max} - \delta_{cc}) - K_2^{post}[\cos(\delta_{max} - K_3^{post}) - \cos(\delta_{cc} - K_3^{post})] \\ \delta_{cc} &= 15.5200 \quad \text{(deg.)} \end{aligned}$$

Since $P_e^f = 0$ is constant, the critical clearing time can be determined in a similar way as shown in Example 4.2. Thus,

$$t_{cc} = \sqrt{\frac{2M}{P_m - P_e^f}(\delta_{cc} - \delta_s^{pre})} = \sqrt{\frac{2M}{P_m}(\delta_{cc} - \delta_s^{pre})} = 0.0744 \quad \text{(s)}$$

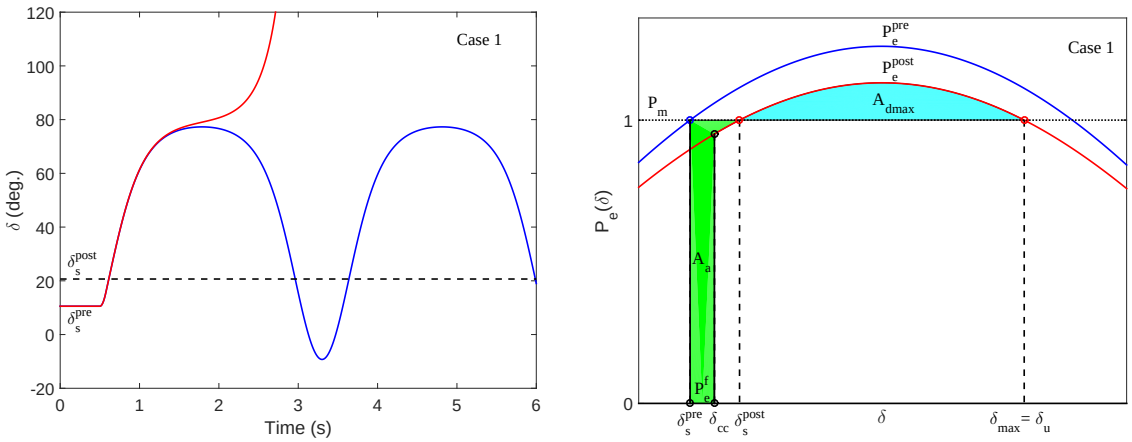

Figure 4.20. Variations of δ and P_e for case 1.

In Case 2, we have

$$K_1^f = 0.1307 \quad , \quad K_2^f = 0 \quad \Rightarrow \quad \delta_{cc} = 16.3096 \quad \text{(deg.)}$$

Since $P_e^f = K_1^f = 0.1307$ is constant, the critical clearing time can analytically be determined by

$$t_{cc} = \sqrt{\frac{2M}{P_m - P_e^f}(\delta_{cc} - \delta_s^{pre})} = 0.0859 \quad \text{(s)}$$

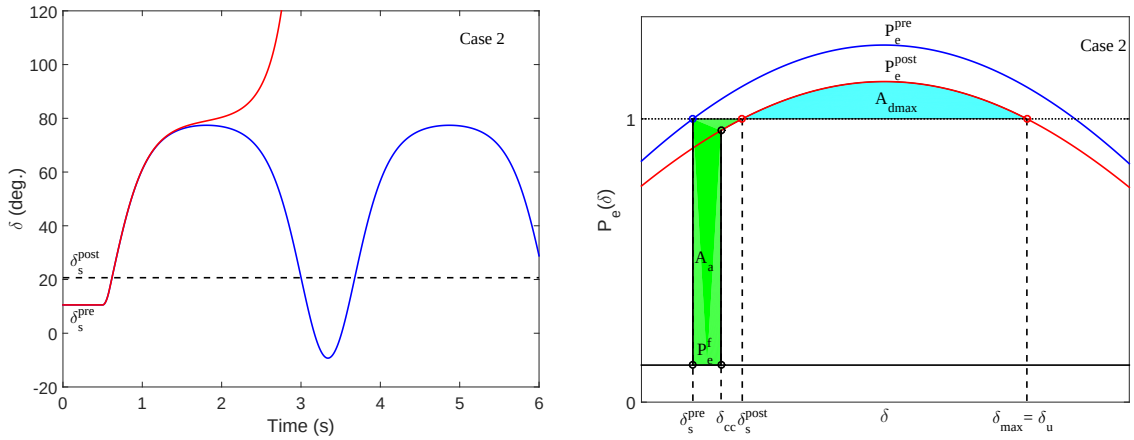

Figure 4.21. Variations of δ and P_e for case 2.

In Case 3, we have

$$K_1^f = 0.1165 \quad , \quad K_2^f = 0.1458 \quad , \quad K_3^f = -0.7516 \quad \Rightarrow \quad \delta_{cc} = 17.1689 \quad \text{(deg.)}$$

Since $P_e^f = K_1^f + K_2^f \sin(\delta - K_3^f)$ is a function of δ (i.e. it is not constant), the critical clearing time cannot analytically be determined. We may apply Transient Energy Function (TEF) method to estimate the critical clearing time as shown in **Example 4.5**.

$$t_{cc} = 0.0981 \quad \text{(s), from } \textbf{Example 4.5}$$

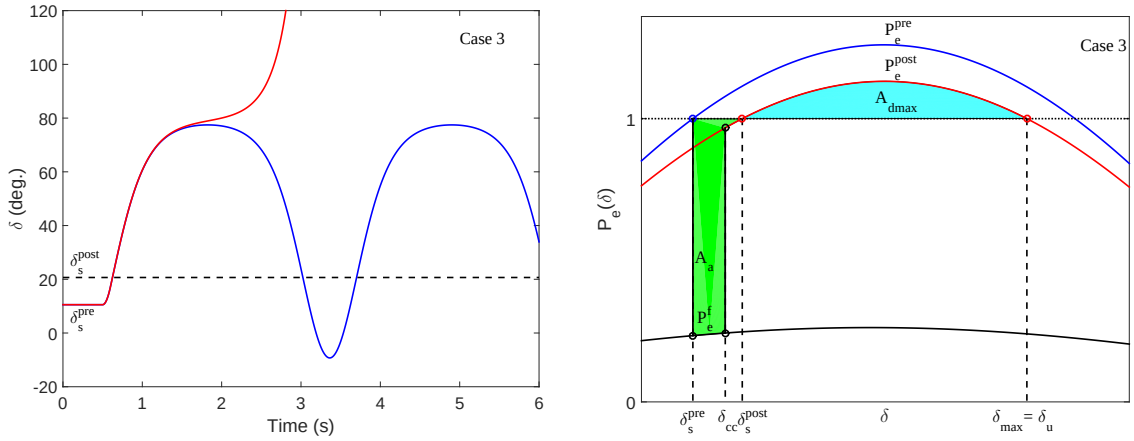

Figure 4.22. Variations of δ and P_e for case 3.

4.3 Transient Energy Function (TEF) method

Another method to estimate the critical clearing time is known as Transient Energy Function (TEF) method. This method (also known as the direct method) is based on

Lyapunov's direct method which gives an estimate of the actual stability region. The simplest estimate is provided by the set

$$\Omega_c = \{x \in R^{n_x} : \mathcal{V}(x) < c\}$$

i.e., for any initial point within Ω_c the system is stable, and the system trajectory will tend to the stable equilibrium point x_s.

Example 4.4 *Consider the following nonlinear system*

$$\begin{aligned} \dot{x}_1 &= -8x_1 + 2x_1x_2^2 \\ \dot{x}_2 &= -18x_2 + 2x_2x_1^2 \end{aligned}$$

By applying the direct method give an estimate of the actual stability region.

By setting $\dot{x}_1 = \dot{x}_2 = 0$, we first find the equilibrium points of the system. It can easily be shown that the equilibrium points are

$$x_{0_1} = (-3,-2) \quad , \quad x_{0_2} = (3,2) \quad , \quad x_{0_3} = (-3,2) \quad , \quad x_{0_4} = (3,-2) \quad , \quad x_{0_5} = (0,0)$$

Based on Theorem 2.1, x_{0_1}, x_{0_2}, x_{0_3}, x_{0_4} are unstable, and $x_{0_5} = x_s$ is (asymptotically) stable.

Consider the positive definite function $\mathcal{V}(x) = x_1^2 + x_2^2$ whose time derivative along the trajectories of the system is given by

$$\dot{\mathcal{V}} = -4(4x_1^2 + 9x_2^2 - 2x_1^2x_2^2)$$

Since our interest is in estimating the stability region, we need to determine a domain $\mathcal{D}$ about the origin where $\dot{\mathcal{V}}$ is negative definite, and a set $\Omega_c \subset \mathcal{D}$ which is bounded. We can find c by minimizing $\mathcal{V}$ subject to $\dot{\mathcal{V}} = 0$. Doing this, we easily find $c = 12.5$, see Section B.1 in Appendix B. Thus, $\mathcal{V} < 12.5$ is the estimate of the stability region as shown in Figure 4.23. Note that $\mathcal{V} = c = 12.5$ is a level surface of Lyapunov function $\mathcal{V}(x) = x_1^2 + x_2^2$.

In the figure, the stability boundary of the actual stability region is indicated in blue, and the stability boundary of the estimated stability region (i.e. $\Omega_c = \{x \in R^{n_x} : \mathcal{V}(x) < c\}$) is indicated in red.

Let $\mathcal{V}_{cr} = c$ be the critical level surface, and x_{ini} be an initial point whose position is known. If $\mathcal{V}(x_{ini}) < \mathcal{V}_{cr}$, then the initial point lies within the estimated stability region, and the system is therefore predicted by the direct method as stable. However, if $\mathcal{V}(x_{ini}) \geq \mathcal{V}_{cr}$, then the system is predicted as unstable.

Let $x_{ini} = (2,2)$ be an initial point. At this point $\mathcal{V}(x_{ini}) = 8$ which is less than $\mathcal{V}_{cr} = 12.5$, and based on the direct method the system with this initial point is predicted as stable. Next, let $x_{ini} = (-1,4)$ be an initial point. At this point $\mathcal{V}(x_{ini}) = 17$ which is greater than $\mathcal{V}_{cr} = 12.5$. Thus by the direct method, the system with this initial point is predicted as unstable.

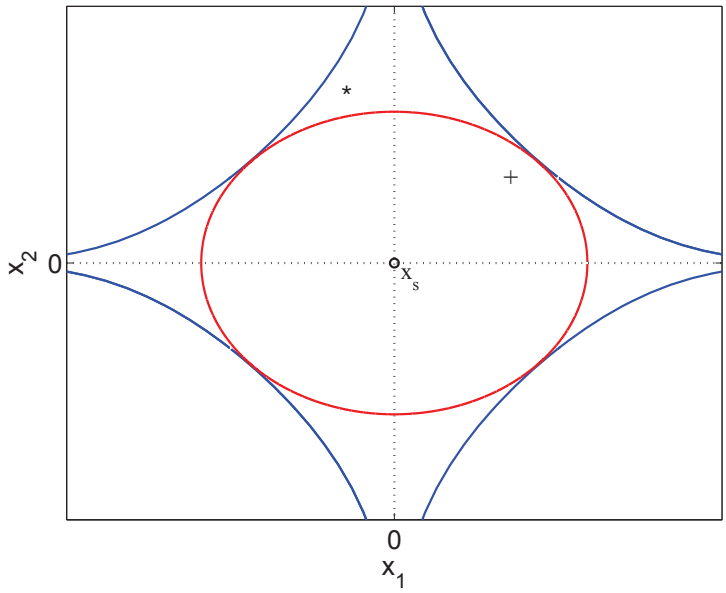

Figure 4.23. Estimate of the stability region of x_s.

The initial points $x_{ini} = (2, 2)$ and $x_{ini} = (-1, 4)$ are indicated with "+" and "*", respectively, in the figure. Obviously, $x_{ini} = (2, 2)$ lies within Ω_c and the direct method correctly predicts the stability of the system. The initial point $x_{ini} = (-1, 4)$ does not lie within Ω_c, but it lies within the actual stability region that is the system will be stable with this initial point. However, the direct method incorrectly predicts the instability of the system. This is a disadvantage of this method which gives a conservative prediction. However, an important feature of this method is that it does not predict an unstable case as a stable case.

This method has received considerable attention for assessment of power system transient stability. In power system literature this method is more known as the Transient Energy Function (TEF) method, since energy functions have been used as Lyapunov function candidates. The energy function for a power system has normally the form

$$\mathcal{V}(x) = W_k + W_p + C_0 \tag{4.19}$$

where, W_k and W_p are known as kinetic and potential energy, respectively. C_0 is a constant such that $\mathcal{V}(x_s) = 0$ at the stable equilibrium point.

Using the TEF method, the assessment of transient stability of a power system after a fault is performed by the following steps [7]:

1. Knowing the structure of the post-fault system, compute the stable equilibrium point (x_s) of the post-fault system.

2. Formulate the energy function of the post-fault system, and calculate $\mathcal{V}_{cr}$ which is the critical energy function.

3. Simulate the system during the fault (i.e. the on-fault system), and compute x_{t_c}

at the specified clearing time t_c. The point x_{t_c} is considered as the initial point of the post-fault system.

4. Calculate $\mathcal{V}(x_{t_c})$. If it is less than $\mathcal{V}_{cr}$, the system is stable.

5. The critical clearing time can also be computed by simulating the on-fault system until at a time t_{cc}, $\mathcal{V}(x_{t_{cc}}) = \mathcal{V}_{cr}$. This time is the critical clearing time.

Example 4.5 *Consider the energy function below.*

$$\begin{aligned} \mathcal{V}(x) =& \frac{1}{2}M\omega^2 - \left[(P_m - K_1^{post})\delta + K_2^{post}\cos(\delta - K_3^{post})\right] + C_0 \\ C_0 =& (P_m - K_1^{post})\delta_s^{post} + K_2^{post}\cos(\delta_s^{post} - K_3^{post}) \end{aligned} \tag{4.20}$$

a) *Show that the function $\mathcal{V}(x)$ in* (4.20) *satisfies the conditions of Theorem 2.2 for $x_0 = x_s^{post}$.*

b) *By using the function $\mathcal{V}(x)$ in* (4.20)*, find (or estimate) the critical clearing time of each case in* **Example 4.3**.

a) It can be shown in a similar way as described in **Example 2.2**.

b) The critical clearing time for each case can be found as follows.

- Find $\mathcal{V}_{cr}$ which is given by (why?)

$$\mathcal{V}_{cr} = -\left[(P_m - K_1^{post})\delta_{max} + K_2^{post}\cos(\delta_{max} - K_3^{post})\right] + C_0$$

- Simulate the system during the fault with appropriate clearing time t_c and integration time step.

- Let the vectors δ_f and ω_f be the simulation results during the fault. Then, substitute these results in $\mathcal{V}(x)$ in (4.20) to obtain the vector

$$\mathcal{V}(x) = \frac{1}{2}M\omega_f^2 - \left[(P_m - K_1^{post})\delta_f + K_2^{post}\cos(\delta_f - K_3^{post})\right] + C_0$$

- The intersection between $\mathcal{V}(x)$ and $\mathcal{V}_{cr}$ gives the estimated critical clearing time as shown in Figure 4.24.

4.4 Transient stability enhancement

In this section, some of the most common methods to improve the transient stability of power systems will be presented. For the purpose of illustration how the proposed methods enhance the transient stability, these methods will be applied to an SMIB

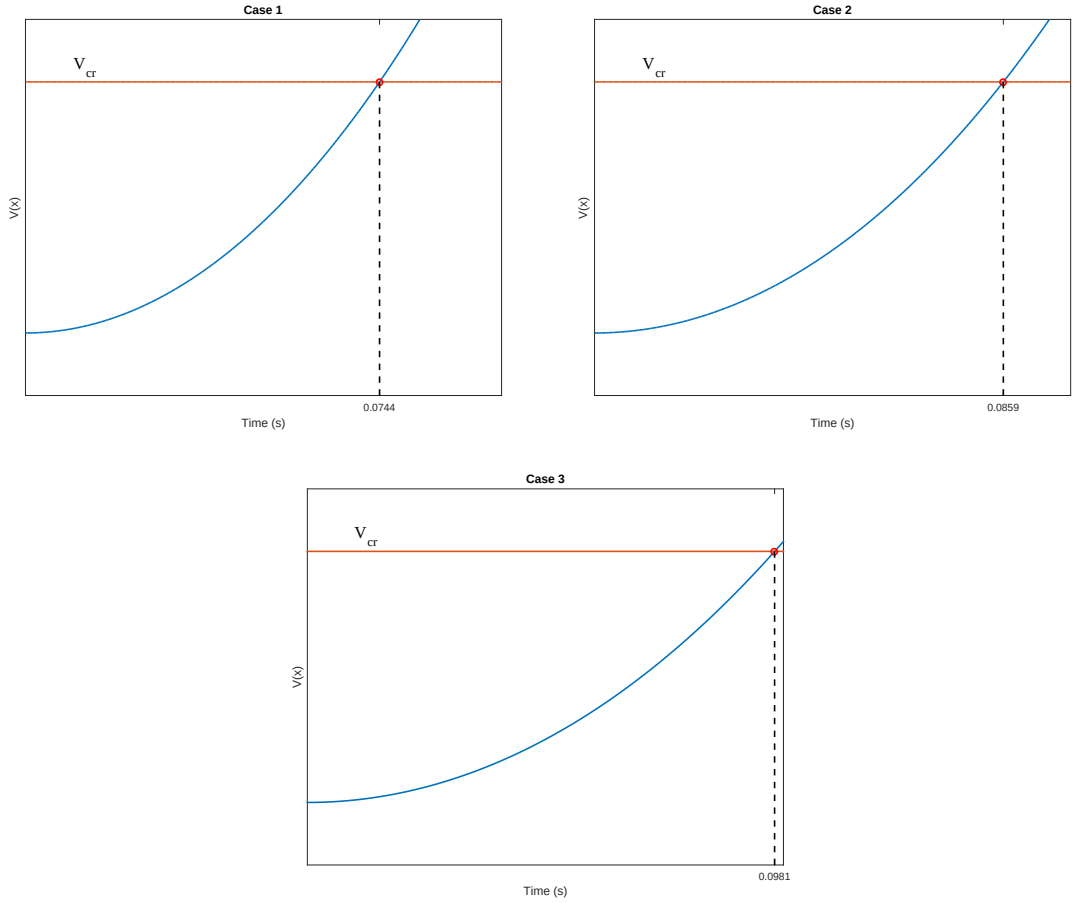

Figure 4.24. Estimation of critical clearing time based on TEF.

system. However, it is to be noted that these methods are general, and can be applied to any real multi-machine power system.

In the previous section, it has been shown that the SMIB system is transiently stable for a given fault and a given clearing time t_c, if $t_c < t_{cc}$ (or $A_1 < A_2$ or $\mathcal{V}(x_c) < \mathcal{V}_{cr}$). Using this relationship, a stability measure may be defined as follows

$$\begin{aligned}
\mathcal{M}_t &= \frac{t_{cc} - t_c}{t_{cc}} 100\,\% = (1 - \frac{t_c}{t_{cc}})\, 100\,\% \\
\mathcal{M}_{\mathcal{V}} &= \frac{\mathcal{V}_{cr} - \mathcal{V}(x_c)}{\mathcal{V}_{cr}} 100\,\% = (1 - \frac{\mathcal{V}(x_c)}{\mathcal{V}_{cr}})\, 100\,\% \\
\mathcal{M}_A &= \frac{A_2 - A_1}{A_2} 100\,\% = (1 - \frac{A_1}{A_2})\, 100\,\%
\end{aligned} \tag{4.21}$$

Increasing $\mathcal{M}_t$ (or $\mathcal{M}_A$ or $\mathcal{M}_{\mathcal{V}}$) results in enhancing the transient stability. Obviously, an important way to improve the transient stability is the use of protection equipments and circuit breakers that quickly detect and clear the faults (which results in shortening of t_c or reduction of A_1), and also the use of automatic line re-closing following the fault clearing (which results in enlargement of A_2 as shown in Exercises).

Consider the SMIB system shown in Figure 4.25. In this study, the clearing time is specified based on the properties of protection equipments and circuit breakers. The objective of the proposed methods is therefore to extend the critical clearing time (which is similar to enlargement of A_2 and/or reduction of A_1).

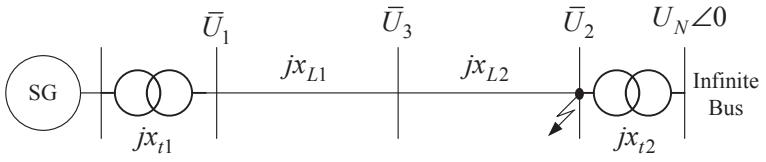

Figure 4.25. An SMIB system.

For this system $H = 4$, $x'_d = 0.15$, $P_m = 1$, $x_{t1} = x_{t2} = 0.1$, $x_{L1} = x_{L2} = 0.2$ and $U_N = 1$ (all in (pu)). A three-phase fault occurs at bus 2, and the fault is cleared after 100 (ms) (i.e. $t_c = 0.1$ (s)). Prior to the fault, $U_1 = 1$ (pu). Since $P_e^f = 0$ during this fault, $A_1 = A_2$ gives the critical clearing time

$$t_{cc} = \sqrt{\frac{2M}{P_m}\,(\delta_{cc} - \delta_s^{pre})} = 0.1458 \ \text{(s)}$$

Therefore, $\mathcal{M}_t = 31.4\%$.

Braking resistors

One method to improve the transient stability is to switch a shunt resistor (normally close to the generator) for a short time following a fault. This action is known as braking resistors by which the rotor acceleration due to the fault will be braked. Switching a shunt resistor R at bus 1 during the fault, then $P_e^f \neq 0$ (but a positive constant), and $A_1^{new} = A_2^{new}$ gives

$$t_{cc}^{new} = \sqrt{\frac{2M}{P_m - P_e^f}\,(\delta_{cc}^{new} - \delta_s^{pre})}$$

For a clearing angle equal to δ_{cc} when $P_e^f = 0$, the accelerating area with $P_e^f \neq 0$ will be less than A_1 with $P_e^f = 0$. To make $A_1^{new} = A_2^{new}$, then A_2^{new} must be less than A_2 which implies that δ_{cc}^{new} must be greater than δ_{cc}. Furthermore, $\frac{2M}{P_m - P_e^f} > \frac{2M}{P_m}$. Therefore, $t_{cc}^{new} > t_{cc}$ which implies that $\mathcal{M}_{tR} > \mathcal{M}_t$.

For $R = 1$ (pu), it can be shown that $t_{cc}^{new} = 0.2370$ (s), and $\mathcal{M}_{tR} = 57.8\%$.

Series capacitor compensation

Another method to enhance transient stability is reduction of transmission system reactance. In the SMIB system,

$$P_e = \frac{E'_q\, U_N}{x'_d + x_{t1} + x_{t2} + x_{L1} + x_{L2}}\,\sin(\delta) = P_{emax}\,\sin(\delta)$$

By compensating each line with a series capacitor, P_{emax} becomes higher which results in enlargement of A_2.

Let each line be compensated with 50% that is $x_{L1}^{new} = x_{L2}^{new} = 0.2 - x_c = 0.2 * (1 - 0.5)$. Thus, by this method $t_{cc}^{new} = 0.2050$ (s), and $\mathcal{M}_{tx_c} = 51.2\%$.

Shunt capacitor compensation
The main function of shunt capacitor compensation is to keep the voltage profile of the (heavily loaded) transmission system within acceptable levels (i.e. close to the nominal value). This compensation also increases the maximum power transfer capability which results in enlargement of A_2.

Let a shunt capacitor with $B_{sh} = 0.58$ (pu) be installed at bus 3 to keep the steady-state voltage magnitude of this bus at 1 (pu).
Thus, by this compensation $t_{cc}^{new} = 0.1505$ (s), and $\mathcal{M}_{tB_{sh}} = 33.5\%$.

Obviously, compared to the shunt capacitor compensation, the braking resistors and series capacitor compensation are more effective of achieving transient stability enhancement.

Other methods
There are other actions that not only significantly enhance transient stability, they also improve damping of electromechanical oscillations, for example high-speed excitation system with Automatic Voltage Regulator (AVR) and Power System Stabilizer (PSS) which will be discussed in this compendium, or power electronics based controllable devices with appropriate control strategies.

Chapter 5

Dynamic modeling of multi-machine power systems

In Chapter 4, the dynamic of a very simple power system (the SMIB system) has been derived and studied. This simple model has of course a limited application to realistic power systems. The analysis of such a simple model is primary motivated by the insight it gives. In this chapter, dynamic modeling of a multi-machine power system is however presented. It will be shown that depending on load modeling this dynamic will be described by either a set of differential-algebraic equations (DAE) or only by a set of differential equations. The dynamic model given by differential-algebraic equations is termed as Structure Preserving Model (SPM), and the dynamic model given by differential equations is termed as Reduced Network Model (RNM).

Before deriving the dynamic model of a multi-machine power system, we start this chapter with presenting different load models.

5.1 Load modeling

As presented in [8], the term "load" can have several meanings. In this compendium the following definition of the load is however of concern

- *"A portion of the system that is not explicitly represented in a system model, but rather is treated as if it were single power-consuming power device connected to a bus in the system model"* [8].

Based on the above definition, the load at a (high voltage) bus represents the aggregation of hundreds or thousands of individual commercial, industrial and residential power-consuming devices such as motors, heating, lighting, and electrical appliances as shown in Figure 5.1.

This aggregate (or composite) load model may be represented by static or dynamic load models, or a combination of both as described in (5.1)

$$\bar{S}_L = \kappa\, \bar{S}_{st} + (1-\kappa)\, \bar{S}_{dyn} \quad \text{where} \quad 0 \leq \kappa \leq 1 \tag{5.1}$$

where, κ is the fraction of the load represented by static load model. $\bar{S}_L = \bar{U}_L\, \bar{I}_L^* = P_L + j\, Q_L$ is a mathematical representation of the composite load model. It gives the relationship between bus voltage and current flowing into the (composite) load.

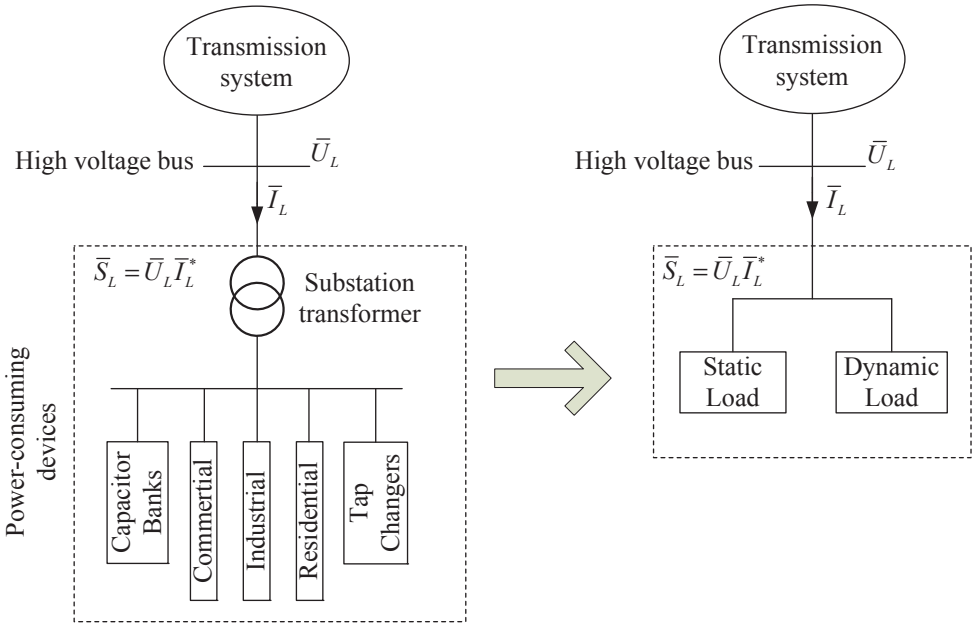

Figure 5.1. A composite load model for representing physical loads.

5.1.1 Static load model

This model expresses the characteristics of the load at any instant of time as functions of the bus voltage magnitude and frequency at the same instant [8]. These characteristics are mathematically described by only algebraic equations. This model has usually been used for transient stability analysis.

The exponential and ZIP models are two types of the static load models which have been widely used to represent the voltage dependency of loads.

In the exponential model, active and reactive components of the load are expressed as (it is assumed that $\kappa = 1$, i.e. $P_L = P_{st}$ and $Q_L = Q_{st}$)

$$P_L = P_{EXP} = P_{L0} \left(\frac{U_L}{U_{L0}} \right)^{mp} \quad \text{and} \quad Q_L = Q_{EXP} = Q_{L0} \left(\frac{U_L}{U_{L0}} \right)^{mq} \tag{5.2}$$

where, U_L is the actual bus voltage magnitude, U_{L0} is the initial value of the voltage, and P_{L0} and Q_{L0} are the active and reactive powers at U_{L0}. The voltage exponents mp and mq represents the parameters of this model.

- With $mp = mq = 0$, the model represents constant power characteristic.
- With $mp = mq = 1$, the model represents constant current characteristic.
- With $mp = mq = 2$, the model represents constant impedance characteristic.

Based on the nature of the composite load characteristics at a given bus these exponents may have different values.

In the ZIP model, active and reactive components of the load are expressed as

$$\begin{aligned} P_L &= P_{ZIP} = P_{L0}\left[k_{pz}\left(\frac{U_L}{U_{L0}}\right)^2 + k_{pi}\left(\frac{U_L}{U_{L0}}\right) + k_{pp}\right] \\ Q_L &= Q_{ZIP} = Q_{L0}\left[k_{qz}\left(\frac{U_L}{U_{L0}}\right)^2 + k_{qi}\left(\frac{U_L}{U_{L0}}\right) + k_{qp}\right] \end{aligned} \tag{5.3}$$

This model is composed of constant impedance (Z), constant current (I), and constant power (P) components. The parameters k_p and k_q define the fraction of each component. Note that $k_{pz} + k_{pi} + k_{pp} = k_{qz} + k_{qi} + k_{qp} = 1$.

A more general representation of the static loads is given by (5.4) where the frequency dependency of load characteristics is also included [9]-[10].

$$\begin{aligned} P_L &= P_{ZIP} + \kappa\, P_{L0}\left(\sum_{k=1}^{2} k_{p_k}\left(\frac{U_L}{U_{L0}}\right)^{mp_k}(1 + D_{p_k}\,\Delta f)\right) \\ Q_L &= Q_{ZIP} + \kappa\, Q_{L0}\left(\sum_{k=1}^{2} k_{q_k}\left(\frac{U_L}{U_{L0}}\right)^{mq_k}(1 + D_{q_k}\,\Delta f)\right) \end{aligned} \tag{5.4}$$

where D_{pk} and D_{qk} are damping constants, and $\Delta f = f - f_s$ is the bus frequency deviation (f is the actual frequency of the bus, and f_s is the nominal frequency of the bus). It is obvious that the load models (5.2)-(5.3) are derivatives of the general model (5.4) in which $k_{pz} + k_{pi} + k_{pp} + k_{p1} + k_{p2} = k_{qz} + k_{qi} + k_{qp} + k_{q1} + k_{q2} = 1$.

5.1.2 Dynamic load model

It is well known that load characteristics have a significant impact on power system dynamics. Therefore, accurate load modeling is vitally important for power system utilities to predict more precisely the power system operating limits and stability margins. Thus, in many stability studies such as long-term stability and voltage stability it is necessary to account for the dynamics of loads.

Electrical motors consume a large amount of the total electrical energy supplied by a power system, and a large number of these motors are induction motors which affect damping of oscillations. Thus, in addition to studies of long-term stability and voltage stability, for improving damping prediction it has also been recommended that major blocks of induction motor load should be represented by dynamic models including both inertial and rotor flux dynamics (known as third-order model) [8]-[10]. For a composite load, the motor components are aggregated into a single dynamic induction motor model as shown in Figure 5.2 which has been derived by applying an appropriate transformation of phase variables into components along rotating axes. For an induction machine the preferred reference frame is one with the axes rotating at synchronous speed [11], i.e. the stator and rotor quantities are transferred to a reference frame which rotates at synchronous speed ω_s.

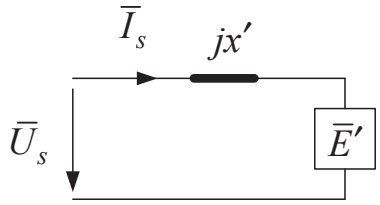

Figure 5.2. Induction motor transient-equivalent circuit (third-order model).

In Figure 5.2, x' is the transient reactance (the stator resistance has been neglected), and based on dq-components of the new reference frame we have the following (all variables are expressed in (pu)):

$$\begin{aligned} \bar{U}_s &= U_q + jU_d \\ \bar{I}_s &= I_q + jI_d \\ \bar{E}' &= E_q + jE_d \end{aligned}$$

Moreover, from the figure the following can be obtained

$$I_q = \frac{U_d - E'_d}{x'} \quad \text{and} \quad I_d = -\frac{U_q - E'_q}{x'} \tag{5.5}$$

Let x_m be the magnetizing reactance, r_r be the rotor resistance, and x_s and x_r be the leakage reactances of the stator and the rotor, respectively. Then, it can be shown that based on the dq-components of the new reference frame the dynamic of this induction motor is given by [4]

$$\begin{aligned} \dot{s} =& \frac{1}{2H}\,(T_m - T_e) \\ \dot{E}'_q =& \omega_s\, s\, E'_d - \frac{1}{T'_0}\,\left(E'_q + (x - x')I_d\right) \\ \dot{E}'_d =& -\omega_s\, s\, E'_q - \frac{1}{T'_0}\,(E'_d - (x - x')I_q) \end{aligned} \tag{5.6}$$

where,

$$\begin{aligned} s &= \frac{\omega_s - \omega_{motor}}{\omega_s} \quad \text{is the slip of the induction motor} \\ T_m &= A + Bs + Cs^2 \quad \text{is the mechanical load torque in terms of the slip} \\ T_e &= E'_q\, I_q + E'_d\, I_d \quad \text{is the electrical torque} \\ T'_0 &= \frac{x_r + x_m}{\omega_s\, r_r} \quad \text{is the transient open-circuit time constant} \\ x' &= x_s + \frac{x_m\, x_r}{x_m + x_r} \quad \text{and} \quad x = x_s + x_m \end{aligned}$$

Note that I_q and I_d in (5.6) are given by (5.5). Furthermore, $\bar{U}_L = \bar{U}_s$, and if $\kappa = 0$ we have $\bar{I}_L = \bar{I}_s$, i.e. $\bar{S}_L = \bar{S}_{dyn}$.

There are also other dynamic load models which are summarized in [10].

5.2 Multi-machine power systems

Figure 5.3 shows a multi–machine power system. The transmission network has a total of N buses including the generators terminal buses (the first n_g buses). Voltages at these buses are given by $\bar{U}_i = U_i \angle \theta_i$.

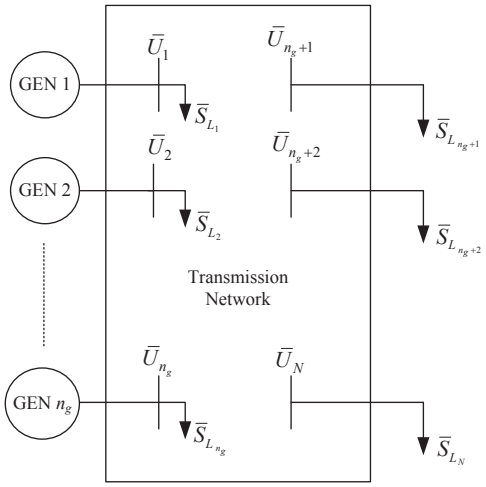

Figure 5.3. A multi–machine power system.

For this system the following assumptions are made:

1. Dynamic of each generator is described by the one-axis model.
2. Mechanical power of each generator (i.e. P_m) is constant.
3. Inherent damping of each generator (i.e. D) is zero.
4. Loads are represented by static load model.
5. Transmission network is lossless.

Based on the assumption 1, the equivalent circuit of the k:th generator is shown in Figure 5.4 where the reactance of the k:th transformer is included in x'_{dk}. The voltage at the generator internal bus is given by $E'_{qk} \angle \delta_k$.

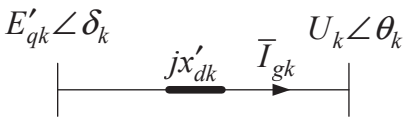

Figure 5.4. Synchronous generator one-axis dynamic circuit.

5.2.1 Structure preserving model

Based on the assumptions 1-3, the dynamic of the k:th generator is given by

for $k = 1 \cdots n_g$

$$\begin{aligned}
\dot{\delta}_k &= \omega_k \\
\dot{\omega}_k &= \frac{1}{M_k}\left(P_{mk} - \frac{E'_{qk}\,U_k}{x'_{dk}}\sin(\delta_k - \theta_k)\right) \\
\dot{E'}_{qk} &= \frac{1}{T'_{dok}}\left(E_{fk} - \frac{x_{dk}}{x'_{dk}}\,E'_{qk} + \frac{x_{dk} - x'_{dk}}{x'_{dk}}\,U_k\cos(\delta_k - \theta_k)\right)
\end{aligned} \tag{5.7}$$

where the reactance of the k:th transformer is also included in x_{dk}.

Next, let Y_{bus} of order $(N \times N)$ be the admittance matrix of the transmission network, and the kl-th element of the admittance matrix be defined by $\bar{Y}_{bus_{kl}} = G_{kl} + jB_{kl}$, where G_{kl} represents solely the resistances of the respective transmission lines. However, based on the assumption 5 (since $R \ll X$) $G_{kl} = 0$, and therefore $\bar{Y}_{bus_{kl}} = jB_{kl}$.

The real and reactive powers injected into bus k are given by

for $k = 1 \cdots n_g$

$$\begin{aligned}
P_k &= \sum_{l=1}^{N} B_{kl}U_kU_l\sin(\theta_k - \theta_l) + \frac{E'_{qk}U_k\sin(\theta_k - \delta_k)}{x'_{dk}} \\
Q_k &= -\sum_{l=1}^{N} B_{kl}U_kU_l\cos(\theta_k - \theta_l) + \frac{U_k^2 - E'_{qk}U_k\cos(\theta_k - \delta_k)}{x'_{dk}}
\end{aligned} \tag{5.8}$$

and for $k = (n_g + 1) \cdots N$

$$\begin{aligned}
P_k &= \sum_{l=1}^{N} B_{kl}U_kU_l\sin(\theta_k - \theta_l) \\
Q_k &= -\sum_{l=1}^{N} B_{kl}U_kU_l\cos(\theta_k - \theta_l)
\end{aligned} \tag{5.9}$$

Let P_{L_k} and Q_{L_k} be the active and reactive loads at bus k. Then, for $k = 1 \cdots N$ the power flow equations (5.8) and (5.9) can be written as

$$\begin{aligned}
P_k + P_{L_k} &= 0 \\
Q_k + Q_{L_k} &= 0
\end{aligned} \tag{5.10}$$

which is a set of algebraic equations.

Let

$$\begin{aligned}
x &= [\delta_1 \cdots \delta_{n_g}\ ,\ \omega_1 \cdots \omega_{n_g}\ ,\ E'_{q1} \cdots E'_{qn_g}]^T \\
y &= [\theta_1 \cdots \theta_N\ ,\ U_1 \cdots U_N]^T
\end{aligned} \tag{5.11}$$

Then, equations (5.7) and (5.10) can be rewritten as

$$\begin{aligned}
\dot{x} &= f(x, y) \\
0 &= g(x, y)
\end{aligned} \tag{5.12}$$

Equation (5.12) is a set of differential-algebraic equations which describe the dynamic of the multi-machine system. The differential equations $\dot{x} = f(x, y)$ describe the dynamic of the generators. In case of having dynamic loads and other dynamical components, their contributions will be included in these differential equations. The algebraic equations consist of the network equations based on Kirchhoff's current law, i.e. the sum of all currents (or powers) flowing into bus k must be equal zero. Equation (5.8) (which is included in (5.10), and gives the power balance equations at the generator terminal buses) is the interface between the algebraic variables (i.e. y) and the state variables (i.e. x).

This model is termed Structure Preserving Model (SPM) since the structure of the system model is preserved. An advantage of using SPM is that from a modeling viewpoint, it allows more realistic representations of power system components, especially load behaviors.

5.2.2 Reduced Network Model

The Reduced Network Model (RNM) can be obtained by replacing assumption 4 with the following assumption

4. Loads are represented as constant impedances $\bar{Z}_{L_k} = R_{L_k} + jX_{L_k} = \dfrac{U_k^2}{P_{L_k} - jQ_{L_k}}$.

Impedance loads can also be given in the form of admittance loads as

$$\bar{y}_{L_k} = \frac{1}{\bar{Z}_{L_k}} = \frac{P_{L_k} - jQ_{L_k}}{U_k^2} \tag{5.13}$$

Let Y of order $(N \times N)$ be the admittance matrix of the transmission network in which the admittance loads are included, i.e. $Y = Y_{bus} + Y_L$, where Y_L is a diagonal matrix of order $N \times N$ whose diagonal entries are $\bar{y}_{L_k}$. Then, the kl-th element of the admittance matrix is given by $\bar{Y}_{kl} = G_{kl} + jB_{kl}$ where $G_{kl} = 0$ for $k \neq l$ due to assumption 5. However, $G_{kk} \neq 0$ because of the admittance loads.

Next, the multi-machine system is augmented with n_g buses which represent the generators internal buses as shown in Figure 5.5, i.e. the total number of buses is $n_g + N$.

The current of the k-th generator (i.e. $\bar{I}_{gk}$) is given by

$$\bar{I}_{gk} = \frac{\bar{E'}_{qk} - \bar{U}_k}{jx'_{dk}} \quad \text{for} \quad k = 1 \cdots n_g \tag{5.14}$$

Based on Kirchhoff's current law, the following can be obtained.

$$0 = \sum_{l=1}^{N} \bar{Y}_{kl}\, \bar{U}_l - \bar{I}_{gk} \quad \text{for} \quad k = 1 \cdots n_g \tag{5.15}$$

$$0 = \sum_{l=1}^{N} \bar{Y}_{kl}\, \bar{U}_l \quad \text{for} \quad k = n_g + 1 \cdots N \tag{5.16}$$

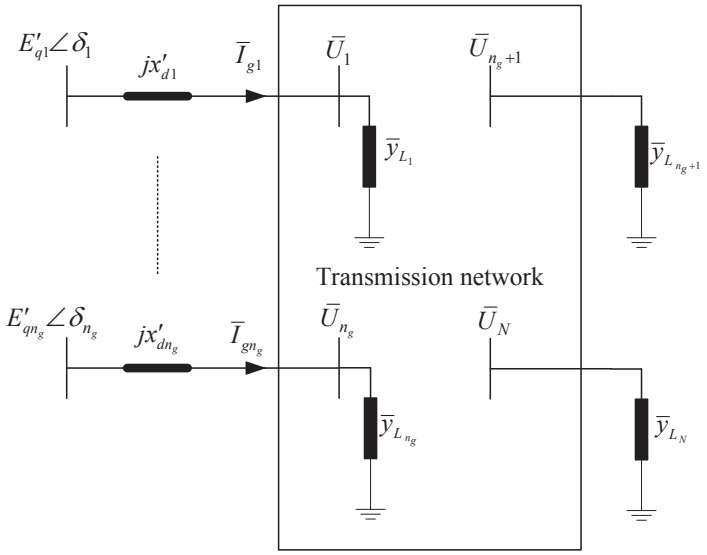

Figure 5.5. The augmented multi–machine power system .

or in compact form

$$\begin{bmatrix} I_G \\ 0_N \end{bmatrix} = \begin{bmatrix} Y_A & Y_B \\ Y_C & Y_D \end{bmatrix} \begin{bmatrix} E_G \\ U_N \end{bmatrix} \tag{5.17}$$

where

- $I_G = [\bar{I}_{g1} \cdots \bar{I}_{gn_g}]^T$, and 0_N is a zero vector of order $N \times 1$.
- $E_G = [\bar{E}'_{q1} \cdots \bar{E}'_{qn_g}]^T$, and $U_N = [\bar{U}_1 \cdots \bar{U}_N]^T$.
- Y_A is a diagonal matrix of order $n_g \times n_g$ whose diagonal entries are $\bar{Y}_{A_{kk}} = \dfrac{1}{jx'_{dk}}$.
- Y_B is a zero matrix of order $n_g \times N$ whose non-zero entries are $\bar{Y}_{B_{kk}} = \dfrac{-1}{jx'_{dk}}$.
- $Y_C = (Y_B)^T$
- Y_D is a matrix of order $N \times N$ which is given by

$$Y_D = Y + \begin{bmatrix} Y_A & 0_1 \\ 0_2 & 0_3 \end{bmatrix}$$

  where, Y is the admittance matrix of the transmission network (including the admittance loads), and 0_1, 0_2 and 0_3 are zero matrices with appropriate orders.

Equation (5.17) can be rewritten as

$$I_G = Y_A\, E_G + Y_B\, U_N \tag{5.18}$$
$$0_N = Y_C\, E_G + Y_D\, U_N \tag{5.19}$$

By solving U_N from equation (5.19), and substituting it in equation (5.18), the following is obtained

$$\begin{aligned} U_N &= -\,Y_D^{-1}\,Y_C\,E_G \\ I_G &= Y_A\,E_G + Y_B\,U_N = \left(Y_A - Y_B\,Y_D^{-1}\,Y_C\,\right)E_G \\ &= Y_{RNM}\,E_G = (G + jB)E_G \end{aligned} \tag{5.20}$$

Thus, for $k = 1 \cdots n_g$

$$\bar{I}_{gk} = (G_{kk} + jB_{kk})\bar{E}'_{qk} + \sum_{\substack{l=1 \\ l\neq k}}^{n_g}(G_{kl} + jB_{kl})\bar{E}'_{ql} \tag{5.21}$$

where,

- $Y_{RNM} = G + jB$ is the admittance matrix of the reduced network model which is of the order $n_g \times n_g$.
- G_{kk} and B_{kk} represent the equivalent short-circuit conductance and susceptance of the k–th generator.
- G_{kl} and B_{kl} represent the transfer conductance and susceptance between internal buses k and l.

Note that G_{kk} and G_{kl} are non-zero in case of having any active load in the system, i.e. $P_L \neq 0$.

By virtue of equation (3.48), the generator current $\bar{I}_{gk}$ can also be written as

$$\bar{I}_{gk} = (I_{qk} + j\,I_{dk})\,e^{j\delta_k} = (G_{kk} + jB_{kk})E'_{qk}\,e^{j\delta_k} + \sum_{\substack{l=1 \\ l\neq k}}^{n_g}(G_{kl} + jB_{kl})E'_{ql}\,e^{j\delta_l} \tag{5.22}$$

from which I_{qk} and I_{dk} can be solved for $k = 1 \cdots n_g$, as

$$\begin{aligned} I_{qk} &= G_{kk}E'_{qk} + \sum_{\substack{l=1 \\ l\neq k}}^{n_g} E'_{ql}\ (G_{kl}\cos(\delta_k - \delta_l) + B_{kl}\sin(\delta_k - \delta_l)) \\ I_{dk} &= B_{kk}E'_{qk} + \sum_{\substack{l=1 \\ l\neq k}}^{n_g} E'_{ql}\ (B_{kl}\cos(\delta_k - \delta_l) - G_{kl}\sin(\delta_k - \delta_l)) \end{aligned} \tag{5.23}$$

Based on equations (3.77) and (3.96), the dynamic of the k:th generator is given by

$$\begin{aligned} \dot{\delta}_k &= \omega_k \\ \dot{\omega}_k &= \frac{1}{M_k}\,(P_{mk} - P_{ek}) = \frac{1}{M_k}\left(P_{mk} - E'_{qk}\,I_{qk}\right) \\ \dot{E}'_{qk} &= \frac{1}{T'_{dok}}\left(E_{fk} - E'_{qk} + (x_{dk} - x'_{dk})I_{dk}\right) \end{aligned} \tag{5.24}$$

Substituting (5.23) into (5.24), the following is obtained

$$\begin{aligned}
\dot{\delta}_k &= \omega_k \\
\dot{\omega}_k &= \frac{1}{M_k}\left[P_{mk} - G_{kk}E'^2_{qk} - \sum_{\substack{l=1\\ l\neq k}}^{n_g} E'_{qk}E'_{ql}\ (G_{kl}\cos(\delta_{kl}) + B_{kl}\sin(\delta_{kl}))\right] \qquad (5.25)\\
\dot{E}'_{qk} &= \frac{1}{T'_{dok}}\left[E_{fk} - E'_{qk} + (x_{dk} - x'_{dk})\left(B_{kk}E'_{qk} + \sum_{\substack{l=1\\ l\neq k}}^{n_g} E'_{ql}\ (B_{kl}\cos(\delta_{kl}) - G_{kl}\sin(\delta_{kl}))\right)\right]
\end{aligned}$$

where, $\delta_{kl} = \delta_k - \delta_l$.

It is obvious that equation (5.25) contains only state variables and constants. The reason is that with the loads represented by constant impedances all N network buses are eliminated by equation (5.20), and there are no algebraic variables (i.e. the voltages at the network buses) in (5.25). Therefore, there is no need of (5.10) to calculate the algebraic variables y.

Using x in (5.11), equation (5.25) can be written as

$$\dot{x} = f(x) \qquad (5.26)$$

i.e., the dynamic of the multi-machine system shown in Figure 5.5 is described by only a set of differential equations. Furthermore, the $(n_g + N)$-bus system in Figure 5.5 is reduced to an n_g-bus system containing only the generators internal buses.

Example 5.1 *Consider the lossless system shown in Figure 5.6. The system data is given in Appendix A (Section A.3).*
Based on assumptions 1-5*, describe mathematically the dynamic of the system, if*

- **a)** *the load model given by* (5.2) *is used, with* $mp = 1$ *and* $mq = 2$*. Also, plot the variations of the electric powers* P_g *when 10% of the active load at BUS 4 is disconnected during 0.1 (s).*
- **b)** *the loads are considered as constant impedances. Also, plot the variations of the electric powers* P_g *for a three-phase fault at BUS 4. The fault is cleared after 100 (ms), i.e.* $t_c = 0.1$ *(s).*

a) Let

$$\begin{aligned}
b_{d1} &= \frac{1}{x'_{d1}} \quad , \quad b_{d2} = \frac{1}{x'_{d2}} \quad , \quad b_{d3} = \frac{1}{x'_{d3}} \\
b_{14} &= \frac{1}{x_{14}} \quad , \quad b_{24} = \frac{1}{x_{24}} \quad , \quad b_{34} = \frac{1}{x_{34}}
\end{aligned}$$

where, the transformer reactance (x_T) is included in x'_d.

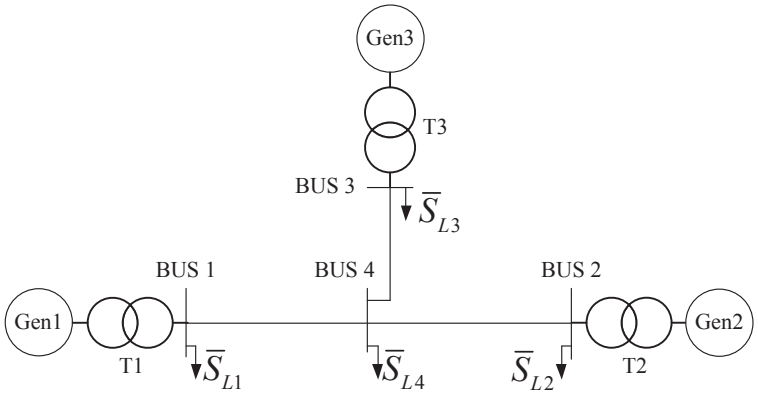

Figure 5.6. A simple multi–machine power system.

The loads are modeled as

$$\begin{aligned}
\bar{S}_{L_1} &= P_{L_1} + jQ_{L_1} = P_{L_{1_0}} \left(\frac{U_1}{U_{1_0}}\right) + jQ_{L_{1_0}} \left(\frac{U_1}{U_{1_0}}\right)^2 \\
\bar{S}_{L_2} &= P_{L_2} + jQ_{L_2} = P_{L_{2_0}} \left(\frac{U_2}{U_{2_0}}\right) + jQ_{L_{2_0}} \left(\frac{U_2}{U_{2_0}}\right)^2 \\
\bar{S}_{L_3} &= P_{L_3} + jQ_{L_3} = P_{L_{3_0}} \left(\frac{U_3}{U_{3_0}}\right) + jQ_{L_{3_0}} \left(\frac{U_3}{U_{3_0}}\right)^2 \\
\bar{S}_{L_4} &= P_{L_4} + jQ_{L_4} = P_{L_{4_0}} \left(\frac{U_4}{U_{4_0}}\right) + jQ_{L_{4_0}} \left(\frac{U_4}{U_{4_0}}\right)^2
\end{aligned}$$

The dynamic of the system is described by a set of differential- algebraic equations. The differential equations are given by (x_T is included in x'_d and x_d)

$$\begin{aligned}
\dot{\delta}_1 &= \omega_1 \\
\dot{\delta}_2 &= \omega_2 \\
\dot{\delta}_3 &= \omega_3 \\
\dot{\omega}_1 &= \frac{1}{M_1}\left(P_{m1} - P_{e1}\right) \\
\dot{\omega}_2 &= \frac{1}{M_2}\left(P_{m2} - P_{e2}\right) \\
\dot{\omega}_3 &= \frac{1}{M_3}\left(P_{m3} - P_{e3}\right) \\
\dot{E}'_{q1} &= \frac{1}{T'_{do1}}\left(E_{f1} - \frac{x_{d1}}{x'_{d1}}E'_{q1} + \frac{x_{d1} - x'_{d1}}{x'_{d1}}U_1\cos(\delta_1 - \theta_1)\right) \\
\dot{E}'_{q2} &= \frac{1}{T'_{do2}}\left(E_{f2} - \frac{x_{d2}}{x'_{d2}}E'_{q2} + \frac{x_{d2} - x'_{d2}}{x'_{d2}}U_2\cos(\delta_2 - \theta_2)\right) \\
\dot{E}'_{q3} &= \frac{1}{T'_{do3}}\left(E_{f3} - \frac{x_{d3}}{x'_{d3}}E'_{q3} + \frac{x_{d3} - x'_{d3}}{x'_{d3}}U_3\cos(\delta_3 - \theta_3)\right)
\end{aligned}$$

The algebraic equations are given by

$$\begin{aligned}
0 &= -P_{g1} + b_{14}\,U_1\,U_4 \sin(\theta_1 - \theta_4) + P_{L_1} \\
0 &= -P_{g2} + b_{24}\,U_2\,U_4 \sin(\theta_2 - \theta_4) + P_{L_2} \\
0 &= -P_{g3} + b_{34}\,U_3\,U_4 \sin(\theta_3 - \theta_4) + P_{L_4} \\
0 &= b_{14}\,U_4\,U_1 \sin(\theta_4 - \theta_1) + b_{24}\,U_4\,U_2 \sin(\theta_4 - \theta_2) + b_{34}\,U_4\,U_3 \sin(\theta_4 - \theta_3) + P_{L_4}
\end{aligned}$$

$$\begin{aligned}
0 &= -Q_{g1} + b_{14}(U_1^2 - U_1\,U_4 \cos(\theta_1 - \theta_4)) + Q_{L_1} \\
0 &= -Q_{g2} + b_{24}(U_2^2 - U_2\,U_4 \cos(\theta_2 - \theta_4)) + Q_{L_2} \\
0 &= -Q_{g3} + b_{34}(U_3^2 - U_3\,U_4 \cos(\theta_3 - \theta_4)) + Q_{L_3} \\
0 &= b_{14}(U_4^2 - U_4\,U_1 \cos(\theta_4 - \theta_1)) + b_{24}(U_4^2 - U_4\,U_2 \cos(\theta_4 - \theta_2)) \\
&\quad + b_{34}(U_4^2 - U_4\,U_3 \cos(\theta_4 - \theta_3)) + Q_{L_4}
\end{aligned}$$

where,

$$\begin{aligned}
P_{ek} &= b_{dk}\,E'_{qk}\,U_k \sin(\delta_k - \theta_k) \\
P_{gk} &= -b_{dk}\,E'_{qk}\,U_k \sin(\theta_k - \delta_k) = P_{ek} \\
Q_{gk} &= -b_{dk}\left(U_k^2 - E'_{qk}\,U_k \cos(\theta_k - \delta_k)\right)
\end{aligned}$$

By defining x and y as follows

$$\begin{aligned}
x &= [\delta_1\ \ \delta_2\ \ \delta_3\ \ \omega_1\ \ \omega_2\ \ \omega_3\ \ E'_{q1}\ \ E'_{q2}\ \ E'_{q3}]^T \\
y &= [\theta_1\ \ \theta_2\ \ \theta_3\ \ \theta_4\ \ U_1\ \ U_2\ \ U_3\ \ U_4]^T
\end{aligned}$$

the dynamic of the system is described in compact form by

$$\begin{aligned}
\dot{x} &= f(x, y) \\
0 &= g(x, y)
\end{aligned}$$

with initial conditions x_0 and y_0 which are computed based on the load flow calculations, and by setting $\dot{x} = f(x_0, y_0) = 0$.

In the load flow calculations, the loads are normally considered as constant loads (i.e. $\bar{S}_{L0} = P_{L0} + jQ_{L0}$). The initial conditions are then computed by the following steps:

1. Run the load flow calculations.
2. From load flow, $y_0 = [\theta_{1_0}\ \ \theta_{2_0}\ \ \theta_{3_0}\ \ \theta_{4_0}\ \ U_{1_0}\ \ U_{2_0}\ \ U_{3_0}\ \ U_{4_0}]^T$ is known.
3. Calculate P_{g1_0}, Q_{g1_0}, Q_{g2_0} and Q_{g3_0}.
4. Calculate $\bar{I}_{g1_0}$, $\bar{I}_{g2_0}$ and $\bar{I}_{g3_0}$

$$\bar{I}_{g1_0} = \frac{P_{g1_0} - jQ_{g1_0}}{\bar{U}^*_{1_0}} \quad , \quad \bar{I}_{g2_0} = \frac{P_{g2_0} - jQ_{g2_0}}{\bar{U}^*_{2_0}} \quad , \quad \bar{I}_{g3_0} = \frac{P_{g3_0} - jQ_{g3_0}}{\bar{U}^*_{3_0}}$$

5. Calculate $\bar{E}'_{q1_0}$, $\bar{E}'_{q2_0}$ and $\bar{E}'_{q3_0}$

$$\begin{aligned}
\bar{E}'_{q1_0} &= E'_{q1_0}\angle\delta_{1_0} = \bar{U}_{1_0} + j\, x'_{d1}\, \bar{I}_{g1_0} \\
\bar{E}'_{q2_0} &= E'_{q2_0}\angle\delta_{2_0} = \bar{U}_{2_0} + j\, x'_{d2}\, \bar{I}_{g2_0} \\
\bar{E}'_{q3_0} &= E'_{q3_0}\angle\delta_{3_0} = \bar{U}_{3_0} + j\, x'_{d3}\, \bar{I}_{g3_0}
\end{aligned}$$

6. $x_0 = [\delta_{1_0}\ \delta_{2_0}\ \delta_{3_0}\ 0\ 0\ 0\ E'_{q1_0}\ E'_{q2_0}\ E'_{q3_0}]^T$ is now known.

7. Finally, P_{m1}, P_{m2}, P_{m3}, E_{f1}, E_{f2} and E_{f3} can be computed by setting $\dot{x} = f(x_0, y_0) = 0$, i.e.

$$\begin{aligned}
P_{m1} &= P_{e1_0} = P_{g1_0} \\
P_{m2} &= P_{e2_0} = P_{g2_0} \\
P_{m3} &= P_{e3_0} = P_{g3_0} \\
E_{f1} &= \frac{x_{d1}}{x'_{d1}}\, E'_{q1_0} - \frac{x_{d1} - x'_{d1}}{x'_{d1}}\, U_{1_0} \cos(\delta_{1_0} - \theta_{1_0}) \\
E_{f2} &= \frac{x_{d2}}{x'_{d2}}\, E'_{q2_0} - \frac{x_{d2} - x'_{d2}}{x'_{d2}}\, U_{2_0} \cos(\delta_{2_0} - \theta_{2_0}) \\
E_{f3} &= \frac{x_{d3}}{x'_{d3}}\, E'_{q3_0} - \frac{x_{d3} - x'_{d3}}{x'_{d3}}\, U_{3_0} \cos(\delta_{3_0} - \theta_{3_0})
\end{aligned}$$

The dynamics of the system in the pre-disturbance state, during-disturbance state and post-disturbance state are given by

Pre-disturbance state:

$$\begin{aligned}
\dot{x} &= f^{pre}(x_0, y_0) = 0 \\
0 &= g^{pre}(x_0, y_0)
\end{aligned}$$

During-disturbance state with $P_{L_4} = 0.9\, P_{L_{4_0}} \left(\frac{U_4}{U_{4_0}}\right)$ **:**

$$\begin{aligned}
\dot{x} &= f^{f}(x, y) \\
0 &= g^{f}(x, y)
\end{aligned}$$

Post-disturbance state with $P_{L_4} = P_{L_{4_0}} \left(\frac{U_4}{U_{4_0}}\right)$ **:**

$$\begin{aligned}
\dot{x} &= f^{post}(x, y) \\
0 &= g^{post}(x, y)
\end{aligned}$$

Figure 5.7 shows the variations of the electric power of each generator for this disturbance. As shown in the figure, Gen 1 oscillates against Gen 2 and Gen 3. Although, $D_1 = D_2 = D_3 = 0$, there is indeed a poor damping in the system (why?).

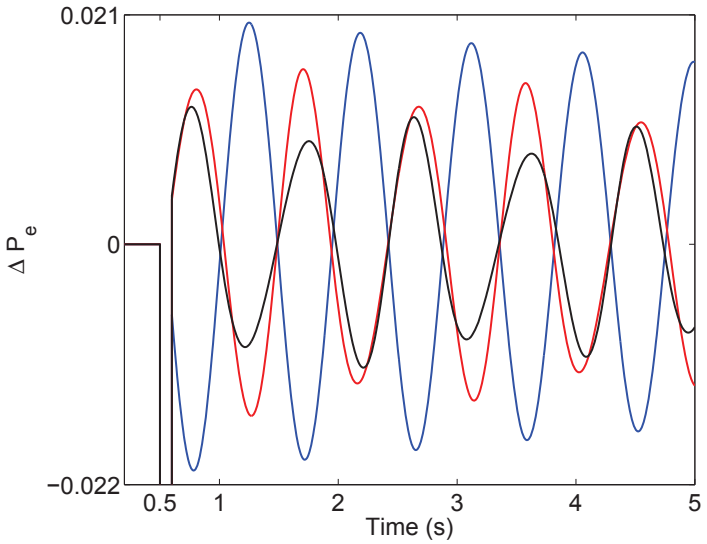

Figure 5.7. Variations of ΔP_{e1} (blue), ΔP_{e2} (red) and ΔP_{e3} (black).

b) In a similar way as described in task **a)**, the initial conditions are firstly obtained. Next, the loads are modeled as admittances as follows

$$\begin{aligned} \bar{y}_{L_1} &= \frac{1}{\bar{Z}_{L_1}} = \frac{P_{L_{1_0}} - jQ_{L_{1_0}}}{U_{1_0}^2} \quad , \quad \bar{y}_{L_2} = \frac{1}{\bar{Z}_{L_2}} = \frac{P_{L_{2_0}} - jQ_{L_{2_0}}}{U_{2_0}^2} \\ \bar{y}_{L_3} &= \frac{1}{\bar{Z}_{L_3}} = \frac{P_{L_{3_0}} - jQ_{L_{3_0}}}{U_{3_0}^2} \quad , \quad \bar{y}_{L_4} = \frac{1}{\bar{Z}_{L_4}} = \frac{P_{L_{4_0}} - jQ_{L_{4_0}}}{U_{4_0}^2} \end{aligned}$$

to make the following Y_L matrix.

$$Y_L = \begin{bmatrix} \bar{y}_{L_1} & 0 & 0 & 0 \\ 0 & \bar{y}_{L_2} & 0 & 0 \\ 0 & 0 & \bar{y}_{L_3} & 0 \\ 0 & 0 & 0 & \bar{y}_{L_4} \end{bmatrix}$$

Let

$$\bar{b}_{d1} = \frac{1}{j\, x'_{d1}} \quad , \quad \bar{b}_{d2} = \frac{1}{j\, x'_{d2}} \quad , \quad \bar{b}_{d3} = \frac{1}{j\, x'_{d3}}$$

and

$$Y_A = \begin{bmatrix} \bar{b}_{d1} & 0 & 0 \\ 0 & \bar{b}_{d2} & 0 \\ 0 & 0 & \bar{b}_{d3} \end{bmatrix}, \; Y_B = \begin{bmatrix} -\bar{b}_{d1} & 0 & 0 & 0 \\ 0 & -\bar{b}_{d2} & 0 & 0 \\ 0 & 0 & -\bar{b}_{d3} & 0 \end{bmatrix}, \; Y_C = \begin{bmatrix} -\bar{b}_{d1} & 0 & 0 \\ 0 & -\bar{b}_{d2} & 0 \\ 0 & 0 & -\bar{b}_{d3} \\ 0 & 0 & 0 \end{bmatrix}$$

Next, with $Y = Y_{bus} + Y_L$, and

$$Y_D = Y + \begin{bmatrix} Y_A & 0_1 \\ 0_2 & 0_3 \end{bmatrix} = \begin{bmatrix} \bar{y}_{11} + \bar{y}_{L_1} & 0 & 0 & \bar{y}_{14} \\ 0 & \bar{y}_{22} + \bar{y}_{L_2} & 0 & \bar{y}_{24} \\ 0 & 0 & \bar{y}_{33} + \bar{y}_{L_3} & \bar{y}_{34} \\ \bar{y}_{14} & \bar{y}_{24} & \bar{y}_{34} & \bar{y}_{44} + \bar{y}_{L_4} \end{bmatrix} + \begin{bmatrix} \bar{b}_{d1} & 0 & 0 & 0 \\ 0 & \bar{b}_{d2} & 0 & 0 \\ 0 & 0 & \bar{b}_{d3} & 0 \\ 0 & 0 & 0 & 0 \end{bmatrix}$$

the admittance matrix of the Reduced Network Model (RNM) is obtained by

$$Y_{RNM} = Y_A - Y_B Y_D^{-1} Y_C = G + j\,B = \begin{bmatrix} G_{11}+j\,B_{11} & G_{12}+j\,B_{12} & G_{13}+j\,B_{13} \\ G_{21}+j\,B_{21} & G_{22}+j\,B_{22} & G_{23}+j\,B_{23} \\ G_{31}+j\,B_{31} & G_{32}+j\,B_{32} & G_{33}+j\,B_{33} \end{bmatrix}$$

$$= \begin{bmatrix} 0.0843 - j\,1.1164 & 0.1476 + j\,0.5463 & 0.1181 + j\,0.4370 \\ 0.1476 + j\,0.5463 & 0.2583 - j\,1.5441 & 0.2066 + j\,0.7648 \\ 0.1181 + j\,0.4370 & 0.2066 + j\,0.7648 & 0.1653 - j\,1.3882 \end{bmatrix}$$

Based on equation (5.21) and the structure of the Y_{RNM}, the figure below shows the reduced model of the system shown in Figure 5.6. In this model, all generator buses are replaced by the corresponding generator internal buses, and all load buses (BUS 4 in this example) are removed. (What are $\bar{y}_{ii}^{RNM}$ and $\bar{y}_{ij}^{RNM}$ in the figure?)

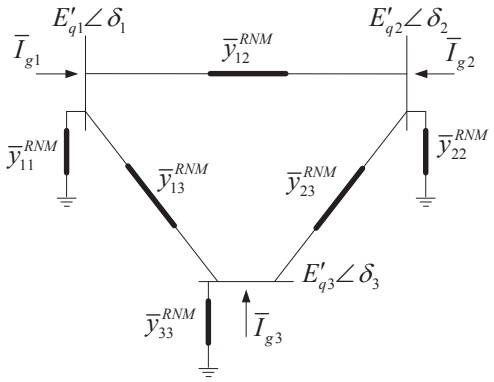

Figure 5.8. The reduced network model of the system shown in Figure 5.6.

For a fault at BUS 4, Y_{RNM} must be modified. This is done by adding a large admittance to the diagonal element of Y_D corresponding to the faulty bus (BUS 4) as follows

$$Y_D^f(4,4) = Y_D(4,4) + (1-j)10^{12} \quad \Rightarrow$$

$$Y_{RNM}^f = Y_A - Y_B (Y_D^f)^{-1} Y_C = G^f + j\,B^f$$

$$= \begin{bmatrix} 0.0000 - j\,1.4286 & 0.0000 + j\,0.0000 & 0.0000 + j\,0.0000 \\ 0.0000 + j\,0.0000 & 0.0000 - j\,2.5000 & 0.0000 + j\,0.0000 \\ 0.0000 + j\,0.0000 & 0.0000 + j\,0.0000 & 0.0000 - j\,2.0000 \end{bmatrix}$$

Next, I_{qk} and I_{dk} with $k = 1, 2, 3$ are obtained by

$$I_{qk} = G_{kk} E'_{qk} + \sum_{\substack{l=1 \\ l \neq k}}^{3} E'_{ql}\ (G_{kl}\cos(\delta_k - \delta_l) + B_{kl}\sin(\delta_k - \delta_l))$$

$$I_{dk} = B_{kk} E'_{qk} + \sum_{\substack{l=1 \\ l \neq k}}^{3} E'_{ql}\ (B_{kl}\cos(\delta_k - \delta_l) - G_{kl}\sin(\delta_k - \delta_l))$$

Thus, the dynamic of the system is given by

$$\begin{aligned}
\dot{\delta}_1 &= \omega_1 \\
\dot{\delta}_2 &= \omega_2 \\
\dot{\delta}_3 &= \omega_3 \\
\dot{\omega}_1 &= \frac{1}{M_1}\left(P_{m1} - E'_{q1}\, I_{q1}\right) \\
\dot{\omega}_2 &= \frac{1}{M_2}\left(P_{m2} - E'_{q2}\, I_{q2}\right) \\
\dot{\omega}_3 &= \frac{1}{M_3}\left(P_{m3} - E'_{q3}\, I_{q3}\right) \\
\dot{E}'_{q1} &= \frac{1}{T'_{do1}}\left(E_{f1} - E'_{q1} + (x_{d1} - x'_{d1})I_{d1}\right) \\
\dot{E}'_{q2} &= \frac{1}{T'_{do2}}\left(E_{f2} - E'_{q2} + (x_{d2} - x'_{d2})I_{d2}\right) \\
\dot{E}'_{q3} &= \frac{1}{T'_{do3}}\left(E_{f3} - E'_{q3} + (x_{d3} - x'_{d3})I_{d3}\right)
\end{aligned}$$

Note that in the during-fault state, $Y_{RNM} = G + j\,B$ is replaced by $Y^f_{RNM} = G^f + j\,B^f$.

Figure 5.9 shows the variations of the electric power of each generator for this fault. Obviously, the power variations are greater for this fault compared to the disturbance in the task **a)** above.

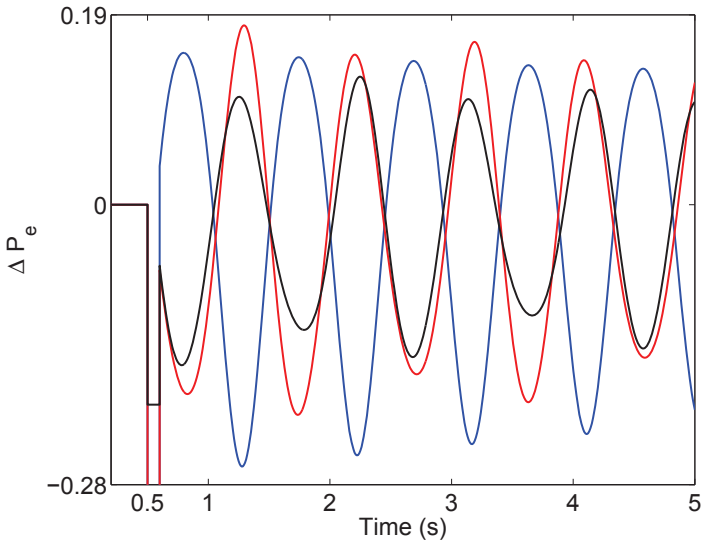

Figure 5.9. Variations of ΔP_{e1} (blue), ΔP_{e2} (red) and ΔP_{e3} (black).

Example 5.2 *Consider again the lossless system shown in Figure 5.6. Let the two-axis model given by* (3.84) *be used for the generators. Describe mathematically the dynamic of the system, if the load model given by* (5.2) *is used, with* $mp = 1$ *and* $mq = 2$. *Also, find the initial values* x_0 *and* y_0.

Since two-axis model is used, the following three differential equations are added into $\dot{x} = f(x, y)$, (x_T is included in x'_q and x_q)

$$\begin{aligned}
\dot{E}'_{d1} &= \frac{1}{T'_{qo1}}\left(-E'_{d1} - (x_{q1} - x'_{q1})I_{q1}\right) = \frac{1}{T'_{qo1}}\left(-\frac{x_{q1}}{x'_{q1}}\,E'_{d1} - \frac{x_{q1} - x'_{q1}}{x'_{q1}}\,U_1 \sin(\delta_1 - \theta_1)\right) \\
\dot{E}'_{d2} &= \frac{1}{T'_{qo2}}\left(-E'_{d2} - (x_{q2} - x'_{q2})I_{q2}\right) = \frac{1}{T'_{qo2}}\left(-\frac{x_{q2}}{x'_{q2}}\,E'_{d2} - \frac{x_{q2} - x'_{q2}}{x'_{q2}}\,U_2 \sin(\delta_2 - \theta_2)\right) \\
\dot{E}'_{d3} &= \frac{1}{T'_{qo3}}\left(-E'_{d3} - (x_{q3} - x'_{q3})I_{q2}\right) = \frac{1}{T'_{qo3}}\left(-\frac{x_{q3}}{x'_{q3}}\,E'_{d3} - \frac{x_{q3} - x'_{q3}}{x'_{q3}}\,U_3 \sin(\delta_3 - \theta_3)\right)
\end{aligned}$$

and the electric power is given by

$$P_{ek} = b_{dk}\left(E'_{qk}\,U_k\,\sin(\delta_k - \theta_k) + E'_{dk}\,U_k\,\cos(\delta_k - \theta_k)\right)$$

The algebraic equations are unchanged, however

$$\begin{aligned}
P_{gk} &= P_{ek} \\
Q_{gk} &= -b_{dk}\left(U_k^2 - E'_{qk}\,U_k \cos(\theta_k - \delta_k) - E'_{dk}\,U_k \sin(\theta_k - \delta_k)\right)
\end{aligned}$$

Note that in the one-axis model, the voltage behind the transient reactance is given by $E'_{qk}\,e^{j\delta_k}$ (see Figure 5.4). However in the two-axis model, the generator internal voltage is $\bar{E}' = (E'_{qk} + jE'_{dk})\,e^{j\delta_k}$ (see Figure 3.11 (a) and equation (3.99)). Furthermore, from Figure 3.6 and equations (3.48) and (3.83) we have

$$\begin{aligned}
U_{dk} &= U_k\,\sin(\theta_k - \delta_k) \\
U_{qk} &= U_k\,\cos(\theta_k - \delta_k) \\
\bar{U}_k &= U_k\,e^{j\theta_k} = (U_{qk} + j\,U_{dk})\,e^{j\delta_k} \\
\bar{I}_k &= \bar{I}_{gk} = (I_{qk} + j\,I_{dk})\,e^{j\delta_k} \\
I_{qk} &= -\frac{U_{dk} - E'_{dk}}{x'_{qk}} \\
I_{dk} &= \frac{U_{qk} - E'_{qk}}{x'_{dk}}
\end{aligned} \tag{5.27}$$

The initial conditions are computed as follows:

- Points "1." to "4." in the task **a)** above.
- Prior to the disturbance

$$\dot{E}'_{dk} = 0 \quad \Rightarrow \quad E'_{dk_0} = -(x_{qk} - x'_{qk})\,I_{qk_0} = -(x_{qk} - x'_{dk})\,I_{qk_0} \tag{5.28}$$

  since it is assumed $x'_{dk} = x'_{qk}$.

From equation (3.99), we have

$$(E'_{qk_0} + jE'_{dk_0})\, e^{j\delta_{k_0}} = \bar{U}_{k_0} + jx'_{dk}\bar{I}_{gk_0} = \bar{U}_{k_0} + jx'_{dk}(I_{qk_0} + j\, I_{dk_0})\, e^{j\delta_{k_0}} \qquad (5.29)$$

Substituting E'_{dk_0} from equation (5.28) into equation (5.29), the following is obtained

$$E'_{qk_0}\, e^{j\delta_{k_0}} + x'_{dk}\, I_{dk_0}\, e^{j\delta_{k_0}} = \bar{U}_{k_0} + jx_{qk}\, I_{qk_0}\, e^{j\delta_{k_0}} \qquad (5.30)$$

Subtracting $x_{qk}\, I_{dk_0}\, e^{j\delta_{k_0}}$ from the both sides of (5.30) results in

$$(E'_{qk_0} - (x_{qk} - x'_{dk})\, I_{dk_0})\, e^{j\delta_{k_0}} = \bar{U}_{k_0} + jx_{qk}(I_{qk_0} + jI_{dk_0})\, e^{j\delta_{k_0}} = \bar{U}_{k_0} + jx_{qk}\bar{I}_{gk_0} \quad (5.31)$$

Thus, δ_{k_0} can be calculated from equation (5.31). When δ_{k_0} is known, U_{q_0}, U_{d_0}, I_{q_0}, I_{d_0}, and finally E'_{dk_0} and E'_{qk_0} can then be calculated from (5.27).

- Point "7.".

Chapter 6

Rotor angle stability

As was presented in Chapter 1, rotor angle stability refers to the ability of synchronous machines of an interconnected power system to remain in synchronism after being subjected to a disturbance. Instability that may result occurs in the form of increasing angular swings of some generators leading to their loss of synchronism with other generators. Loss of synchronism can occur between one machine and the rest of the system, or between groups of machines, with synchronism maintained within each group after separating from each other. This stability is characterized as:

- **Transient stability** which is concerned with the ability of the power system to maintain synchronism when subjected to a large disturbance, such as a short–circuit on a transmission line. Transient stability depends on the initial operating conditions of the system as well as the type, severity and location of the disturbance.
- **Small-signal stability** which is concerned with the ability of the power system to maintain synchronism under small disturbances. The disturbances are considered to be sufficiently small that linearization of system equations is permissible for purposes of analysis.

Transient stability has already been discussed for an SMIB system. Due to the simplicity of the SMIB system, it was possible to study its transient stability by means of Equal Area Criterion without running time-domain simulation. However, since this method is not analytically applicable to multi-machine power systems, some techniques applicable to transient stability analysis of multi-machine power systems are presented in this chapter.

6.1 Transient stability

The main aim of transient stability analysis of a power system is to study whether the system after a large disturbance will settle to an acceptable steady-state as time passes. To ensure power system stability (or security), power system utilities would like to assess the performance of either current or postulated power system configuration under a variety of actual or hypothesized operating conditions and disturbances. Then based on the results of the stability studies, they take preventive control action if necessary.

For transient stability study, power system utilities broadly apply time-domain simulation programs to predict the response of the system(s) to various large disturbances. In these programs, the dynamic of the system may be described by a set of differential-algebraic equations of the form (5.12) (or only differential equations) which are solved

by using step-by-step numerical integration methods. Based on simulation results, the behavior of the system is evaluated to predict the system stability and operating limits. An advantage of applying time-domain simulations is that it is possible to have more detailed models for generators and other power system components. By these detailed models, the dynamic behaviors of the actual power system components are then more accurately represented.

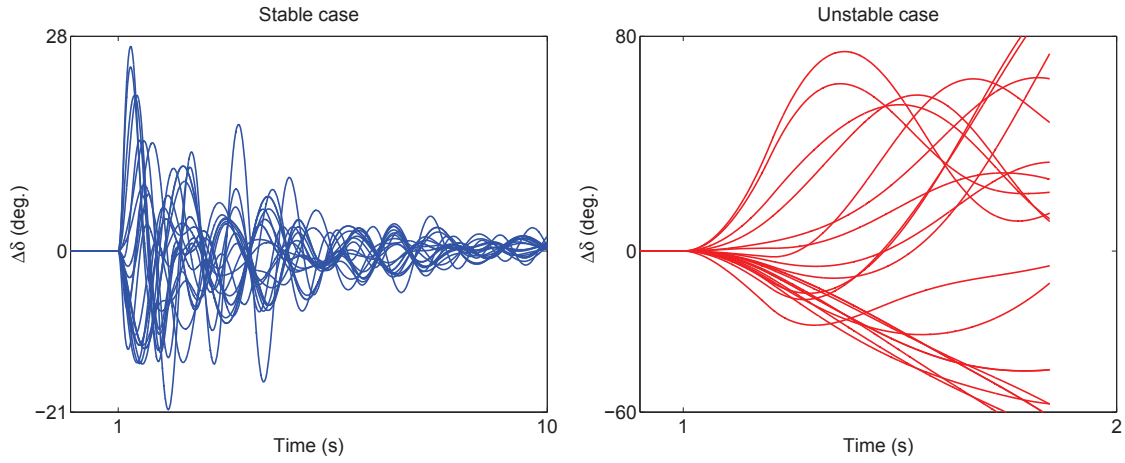

Figure 6.1. Rotor angle deviations of each generator.

Figure 6.1 shows the dynamic behaviors of the generators in the Nordic32 test system proposed by CIGRE after a large disturbance for different clearing times. For the unstable case, the system loses its synchronism and it is transiently unstable for the specified disturbance and clearing time. Simulations were performed by using the simulation program SIMPOW, and the results were plotted in MATLAB.

The time-domain approach has however disadvantages such as heavy and time-consuming computations (especially for large interconnected power systems). Moreover (as shown in the above figure), it does not provide any information regarding the stability margin.

To overcome these disadvantages, other transient stability analysis methods have been developed. In this compendium two methods will be presented, namely the Transient Energy Function (TEF) method and the SIngle Machine Equivalent (SIME) method.

6.1.1 Transient Energy Function (TEF) method

As explained in Section 4.3, TEF method has received considerable attention for assessment of power system transient stability. The most challenge of the application of TEF method to a multi-machine power system is calculation of $\mathcal{V}_{cr}$ to have a less conservative estimation. There are different techniques for calculating $\mathcal{V}_{cr}$. These techniques have been presented and discussed in [7] and related references therein.

In the development of energy functions for multi-machine power systems, and also in order to clearly distinguish between the forces that accelerate the whole system

and those that tend to separate the system into different parts, it is convenient to transform the system (5.12) into the so called Center Of Inertia (COI) reference frame. The position of the COI is defined by

$$\delta_{COI} = \frac{1}{M_T}\sum_{k=1}^{n_g} M_k\delta_k \quad , \quad \omega_{COI} = \frac{1}{M_T}\sum_{k=1}^{n_g} M_k\omega_k \quad \text{where} \quad M_T = \sum_{k=1}^{n_g} M_k \tag{6.1}$$

Furthermore,

$$\dot{\omega}_{COI} = \frac{1}{M_T}\sum_{k=1}^{n_g} M_k\,\dot{\omega}_k = \frac{1}{M_T}\sum_{k=1}^{n_g}(P_{mk} - P_{ek}) = \frac{P_{COI}}{M_T} \tag{6.2}$$

Next, the state variables δ_k and ω_k are transformed to the COI variables as

$$\tilde{\delta}_k = \delta_k - \delta_{COI} \quad , \quad \tilde{\omega}_k = \omega_k - \omega_{COI} \tag{6.3}$$

These COI variables are constrained by

$$\sum_{k=1}^{n_g} M_k\tilde{\delta}_k = 0 \quad , \quad \sum_{k=1}^{n_g} M_k\tilde{\omega}_k = 0 \tag{6.4}$$

The load buses angles are also transformed to the COI reference frame by

$$\tilde{\theta}_k = \theta_k - \delta_{COI}$$

Time derivation of equation (6.3) gives

$$\begin{aligned}
\dot{\tilde{\delta}}_k &= \dot{\delta}_k - \dot{\delta}_{COI} = \omega_k - \omega_{COI} = \tilde{\omega}_k \\
\dot{\tilde{\omega}}_k &= \dot{\omega}_k - \dot{\omega}_{COI} = \frac{1}{M_k}\left(P_{mk} - P_{ek} - \frac{M_k}{M_T}P_{COI}\right)
\end{aligned}$$

The system (5.12) in the COI reference frame is then expressed as (for $k = 1 \cdots n_g$)

$$\begin{aligned}
\dot{\tilde{\delta}}_k &= \tilde{\omega}_k \\
\dot{\tilde{\omega}}_k &= \frac{1}{M_k}\left(P_{mk} - \frac{E'_{qk}\,U_k}{x'_{dk}}\sin(\tilde{\delta}_k - \tilde{\theta}_k) - \frac{M_k}{M_T}P_{COI}\right) \\
\dot{E}'_{qk} &= \frac{1}{T'_{dok}}\left(E_{fk} - \frac{x_{dk}}{x'_{dk}}\,E'_{qk} + \frac{x_{dk} - x'_{dk}}{x'_{dk}}\,U_k\cos(\tilde{\delta}_k - \tilde{\theta}_k)\right)
\end{aligned} \tag{6.5}$$

and

$$\begin{aligned}
P_k + P_{L_k} &= 0 \\
Q_k + Q_{L_k} &= 0
\end{aligned} \tag{6.6}$$

where, P_k and Q_k are given by (5.8) and (5.9) in which θ and δ are replaced by $\tilde{\theta}$ and $\tilde{\delta}$. Note however that $\tilde{\theta}_k - \tilde{\theta}_l = \theta_k - \theta_l$ and $\tilde{\delta}_k - \tilde{\theta}_k = \delta_k - \theta_k$.

Let the loads (i.e. P_{L_k} and Q_{L_k}) be modeled based on (5.2) with $mp = 0$ and an arbitrary mq. Then, the following energy function is given for the DAE system (6.5) and (6.6)

$$\mathcal{V}(\tilde{\omega}, \tilde{\delta}, E'_q, U, \tilde{\theta}) = W_K + W_P + C_o \tag{6.7}$$

where

$$W_K = \frac{1}{2}\sum_{k=1}^{n_g} M_k \tilde{\omega}_k^2 \quad \text{and} \quad W_P = \sum_{p=1}^{7} \mathcal{V}_{2p}$$

with

$$\begin{aligned}
\mathcal{V}_{21} &= -\sum_{k=1}^{n_g} P_{mk}\tilde{\delta}_k \quad , \quad \mathcal{V}_{22} = \sum_{k=1}^{N} P_{Lk}\tilde{\theta}_k \quad , \quad \mathcal{V}_{23} = \sum_{k=1}^{N} \int \frac{Q_{Lk}}{U_k}\, dU_k \\
\mathcal{V}_{24} &= \sum_{k=1}^{n_g} \frac{1}{2x'_{dk}}[E'^2_{qk} + U_k^2 - 2E'_{qk}U_k\cos(\tilde{\delta}_k - \tilde{\theta}_k)] \\
\mathcal{V}_{25} &= -\frac{1}{2}\sum_{k=1}^{N}\sum_{l=1}^{N} B_{kl}\, U_k\, U_l \cos(\tilde{\theta}_k - \tilde{\theta}_l) \\
\mathcal{V}_{26} &= -\sum_{k=1}^{n_g} \frac{E_{fdk}E'_{qk}}{x_{dk} - x'_{dk}} \quad \text{and} \quad \mathcal{V}_{27} = \sum_{k=1}^{n_g} \frac{E'^2_{qk}}{2(x_{dk} - x'_{dk})}
\end{aligned}$$

Using the notation

$$[\frac{d\mathcal{V}}{dt}]_{\tilde{\omega}} \quad \text{for} \quad \frac{\partial \mathcal{V}}{\partial \tilde{\omega}}\,\frac{d\tilde{\omega}}{dt}$$

and similarly for the other states, the following are then obtained

$$[\frac{d\mathcal{V}_1}{dt}]_{\tilde{\omega}} + [\frac{d\mathcal{V}_{21}}{dt} + \frac{d\mathcal{V}_{24}}{dt}]_{\tilde{\delta}} = 0 \tag{6.8}$$

$$[\frac{d\mathcal{V}_{22}}{dt} + \frac{d\mathcal{V}_{24}}{dt} + \frac{d\mathcal{V}_{25}}{dt}]_{\tilde{\theta}} = \sum (P_k + P_{Lk})\dot{\tilde{\theta}}_k = 0 \tag{6.9}$$

$$[\frac{d\mathcal{V}_{23}}{dt} + \frac{d\mathcal{V}_{24}}{dt} + \frac{d\mathcal{V}_{25}}{dt}]_{U} = \sum (Q_k + Q_{Lk})\frac{\dot{U}_k}{U_k} = 0 \tag{6.10}$$

$$[\frac{d\mathcal{V}_{24}}{dt} + \frac{d\mathcal{V}_{26}}{dt} + \frac{d\mathcal{V}_{27}}{dt}]_{E'_q} = -\sum_{k=1}^{n_g} \frac{T'_{dok}}{x_{dk} - x'_{dk}}(\dot{E}'_{qk})^2 \tag{6.11}$$

which results in the following time derivative of the energy function

$$\frac{d\mathcal{V}}{dt} = -\sum_{k=1}^{n_g} \frac{T'_{dok}}{x_{dk} - x'_{dk}}(\dot{E}'_{qk})^2 \leq 0 \tag{6.12}$$

6.1.2 SIngle Machine Equivalent (SIME) method

The SIME method is a hybrid direct-temporal transient stability method, which transforms the trajectories of a multi-machine power system into the trajectory of a single machine equivalent system of the form

$$\begin{aligned} \dot{\delta}_{SIME} &= \omega_{SIME} \\ \dot{\omega}_{SIME} &= M^{-1}\left[P_{m_{SIME}} - P_{e_{SIME}}\right] \end{aligned} \tag{6.13}$$

whose parameters (which are derived from multi-machine power system) are time-varying [12].

Basically, the SIME method deals with the post-fault configuration of a power system subjected to a disturbance which presumably drives it to instability. Under such condition, the SIME method uses a time-domain program in order to identify the mode of separation of its machines into two groups, namely critical (subscript C) and non-critical machines (subscript NC) which are replaced by successively a two-machine equivalent. Then, this two-machine equivalent is replaced by a single machine equivalent system. By definition, the critical machines are the machines responsible of the loss of synchronism.

The parameters of (6.13) are given by

$$\begin{aligned} \delta_{SIME} &= \delta_C - \delta_{NC} \\ \omega_{SIME} &= \omega_C - \omega_{NC} \\ P_{m_{SIME}} &= M_T^{-1}\left(M_C \sum_{i\in C} P_{mi} - M_{NC} \sum_{j\in NC} P_{mj}\right) \\ P_{e_{SIME}} &= M_T^{-1}\left(M_C \sum_{i\in C} P_{ei} - M_{NC} \sum_{j\in NC} P_{ej}\right) \\ M &= \frac{M_C\, M_{NC}}{M_T} \quad \text{and} \quad M_T = M_C + M_{NC} \end{aligned} \tag{6.14}$$

where

$$\begin{aligned} M_C &= \sum_{i\in C} M_i \quad , \quad M_{NC} = \sum_{j\in NC} M_j \\ \delta_C &= M_C^{-1} \sum_{i\in C} M_i\delta_i \quad , \quad \delta_{NC} = M_{NC}^{-1} \sum_{j\in NC} M_j\delta_j \\ \omega_C &= M_C^{-1} \sum_{i\in C} M_i\omega_i \quad , \quad \omega_{NC} = M_{NC}^{-1} \sum_{j\in NC} M_j\omega_j \end{aligned} \tag{6.15}$$

By refreshing the parameters of the single machine equivalent system at each integration time–step and numerically assessing the transient stability of this equivalent system based on the equal area criterion, the SIME method provides accurate and fast transient stability assessment of multi-machine power systems, and also additional interesting information such as stability margins, identification of the mode of instability and corresponding critical machines, sensitivity analysis and control techniques [12]-[13].

6.2 Small-signal stability

As was mentioned, small-signal stability analysis deals with small disturbances, and it is applied to linearized system models. This analysis provides valuable information about the inherent dynamic characteristics of the power system. It also provides a valuable complement to information gained by time-domain simulation.

Small disturbances, such as the normal small fluctuations in the system loads or small changes of the set values of some parameters, are always present in a power system and normally the resulting power (or electromechanical) oscillations are stable that is the oscillations are positively damped and decay with time. However, these spontaneous oscillations may due to insufficient damping occasionally grow in amplitude with time, and result in sustained low frequency oscillations that cause loss of synchronism.

The change in electrical torque (ΔT_e) of a synchronous generator following a disturbance can be resolved into two components, namely the synchronizing torque component (ΔT_S) and the damping torque component (ΔT_D) as follows [6]:

$$\Delta T_e = \Delta T_S + \Delta T_D = K_S\,\Delta\delta + K_D\,\Delta\omega \tag{6.16}$$

where,

- ΔT_S is in phase with $\Delta\delta$, and K_S is the synchronizing torque coefficient.
- ΔT_D is in phase with $\Delta\omega$, and K_D is the damping torque coefficient.

Lack of sufficient synchronizing torque results in non-oscillatory instability in the first few seconds following a fault, i.e. loss of synchronism between interconnected generators. This type of instability is essentially caused by the non-linear nature of the dynamics of interconnected generators [14]. Therefore, (fast) automatic voltage regulators have been used to increase the synchronizing torques between interconnected generators. However, they have also an effect of reducing the damping torques which may result in oscillatory instability. This phenomenon is a typical small-signal stability problem in today's power systems. Thus to ensure system stability, a power system should be designed and planned such that both synchronizing and damping torques (with sufficient positive K_S and K_D) exist for each of the synchronous machines.

In this section, application of small-signal stability analysis to power systems and the impact of AVR and PSS on the synchronizing and damping torques will be presented. But first, the essential characteristics (also known as modal analysis) of a Linear Time-Invariant (LTI) system of the form

$$\begin{aligned} \dot{x}(t) &= A\,x(t) + B\,\mathcal{U}(t) \\ \mathcal{Y}(t) &= C\,x(t) \end{aligned} \tag{6.17}$$

are reviewed in terms of the eigen-properties of matrix A.

6.2.1 Modal analysis

Consider the LTI system (6.17), where

- x is a vector of order $n_x \times 1$ containing the system state variables.
- $\mathcal{Y}$ is a vector of order $m \times 1$ containing the system outputs or measured variables.
- $\mathcal{U}$ is a vector of order $r \times 1$ containing the system inputs (or control) variables.
- A is a matrix termed as the state matrix of order $n_x \times n_x$.
- B is a matrix termed as the input matrix of order $n_x \times r$.
- C is a matrix termed as the output matrix of order $m \times n_x$.

For now, let $\mathcal{U}$ be zero and consider the unforced LTI system

$$\dot{x}(t) = A\,x(t) \tag{6.18}$$

Eigenvalues

The eigenvalues of A are defined as the n_x solutions of $\lambda = \lambda_1 \cdots \lambda_{n_x}$ which satisfy

$$det(\, A - \lambda\, \underline{\mathbf{1}}\,) = 0 \tag{6.19}$$

where "*det*" stands for determinant, and $\underline{\mathbf{1}}$ is the identity matrix. The eigenvalues may be real or complex. It is common to associate each eigenvalue λ_i with a **mode** of the system. The stability of an equilibrium point can be determined based on the eigenvalues of the system by applying Theorem 2.1. A real eigenvalue corresponds to a non-oscillatory mode. A negative real eigenvalue represents a decaying mode whereas a positive real eigenvalue monotonic instability.

If A is real, complex eigenvalues always occur in conjugate pairs. Each pair corresponds to an oscillatory mode, and is expressed (for the i-th mode) by

$$\lambda_i = \sigma_i \pm j\omega_{p_i} \tag{6.20}$$

The real component σ_i gives the damping of the i-th mode. A negative σ represents a damped oscillatory mode, however a positive σ represents an oscillatory instability. The imaginary component ω_{p_i} gives the oscillation frequency of the i-th mode, and is expressed by

$$f_{p_i} = \frac{\omega_{p_i}}{2\,\pi} \tag{6.21}$$

The damping ratio of the i-th mode is given by

$$\zeta_i = \frac{-\sigma_i}{\sqrt{\sigma_i^2 + \omega_{p_i}^2}} = \frac{-\sigma_i}{|\lambda_i|} \tag{6.22}$$

A positive damping ratio determines the decay rate of the oscillation amplitude.

In this compendium we assume that the eigenvalues are distinct, i.e. $\lambda_i \neq \lambda_j$.

Eigenvectors

Any non-zero vector V_i^r which satisfies

$$A\,V_i^r = \lambda_i\,V_i^r \tag{6.23}$$

is termed the right eigenvector of A corresponding to the eigenvalue λ_i. Note that V_i^r is a column vector of order $n_x \times 1$.

Similarly, any non-zero vector V_i^l which satisfies

$$V_i^l\,A = \lambda_i\,V_i^l \tag{6.24}$$

is termed the left eigenvector of A corresponding to the eigenvalue λ_i. Note that V_i^l is a row vector of order $1 \times n_x$.

It can be shown that

$$\begin{aligned} V_i^l\,V_j^r &= 0 \\ V_i^l\,V_i^r &= C_i \neq 0 \end{aligned} \tag{6.25}$$

Note that V_i^r (or V_i^l) is not a unique solution, $k\,V_i^r$ (where k is a scalar) can also be a solution. Due to this property, it is possible to normalize the right and left eigenvectors so that

$$V_i^l\,V_i^r = \begin{bmatrix} v_{i1}^l & v_{i2}^l & \cdots & v_{in_x}^l \end{bmatrix} \begin{bmatrix} v_{1i}^r \\ v_{2i}^r \\ \vdots \\ v_{n_x i}^r \end{bmatrix} = 1 \tag{6.26}$$

Modal matrices

For the purpose of modal analysis, it is convenient to introduce the following modal matrices:

$$V^R = \begin{bmatrix} V_1^r & V_2^r & \cdots & V_{n_x}^r \end{bmatrix} = \begin{bmatrix} v_{11}^r & v_{12}^r & \cdots & v_{1n_x}^r \\ v_{21}^r & v_{22}^r & \cdots & v_{2n_x}^r \\ \vdots & \vdots & \ddots & \vdots \\ v_{n_x1}^r & v_{n_x2}^r & \cdots & v_{n_xn_x}^r \end{bmatrix} \tag{6.27}$$

$$\begin{aligned} V^L &= \begin{bmatrix} \left(V_1^l\right)^T & \left(V_2^l\right)^T & \cdots & \left(V_{n_x}^l\right)^T \end{bmatrix}^T = \begin{bmatrix} v_{11}^l & v_{12}^l & \cdots & v_{1n_x}^l \\ v_{21}^l & v_{22}^l & \cdots & v_{2n_x}^l \\ \vdots & \vdots & \ddots & \vdots \\ v_{n_x1}^l & v_{n_x2}^l & \cdots & v_{n_xn_x}^l \end{bmatrix} \\ &= \left(V^R\right)^{-1} \quad \text{(by virtue of equations (6.25)-(6.26))} \end{aligned} \tag{6.28}$$

and the diagonal matrix

$$\Lambda = \begin{bmatrix} \lambda_1 & 0 & \cdots & 0 \\ 0 & \lambda_2 & \cdots & 0 \\ \vdots & \vdots & \ddots & \vdots \\ 0 & 0 & \cdots & \lambda_{n_x} \end{bmatrix} \tag{6.29}$$

In terms of the above matrices, equation (6.23) can also be expressed as

$$A\,V^R = V^R\,\Lambda \quad \Rightarrow \quad (V^R)^{-1}\,A\,V^R = (V^R)^{-1}\,V^R\,\Lambda = \Lambda \tag{6.30}$$

that is, the matrix A can be diagonalized by its modal matrix V^R.

System modes

Since the state matrix A is (normally) not a diagonal matrix, the dynamic of each state variable of the unforced LTI system (6.18) is a linear combination of the other state variables. Therefore, it may be difficult to analytically identify the parameters that have significant impact on the dynamic of each state variable. To overcome this difficulty, the system (6.18) is (based on the modal matrices) transformed to an LTI system whose state matrix is diagonalized as follows.

First, a new state vector ξ is established by the transformation

$$\xi(t) = V^L\,x(t) = (V^R)^{-1}\,x(t) \tag{6.31}$$

which implies that

$$x(t) = V^R\,\xi(t) \tag{6.32}$$

Substitution of this transformation (i.e. (6.32)) in the original system (6.18) results in the following transformed system

$$\begin{aligned} V^R\,\dot{\xi}(t) &= A\,V^R\,\xi(t) \quad \Rightarrow \\ \dot{\xi}(t) &= (V^R)^{-1}\,A\,V^R\,\xi(t) \\ &= \Lambda\,\xi(t) \qquad \text{(by virtue of equation (6.30))} \end{aligned} \tag{6.33}$$

Based on the above transformation, we are now dealing with an LTI system whose state matrix is diagonal, i.e. Λ. The dynamic system (6.33) represents n_x uncoupled first-order differential equations of the form

$$\dot{\xi}_i(t) = \lambda_i\,\xi_i(t) \qquad \text{for} \quad i = 1 \cdots n_x \tag{6.34}$$

whose solutions with respect to time t are given by

$$\xi_i(t) = \xi_i(0)\,e^{\lambda_i t} \qquad \text{for} \quad i = 1 \cdots n_x \tag{6.35}$$

where, $\xi_i(0)$ is the initial value of $\xi_i(t)$ at $t = 0$. From (6.31), we have

$$\xi_i(0) = V_i^l\,x(0) \tag{6.36}$$

which is a scalar, and will henceforth be denoted by α_i. Moreover, $x(0)$ is the initial values of all the original state variables $x(t)$ at $t = 0$.

Next, by virtue of the expression for x in (6.31) and also equations (6.35)-(6.36), the solution of the original dynamic system (6.18) can be expressed by

$$x(t) = \sum_{i=1}^{n_x} V_i^r \left[V_i^l \, x(0)\right] \, e^{\lambda_i t} = \sum_{i=1}^{n_x} V_i^r \, \alpha_i \, e^{\lambda_i t} \tag{6.37}$$

or for the k-th state variable

$$x_k(t) = \sum_{i=1}^{n_x} v_{ki}^r \, \alpha_i \, e^{\lambda_i t} \tag{6.38}$$

Equation (6.35) gives the each dynamic mode (corresponding to $e^{\lambda_i t}$) of the system with magnitude α_i. However, the dynamic response of each state variable is given by equation (6.38) which is a linear combination of n_x dynamic modes.

From equation (6.32) (and also (6.37)) we can see that the right eigenvector V_i^r describes how each dynamic mode is distributed among the system states x that is it describes the mode shape. From equation (6.36) we can however see that the left eigenvector V_i^l weighs the contribution of the initial condition $x(0)$ to the i-th mode. Thus, the k-th element of V_i^r measures the activity of the state variable x_k in the i-th mode, and the k-th element of V_i^l weighs the contribution of this activity to the i-th mode [15].

Eigenvalue sensitivity

Let a_{kj} be the element of the state matrix A in the k-th row and j-th column. The sensitivity of the eigenvalue λ_i to a_{kj} is then determined by differentiating (6.23) with respect to a_{kj} which yields

$$\frac{\partial A}{\partial a_{kj}} V_i^r + A \frac{\partial V_i^r}{\partial a_{kj}} = \frac{\partial \lambda_i}{\partial a_{kj}} V_i^r + \lambda_i \frac{\partial V_i^r}{\partial a_{kj}} \tag{6.39}$$

Pre-multiplication of (6.39) by V_i^l gives

$$V_i^l \frac{\partial A}{\partial a_{kj}} V_i^r + V_i^l A \frac{\partial V_i^r}{\partial a_{kj}} = V_i^l \frac{\partial \lambda_i}{\partial a_{kj}} V_i^r + V_i^l \lambda_i \frac{\partial V_i^r}{\partial a_{kj}}$$

or

$$\underbrace{V_i^l \, V_i^r}_{=1} \frac{\partial \lambda_i}{\partial a_{kj}} = V_i^l \frac{\partial A}{\partial a_{kj}} V_i^r + \underbrace{(V_i^l A - V_i^l \lambda_i)}_{=0} \frac{\partial V_i^r}{\partial a_{kj}}$$

which results in

$$\frac{\partial \lambda_i}{\partial a_{kj}} = v_{ik}^l v_{ji}^r \tag{6.40}$$

since all elements of $\frac{\partial A}{\partial a_{kj}}$ are zero, except for the element in the k-th row and j-th column which is equal to 1.

Information about the sensitivity of eigenvalues to system parameters such as excitation system gain, generator inertia and line reactance is of importance in power system stability analysis and control. Eigenvalue sensitivity can also be used to ascertain which power system parameters have a major impact on damping of particular modes.

Participation factor

For small-signal stability and control, it is of importance to measure properly the participation of state variables within a mode i. The right eigenvector V_i^r might be a possible choice for this issue since its elements measure the activity of the state variables in the mode i. However, these elements are dependent on the dimensions and scaling of the state variables which are incommensurable. As a solution to this problem, a related but dimensionless measure p_{ki} termed participation factor has been presented in [15]. The participation factor p_{ki} is a measure of the relative participation of the k-th state variable in the i-th mode, and vice versa. It is given by

$$p_{ki} = v_{ik}^l \, v_{ki}^r = v_{ki}^r \, v_{ik}^l \tag{6.41}$$

Since the v_{ki}^r measures the activity of the state variable x_k in the i-th mode and the v_{ik}^l weighs the contribution of this activity to the mode, the product p_{ki} measures the net participation. Furthermore, a comparison between (6.41) and (6.40) shows that

$$\frac{\partial \lambda_i}{\partial a_{kk}} = p_{ki} \tag{6.42}$$

For the purpose of small-signal analysis, it is convenient to introduce a matrix $\mathcal{P}$ containing all participation factors. This matrix is termed participation matrix, and has the form

$$\begin{aligned} \mathcal{P} &= [\mathcal{P}_1 \quad \mathcal{P}_2 \quad \cdots \quad \mathcal{P}_{n_x}] \\ &= \begin{bmatrix} p_{11} & p_{12} & \cdots & p_{1n_x} \\ p_{21} & p_{22} & \cdots & p_{2n_x} \\ \vdots & \vdots & \ddots & \vdots \\ p_{n_x1} & p_{n_x2} & \cdots & p_{n_xn_x} \end{bmatrix} = \begin{bmatrix} v_{11}^r \, v_{11}^l & v_{12}^r \, v_{21}^l & \cdots & v_{1n_x}^r \, v_{n_x1}^l \\ v_{21}^r \, v_{12}^l & v_{22}^r \, v_{22}^l & \cdots & v_{2n_x}^r \, v_{n_x2}^l \\ \vdots & \vdots & \ddots & \vdots \\ v_{n_x1}^r \, v_{1n_x}^l & v_{n_x2}^r \, v_{2n_x}^l & \cdots & v_{n_xn_x}^r \, v_{n_xn_x}^l \end{bmatrix} \end{aligned} \tag{6.43}$$

Modal controllability and observability

Consider the LTI system (6.17). By applying the transformation (6.32) to (6.17), the following is obtained

$$\dot{\xi}(t) = \Lambda \, \xi(t) + V^L B \, \mathcal{U}(t) \tag{6.44}$$

$$\mathcal{Y}(t) = C \, V^R \, \xi(t) \tag{6.45}$$

Equation (6.44) can be written as n_x uncoupled equations

$$\dot{\xi}_i(t) = \lambda_i \xi_i(t) + \sum_{j=1}^{r} V_i^l B_j u_j(t) = \lambda_i \xi_i(t) + \sum_{j=1}^{r} c_{ij} u_j(t) \qquad \text{for} \quad i = 1 \cdots n_x \quad (6.46)$$

where, $c_{ij} = V_i^l B_j$, V_i^l is the i-th row of V^L, B_j is the j-th column of B and $u_j(t)$ is the j-th element of $\mathcal{U}(t)$.

Obviously, the input u_j has no effect on the i-th mode if $c_{ij} = 0$. Thus, the i-th mode is controllable if and only if there is any $c_{ij} \neq 0$.

The $n_x \times r$ matrix $V^L B$ is termed as the mode controllability matrix whose element in the i-th row and j-th column is c_{ij}. By inspecting this matrix, the controllable (or uncontrollable) modes can be identified. For instance, the i-th mode is uncontrollable if the i-th row of this matrix is zero.

Equation (6.45) can also be written as

$$\mathcal{Y}_j(t) = \sum_{i=1}^{n_x} C_j V_i^r \xi_i(t) = \sum_{i=1}^{n_x} o_{ji} \xi_i(t) \qquad \text{for} \quad j = 1 \cdots m \quad (6.47)$$

where, $o_{ji} = C_j V_i^r$, C_j is the j-th row of C and V_i^r is the i-th column of V^R.

It is evident that the i-the mode cannot be observed in the j-th output variable (i.e. $\mathcal{Y}_j(t)$) if $o_{ji} = 0$. Thus, the i-the mode is observable if and only if there is any $o_{ji} \neq 0$.

The $m \times n_x$ matrix $C\,V^R$ is termed as the mode observability matrix whose element in the j-th row and i-th column is o_{ji}. By inspecting this matrix, the observable (or unobservable) modes can be identified. For instance, the i-th mode is unobservable if the i-th column of this matrix is zero.

Residues

Consider again equations (6.44). Let $m = r = 1$, i.e. a Single Input Single Output (SISO) system. Taking Laplace transform, the following is obtained

$$\xi(s) = (s\underline{\mathbf{1}} - \Lambda)^{-1} V^L B \mathcal{U}(s) \quad (6.48)$$

Taking Laplace transform of (6.45), and substituting (6.48) into it, we have then

$$\mathcal{Y}(s) = C\,V^R (s\underline{\mathbf{1}} - \Lambda)^{-1} V^L B \mathcal{U}(s) \quad (6.49)$$

where, s is the Laplace operator. Since Λ is a diagonal matrix, the transfer function of (6.17) can be expressed in partial function as

$$G(s) = \frac{\mathcal{Y}(s)}{\mathcal{U}(s)} = \sum_{i=1}^{n_x} \frac{\bar{R}_i}{s - \lambda_i} \quad (6.50)$$

where, $\bar{R}_i$ is the residue of $G(s)$ at λ_i and is expressed as

$$\bar{R}_i = C\,V_i^r\,V_i^l\,B \quad (6.51)$$

Note that $R_i = |\bar{R}_i|$ is indeed the product of the controllability and observability of the i-th mode.

Having a feedback transfer function of the form $H(s,k) = kH(s)$ (where, k is a constant gain) between output and input, it can be shown that [16]

$$\frac{\partial \lambda_i}{\partial k} = \bar{R}_i \, H(\lambda_i) \tag{6.52}$$

For small values of gain, equation (6.52) can be written as

$$\frac{\Delta \lambda_i}{\Delta k} = \bar{R}_i \, H(\lambda_i) \tag{6.53}$$

Thus, if a feedback transfer function is added to the system, the i-th eigenvalue will be changed as

$$\Delta \lambda_i = \bar{R}_i \, H(\lambda_i, k) \tag{6.54}$$

Equations (6.53)-(6.54) will be used later on designing a PSS for improving damping of electromechanical oscillations.

6.2.2 Small signal stability of power systems

Let the dynamic of a power system be described by

$$\begin{aligned} \dot{x} &= f(x,y) \\ 0 &= g(x,y) \end{aligned} \tag{6.55}$$

where, $f(x,y)$ and $g(x,y)$ are given by equations (5.7)-(5.11).

By linearizing the above non-linear system around an operating point (x_0, y_0), the small signal analysis can be applied to the linearized system. In Example 5.1, it has been shown how (x_0, y_0) can be calculated.

The linearized system is given by

$$\Delta \dot{x} = f_x \Delta x + f_y \Delta y \tag{6.56}$$

$$0 = g_x \Delta x + g_y \Delta y \tag{6.57}$$

where

$$f_x = \left[\frac{\partial f(x,y)}{\partial x}\right]_{x=x_o \, ; \, y=y_o} \quad , \quad f_y = \left[\frac{\partial f(x,y)}{\partial y}\right]_{x=x_o \, ; \, y=y_o}$$

$$g_x = \left[\frac{\partial g(x,y)}{\partial x}\right]_{x=x_o \, ; \, y=y_o} \quad , \quad g_y = \left[\frac{\partial g(x,y)}{\partial y}\right]_{x=x_o \, ; \, y=y_o}$$

f_x, f_y, g_x and g_y are Jacobian matrices which are explained in Section B.2 of Appendix B.

From equation (6.57), Δy can be solved as

$$\Delta y = -(g_y)^{-1} g_x \Delta x \tag{6.58}$$

Assuming $(g_y)^{-1}$ is non-singular, and substituting Δy into equation (6.56), the following is obtained

$$\Delta \dot{x} = \left(f_x - f_y (g_y)^{-1} g_x\right) \Delta x = A_s \, \Delta x \tag{6.59}$$

where, A_s is the overall system state matrix.

Equation (6.59) is the linearized system of the non-linear system (6.55). The eigenvalues of the linearized system are given by equation (6.19) where the state matrix A is replaced by A_s. Note however that the linearized system (6.59) has (at least) two zero eigenvalues which are not of interest in this analysis. The first zero eigenvalue is due to use of absolute changes in rotor angles (i.e. $\Delta\delta$) as state variables. Since angles appear as differences, an equal change in each of the rotor angles has no effect on power flow equations. Therefore, the state matrix columns associated with the rotor angles are linearly dependent, and make the state matrix A_s singular. The second zero eigenvalue is due to zero damping constant, i.e. $D_i = 0$. If there is any non-zero damping constant in the system, the second zero eigenvalue vanishes. If the system contains an infinite bus, these two eigenvalues vanish.

Example 6.1 *Consider the system shown in Figure 6.2.*

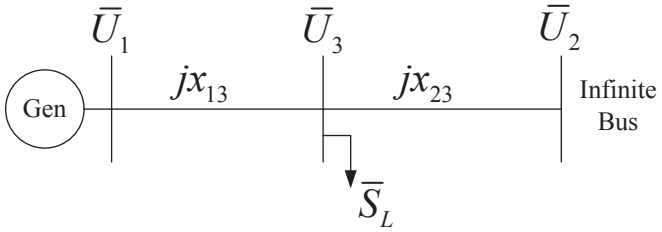

Figure 6.2. A single generator connected to an infinite bus.

The system data is given as follows (all values are expressed in pu):

Gen: *One-axis model is used with* $H = 4$, $D = 0$, $x'_d = 0.15$, $x_d = 1$, $x_t = 0.1$, $T'_{do} = 6$ *and* $P_m = 1$

Network: $\bar{U}_1 = 1\angle\theta_1$, $\bar{U}_2 = 1\angle 0$ *(infinite bus),* $x_{13} = 0.3$, $x_{23} = 0.5$ *the load model* (5.2) *is used with* $P_{L0} = 0.7$, $Q_{L0} = 0.01$, $mp = 1$ *and* $mq = 2$.

a) *Linearize the system around its equilibrium point, and calculate the eigenvalues. Calculate also the damping ratio and frequency of the oscillatory mode.*

b) *Draw the block diagram of the linearized system and calculate the synchronizing and damping torque coefficients at the oscillatory mode.*

c) *Simulate the non-linear dynamic system for the following cases*

Case 1: *A three-phase fault occurs at bus 3. The fault is cleared after 100 (ms) (large disturbance).*

Case 2: *20% of the active load is disconnected during 100 (ms) (small disturbance).*

a) The system dynamic is given by

$$\begin{aligned}\dot{x} &= f(x,y)\\ 0 &= g(x,y)\end{aligned}$$

From load flow, x_0 and y_0 are calculated.

$$\begin{aligned}x_0 &= [\delta_0 \quad \omega_0 \quad E'_{q_0}]^T = [40.2667\,(\text{deg.}) \quad 0 \quad 1.1001]^T\\ y_0 &= [\theta_{1_0} \quad \theta_{3_0} \quad U_{1_0} \quad U_{3_0}]^T = [27.1319\,(\text{deg.}) \quad 8.9674\,(\text{deg.}) \quad 1 \quad 0.9623]^T\end{aligned}$$

Linearizing the non-linear system around (x_0, y_0), the following is obtained

$$\Delta\dot{x} = A_s\,\Delta x + B\,\mathcal{U}$$

or

$$\begin{aligned}\begin{bmatrix}\Delta\dot{\delta}\\ \Delta\dot{\omega}\\ \Delta\dot{E}'_q\end{bmatrix} &= \begin{bmatrix}a_{11} & a_{12} & a_{13}\\ a_{21} & a_{22} & a_{23}\\ a_{31} & a_{32} & a_{33}\end{bmatrix}\begin{bmatrix}\Delta\delta\\ \Delta\omega\\ \Delta E'_q\end{bmatrix} + \begin{bmatrix}0 & 0\\ \frac{1}{M} & 0\\ 0 & \frac{1}{T'_{do}}\end{bmatrix}\begin{bmatrix}\Delta P_m\\ \Delta E_f\end{bmatrix}\\ &= \begin{bmatrix}0 & 1 & 0\\ -27.1507 & 0 & -37.6825\\ -0.1094 & 0 & -0.2912\end{bmatrix}\begin{bmatrix}\Delta\delta\\ \Delta\omega\\ \Delta E'_q\end{bmatrix} + \begin{bmatrix}0 & 0\\ 39.2699 & 0\\ 0 & 0.1667\end{bmatrix}\begin{bmatrix}\Delta P_m\\ \Delta E_f\end{bmatrix}\end{aligned}$$

where, $\Delta P_m = \Delta E_f = 0$.

The eigenvalues are

$$\begin{aligned}\lambda_1, \lambda_2 &= -0.0758 \pm j\,5.2081\\ \lambda_3 &= -0.1395\end{aligned}$$

Therefore, the equilibrium point is asymptotically stable. The damping ratio and the frequency of the oscillatory mode (λ_1 or λ_2) are

$$\begin{aligned}\zeta_1 &= \frac{-\sigma_1}{|\lambda_1|} = 0.0146\\ f_{p1} &= \frac{\omega_{p_1}}{2\,\pi} = 0.8289\,(Hz)\end{aligned}$$

b) Figure 6.3 shows the block diagram of the linearized system which is redrawn as shown in Figure 6.4 to have a representation similar to the well-known K representation.

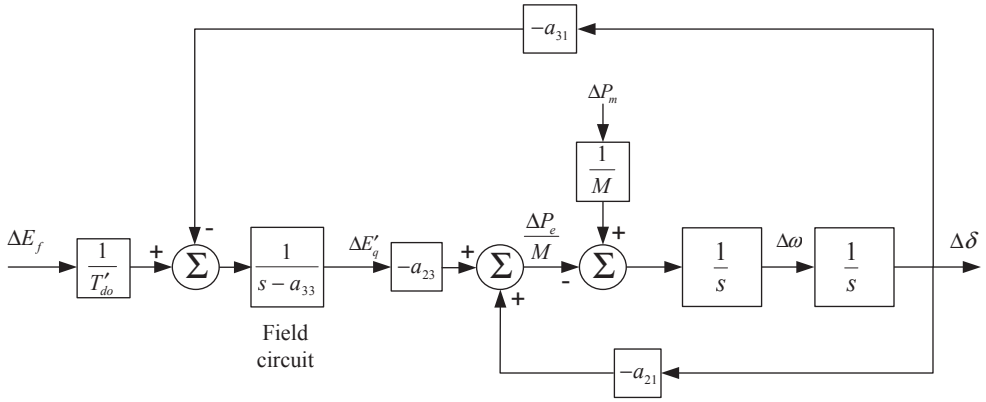

Figure 6.3. Block diagram representation with one-axis model.

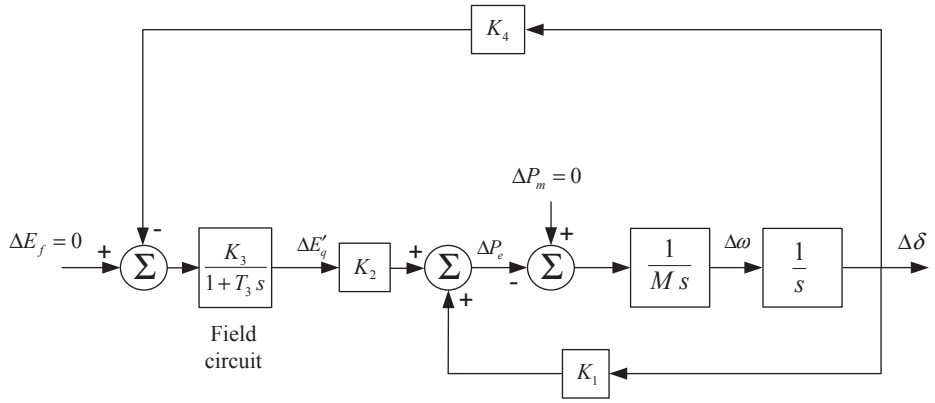

Figure 6.4. The well-known K block diagram representation with one-axis model.

In Figure 6.4

$$\begin{aligned} K_1 &= -M\,a_{21} = 0.6914 \quad , \quad K_2 = -M\,a_{23} = 0.9596 \\ T_3 &= -\frac{1}{a_{33}} = 3.4339 \quad , \quad K_3 = \frac{T_3}{T'_{do}} = 0.5723 \\ K_4 &= -T'_{do}\,a_{31} = 0.6563 \end{aligned} \tag{6.60}$$

In the steady-state, $\Delta P_e = \frac{\omega_s}{\omega_g}\,\Delta T_e = \Delta T_e$ (expressed in (pu)), since $\omega_s = \omega_g$. In the transient-state based on the assumption $\frac{\omega_s}{\omega_g} \approx 1$, we may also assume that $\Delta P_e \approx \Delta T_e$. Therefore, the synchronizing and damping torque coefficients at the oscillatory mode λ_1 are calculated by setting $s = \lambda_1 = \sigma_1 + j\,\omega_{p_1}$ as follows.

From the block diagram of Figure 6.4

$$\begin{aligned} \Delta\delta = \frac{1}{s}\,\Delta\omega = \frac{1}{\sigma_1 + j\,\omega_{p_1}}\,\Delta\omega \qquad \Rightarrow \\ j\Delta\delta = \frac{1}{\omega_{p_1}}\,\Delta\omega - \frac{\sigma_1}{\omega_{p_1}}\,\Delta\delta \end{aligned} \tag{6.61}$$

Also,

$$\begin{aligned}\Delta T_e &= \Delta P_e = K_1\,\Delta\delta + K_2\,\Delta E'_q \\ &= K_1\,\Delta\delta + K_2\,F(s=\lambda_1)\,\Delta\delta \\ &= K_1\,\Delta\delta + K_2\,(F_{re} + jF_{im})\,\Delta\delta \\ &= K_1\,\Delta\delta + K_2\;F_{re}\,\Delta\delta + K_2\,F_{im}\,j\Delta\delta\end{aligned} \tag{6.62}$$

where,

$$F(s=\lambda_1) = -\frac{K_3\,K_4}{1+T_3\,s} = -\frac{K_3\,K_4}{1+T_3\,\lambda_1} = F_{re} + jF_{im}$$

Substituting $j\Delta\delta$ from (6.61) into (6.62), the following is obtained

$$\begin{aligned}\Delta T_e &= \left[K_1 + K_2\,\left(F_{re} - F_{im}\frac{\sigma_1}{\omega_{p_1}}\right)\right]\,\Delta\delta + \left[\frac{K_2\,F_{im}}{\omega_{p_1}}\right]\,\Delta\omega \\ &= (K_1 + K_S|_{1axis})\;\Delta\delta + K_D|_{1axis}\,\Delta\omega \\ &= K_S\,\Delta\delta + K_D\,\Delta\omega \\ &= 0.6908\,\Delta\delta + 0.0039\,\Delta\omega\end{aligned} \tag{6.63}$$

The synchronizing and damping torque coefficients can also be calculated as follows.

From the block diagram of Figure 6.4

$$\begin{aligned}\Delta\delta = \frac{1}{s}\,\Delta\omega = \frac{1}{\sigma_1 + j\,\omega_{p_1}}\,\Delta\omega = \frac{\sigma_1 - j\,\omega_{p_1}}{|\lambda_1|^2}\,\Delta\omega \qquad \Rightarrow \\ j\omega_{p_1}\Delta\omega = \sigma_1\,\Delta\omega - |\lambda_1|^2\,\Delta\delta\end{aligned} \tag{6.64}$$

Also,

$$\begin{aligned}\Delta T_e &= \Delta P_e = -M\,s\,\Delta\omega = -M\,[(\sigma_1 + j\,\omega_{p_1})\,\Delta\omega] \\ &= -\,M\,[\sigma_1\,\Delta\omega + j\,\omega_{p_1}\,\Delta\omega] \\ &= -\,M\,[\sigma_1\,\Delta\omega + \sigma_1\,\Delta\omega - |\lambda_1|^2\,\Delta\delta] \\ &= M\,|\lambda_1|^2\,\Delta\delta + (-2\,M\,\sigma_1)\,\Delta\omega \\ &= K_S\,\Delta\delta + K_D\,\Delta\omega \\ &= 0.6908\,\Delta\delta + 0.0039\,\Delta\omega\end{aligned} \tag{6.65}$$

Comments:

- With the classical model $\Delta E'_q = 0$. Therefore, the synchronizing torque coefficient would be $K_S = K_1 = 0.6914$. Moreover, since there is no inherent damping in the system (i.e. $D = 0$), the damping torque coefficient would be $K_D = D = 0$.
- With one-axis model, we see that a positive damping torque component exists, i.e. $K_D = K_D|_{1axis} = 0.0039$. This is due to variation of E'_q since it is a state variable. Having an inherent damping in the system, the damping torque coefficient is then

$K_D = D + K_D|_{1axis}$. The effect of field flux variation (i.e. E'_q) on the system damping can also be observed in (6.12) which is the time derivative of the energy function (i.e. $\dot{\mathcal{V}}$) along the non-linear system. Since $\dot{\mathcal{V}} < 0$, the equilibrium point is asymptotically stable that is the system is dissipative (or there is a positive damping in the system). If E'_q is constant, then $\dot{E'}_q = 0$ which results in $\dot{\mathcal{V}} = 0$ that is the system is conservative (or there is no damping in the system).

- The contributions of the state variable E'_q to the synchronizing and damping torques coefficients are $K_S|_{1axis} = K_S - K_1 = -0.0006$ and $K_D|_{1axis} = 0.0039$ that is a (small) negative contribution to the synchronizing torque, but a (small) positive contribution to the damping torque.

c) Figure 6.5 shows variations of the rotor angle for each case. Obviously the system is transiently unstable for case 1, however it is stable for case 2 (small-signal stability). For case 2, we see that the amplitude of the oscillation decays with time that is there is a positive damping in the system. Note that the damping ratio is about 1.5%. It can also be observed that the oscillation frequency is about

$$f_p = \frac{1}{T} = \frac{1}{t_2 - t_1} = \frac{1}{3.27 - 2.06} = 0.8264\,(Hz)$$

Thus, the calculated frequency $f_p = \dfrac{\omega_p}{2\,\pi} = 0.8289\,(Hz)$ (which is based on the linearized system) gives a good estimation of the oscillation frequency.

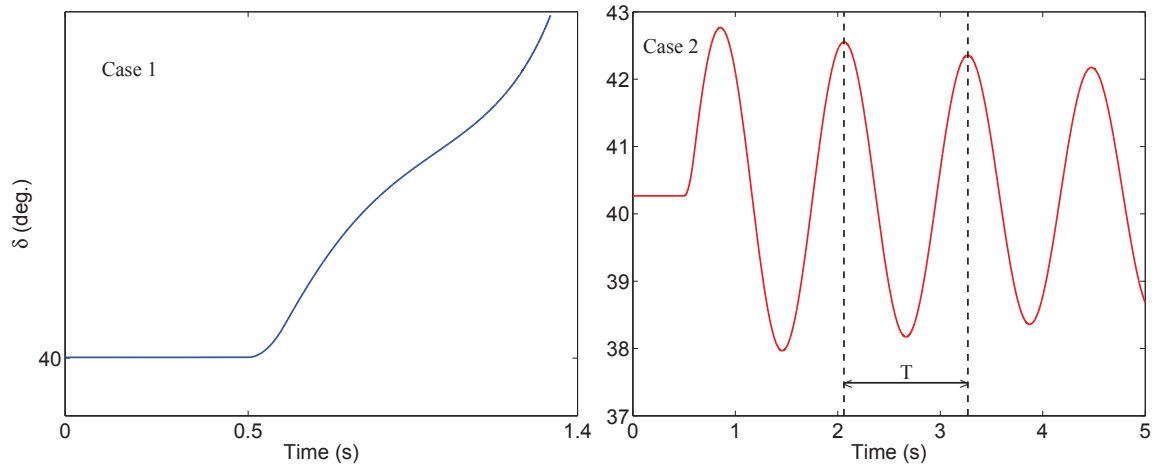

Figure 6.5. Variations of rotor angle with one-axis model.

Example 6.2 *To improve the transient stability of the above system, the AVR shown in Figure 3.14 is added to the generator with* $T_e = 0.01$ *and* $K_A = 150$ *(*$E_{f_{max}}$ *and* $E_{f_{min}}$ *are not considered in this example).*

a) *Simulate the non-linear dynamic system for the two cases in Example 6.1.*

b) *Based on the small-signal analysis, describe the effect of the AVR on the system stability.*

a) Figure 6.6 shows variations of the rotor angle for each case. For case 1, it is obvious that the AVR with its high gain (i.e. K_A) has improved the transient (or first swing) stability. However, it has introduced a negative damping in electromechanical oscillations which results in oscillatory instability. This phenomenon is a typical small-signal stability problem in today's power systems. In case 2, small-signal instability is obvious.

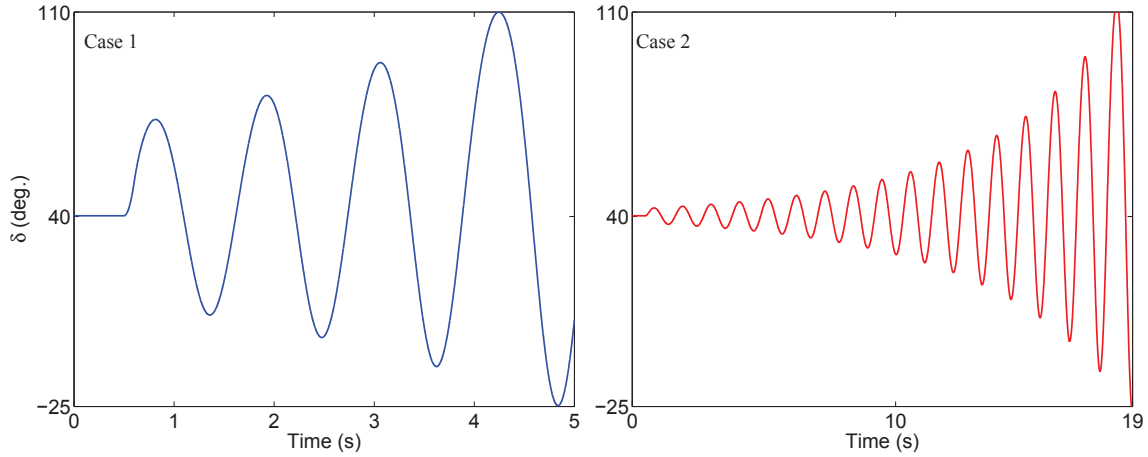

Figure 6.6. Variations of rotor angle with AVR in the system.

b) Because of the AVR, the differential equation (3.101) with $U_{PSS} = 0$ is added to the $f(x, y)$. From load flow, x_0 and y_0 are calculated.

$$\begin{aligned} x_0 &= [\delta_0 \quad \omega_0 \quad E'_{q_0} \quad E_{f_0}]^T = [40.2670\,(\text{deg.}) \quad 0 \quad 1.1001 \quad 1.5296]^T \\ y_0 &= [\theta_{1_0} \quad \theta_{3_0} \quad U_{1_0} \quad U_{3_0}]^T = [27.1320\,(\text{deg.}) \quad 8.9674\,(\text{deg.}) \quad 1 \quad 0.9623]^T \end{aligned}$$

Linearization of the non-linear system around (x_0, y_0) gives

$$\Delta\dot{x} = A_s\,\Delta x(t) + B\,\mathcal{U}(t)$$

or

$$\begin{aligned} \begin{bmatrix} \Delta\dot{\delta} \\ \Delta\dot{\omega} \\ \Delta\dot{E}'_q \\ \Delta\dot{E}_f \end{bmatrix} &= \begin{bmatrix} a_{11} & a_{12} & a_{13} & a_{14} \\ a_{21} & a_{22} & a_{23} & a_{24} \\ a_{31} & a_{32} & a_{33} & a_{34} \\ a_{41} & a_{42} & a_{43} & a_{44} \end{bmatrix} \begin{bmatrix} \Delta\delta \\ \Delta\omega \\ \Delta E'_q \\ \Delta E_f \end{bmatrix} + \begin{bmatrix} 0 \\ 0 \\ 0 \\ \frac{K_A}{T_e} \end{bmatrix} \Delta U_{ref} \\ &= \begin{bmatrix} 0 & 1 & 0 & 0 \\ -27.1507 & 0 & -37.6825 & 0 \\ -0.1094 & 0 & -0.2912 & 0.1667 \\ 2283.9790 & 0 & -11436.1545 & -100 \end{bmatrix} \begin{bmatrix} \Delta\delta \\ \Delta\omega \\ \Delta E'_q \\ \Delta E_f \end{bmatrix} + \begin{bmatrix} 0 \\ 0 \\ 0 \\ 15000 \end{bmatrix} \Delta U_{ref} \end{aligned} \tag{6.66}$$

The eigenvalues are

$$\begin{aligned} \lambda_1, \lambda_2 &= 0.1752 \pm j\,5.8155 \\ \lambda_3 &= -74.1635 \\ \lambda_4 &= -26.4780 \end{aligned}$$

The damping ratio and the frequency of the oscillatory mode are

$$\begin{aligned} \zeta_1 &= \frac{-\sigma_1}{|\lambda_1|} = -0.0301 \\ f_{p1} &= \frac{\omega_{p_1}}{2\,\pi} = 0.9256\,(Hz) \end{aligned}$$

Obviously, the equilibrium point is unstable.

Figure 6.7 shows the block diagram of the linearized system.

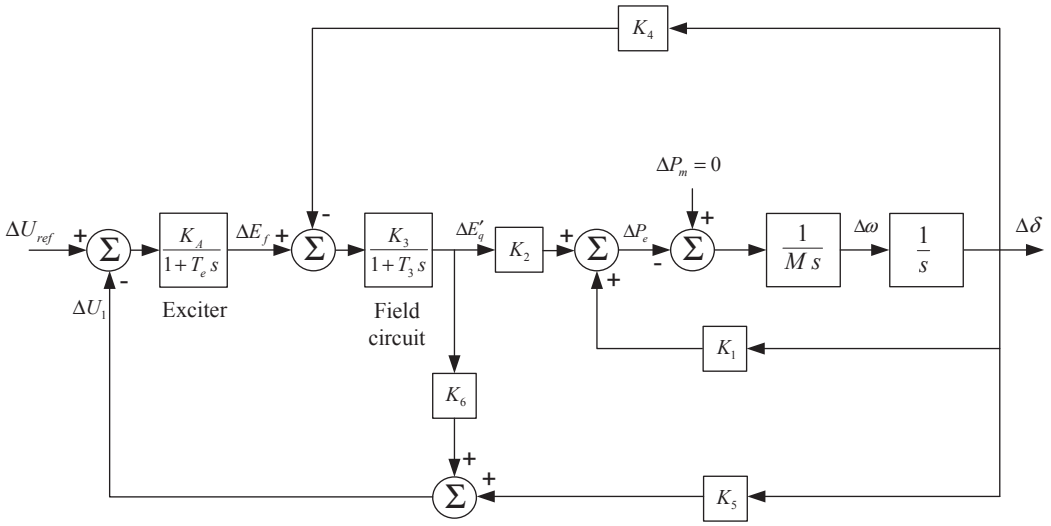

Figure 6.7. Block diagram representation with AVR.

where,

$$K_5 = -\frac{K_A}{T_e} a_{41} = -0.1523 \quad \text{and} \quad K_6 = -\frac{K_A}{T_e} a_{43} = 0.7624$$

From the block diagram of Figure 6.7 (with $\Delta U_{ref} = 0$)

$$\begin{aligned} \Delta T_e &= K_1\,\Delta\delta + K_2\,\Delta E'_q \\ &= K_1\,\Delta\delta + K_2\,F(s=\lambda_1)\,\Delta\delta \\ &= (K_1 + K_S|_{AVR})\;\Delta\delta + K_D|_{AVR}\,\Delta\omega \\ &= K_S\,\Delta\delta + K_D\,\Delta\omega \\ &= 0.8620\,\Delta\delta - 0.0089\,\Delta\omega \end{aligned} \tag{6.67}$$

where,

$$F(s=\lambda_1) = -\frac{K_3\,K_5\,K_A + K_3\,K_4\,(1+T_e\,s)}{(1+T_e\,s)(1+T_3\,s) + K_3\,K_6\,K_A} = F_{re} + jF_{im}$$

The contributions of the AVR to the synchronizing and damping torques coefficients are $K_S|_{AVR} = K_S - K_1 = 0.1706$ and $K_D|_{AVR} = -0.0089$ that is a positive contribution to the synchronizing torque, but a negative contribution to the damping torque.

As discussed earlier, participation factors are useful in identifying those states which have the most impact on a selected mode. Furthermore, p_{ki} gives the sensitivity of λ_i to the diagonal element a_{kk} of the state matrix. The participation matrix (only the magnitudes of the participation factors are of interest) of system (6.66) is

$$|\mathcal{P}| = \begin{array}{c} \begin{matrix} \lambda_1 & \lambda_2 & \lambda_3 & \lambda_4 \end{matrix} \\ \begin{bmatrix} 0.4933 & 0.4933 & 0.0007 & 0.0144 \\ 0.4933 & 0.4933 & 0.0007 & 0.0144 \\ 0.0295 & 0.0295 & 0.5386 & 1.5087 \\ 0.0018 & 0.0018 & 1.5401 & 0.5375 \end{bmatrix} \end{array} \begin{matrix} \Delta\delta \\ \Delta\omega \\ \Delta E'_q \\ \Delta E_f \end{matrix}$$

From the participation matrix we see that $\Delta\delta$ and $\Delta\omega$ are the state variables which have the most influence on the unstable mode. Furthermore, the state variables ΔE_f and $\Delta E'_q$ are the state variables which have most influence on the third and forth modes, respectively.

To stabilize the unstable mode, a power system stabilizer (PSS) is added in the excitation system. To provide positive damping, the PSS must be tuned such that it produces a component in phase with $\Delta\omega$.

Example 6.3 *Use the PSS shown in Figure 3.17 without the washout block and with only one lead-lag filter. Let ω be the input signal.*

- **a)** *For the unstable mode (i.e. $s = \lambda_1$), tune the lead-lag block of the PSS so that the PSS produces a component in phase with $\Delta\omega$, and find a value for K_{PSS} so that the damping ratio of this mode is about 15%.*
- **b)** *Simulate the non-linear dynamic system for the two cases in Example 6.1.*
- **c)** *Linearize the system, and calculate the eigenvalues. Calculate also the damping ratio and frequency of the oscillatory mode.*

a) Figure 6.8 shows the block diagram representation with PSS. In the figure

$$\begin{aligned} \Delta U_{PSS} =& K_{PSS}\, H(s)\, \Delta\omega = K_{PSS}\, \frac{1+T_1\, s}{1+T_2\, s}\, \Delta\omega \\ =& K_{PSS}\, |H(s)|\, e^{j\, arg(H(s))}\, \Delta\omega \end{aligned}$$

From the block diagram of Figure 6.8 (with $\Delta U_{ref} = 0$)

$$\begin{aligned} \Delta T_e =& K_1\, \Delta\delta + K_2\, \Delta E'_q \\ =& K_1\, \Delta\delta + K_2(\Delta E'_q|_{AVR} + \Delta E'_q|_{PSS}) \\ =& (K_1 + K_S|_{AVR})\ \Delta\delta + K_D|_{AVR}\, \Delta\omega + K_2\, \Delta E'_q|_{PSS} \end{aligned} \tag{6.68}$$

where

$$\begin{aligned} \Delta E'_q|_{PSS} =& F(s)\, \Delta U_{PSS} = \frac{K_A\, K_3}{(1+T_e\, s)(1+T_3\, s) + K_3\, K_6\, K_A}\, \Delta U_{PSS} \\ =& K_{PSS}\, |H(s)|\, |F(s)|\, e^{j\,\varphi}\, \Delta\omega \end{aligned} \tag{6.69}$$

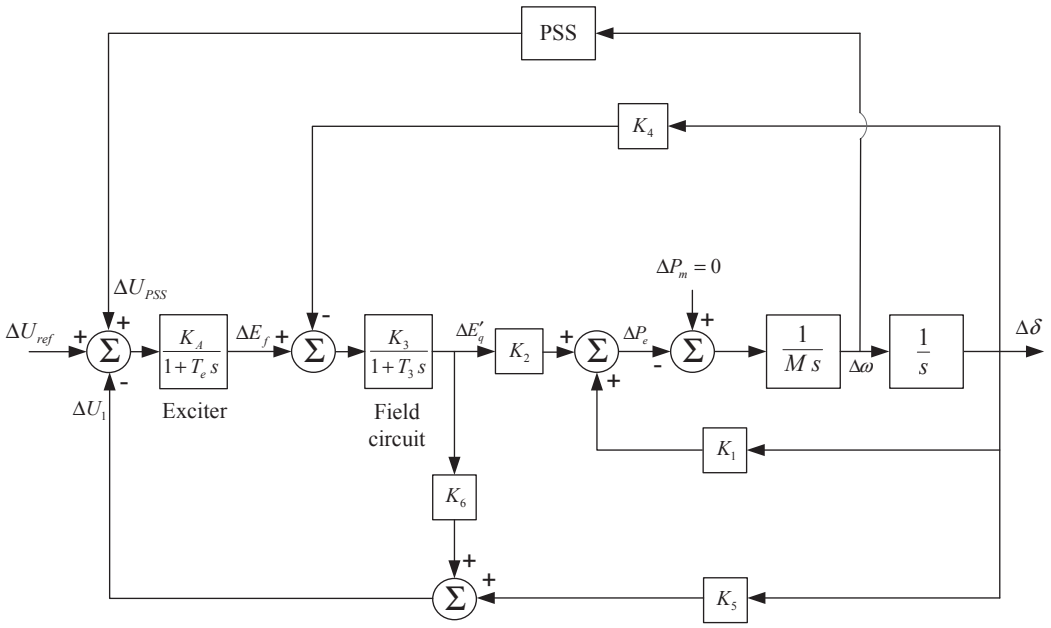

Figure 6.8. Block diagram representation with PSS.

where,

$$\varphi = arg(H(s)) + arg(F(s))$$

From equation (6.69) we can see that $\Delta E'_q|_{PSS}$ will be in phase with $\Delta\omega$ if $\varphi = 0$.

Let $\phi = -arg(F(s = \lambda_1)) = 16.9619$ (deg.). Then, $\Delta E'_q|_{PSS}$ will be in phase with $\Delta\omega$ if

$$\arctan\left(\frac{\omega_{p_1} T_1}{1 + \sigma_1 T_1}\right) - \arctan\left(\frac{\omega_{p_1} T_2}{1 + \sigma_1 T_2}\right) = \phi \tag{6.70}$$

Now, by setting a value for T_1 (or T_2), then T_2 (or T_1) can easily be determined.

T_1 and T_2 can also (**approximately**) be determined by setting $s = \lambda_1 \approx j\omega_{p_1}$ (i.e. $\sigma_1 \approx 0$ in equation (6.70)), and

$$T_1 = \alpha\, T \quad , \quad T_2 = T \quad \text{where,} \quad T = \frac{1}{\omega_{p_1}\sqrt{\alpha}} \quad \text{and} \quad \alpha > 1 \tag{6.71}$$

Then from equation (6.70) (with $\sigma_1 \approx 0$), α and T can easily be determined as follows

$$\begin{aligned}
\alpha &= \left(1 + 2\tan^2(\phi)\right) + \sqrt{\left(1 + 2\tan^2(\phi)\right)^2 - 1} = \frac{1 + \sin(\phi)}{1 - \sin(\phi)} = 1.8238 \\
T &= \frac{1}{\omega_{p_1}\sqrt{\alpha}} = 0.1273 \\
T_1 &= 0.2322 \\
T_2 &= 0.1273
\end{aligned} \tag{6.72}$$

With the above T_1 and T_2, the total damping torque coefficient is then

$$K_D = K_D|_{AVR} + K_2\, K_{PSS}\, |H(s)|\, |F(s)| \tag{6.73}$$

Note that $|H(s)|$ and $|F(s)|$ are the magnitudes of the transfer functions $H(s = \lambda_1)$ and $F(s = \lambda_1)$ (with $\lambda_1 = \sigma_1 + j\omega_{p_1}$), respectively.

The desired damping ratio for the unstable mode is $\zeta_{des} = 0.15$. Based on equations (6.22), (6.65) and (6.73), K_{PSS} can be determined as follows so that the ζ_{des} is obtained.

$$\begin{aligned} \sigma_{des} &= -\frac{\zeta_{des}\,\omega_{p_1}}{\sqrt{1-\zeta_{des}^2}} = -0.8823 \\ K_{D_{des}} &= -2\,M\,\sigma_{des} = 0.0449 \\ K_{PSS} &= \frac{K_{D_{des}} - K_D|_{AVR}}{K_2\,|H(s)|\,|F(s)|} = 0.0333 \end{aligned} \tag{6.74}$$

Note that the aim is to shift only the real part of the unstable mode (i.e. $\sigma_1 = 0.1751$) to the new position $\sigma_{des} = -0.8823$. Therefore, we let the imaginary part be unchanged, i.e. $\omega_{p_{des}} = \omega_{p_1} = 5.8155$.

b) Because of the power system stabilizer, the differential equation (3.102) is added to the $f(x, y)$ of Example 6.2. Note that in differential equation $\dot{E}_f$, the auxiliary signal U_{PSS} is not longer zero since it is now a state variable.

From load flow, x_0 and y_0 are calculated.

$$\begin{aligned} x_0 &= [\delta_0 \quad \omega_0 \quad E'_{q_0} \quad E_{f_0} \quad U_{PSS_0}]^T = [40.2670\,(\text{deg.}) \quad 0 \quad 1.1001 \quad 1.5296 \quad 0]^T \\ y_0 &= [\theta_{1_0} \quad \theta_{3_0} \quad U_{1_0} \quad U_{3_0}]^T = [27.1320\,(\text{deg.}) \quad 8.9674\,(\text{deg.}) \quad 1 \quad 0.9623]^T \end{aligned}$$

Figure 6.9 shows variations of the rotor speed for each case. It is obvious that not only the system is stabilized, but also it is well-damped for both cases.

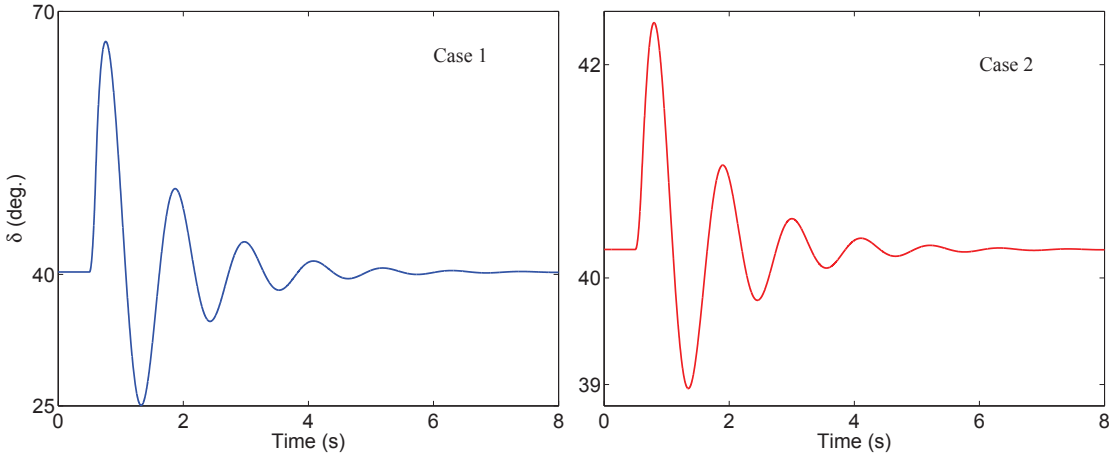

Figure 6.9. Variations of rotor angle with PSS in the system.

c) Linearization of the non-linear system around (x_0, y_0) gives

$$\Delta\dot{x} = A_s\,\Delta x(t) + B\,\mathcal{U}(t)$$

or

$$\begin{bmatrix} \Delta\dot{\delta} \\ \Delta\dot{\omega} \\ \Delta\dot{E}'_q \\ \Delta\dot{E}_f \\ \Delta\dot{U}_{PSS} \end{bmatrix} = \begin{bmatrix} a_{11} & a_{12} & a_{13} & a_{14} & a_{15} \\ a_{21} & a_{22} & a_{23} & a_{24} & a_{25} \\ a_{31} & a_{32} & a_{33} & a_{34} & a_{25} \\ a_{41} & a_{42} & a_{43} & a_{44} & a_{45} \\ a_{51} & a_{52} & a_{53} & a_{54} & a_{55} \end{bmatrix} \begin{bmatrix} \Delta\delta \\ \Delta\omega \\ \Delta E'_q \\ \Delta E_f \\ \Delta U_{PSS} \end{bmatrix} + \begin{bmatrix} 0 \\ 0 \\ 0 \\ \frac{K_A}{T_e} \\ 0 \end{bmatrix} \Delta U_{ref}$$

$$= \begin{bmatrix} 0 & 1 & 0 & 0 & 0 \\ -27.1507 & 0 & -37.6825 & 0 & 0 \\ -0.1094 & 0 & -0.2912 & 0.1667 & 0 \\ 2283.9790 & 0 & -11436.1545 & -100 & 15000 \\ -1.6512 & 0.2619 & -2.2917 & 0 & -7.8537 \end{bmatrix} \begin{bmatrix} \Delta\delta \\ \Delta\omega \\ \Delta E'_q \\ \Delta E_f \\ \Delta U_{PSS} \end{bmatrix} + \begin{bmatrix} 0 \\ 0 \\ 0 \\ 15000 \\ 0 \end{bmatrix} \Delta U_{ref}$$

The eigenvalues are

$$\begin{aligned} \lambda_1, \lambda_2 &= -0.9136 \pm j\, 5.6900 \\ \lambda_3 &= -75.7613 \\ \lambda_4 &= -20.3710 \\ \lambda_5 &= -10.1854 \end{aligned}$$

The damping ratio and the frequency of the oscillatory mode are

$$\begin{aligned} \zeta_1 &= \frac{-\sigma_1}{|\lambda_1|} = 0.1585 \\ f_{p1} &= \frac{\omega_{p_1}}{2\,\pi} = 0.9056\,(Hz) \end{aligned}$$

We see that σ_1, ω_{p_1} and ζ_1 do not have exactly the values which were desired. However, the differences are small.

Example 6.4 *For the unstable mode (i.e. λ_1), use equations* (6.51)-(6.54) *to tune the PSS so that the damping ratio of this mode is about 15%. Let T_1 and T_2 be defined as in equation* (6.71).

We select $\Delta\omega$ as output variable, to have the following system which is of form given by (6.17)

$$\begin{aligned} \dot{x}(t) &= A\,x(t) + B\,\mathcal{U}(t) \\ \mathcal{Y}(t) &= C\,x(t) \end{aligned} \tag{6.75}$$

where, $x(t)$, A, B and $\mathcal{U}(t)$ are given in equation (6.66), and $C = [0 \quad 1 \quad 0 \quad 0]$. The transfer function of the system without PSS is given by

$$G(s) = \frac{\mathcal{Y}(s)}{\mathcal{U}(s)} = \frac{\Delta\,\omega(s)}{\Delta\,U_{ref}(s)} = \sum_{i=1}^{4} \frac{\bar{R}_i}{s - \lambda_i} \tag{6.76}$$

The residue of the unstable mode is given by

$$\bar{R}_1 = C\, V_1^r\, V_1^l\, B = -21.968 + j7.3534 = 23.166 \angle 161.49\,(\text{deg.}) \qquad (6.77)$$

Adding a PSS in the generator, we are then dealing with the following feedback control system

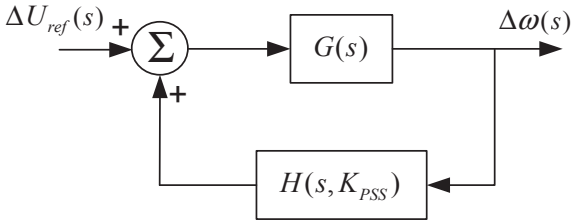

Figure 6.10. Feedback control system.

It is well-known that the residue of an eigenvalue gives the direction of the eigenvalue departure for a small change of system parameters.

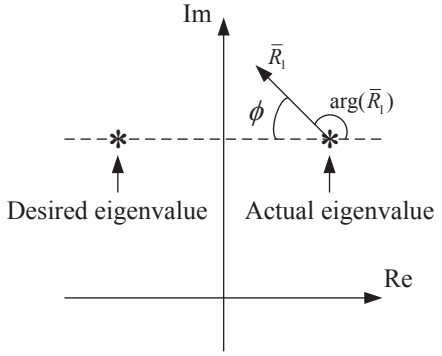

Figure 6.11. Direction of the eigenvalue departure for small changes.

From equation (6.54) and Figure 6.11, it is obvious that to move the actual eigenvalue to the desired position (only the real part is changed) the argument of $H(s = \lambda_1)$ (denoted by ϕ) must be $\phi = 180 - arg(\bar{R}_1)$.

In this case the residue argument of the interest mode is $arg(\bar{R}_1) = 161.49$ (deg.). Substituting $\phi = 18.51$ into equation (6.72), $T_1 = 0.2389$ and $T_2 = 0.1238$ are obtained.

From equation (6.54) we have

$$\Delta\lambda_1 = \sigma_{des} - \sigma_1 = \bar{R}_1\, H(s,k) = K_{PSS}\, R_1\, |H(s)|\, e^{j\,\pi} \quad \Rightarrow$$

$$K_{PSS} = \frac{|\Delta\lambda_1|}{R_1\, |H(s)|} = 0.0329$$

where, $s = \lambda_1$, $R_1 = 23.166$ is the magnitude of the residue $\bar{R}_1$ and $|H(s)| = 1.3895$ is the magnitude of the lead-lag block of the PSS.

We can see that the obtained values to tune the PSS with this method (also known as the residue technique) are almost similar to the values obtained in Example 6.3.

Example 6.5 *Consider again the lossless system shown in Figure 5.6. The one-axis model is used for the generators, and the loads are considered as impedance loads. Furthermore, all generators are equipped with AVR shown in Figure 3.14 where* $E_{fmax} = 5$ *and* $E_{fmin} = -5$ *(pu). By using the PSS shown in Figure 3.17, make an appropriate damping in the system.*

We firstly analyse the system without PSS. The RNM is used to describe the dynamic of the system. Figure 6.12 shows the simulation results for a fault at BUS 4 with clearing time $t_c = 0.1$ (s). The plotted rotor angles are defined in the COI reference frame. As shown in the figure, the system is unstable. The variations of the field voltages of the generators are shown in the figure. As the system approaches its separation (i.e. losing its synchronism), the AVRs behave in a "bang-bang" control manner between their limits.

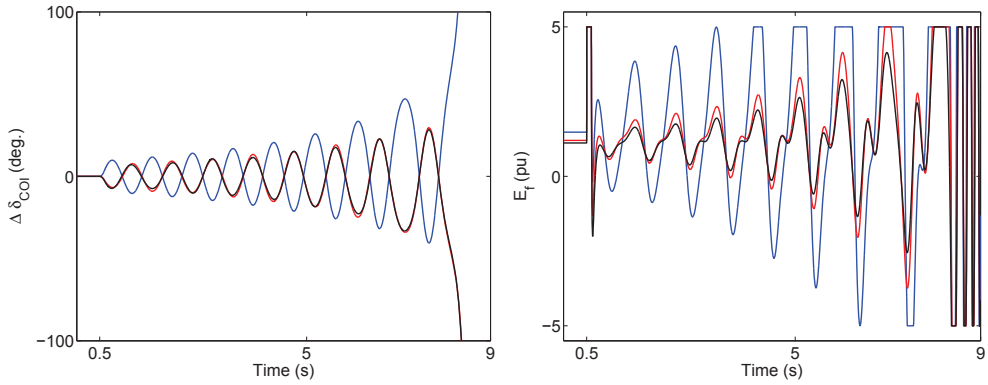

Figure 6.12. Variations of $\Delta\delta$ in the COI reference frame and E_f of Gen1 (blue), Gen2 (red) and Gen3 (black).

Next, the system is linearized around its stable equilibrium point (see also Appendix B). Table 6.1 shows some results from the linear analysis of the system.

Mode	λ	f_p	ζ
1	-80.3517	0	1
2	-86.7215	0	1
3	-89.7353	0	1
4	-19.9922	0	1
5	0.1918 + j 7.2317	1.1510	-0.0265
6	0.1918 - j 7.2317	1.1510	-0.0265
7	0.0136 + j 10.0342	1.5970	-0.0014
8	0.0136 - j 10.0342	1.5970	-0.0014
9	-13.8411	0	1
10	-10.6692	0	1
11	0.0022		
12	-0.0022		

Table 6.1. Some results from the linear analysis of the system.

The last two eigenvalues can be considered as zero eigenvalues. As shown in the table, since the system has $3 \times 4 = 12$ state variables, there are twelve eigenvalues two of which are zeros (why?). The linearized system has two unstable oscillatory modes, namely mode 5 and mode 7. Below, the participation matrix (with the magnitudes of the participation factors) of these two unstable modes is given. In mode 5, the participation factor of the rotor speed of the Gen 1 has the highest value. However in mode 7, the participation factor of the rotor speed of the Gen 3 has the highest value.

$$|\mathcal{P}| = \begin{matrix} \\ \\ \\ \\ \\ \\ \\ \\ \\ \\ \\ \end{matrix} \begin{matrix} \lambda_5 & \lambda_7 \\ \end{matrix} \begin{bmatrix} 0.2618 & 0.0001 \\ 0.1367 & 0.2076 \\ 0.0919 & 0.2917 \\ 0.2618 & 0.0001 \\ 0.1367 & 0.2076 \\ 0.0919 & 0.2917 \\ 0.0270 & 0.0000 \\ 0.0010 & 0.0008 \\ 0.0004 & 0.0005 \\ 0.0021 & 0.0000 \\ 0.0001 & 0.0001 \\ 0.0000 & 0.0001 \end{bmatrix} \begin{matrix} \Delta\delta_1 \\ \Delta\delta_2 \\ \Delta\delta_3 \\ \Delta\omega_1 \\ \Delta\omega_2 \\ \Delta\omega_3 \\ \Delta E'_{q1} \\ \Delta E'_{q2} \\ \Delta E'_{q3} \\ \Delta E_{f1} \\ \Delta E_{f2} \\ \Delta E_{f3} \end{matrix} \tag{6.78}$$

Figure 6.13 shows the mode shapes of the unstable modes based on the right eigenvector (the elements corresponding to the rotor angles) of each mode, Gen 1 (in blue), Gen 2 (in red) and Gen 3 (in black).

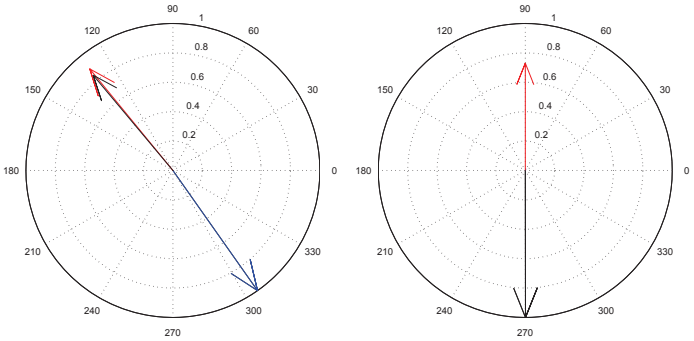

Figure 6.13. The mode shapes of the unstable modes.

From Table 6.1, it can be found that mode 5 has the lowest damping ratio and frequency. From the participation matrix and the compass plots, it can be concluded that Gen 1 is mostly participated in this mode. Therefore, a PSS is used in Gen 1 with ω_1 as its input signal. Based on the linearized system (6.17), $\mathcal{U} = \Delta U_{1ref}$ and

$$\begin{aligned} B =& [0 \ 0 \ 0 \ 0 \ 0 \ 0 \ 0 \ 0 \ 0 \ \frac{K_{A1}}{T_{e1}} \ 0 \ 0]^T \quad \text{i.e. of order } 12 \times 1 \\ C =& [0 \ 0 \ 0 \ 1 \ 0 \ 0 \ 0 \ 0 \ 0 \ 0 \ 0 \ 0] \quad \text{i.e. of order } 1 \times 12 \end{aligned} \tag{6.79}$$

the feedback control system is shown in Figure 6.14 which will be studied.

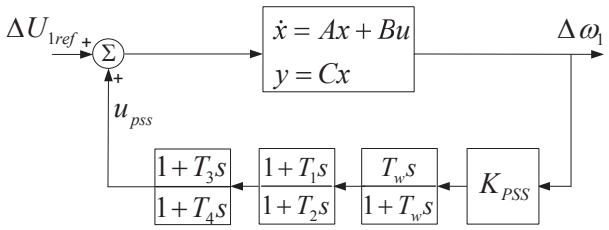

Figure 6.14. The closed-loop of the linearized system with a PSS in Gen1.

To find appropriate values for T_1-T_4, the residue of the selected unstable mode and the angle ϕ must firstly be calculated, and they are

$$\bar{R}_5 = CV_5^r V_5^l B = 12.0799 \angle 146.2486 \quad \Rightarrow \quad \phi = 180 - arg(\bar{R}_5) = 33.7514 \tag{6.80}$$

Let "n_f" be the number of the lead-lag filters. Then, if

$$\begin{aligned} 0 < |\phi| \leq \ \ 60 &\Rightarrow n_f = 1 \\ 60 < |\phi| \leq 120 &\Rightarrow n_f = 2 \\ 120 < |\phi| \leq 180 &\Rightarrow n_f = 1 \quad \text{set} \quad \phi = -arg(\bar{R}_i) \quad , \quad K_{PSS} = K_{PSS}\, e^{j\,\pi} \end{aligned} \tag{6.81}$$

Now, T_1-T_4 can be obtained by

$$\begin{aligned} \alpha = & \frac{1+\sin(\frac{\phi}{n_f})}{1-\sin(\frac{\phi}{n_f})} \quad , \quad T = \frac{1}{\omega_p \sqrt{\alpha}} \quad , \quad T_1 = \alpha\, T \quad , \quad T_2 = T \\ n_f = & 1 \quad \Rightarrow \quad T_3 = T_4 \quad \text{to remove the second lead-lag filter.} \\ n_f = & 2 \quad \Rightarrow \quad T_3 = T_1 \quad T_4 = T_2 \end{aligned} \tag{6.82}$$

The above equations are also valid for a negative $arg(\bar{R}_i)$, but then $\phi = -180 - arg(\bar{R}_i)$.

In this example for the PSS of Gen 1, $n_f = 1$, $T_1 = 0.2587$ and $T_2 = 0.0739$ are obtained. Setting $T_3 = T_4 = 1$, the contribution of the second lead-lag filter is removed. Having obtained the parameters of the PSS, the root locus diagram of the feedback control system as a function of K_{PSS} can be drawn as shown in Figure 6.15.

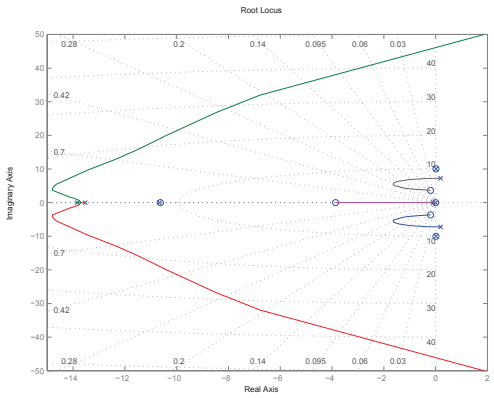

Figure 6.15. The root locus of the system modes and the selected unstable mode 5.

The next step is to choose an appropriate gain K_{PSS} to stabilize the unstable mod 5, but not destabilize the other modes. To find an appropriate gain, the eigenvalues of the closed-loop system will be determined for $K_{PSS} = [0 : 0.001 : 0.2]$. For each K_{PSS} the least damping ratio of all the oscillatory modes is obtained which will be plotted as shown in Figure 6.16. The appropriate gain is the one which gives the maximum of the least damping ratios, i.e. $K_{PSS} = 0.0920$.

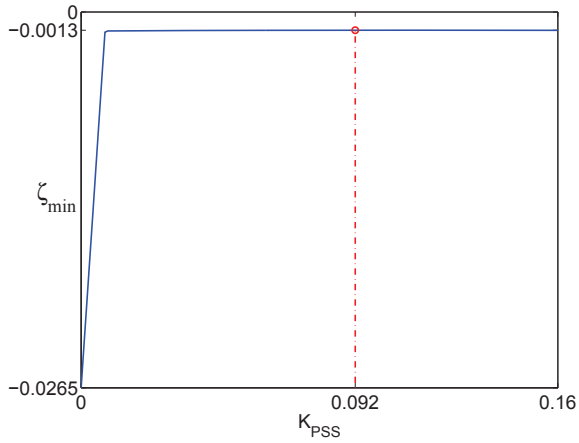

Figure 6.16. The least damping ratios of all the oscillatory modes versus the gain K_{PSS}.

Table 6.2 shows some linear analysis results of the closed-loop system with the obtained T_1, T_2 and K_{PSS} for the first PSS which is installed in Gen 1. As shown in the table, the

Mode	λ	f_p	ζ
1	-89.7262	0	1
2	-88.1906	0	1
3	-82.1920	0	1
4	-12.2383 + j 13.2524	2.1092	0.6784
5	-12.2383 - j 13.2524	2.1092	0.6784
6	-15.5262	0	1
7	-10.6337	0	1
8	0.0129 + j 10.0337	1.5969	-0.0013
9	0.0129 - j 10.0337	1.5969	-0.0013
10	-1.4835 + j 6.2597	0.9963	0.2306
11	-1.4835 - j 6.2597	0.9963	0.2306
12	-0.8440	0	1
13	0.0007		
14	-0.0007		

Table 6.2. Some results from the linear analysis with a PSS in Gen1.

system is still unstable since it has an unstable mode, i.e. mode 8 whose participation factors corresponding to each state variable are given below where S_{11} and S_{21} are the state variables defined in (3.103).

$$|\mathcal{P}| =$$

$\Delta\delta_1$	$\Delta\delta_2$	$\Delta\delta_3$	$\Delta\omega_1$	$\Delta\omega_2$	$\Delta\omega_3$	$\Delta E'_{q1}$	$\Delta E'_{q2}$	$\Delta E'_{q3}$	ΔE_{f1}	ΔE_{f2}	ΔE_{f3}	S_{11}	S_{21}
[0.00	0.2093	0.2900	0.00	0.2093	0.2900	0.00	0.0008	0.0005	0.00	0.0001	0.0001	0.0	0.0]^T

Figure 6.17 shows the variations of $\Delta\delta_{COI}$ for the same fault, and the mode shape of mode 8.

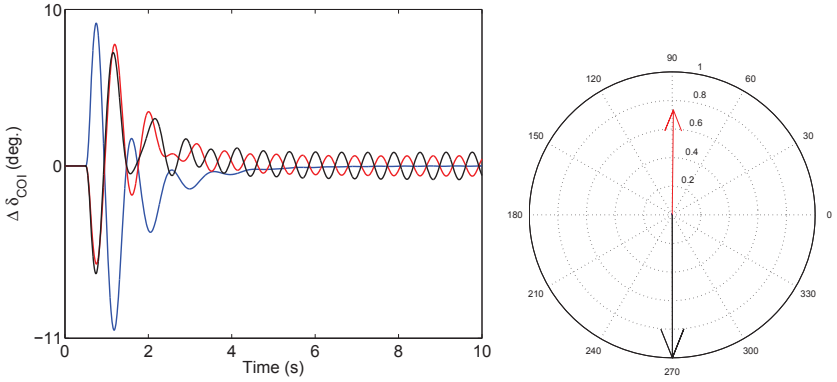

Figure 6.17. Variations of $\Delta\delta$ in the COI reference frame and the mode shape of mode 8. Gen 1 (blue), Gen 2 (red) and Gen 3 (black).

From the participation factors and the mode shape in Figure 6.17, it can be concluded that Gen 3 is mostly participated in this unstable mode, and the second PSS should be used in Gen 3 whose rotor speed will be the input signal of the PSS. Then, we will have a similar closed-loop system as shown in Figure 6.14, but with different A, B and C. Note that the new open-loop system includes the dynamic of the first PSS, therefore the new A is of order 14×14, and the new B and C must be defined.

In a similar manner as described above for the first PSS, we find that $n_f = 1$, $T_1 = 0.2718$ and $T_2 = 0.0365$ for the second PSS. The appropriate gain ($K_{PSS} = 0.1320$) is obtained from Figure 6.18.

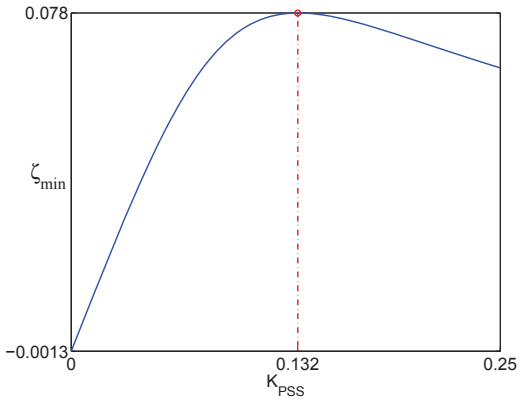

Figure 6.18. The least damping ratios of all the oscillatory modes versus the gain K_{PSS}.

The data of each PSS and their impact on the system are summarized in Table 6.3. As shown in the table, by using the second PSS the system becomes stable and its least damping ratio is about 8%. The PSS parameters obtained from the linearized system, are now used in the nonlinear system.

PSS	Gen	T_1	T_2	K_{PSS}	ζ_{min}	f_p
0					-0.0265	1.1510
1	1	0.2587	0.0739	0.0920	-0.0013	1.5969
2	3	0.2718	0.0365	0.1320	0.078	1.4819

Table 6.3. The obtained values of the parameters of each PSS and their impact on the system.

Figure 6.19 shows the response of the nonlinear system for the same fault at BUS 4.

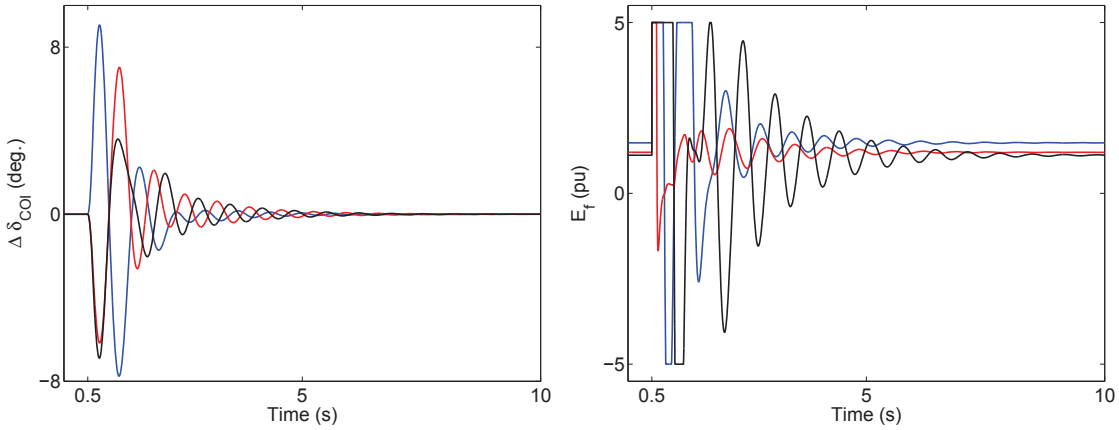

Figure 6.19. Variations of $\Delta\delta$ in the COI reference frame and E_f of Gen1 (blue), Gen2 (red) and Gen3 (black).

Next, we will study how the other input signals will affect the system damping and stability. Using ω_{sime} (see equations (6.14) and (6.15)) as input signal, then based on Figure 6.12 and Figure 6.13 the following ω_{sime} is used for the first PSS,

$$\omega_{sime1} = \frac{H_1\,\omega_1}{H_1} - \frac{H_2\,\omega_2 + H_3\,\omega_3}{H_2 + H_3} = \omega_1 - \frac{H_2\,\omega_2 + H_3\,\omega_3}{H_2 + H_3}$$

which results in the following output vector C.

$$C = [0\ 0\ 0\ 1\ \ -\frac{H_2}{H_2+H_3}\ \ -\frac{H_3}{H_2+H_3}\ \ 0\ 0\ 0\ 0\ 0\ 0] \tag{6.83}$$

For the second PSS, based on Figure 6.17, the following ω_{sime} is used

$$\omega_{sime2} = \frac{H_3\,\omega_3}{H_3} - \frac{H_2\,\omega_2}{H_2} = \omega_3 - \omega_2$$

Then for the second PSS, we have the following B and C.

$$\begin{aligned} B =& [0\ 0\ 0\ 0\ 0\ 0\ 0\ 0\ 0\ 0\ 0\ \frac{K_{A3}}{T_{e3}}\ 0\ 0]^T \quad \text{i.e. of order } 14\times 1 \\ C =& [0\ 0\ 0\ 0\ \ -1\ 1\ 0\ 0\ 0\ 0\ 0\ 0\ 0\ 0] \quad \text{i.e. of order } 1\times 14 \end{aligned} \tag{6.84}$$

Using P_{ei} as input signal (see equation (B.12)), the output vector C is obtained by equation (B.14).

The data of each PSS and their impact on the system are summarized in Table 6.4.

PSS	Gen	u_{in}	T_1	T_2	n_f	K_{PSS}	ζ_{min}	f_p
0							-0.0265	1.1510
1	1	ω_1	0.2587	0.0739	1	0.0920	-0.0013	1.5969
		ω_{sime1}	0.2480	0.0771	1	0.0520	-0.0013	1.5969
		P_{e1}	0.0440	0.4350	1	-2.6710	-0.0013	1.5969
2	3	ω_3	0.2718	0.0365	1	0.1320	0.0780	1.4819
		ω_{sime2}	0.2702	0.0368	1	0.1450	0.2942	1.0246
		P_{e3}	0.0462	0.2148	1	-3.8910	0.0809	1.4828

Table 6.4. The obtained values of the parameters of each PSS and their impact on the system.

Figure 6.20 also shows the response of the nonlinear system for the same fault at BUS 4, with different input signals.

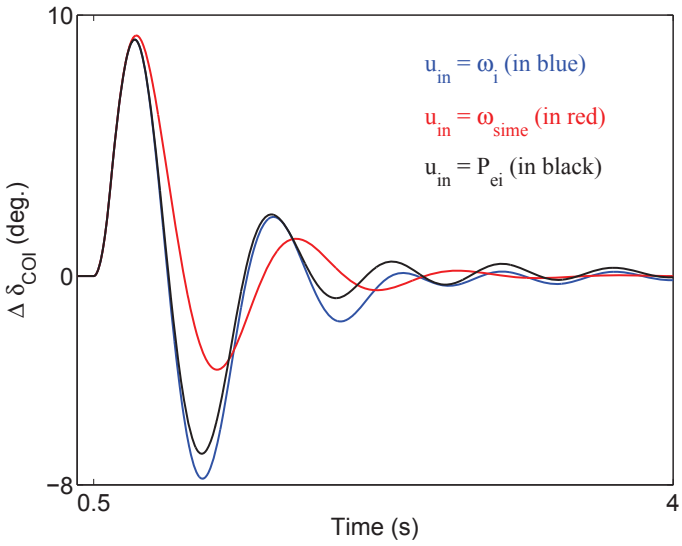

Figure 6.20. Variations of $\Delta\delta_1$ in the COI reference frame with different input signals.

From Table 6.4 and Figure 6.20, it is obvious that ω_{sime} as input signal implies a better power oscillations damping. However, it should be noted that ω_{sime} is based on remote information. The geographical distances between the source of information (i.e. the generators in this example) may be from 500 (km) to 2000 (km). Therefore, the quality and reliability of the remote information are important factors for power system stability and control.

Chapter 7

Voltage stability

It is well-known that the reactive power and the voltage are closely coupled. An injection of reactive power into a bus will result in increasing of the bus voltage, and a consumption of reactive power at a bus will result in decreasing of the bus voltage. In this chapter it will be shown that reactive power has a fundamental impact on voltage stability.

In recent decays, the term "voltage collapse" (or voltage instability) has been used to describe the reason for the blackouts of December 19, 1978, in France; December 27, 1983, in Sweden; July 23, 1987, in Tokyo; September 23, 2003, in Sweden and Denmark [17], and September 28, 2003, in Italy [18]. As introduced in Chapter 1, voltage stability refers to the ability of a power system to maintain steady voltages at all buses in the system after being subjected to a disturbance from a given initial operating condition. Voltage instability normally occurs in heavily stressed systems in the form of a progressive and uncontrollable fall in voltage. A main factor causing voltage instability is inadequate reactive power supply which is normally a consequence of load demand increase, line outages, as well as shortage of reactive power resources.

A criterion for voltage stability is that at a given operating point for every bus i

$$\frac{d\,Q_i}{d\,U_i} > 0 \tag{7.1}$$

where Q_i is the injected reactive power at bus i. The physical interpretation of (7.1) is that reactive power injection at a bus i will result in increasing of the voltage magnitude of bus i. The system is voltage unstable if for any bus i, the condition (7.1) is not satisfied [6].

7.1 Voltage stability analysis

Like transient stability analysis, voltage stability analysis of a power system is also an extensive and complicated task. However, it turns out that many of the most important phenomena and mechanism can be found in very simple systems. In large and complicated systems it is often hard to distinguish the fundamental and decisive phenomena from the more irrelevant ones. It is therefore of importance to study simple systems to get an insight into and understanding of the basics, that can be used in the analysis of more complex systems.

Consider the Single-Load-Infinite-Bus (SLIB) system shown in Figure 7.1.

This simple system may represent a generation area from which power is delivered to a load area via a transmission system with long lines (this is indeed a good representation of the Swedish power system). In the figure, the generation area is considered as a

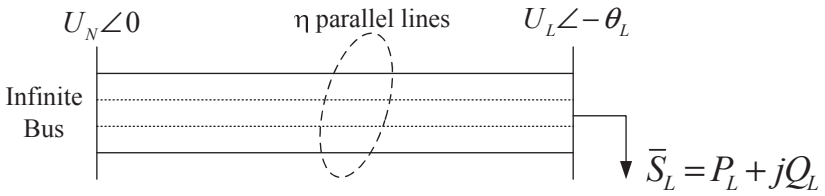

Figure 7.1. SLIB system.

strong system (represented by an infinite bus) and the load area as an equivalent load represented by $\bar{S}_L$. The transmission system is composed of η identical parallel long lines. Each line is represented by a series reactance x (i.e. the transmission system is assumed lossless). The short-circuit power at the load bus is given by

$$S_{sc} = \frac{U_N^2}{X_{eq}}\,(\text{pu}), \quad \text{where} \quad X_{eq} = \frac{x}{\eta}\,(\text{pu}) \tag{7.2}$$

The short-circuit power S_{sc} measures the system voltage strength. As seen from a point in the system, the network can be considered as "weak" if the short-circuit power is low at this point (normally due to high X_{eq}), and strong or stiff if the short-circuit power is high. At a point in the network with high short-circuit power, switching on a load will not change the voltage magnitude very much.

At the load bus, the active and reactive load can be expressed as

$$\begin{aligned} P_L &= \frac{U_N\,U_L}{X_{eq}}\,\sin(\theta_L) \\ Q_L &= -\left(\frac{U_L^2}{X_{eq}} - \frac{U_N\,U_L\,\cos(\theta_L)}{X_{eq}}\right) \end{aligned} \tag{7.3}$$

Since the angle θ_L is not of interest in this study, it can be eliminated from (7.3) which results in [19]:

$$(U_L^2)^2 + (2Q_L X_{eq} - U_N^2)U_L^2 + X_{eq}^2(P_L^2 + Q_L^2) = 0$$

Solving for U_L^2 and using (7.2), the following is obtained:

$$U_L^2 = X_{eq}\left[(0.5\,S_{sc} - Q_L) \pm \sqrt{(0.5\,S_{sc})^2 - (P_L^2 + S_{sc}Q_L)}\right] \tag{7.4}$$

A necessary condition for having a real solution for (7.4) is that

$$P_L^2 + S_{sc}Q_L \le (0.5\,S_{sc})^2 \tag{7.5}$$

From (7.5) it can be obtained that setting $P_L = 0$, the maximum of purely reactive load is one fourth of the short-circuit power S_{sc} that is $Q_{Lmax} = 0.25\,S_{sc}$. Thus, it may be difficult to supply large amounts of reactive power load via transmission system with long lines, especially via the weak one. Therefore, the required reactive power load should be compensated locally. From (7.5) it can also be obtained that setting $Q_L = 0$, the maximum of purely active load is one half of the short-circuit power that is $P_{Lmax} = 0.5\,S_{sc}$.

Theoretically, any amount of active power load can be consumed as long as required reactive power compensation is available at the load bus. Practically for a normal operation, the voltage (in the steady-state) should be held within an acceptable range at all load levels.

For the SLIB system shown in Figure 7.1, let $U_N = 1.044$, $x = 1.2$, $\eta = 4$ and $Q_L = P_L \dfrac{\sin(\varphi)}{\cos(\varphi)} = P_L \tan(\varphi)$, where $\cos(\varphi)$ is the load power factor, and assumed constant.

Figure 7.2 shows the variation of the voltage at the load bus versus the active load with $\tan(\varphi) = 0$ (i.e. purely active load). The diagram is known as U-P curve, P-U curve and also nose curve. As shown in the figure, $P_{Lmax} = 1.8166$ (pu) which is indeed one half of $S_{sc} = 3.6331$ (pu) since $Q_L = 0$. For $P_L > P_{Lmax}$, it is obvious that the system is unstable since there is no solution (or operating point). For $P_L = P_{Lmax}$, the maximum active power is transferred. This maximum power is termed as the theoretical transfer limit, and the corresponding voltage is termed as the critical voltage (for this case $U_{Lcr} = 0.7382$ (pu)). For $P_L < P_{Lmax}$, any value of power can be transferred at two different values of U_L. For instance, $P_L = 1$ (pu) is transferred at $U_{L1} = 1$ (pu) (on the blue line) and $U_{L2} = 0.3$ (pu) (on the red line). Thus, to transfer this amount of active power at U_{L2}, the current through the transmission system will be about 3.3 times larger than the current at U_{L1}. Since real transmission systems are not lossless, with the current at U_{L2} the active and reactive losses in the transmission system will significantly be higher. Therefore, the upper solution (i.e. U_{L1}) corresponds to normal operating condition, and it is practically considered as stable solution.

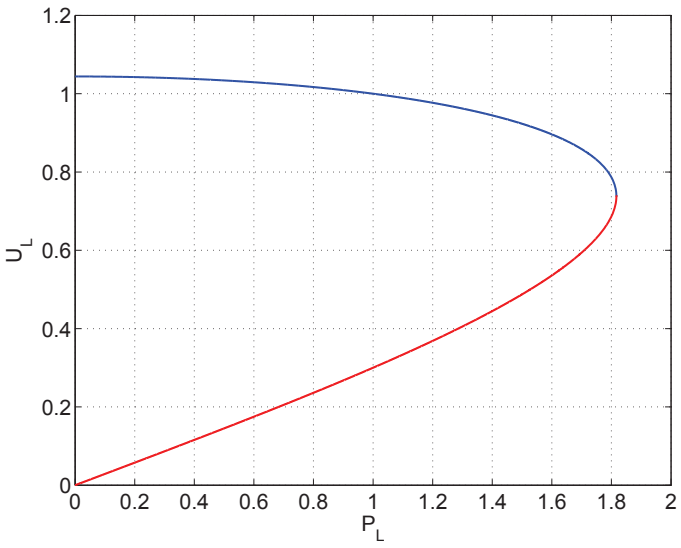

Figure 7.2. U-P curve (or nose curve).

Figure 7.3 shows the family of U-P curves for different power factors. The black curve corresponds to $\tan(\varphi) = 0.25$ that is lagging power factor ($Q_L > 0$), the blue curve corresponds to $\tan(\varphi) = 0$ that is unity power factor ($Q_L = 0$), and the red curve corresponds to $\tan(\varphi) = -0.25$ that is leading power factor ($Q_L < 0$). Leading power

factor is obtained by shunt compensation. As shown in the figure, the load power factor has a significant influence on the U-P curve, and thereby on the voltage stability. As compared with the unity power factor, with lagging power factor P_{Lmax} is lower, and U_L (the upper solution) declines faster. However, with leading power factor P_{Lmax} is higher and the voltage profile of the upper solution is flatter. The conclusion is that (due to the inductive nature of the transmission system) for being able to transfer more active power to a load bus (i.e. the load center) and to keep the voltage of the load bus close to its nominal (or rated) value, the reactive power demand should be compensated at the load bus. Note that in the steady-state, typical limits are ±10% of the rated voltage that is $\Delta U_L = \pm 0.1$ (pu) for a rated voltage of 1 (pu).

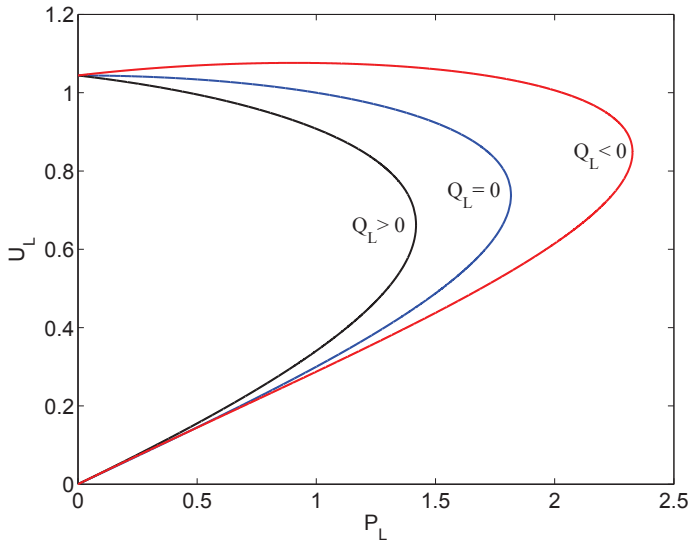

Figure 7.3. U-P curves with different power factors.

Another method to analyze voltage stability is based on the so called Q-U curves as shown in Figure 7.4.

The curves are obtained by a series of power flow calculations as follows [20]:

- Let a fictitious synchronous condenser (i.e. a generator with $P_g = 0$) without reactive power limits be placed at the load bus to make it as a PU-bus type. The specified active power at this bus is $P_{Sk} = 0 - P_L$.
- Run power flow calculation for a series of specified voltages from U_{Lmax} to U_{Lmin}.
- For each specified voltage U_L calculate the generated reactive power Q_g.
- Plot Q_g versus the specified voltages as shown in Figure 7.4

$Q_g < 0$ indicates that the generator absorbs (or consumes) reactive power, and $Q_g > 0$ indicates that the generator injects (or produces) reactive power.

Figure 7.4 shows the Q-U curves for $P_L = 1$ and $P_L = P_{Lmax}$ (pu) with $\tan(\varphi) = 0$. The intersection between the Q-U curve and $Q_g = 0$ gives the operating point (or solution)

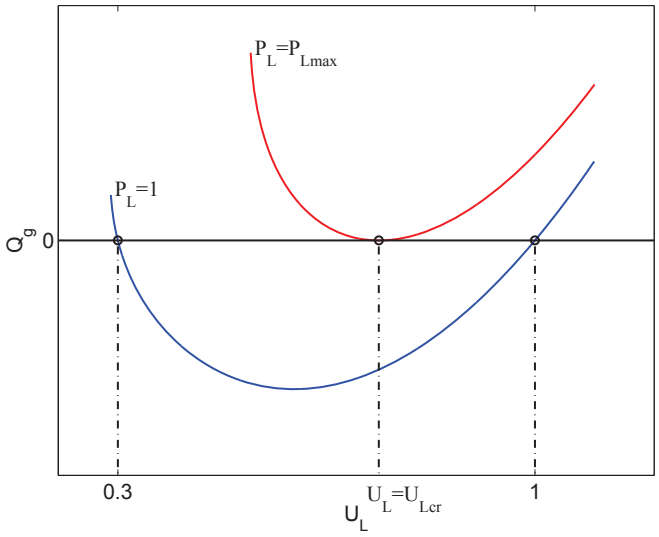

Figure 7.4. Q-U curves with different active power loading ($\tan(\varphi) = 0$).

of the system (why?). For $P_L = 1$, there are two solutions which are indeed the same solutions in Figure 7.2. According to the voltage stability criterion (7.1), $U_L = 1$ (pu) is the stable operating point since $\dfrac{dQ_g}{dU_L} > 0$ at this point. The critical operating point is reached when $\dfrac{dQ_g}{dU_L} = 0$. For $P_L = P_{Lmax}$, there is only one operating point (i.e. the intersection between the Q-U curve and $Q_g = 0$) at which $\dfrac{dQ_g}{dU_L} = 0$. The voltage at this point is the critical voltage shown in Figure 7.2.

Since voltage security is strongly coupled to reactive power, the Q-U curve may be a powerful tool to measure reactive power margin at a bus of interest.

Figure 7.5 shows the Q-U and P-U curves for $P_L = 0.8$ ($\tan(\varphi) = 0.25$) with different X_{eq}. For $\eta = 4$ there are two solutions (or operating points), with the stable operating

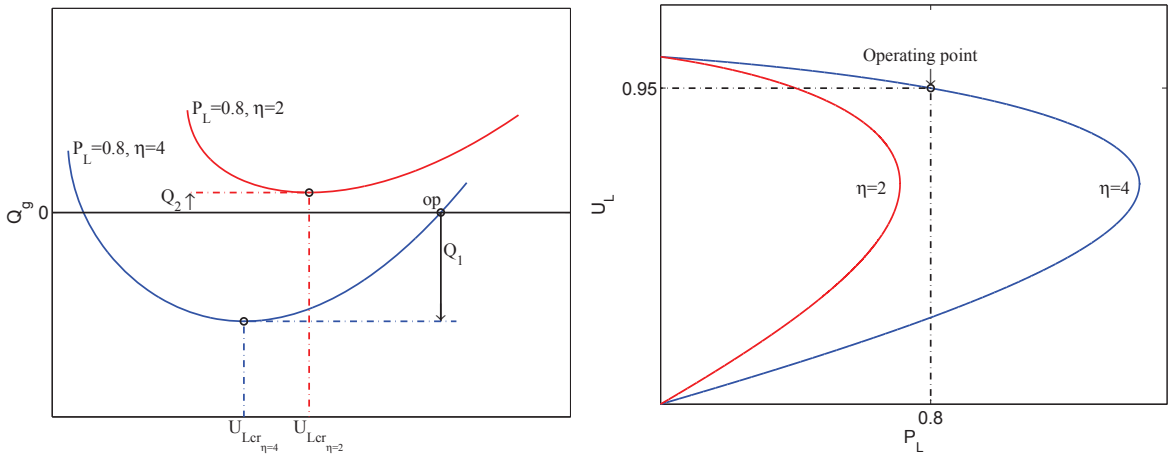

Figure 7.5. Q-U and P-U curves with different X_{eq} ($\tan(\varphi) = 0.25$).

point to the right of $\frac{dQ_g}{dU_L} = 0$ (indicated by "op" in the figure). However, when two lines are disconnected (i.e. $\eta = 2$) there is no operating point in the system that is the system is unstable. It is assumed that P_L is constant and $Q_L = 0.25\,P_L$.

Q_1 and Q_2 values shown in Figure 7.5 are reactive power margins with respect to the corresponding transfer power limit P_{Lmax}, or U_{Lcr}. Since $Q_1 < 0$, it corresponds to the maximum amount of more reactive load consumption without losing an operating point that is if $Q_L > P_L \tan(\varphi) + |Q_1|$, then there is no operating point in the system. However, since $Q_2 > 0$ in case $\eta = 2$, it corresponds to the minimum requirement of reactive power injection (or compensation) at the load bus to have an operating point.

Note that Q_2 corresponds to a constant reactive power injection independent of the load bus voltage. If compensation at the load bus is provided by a shunt capacitor $Q_c = B\,U_L^2$, the minimum requirement of reactive power compensation for having an operating point is the distance between $Q_g = 0$ and a point where Q_c is tangent to the Q-U curve.

Example 7.1 *Consider the system shown in Figure 7.1. With* $\eta = 4$, $\tan(\varphi) = 0.25$, $P_L = 0.8$ *(pu) and* $Q_L = P_L \tan(\varphi)$ *(pu) the voltage magnitude of the load bus is* $U_L = 0.95$ *(pu). Due to a disturbance two lines in the transmission system have been disconnected (i.e.* $\eta = 2$*). Assume that a shunt capacitor is available at the load bus.*

a) *Determine the minimum reactive power compensation* Q_{cmin} *such that the post-disturbance system has an operating point.*

b) *Determine the required reactive power reserve (i.e.* $Q_{cres} = Q_c - Q_{cmin}$*) such that the voltage magnitude of the load bus is restored to the pre-disturbance value, i.e.* $U_L = 0.95$ *(pu).*

Figure 7.6 shows the Q-U characteristic of the post-disturbance system.

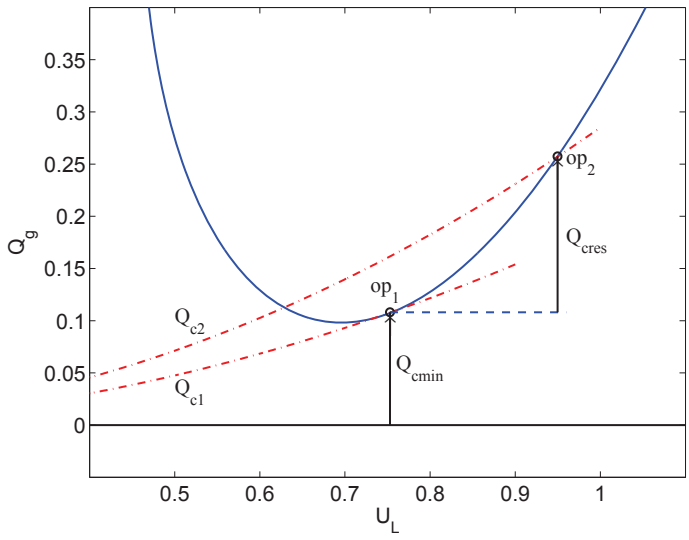

Figure 7.6. Q-U curve of the Example 7.1 ($\eta = 2$).

a) At the operating point "op$_1$", $Q_{c1} = B_{min}\,U_L^2$ is tangent to the Q-U curve. The distance from "op$_1$" to $Q_g = 0$ gives the minimum reactive power compensation $Q_{cmin} = Q_{c_{op_1}} = B_{min}\,U_{L_{op_1}}^2 \approx 0.11$ (pu) which can be read from the figure.

b) The operating point "op$_2$" corresponds to the desired voltage (i.e. $U_L = 0.95$ (pu)) at the load bus. The intersection between $Q_{c2} = (B_{min} + \Delta B)\,U_L^2$ and "op$_2$" gives the required reactive power compensation to obtain the desired voltage. From the figure it is easy to find that $Q_{creq} = Q_{c_{op_2}} = (B_{min} + \Delta B)\,U_{L_{op_2}}^2 \approx 0.26$ (pu). Thus, $Q_{cres} = Q_{c_{op_2}} - Q_{c_{op_1}}$.

7.2 Voltage instability mechanisms and prevention

Voltage instability occurs in a time interval ranging from a few seconds to tens of minutes, and is classified into slow and fast instabilities. The loads characteristics and the voltage control actions are usually the main reason for this instability. A large amount of the loads have voltage-dependent characteristics with a tendency to restore the power demands, for instance induction motor slip adjustment, and thermostatically-controlled heating loads. The power demand (or load) restoration may also be performed by Load Tap Changers (LTC) which have also significant impact on voltage instability. Voltage instability may also be experienced at the terminals of line commutated High Voltage Direct Current (HVDC) links connected to weak power systems. The converters of this kind of HVDC consume reactive power of 50-60% of the dc power.

7.2.1 Fast voltage instability

The fast voltage instability takes place just a few seconds or less after a disturbance. The main reason for this instability is the fast load-restoring actions by components such as induction motors, line commutated HVDC, and electronically-controlled loads.

After a large disturbance (such as short-circuit or tripping of a long transmission line), induction motor responds rapidly to match the mechanical torque due to its dynamic $2H\,\dot{s} = T_m - T_e(U_L, s)$, where (all quantities are expressed in pu) s is the motor slip (note that the motor speed is given by $\omega = 1 - s$), and U_L is the voltage at the bus where the motor is located. If there is no intersection between the mechanical torque (which is assumed constant) and the electrical torque after the disturbance, the system loses a post-disturbance equilibrium point which results in stalling of the motor (i.e. the motor decelerates to a complete stop, and $s = 1$). The motor stalling implies a higher reactive power consumption which causes the voltage to collapse. Another situation may be that the motor slip is greater than the unstable slip s_u when a fault is cleared. At that point T_e (which is a function of U_L and s) is less than T_m. Thus due to the motor dynamic, s increases and approaches $s = 1$ at which the motor stalls.

Assume that the load in Figure 7.1 is an induction motor, see Figure 5.2. In this study, $\dot{E}'_q$ and $\dot{E}'_d$ are set to zero in equation (5.6). A shunt capacitor is installed at the load bus to compensate the reactive power consumption of the motor such that the voltage

at the load bus is 1 (pu). A three-phase fault occurs at the load bus, and it is cleared at the clearing time t_c. Figure 7.7 shows the system response for $t_c = t_{c1}$, and Figure 7.8 shows the system response for $t_c = t_{c2} > t_{c1}$. In the figures, the post-fault electrical torques are shown.

At the clearing time $t_c = t_{c1}$, the initial value of the post-fault electrical torque (indicated in the figure with "o") is greater than T_m, and the motor slip is less than s_u. Thus, s decreases and returns to the equilibrium point at which $T_e = T_m$. Also, P_L and Q_L (which are functions of U_L and s) are restored. The reactive power consumption is also proportional to s and P_L that is $Q_L \sim sP_L$.

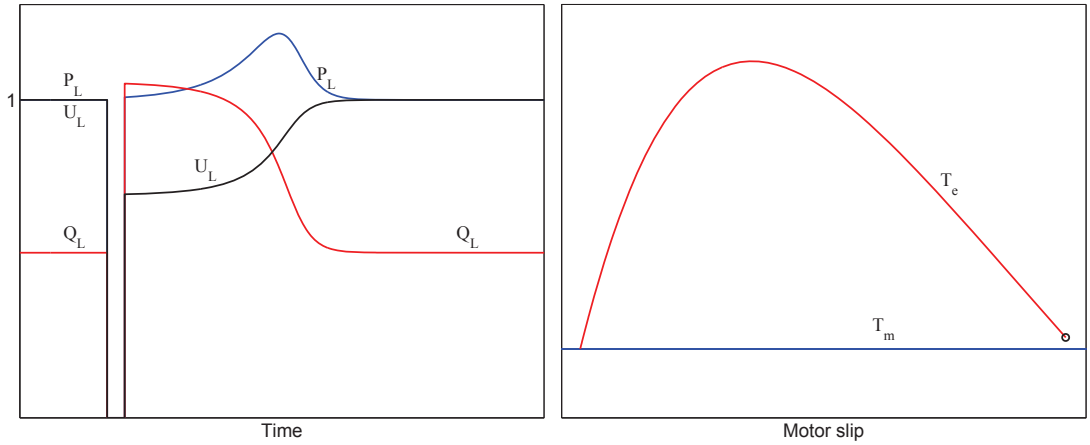

Figure 7.7. Dynamic response of the system with $t_c = t_{c1}$.

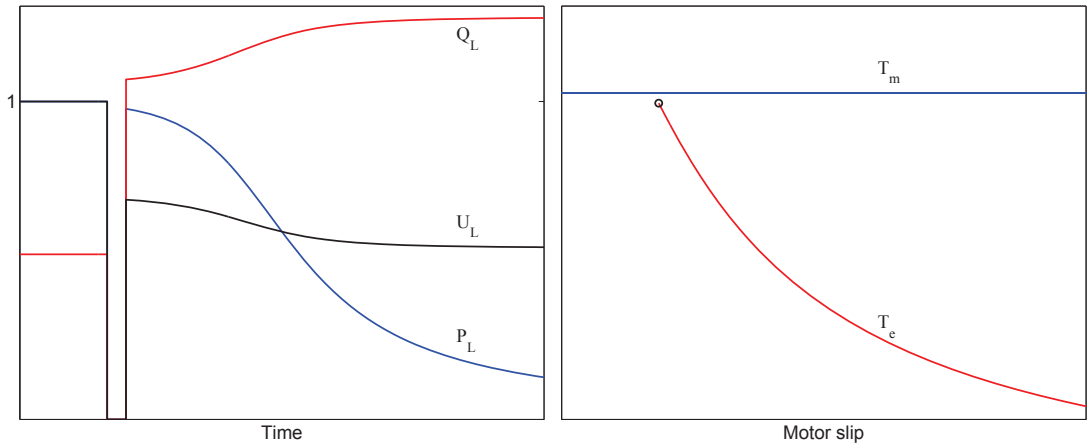

Figure 7.8. Dynamic response of the system with $t_c = t_{c2} > t_{c1}$.

At the clearing time $t_c = t_{c2} > t_{c1}$, the electrical torque (indicated in the figure with "o") is less than T_m, and the motor slip is greater than s_u. Thus, s increases and so does Q_L which causes the voltage to drop.

In a similar manner (especially due to a reduction in the voltage at the ac terminal), the power control of HVDC responds rapidly to restore the demanded active power which results in more reactive consumption in converters, and causing further voltage reduction at the ac terminal. This process leads to progressive fall of voltage.

7.2.2 Slow voltage instability

The time frame of this instability may extend from tens of seconds to several minutes. Equipments such as LTC, thermostatically-controlled loads and generator reactive power limiters (which have slow dynamics) are mostly involved in the slow voltage instability.

The mechanism of the slow voltage instability is similar to that for the fast voltage instability, however within a longer time frame. This mechanism will be presented below by using a Load Tap Changer (LTC).

Assume that the load in Figure 7.1 is connected to the transmission system via an LTC as shown in Figure 7.9

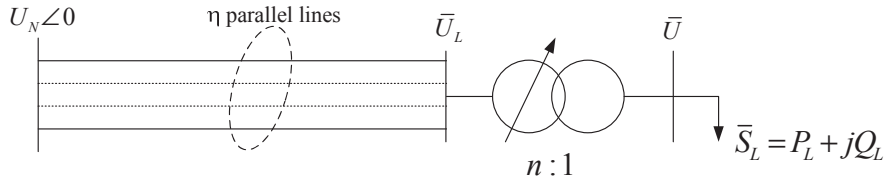

Figure 7.9. Load tap changer in the SLIB system.

An LTC is a transformer with variable turns-ratio (or tap changer, i.e. n). The function of the LTC is to (automatically) control the voltage at the load (i.e. U) by changing n. Normally, the tap is on the high voltage side where it is easier to change the tap since the current on this side is lower. The relation between U_L and U is given by

$$U = \frac{U_L}{n} \tag{7.6}$$

The dynamic of an LTC is usually described by a discrete tap changing logic. However, in our analysis a continuous tap changing model is applied as follows

$$\dot{n} = \frac{1}{T}(U - U_0) = \frac{1}{T}(\frac{U_L}{n} - U_0), \quad n_{min} \le n \le n_{max} \tag{7.7}$$

where T is a time constant which is typically some ten seconds, and U_0 is the reference voltage.

In Figure 7.9, we assume an ideal LTC (i.e. the transformer impedance is omitted). Typical tap changer range is $\pm 10\%$, but in this study we assume that the LTC does not hit its limit. Also, the load is represented by an impedance with $X_L = Q_L = 0$ that is

$$\bar{S}_L = P_L = \frac{U^2}{R_L} = G_L\, U^2 = G_L \left(\frac{U_L}{n}\right)^2 \tag{7.8}$$

Consider now the SLIB system shown in Figure 7.9. The pre-disturbance system data are as follows

$$\eta = 4\,,\; U_N = 1.044\,,\; P_L = U_L = U = n = G_L = 1\,,\; Q_{Loss} = X_{eq}\, I^2_{Line} = 0.3\,(\text{pu})$$

Figure 7.10 shows the system response after disconnection of a line in the transmission system (i.e. $\eta = 3$). The diagram on the left hand side shows variations of P_L, U_L, U and n versus time.

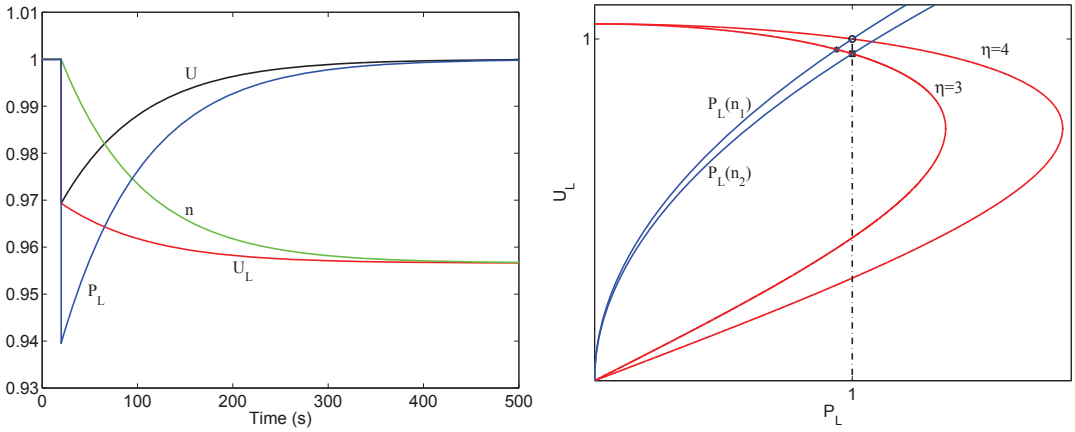

Figure 7.10. Dynamic response of the system with $\eta = 3$.

When the line is disconnected, P_L, U_L, and U decrease. Thus, the LTC starts to restore the load voltage U which results in decreasing of n. When n decreases, the load voltage U increases, and so does P_L since it is voltage dependent. An increase of P_L implies higher current trough the transmission system which results in higher reactive power loss in the transmission system (i.e. Q_{Loss}), and causing further voltage reduction (i.e. U_L). This situation continues until the load is restored that is $P_L = P_{L0} = 1$ and $U = U_0 = 1$. The diagram on the right hand side shows the U-P curves of the pre-disturbance and post-disturbance systems, as seen from the high voltage side of the LTC. The red curves are the pre-disturbance and post-disturbance systems characteristics. The vertical dashed line is the steady-state (or long-term) load characteristic. In the steady-state, the load is considered as constant power, and it is restored to its set value $P_{L0} = 1$. The intersection between the system characteristic and the steady-state load characteristic gives the equilibrium point of the system. The blue curve is the dynamic characteristic of the load (i.e. $P_L(n)$) as a function of the state variable n, also as a function of U_L (see equation (7.8)). The equilibrium point of the pre-disturbance system is indicated by "o" at which $P_L(n) = 1$ with $n = n_1 = 1$ and $U_L = 1$. When the line is disconnected (i.e. $\eta = 3$) , the operating point moves to the point "*" on the post-disturbance system characteristic. Due to the dynamic of the LTC, $P_L(n)$ will be varied until it reaches the post-disturbance equilibrium point indicated by "⊠" (i.e. the intersection point between $P_L(n_2)$ and the U-P curve of $\eta = 3$). Note that $n_2 < n_1$.

Now assume that due to a protection action in the transmission system, another line is disconnected (i.e. $\eta = 2$) just eight minutes after the first disconnection. The post-disturbance system (i.e. $\eta = 2$) characteristic is shown in Figure 7.11. Since there is no intersection between the post-disturbance system characteristic and the steady-state load characteristic (i.e. the dashed line), this post-fault system has no equilibrium point. When the second line is disconnected (i.e. $\eta = 2$) , the operating point moves to the point "◇" on the post-disturbance system characteristic. At that point U is less

than U_0. Thus, the LTC starts to restore the load voltage U which results in decreasing of n. When n decreases, the load voltage U increases, and so does P_L since it is voltage dependent. An increase of P_L implies higher current trough the transmission system which results in higher reactive power loss in the transmission system, and causing further voltage reduction (i.e. U_L). Since there is no equilibrium point in the system, this situation continues slowly due to the slow dynamic of the LTC. However, when $P_L(n)$ crosses the critical voltage indicated by "⊛", and enters into the lower side of the U-P curve the load restoration by the LTC fails which results in decreasing of U and P_L (i.e. when $n < n_3$). This situation leads to voltage instability (or collapse) in the system as shown in Figure 7.11.

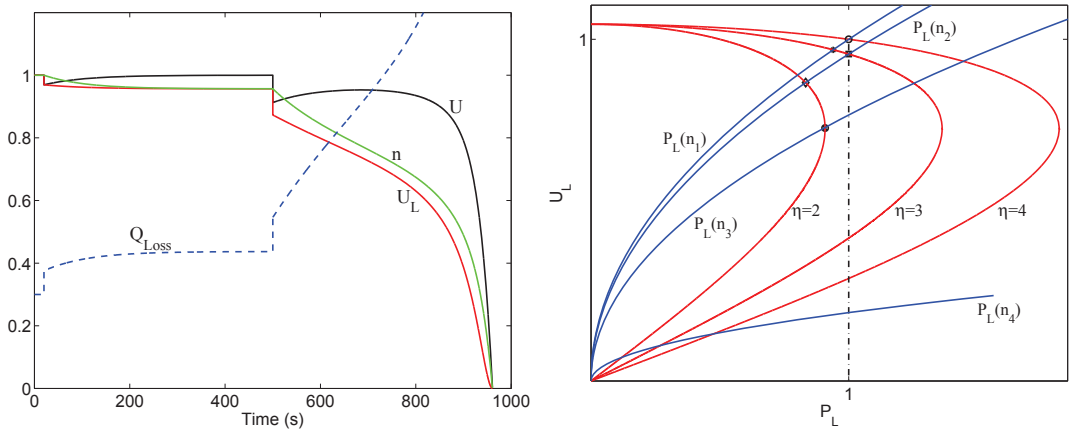

Figure 7.11. Dynamic response of the system with $\eta = 2$.

It should be noted that if the LTC had a limited range of action (i.e. $n_{min} \leq n \leq n_{max}$), the LTC could hit its limit before reaching the critical point "⊛" as shown in Figure 7.12. Since the LTC hits its limit there is no dynamic in the system (i.e. $\dot{n} = 0$), and the load will not be restored. Thus, the point indicated by "⊞" (i.e. the intersection point between $P_L(n = 0.9)$ and the U-P curve of $\eta = 2$) is the equilibrium point of the post-disturbance system.

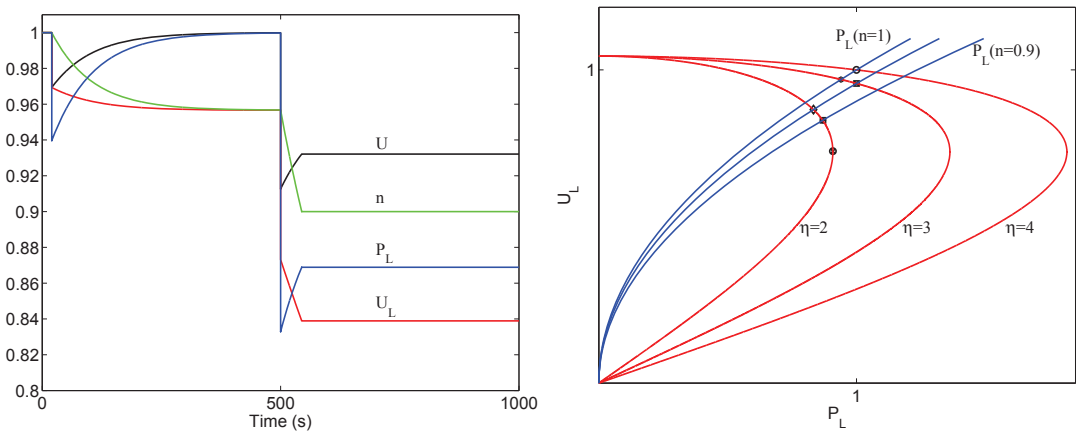

Figure 7.12. Dynamic response of the system with $n_{min} = 0.9$.

In case of having a limited range of LTC action we should, however, consider the thermostatically-controlled action of the load for restoring the load. The simplest dynamic of the thermostatically-controlled load is given by

$$\dot{G}_L = \frac{1}{T_G}\left(\frac{n}{U_L}\right)^2 (P_{L0} - P_L) \tag{7.9}$$

where T_G is a time constant which is usually in order of several minutes, P_{L0} is the reference active power, and P_L is given by equation (7.8).

Figure 7.13 shows the dynamic response of the system when the LTC has a limited range of action, and the load self-restoration action (i.e. equation (7.9)) is considered.

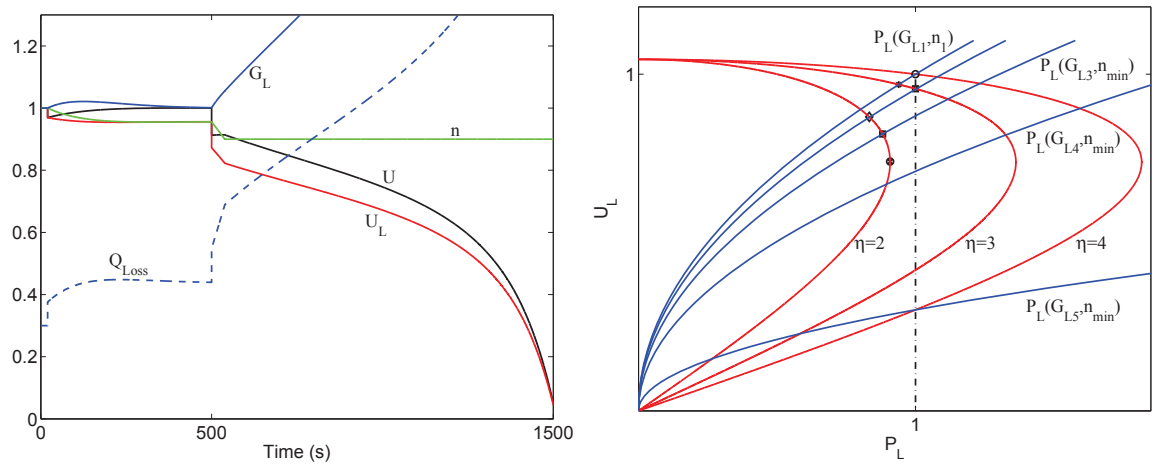

Figure 7.13. Dynamic response of the system with the load self-restoration action.

At point "⊞" (i.e. the intersection point between $P_L(G_{L3}, n_{min})$ and the U-P curve of $\eta = 2$), the LTC hits its limit, and the only dynamic in the system is given by equation (7.9) which continues to restore the load by increasing G_L which results in higher reactive power loss in the transmission system (i.e. Q_{Loss}), and causing further voltage reduction (i.e. U_L). Since there is no equilibrium point in the system, this situation continues slowly due to the slow dynamic of the thermostatically-controlled action, and leads to voltage collapse.

Obviously, the dynamic response of the system shown in Figure 7.13 is similar to that shown in Figure 7.11 where we took the unrealistic assumption that having an unlimited range of LTC action. However, by that assumption the dynamic of the thermostatically-controlled action of the load was indirectly included in equation (7.7).

7.3 Prevention of voltage instability

In [6]-[20], different preventive and corrective actions to counteract voltage instability are comprehensively described. However, the two essential (or general) corrective actions to prevent a voltage instability (or collapse) are the following:

Reactive power support

Naturally, the reactive power support should take place close to the load which leads to a decrease of reactive power losses in the transmission system, and an increase of the maximum deliverable active power.

Consider the case shown in Figure 7.11, by applying reactive power support a new stable equilibrium point is restored, and the system will be stable if this reactive power support is performed fast enough as shown in Figure 7.14.

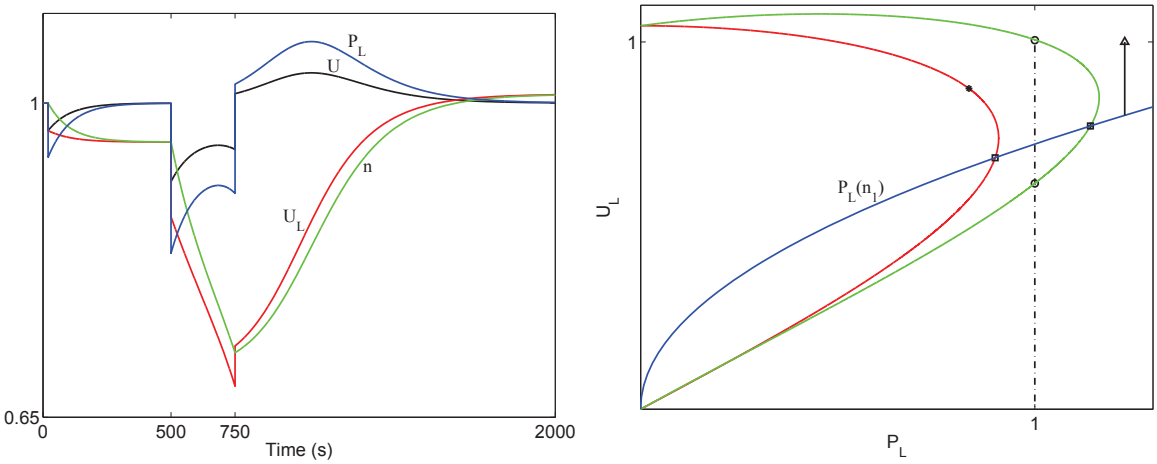

Figure 7.14. Dynamic response of the system with fast enough reactive power support.

The diagram on the right hand side shows the U-P curves of the post-disturbance system with $\eta = 2$. The red curve is the same curve shown in Figure 7.11 (with $\eta = 2$) for which the system has no equilibrium point. The green curve shows the system U-P characteristic when a shunt capacitor is switched in the transmission system close to the load. By this action two new equilibrium points (indicated by "o") are restored in the system. The upper one is a stable equilibrium point, and the lower one is unstable. The point "*" is the initial point of the post-disturbance system when the second line was tripped (i.e $\eta = 2$) at $t = 500$ (s). The intersection point (indicated by "□") between $P_L(n_1)$ and the dotted U-P curve corresponds to the operating point just before the capacitor switching at $t = 750$ (s). When the capacitor is switched, the operating point jumps to the new one indicated by "⊞" at which $U > U_0$ since at this point $P_L > 1$ and $P_L = GU^2 = 1\,U^2$. Note that in this example $U_0 = 1$. Thus, based on the LTC dynamic (see equation (7.7)) the tap n increases, and so does U_L. Since P_L (see equation (7.8)) is a function of n and U_L, it takes the direction indicated by the arrow and tends to the stable equilibrium point.

Figure 7.15 shows the dynamic response of the system when the shunt capacitor is switched at $t = 800$ (s). When the capacitor is switched, the operating point jumps from the point indicated by "□" to the one indicated by "⊞" which is the initial point of the post-disturbance system with reactive power support. At this point $U < U_0$ since $P_L < 1$. Thus, based on the LTC dynamic the tap n decreases, and so does U_L. Therefore, P_L takes the direction indicated by the arrow. This situation leads to voltage collapse.

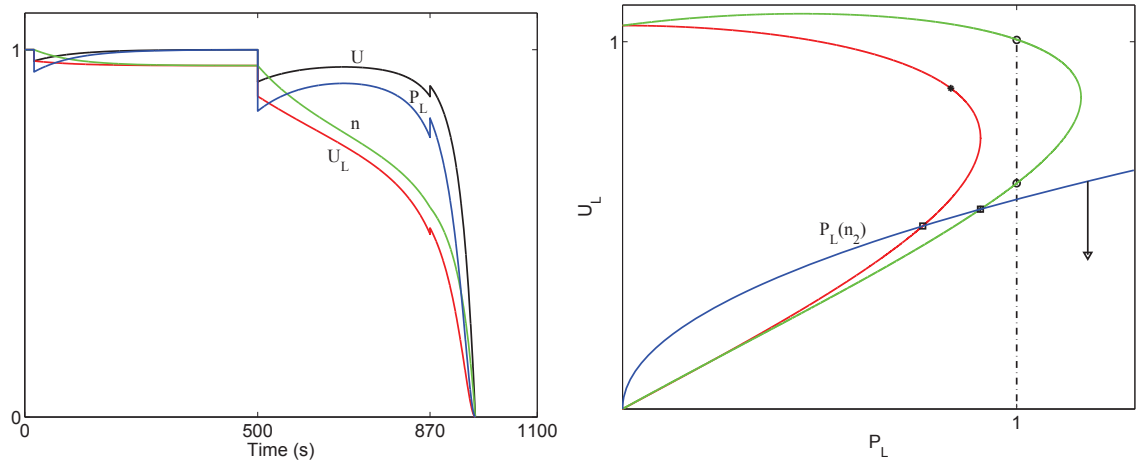

Figure 7.15. Dynamic response of the system with too slow reactive power support.

In this example for any initial point (of the post-disturbance system with reactive power support) under the unstable equilibrium point the system will be unstable. Thus, the switching time, and also the size of the shunt capacitor should be carefully selected so that the initial point does not lie under the unstable equilibrium point.

For the case shown in Figure 7.8, a fast-acting of reactive power support may prevent the motor slip to reach the unstable slip s_u. Power electronic based devices (such as SVCs and STATCOMs which will be presented in EG2120 FACTS and HVDC in power systems), generators, and synchronous condensers can be mentioned as fast reactive power support devices. A synchronous condenser is a synchronous generator that only produces or consumes reactive power. Such a synchronous condenser is installed in the Swedish island Gotland due to the (line commutated) HVDC link between the weak network of the island and the power system of the mainland.

Reactive power support can also be performed by switching series reactances, automatic line re-closing following the fault clearing, switching off shunt inductors in the transmission system. However, these actions should be fast enough to lead the system to the stable equilibrium point.

Load reduction

This action can be performed by

- blocking the LTC tap changing, see P_L in Figure 7.12. Note that if other load restoration exists, this action may only delay the process of a voltage collapse, see Figure 7.13,
- load shedding (i.e. by reducing G_L, see Figure 7.16, the figure on the left hand side),
- reducing the LTC set point (i.e. U_0 in equation (7.7), see Figure 7.16, the figure on the right hand side).

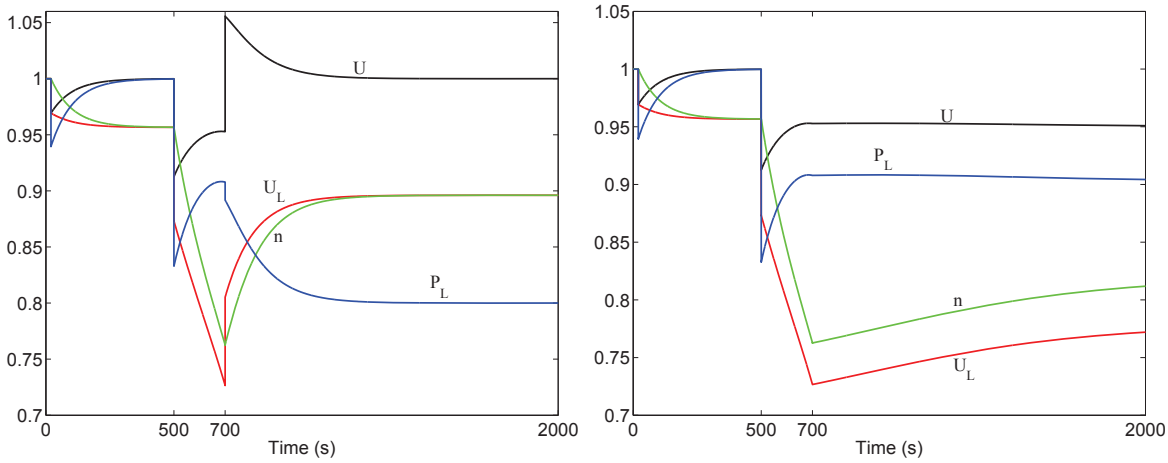

Figure 7.16. Dynamic response of the system by reducing G_L with 20% (on the left) and by reducing U_0 with 5% (on the right) at $t = 700$ (s).

Note however that U_L in the figure on the right hand side is still very low. This low voltage may lead to other protection actions in the transmission system.

Example 7.2 *Consider the SLIB system shown in Figure 7.17 where* $U_N = 1$, $\theta_N = 0$ *and the load is considered as a constat power load.*

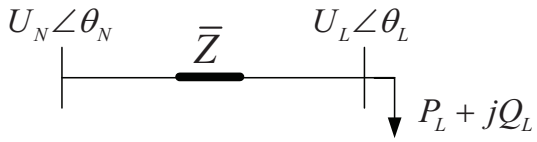

Figure 7.17. The SLIB system.

Let $\bar{Z} = R + j\,X = 0 + j\,0.35$ *and* $\bar{Z} = R + j\,X = 0.035 + j\,0.35$, *respectively.*
a) *Normalize the equivalent model with respect to the base values* U_N, S_{sc}, Z *and plot the* u_n-p_n *curve with* $Q_L = 0$.

Now, let $\bar{Z} = 0 + j\,0.35$ *and* $Q_L = P_L \tan(\varphi)$.
b) *Plot the* u_n-p_n *curve with* $\tan(\varphi) = -0.25$, $\tan(\varphi) = 0$ *and* $\tan(\varphi) = 0.25$, *respectively.*

c) *Plot the* q_n-u_n *curve with* $p_n = p_n^{max}$ *and* $p_n = p_n^{max}/3$, *respectively.*

d) *Using the non-normalized values (i.e.* P_L, Q_L *and* U_L*), plot the stability region in which for any active and reactive loads there is a real solution for the voltage. Plot also the security region in which for any active and reactive loads the voltage* (U_L) *is greater than 0.9.*

a)

$$\text{With } \bar{Z} = 0.000 + j\,0.35 \quad S_{sc} = \frac{U_N^2}{Z} = 3.4571$$

$$\text{With } \bar{Z} = 0.035 + j\,0.35 \quad S_{sc} = \frac{U_N^2}{Z} = 3.4400$$

Let,

$$\begin{aligned} \alpha &= \theta_L - \theta_N - \arctan(\frac{R}{X}) \quad , \quad p_n = \frac{P_L}{S_{sc}} \quad , \quad q_n = \frac{Q_L}{S_{sc}} \\ u_n &= \frac{U_L}{U_N} \quad , \quad r_n = \frac{R}{Z} \quad , \quad x_n = \frac{X}{Z} = \sqrt{1 - r_n^2} \end{aligned}$$

The mismatch equations at load bus give the following normalized equations.

$$\begin{aligned} &\frac{R}{Z^2} U_L^2 + \frac{U_N}{Z} U_L \sin(\alpha) + P_L = 0 \quad \Rightarrow \quad r_n u_n^2 + u_n \sin(\alpha) + p_n = 0 \\ &\frac{X}{Z^2} U_L^2 - \frac{U_N}{Z} U_L \cos(\alpha) + Q_L = 0 \quad \Rightarrow \quad x_n u_n^2 - u_n \cos(\alpha) + q_n = 0 \end{aligned} \tag{7.10}$$

Furthermore,

$$\begin{aligned} &p_n^2 + q_n^2 \quad \Rightarrow \quad u_n^2 = a \pm \sqrt{b} \quad \Rightarrow \\ &u_n^2 = (0.5 - (r_n p_n + x_n q_n)) \pm \sqrt{(0.5 - (r_n p_n + x_n q_n))^2 - (p_n^2 + q_n^2)} \end{aligned} \tag{7.11}$$

A necessary condition to have a real u_n is that $b \geq 0$ which implies that

$$p_n^2 + q_n^2 \leq (0.5 - (r_n p_n + x_n q_n))^2 \tag{7.12}$$

Thus,

$$\begin{aligned} q_n = 0 \quad &\Rightarrow \quad p_n^{max} = \frac{0.5}{1 + r_n} \quad \Rightarrow \quad u_{ncr} = \sqrt{\frac{0.5}{1 + r_n}} \\ p_n = 0 \quad &\Rightarrow \quad q_n^{max} = \frac{0.5}{1 + x_n} \quad \Rightarrow \quad u_{ncr} = \sqrt{\frac{0.5}{1 + x_n}} \end{aligned} \tag{7.13}$$

Figure 7.18 shows the u_n-p_n curves with $R = 0$ (in blue) and $R = 0.035$ (in red). Note that $q_n = 0$ in the both cases.

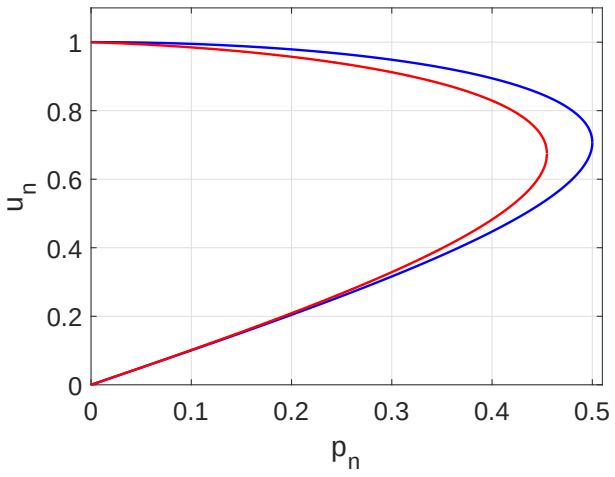

Figure 7.18. The u_n-p_n curves with $R = 0$ (in blue) and $R = 0.035$ (in red).

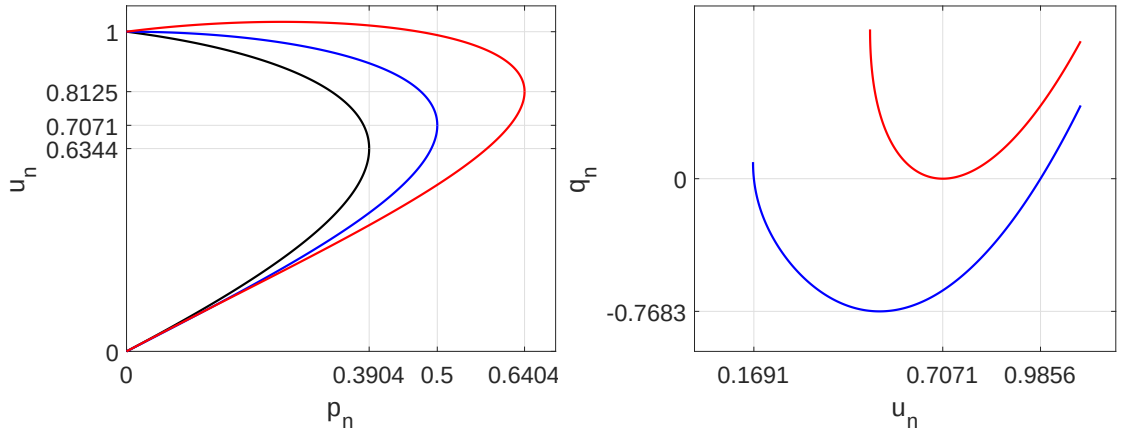

Figure 7.19. The u_n-p_n curves with different power factors, and the q_n-u_n curves with $p_n = p_n^{max}$ and $p_n = p_n^{max}/3$.

b-c) Figure 7.19 shows the u_n-p_n curves with $\tan(\varphi) = 0.25$ (in black), $\tan(\varphi) = 0$ (in blue) and $\tan(\varphi) = -0.25$ (in red), and also the q_n-u_n curves with $p_n = p_n^{max}$ (in red) and $p_n = p_n^{max}/3$ (in red).

d) Figure 7.20 shows the stability region (in cyan) and the security region (in yellow) for P_L and Q_L without reactive power compensation. The stability region indicates for which P_L and Q_L there is a real solution for U_L. However, due to practical issues the voltage in the steady state cannot be less than a specified minimum value (0.9 in this example). The security region indicates for which P_L and Q_L the voltage U_L is still over the minimum value. It also gives some information to the system operator, for a given P_L and Q_L how much reactive power should be compensated to have the operating point in the security region.

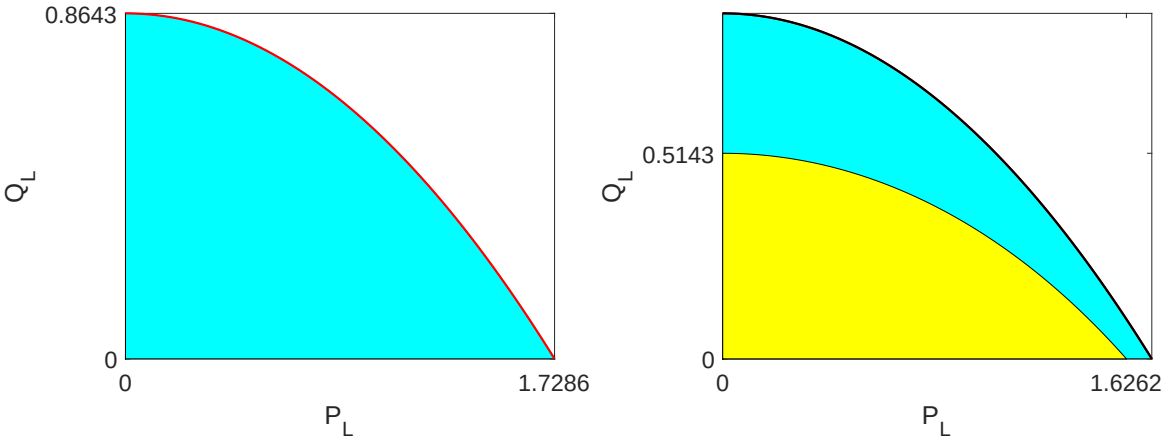

Figure 7.20. the stability region (in cyan) and the security region (in yellow) for P_L and Q_L.

Chapter 8

Frequency control

(*Part of this chapter follows in large the discussion in [21].*)

Power system frequency is an appropriate measure on the active power balance in a power system. The frequency is constant when the same amount of electrical power is produced as consumed by the loads, including system losses. If this is not the case frequency changes will occur. The frequency is reduced when a load increase or a loss of production is not compensated by a corresponding increase of the turbine power of the connected generators. The power deficit decelerates the generator rotors and consequently the frequency is reduced. Too large reductions of the frequency can trigger protection system which may result in system separation, loss of load and costumer outages, since many equipments in a power system, e.g. power supply systems, do not tolerate too low frequencies.

Since the stored kinetic energy in the system is relatively small (the inertia constant of a typical generator is about 5 (s)), the electrical energy must be produced at the same moment as it is consumed by the loads. As the power consumption varies and also due to disturbances such as outage of generation and load, the active power production must be regulated accordingly to keep the frequency within the acceptable limits. In accordance with the European Network of Transmission System Operators for Electricity (ENSTO-E) terminology [22]-[23], this frequency control is performed in three processes, namely

- **Frequency Containment Reserves (FCR)**,
- **Frequency Restoration Reserves (FRR)**,
- **Replacement Reserves (RR)**.

In this compendium, FCR and FRR will be discussed.

The objective of FCR is to stabilize the system frequency after a disturbance at a steady-state value within the permissible maximum Steady-State Frequency Deviation (SSFD). At the maximum SSFD, the FCR are fully activated. In this process, the turbine control (governor) is automatically activated to adjust the active power generation based on frequency deviation. In order to share the control between different generators involved in FCR, a permanent frequency droop is used. In some power systems, the term primary control is used for this process.

In the Northern Europe (NE) synchronous area (comprises Sweden, Norway, Finland and Eastern Denmark), FCR are above all located in hydro units, and are divided up into

- **FCR for Normal operation (FCR-N)** which is at least 600 (MW) at 50 (Hz), and will be fully activated when the permissible maximum SSFD ($\pm$ 0.1 (Hz))

is reached. The full activation time of FCR-N is within 180 (s), (about 63% is activated within 60 (s) and a full activation within 180 (s)).

- **FCR for Disturbances (FCR-D)** which is about 1000 (MW), and is used in case of contingencies (such as the trip of the largest generating unit) so that post-disturbance steady-state frequency does not become less than 49.5 (Hz), i.e. the permissible maximum SSFD is -0.5 (Hz). This action is supposed to start at 49.9 (Hz) and will be fully activated at 49.5 (Hz). The full activation time of FCR-D is within 30 (s), (about 50% is activated within 5 (s) and a full activation within 30 (s)).

Note however that when the system frequency is changed the power demand of certain loads is also changed, specially for motors, in such a way that a frequency increase leads to increased power consumption and a frequency decrease gives lower power consumption. This load frequency dependency thereby stabilizes the frequency.

The objective of FRR is to restore the system frequency to its nominal (or scheduled) value, and to replace the activated FCR. This process may be performed manually and/or automatically by applying a supplementary control loop (an integrator). Since year 2013, an automatic FRR has been introduced in the NE synchronous area to improve frequency quality performance. However, manual regulation is predominant FRR [22]. For the both cases the frequency is used as the input signal. From the actual frequency deviation and the knowledge about the system frequency droop it is straightforward for the system operators to compute how much additional power is needed to restore the system frequency and the used FCR. In the NE synchronous area, the full activation time of the automatic FRR is about 2 minutes, and the full activation time of the manual FRR is about 15 minutes. In some power systems, the term secondary control is used for this process.

Another important parameter for frequency control is Instantaneous Frequency Deviation (IFD) on which the system inertia has a significant impact. The system inertia should be sufficiently large in such a way that the instantaneous frequency does not exceed a permissable maximum IFD. For instance in the NE synchronous area, a frequency between 49 and 47 (Hz) will trigger the protection systems to under-frequency load-shedding and system separation, and also a frequency less than 47.5 (Hz) will trigger the protection systems of large steam turbines to be disconnected.

8.1 System model

Consider the multi-machine power system shown in Figure 5.3. The swing equation of the k-th generator is given by (all variables including ω are expressed in (pu))

$$M'_k \, \dot{\omega}_k = (P_{mk} - P_{ek})$$

where,

$$M'_k = 2\, H_k \, \frac{S_{ngk}}{S_{base}}$$

Transforming the swing equations to the COI reference frame, the following is obtained.

$$\dot{\omega}_{COI} = \frac{1}{M'_T}\sum_{k=1}^{n_g} M'_k\,\dot{\omega}_k = \frac{1}{M'_T}\sum_{k=1}^{n_g}(P_{mk} - P_{ek}) \tag{8.1}$$

where

$$M'_T = \sum_{k=1}^{n_g} M'_k$$

By considering a small deviation (denoted by Δ) from initial values (denoted by 0), we may write

$$\begin{aligned} P_m &= \sum_{k=1}^{n_g} P_{mk} = \sum_{k=1}^{n_g} P_{m0_k} + \sum_{k=1}^{n_g} \Delta P_{mk} = P_{m0} + \Delta P_m \\ P_e &= \sum_{k=1}^{n_g} P_{ek} = \sum_{k=1}^{n_g} P_{e0_k} + \sum_{k=1}^{n_g} \Delta P_{ek} = P_{e0} + \Delta P_e \end{aligned}$$

Thus, equation (8.1) may be rewritten as

$$M'_T\,\Delta\dot{\omega}_{COI} = (\underbrace{P_{m0} - P_{e0}}_{=0}) + (\Delta P_m - \Delta P_e) = \Delta P_m - \Delta P_e \tag{8.2}$$

Assume that the overall load is modeled as a composite load (see equation (5.4)) which has both frequency-dependent and non-frequency-dependent characteristics. Then, ΔP_e may be expressed as

$$\Delta P_e = \Delta P_L + D_{COI}\,\Delta\omega_{COI} \tag{8.3}$$

where, ΔP_L denotes the non-frequency-sensitive load change, $D_{COI}\,\Delta\omega_{COI}$ denotes the frequency-sensitive load change, and D_{COI} is a small positive damping constant.

If the system losses are included in P_e, the term ΔP_{loss} is then added to (8.3). However, since ΔP_{loss} is much smaller than the sum of the two other terms, it can be neglected that is we may set $\Delta P_{loss} \approx 0$.

Let $\Delta\omega_{COI}$, D_{COI} and M'_T be henceforth denoted by $\Delta\omega$, D and M, respectively, where M is referred to as the system inertia and $\Delta\omega$ is termed the system (or average) frequency deviation, since $\Delta\omega = \Delta f$ in (pu).

Equation (8.2) can now be rewritten as

$$M\,\Delta\dot{\omega} = \Delta P_m - \Delta P_L - D\,\Delta\omega \tag{8.4}$$

whose block diagram representation is shown in Figure 8.1. From equation (8.4), we see that the steady-state frequency deviation (SSFD) for a load change is given by

$$\Delta f = \Delta\omega = -\frac{\Delta P_L}{D}\ (\text{pu}) \ \Rightarrow\ \Delta f = -\frac{\Delta P_L}{D}\,f_s\ (\text{Hz}) \tag{8.5}$$

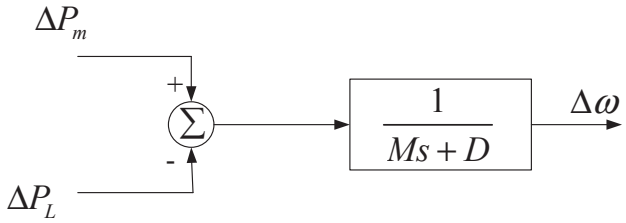

Figure 8.1. Block diagram representation of system (8.4).

8.2 Turbine and turbine governor

The objective of a turbine governing system installed in a generating unit is to produce a desired power which is partly determined by the set value for the produced power and partly by a contribution originating from the frequency control. In this context, the latter is of interest. Figure 8.2 shows a schematic diagram of the mechanical part of the generating unit k, where ΔP_{mk} is the contribution of the k-th generator to ΔP_m in Figure 8.1, $\Delta\omega$ is the system frequency deviation, and ΔY represents the change of the gate position of a hydro turbine, or the change of the valve position of a steam turbine. The block indicated with "turbine" represents the dynamic of the turbine, and the block indicated with "governor" represents the dynamic of the governing system.

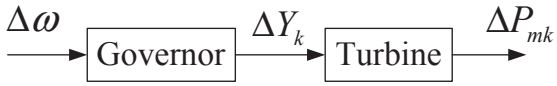

Figure 8.2. Schematic diagram of the mechanical part of a generating unit.

In this compendium, only the hydro turbine and turbine governor are discussed. For steam turbines and governing systems, the readers are referred to [6] and associated references therein.

8.2.1 Hydro turbine model

Figure 8.3 depicts a hydro turbine with penstock and hydro reservoir, and defines the notation that will be used from now on. Bernoulli's equation for a trajectory between the points P_1 and P_2 can be written as

$$\int_{P_1}^{P_2} \frac{\partial \overline{v}}{\partial t} \cdot d\overline{r} + \frac{1}{2}(v_2^2 - v_1^2) + \Omega_2 - \Omega_1 + \int_{P_1}^{P_2} \frac{1}{\rho} dp = 0 \tag{8.6}$$

The following assumptions are usually made:

- $v_1 = 0$, since the reservoir is large and the water level does not change during the time scale that is of interest here.
- The water velocity is non–zero only in the penstock.

- The water is incompressible, i.e. ρ does not change with water pressure.
- The water pressure is the same at P_1 and P_2, i.e. $p_1 = p_2$.

Further,

$$\Omega_2 - \Omega_1 = -gh \tag{8.7}$$

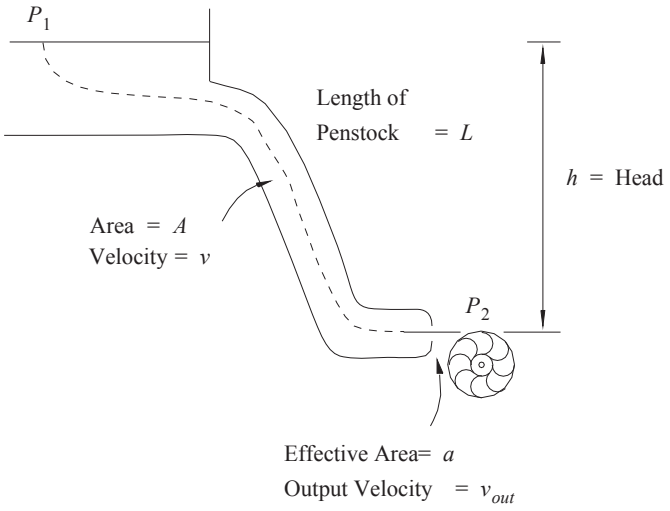

Figure 8.3. Schematic drawing of hydro turbine with water paths.

The above assumptions together with equation (8.7) make it possible to rewrite equation (8.6), with $v_{out} = v_2$ and the length of the penstock L, as

$$L\frac{dv}{dt} + \frac{1}{2}v_{out}^2 - gh = 0 \tag{8.8}$$

where, v is the water velocity in the penstock.

Let a denote the effective opening of the penstock (determined by the opening of the control gate of the turbine) and A denote the area of the penstock. Since the water is assumed incompressible, the rate of the water flow is the same at P_1 and P_2, i.e.

$$a\, v_{out} = A\, v \quad \Rightarrow \quad v_{out} = \frac{A}{a}v \tag{8.9}$$

Thus, equation (8.8) can be written as

$$\frac{dv}{dt} = \frac{1}{L}gh - \frac{1}{2L}\left(\frac{A}{a}v\right)^2 \tag{8.10}$$

The maximum available power at the turbine is

$$P_m = \frac{1}{2}\,\rho\, a\, v_{out}^3 = \frac{1}{2}\,\rho\,\frac{A^3 v^3}{a^2} \tag{8.11}$$

To get the system into standard form,

$$x = v \quad , \quad u = \frac{a}{A} \quad , \quad y = P_m \tag{8.12}$$

are introduced. The system can now be written as

$$\begin{aligned} \dot{x} =& \frac{gh}{L} - x^2 \frac{1}{2Lu^2} \\ y =& \rho A \frac{x^3}{2u^2} \end{aligned} \tag{8.13}$$

whose block diagram is shown in Figure 8.4.

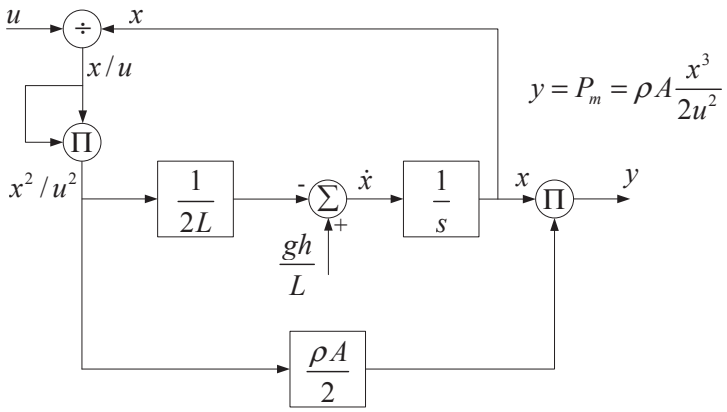

Figure 8.4. Block diagram representation of hydro turbine.

Equation (8.13) describes the dynamic of a nonlinear system of the form

$$\begin{aligned} \dot{x} =& f(x,u) \\ y =& \hbar(x,u) \end{aligned} \tag{8.14}$$

To get an idea of the properties of this system, the nonlinear system is linearized around its equilibrium point. In the steady-state $\dot{x} = 0$. For a given u_0, the equilibrium point x_0 and the initial value of y, i.e. y_0 are obtained as follows

$$\begin{aligned} x_0 =& u_0 \sqrt{2gh} \\ y_0 =& \frac{\rho A x_0^3}{2u_0^2} \end{aligned} \tag{8.15}$$

Linearization of (8.14) around its equilibrium gives

$$\begin{aligned} \Delta\dot{x} =& f_x \, \Delta x + f_u \, \Delta u \\ \Delta y =& \hbar_x \, \Delta x + \hbar_u \, \Delta u \end{aligned} \tag{8.16}$$

or

$$\begin{aligned} \Delta\dot{x} =& -2x_0 \frac{1}{2Lu_0^2} \Delta x + \frac{2x_0^2}{2Lu_0^3} \Delta u \\ \Delta y =& 3\rho \frac{Ax_0^2}{2u_0^2} \Delta x - 2\rho \frac{Ax_0^3}{2u_0^3} \Delta u \end{aligned} \tag{8.17}$$

which, using equations (8.15), can be rewritten as

$$\begin{aligned}\Delta\dot{x} &= -\frac{\sqrt{2gh}}{u_0 L}\Delta x + \frac{2gh}{u_0 L}\Delta u \\ \Delta y &= \frac{3y_0}{u_0\sqrt{2gh}}\Delta x - \frac{2y_0}{u_0}\Delta u\end{aligned} \tag{8.18}$$

Note that $L/\sqrt{2gh}$ has dimension of time, and from the above equations it is apparent that this is the time it takes the water to flow through the penstock if $a = A$. That time is denoted by T:

$$T = L/\sqrt{2gh} \tag{8.19}$$

The Laplace transformation of (8.18) leads to

$$\Delta x = \frac{L/T}{1 + su_0 T}\Delta u \tag{8.20}$$

Based on (8.20), the relationship between the input Δu and the output Δy is then given by

$$\Delta y = \frac{y_0}{u_0} \cdot \frac{1 - 2u_0 Ts}{1 + u_0 Ts}\Delta u \tag{8.21}$$

Note that $u_0 T = a_0 T/A$ also has dimension of time and is denoted by T_w. Thus, equation (8.21) can be rewritten as

$$\Delta y = \frac{y_0}{u_0} \cdot \frac{1 - 2T_w s}{1 + T_w s}\Delta u \tag{8.22}$$

It is obvious that the transfer function in equation (8.22) is of non–minimum phase, i.e. not all zeros are in the left half plane. In this case, one zero is in the right half plane. That is evident from the step response to equation (8.22), depicted in Figure 8.5.

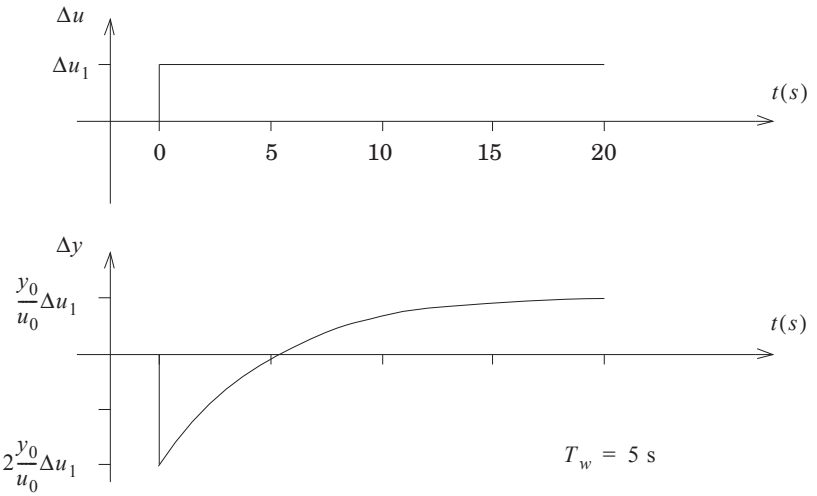

Figure 8.5. Variation of produced power, Δy, after a step change in control gate.

The system has the (unpleasant) property to give a lower power just after the opening of the control gate is increased before the desired increased power generation is reached. The physical explanation is the lower pressure appearing after the control gate is opened, so that the water in the penstock can be accelerated. When the water has been accelerated, the generated power is increased as a consequence of the increased flow. That property of water turbines places certain demands on the design of the control system for the turbines.

Normalizing the input and output variables of equation (8.22), this equation can be rewritten as

$$\Delta P_m = \frac{1 - 2T_w s}{1 + T_w s} \Delta Y \tag{8.23}$$

where,

$$\Delta P_m = \frac{\Delta y}{y_0} \quad \text{and} \quad \Delta Y = \frac{\Delta u}{u_0}$$

In this compendium, the transfer function (8.23) is used to represent the dynamic of a hydro turbine. Thus, for the k-th generator we have (see Figure 8.2)

$$\Delta P_{mk} = \frac{1 - 2T_w s}{1 + T_w s} \Delta Y_k \tag{8.24}$$

8.2.2 Hydro turbine governor model

It is the task of the turbine governor to control the control gate such that the desired power is produced by the generator in question. That power is partly determined by the set value for the produced power and partly by a contribution originating from the frequency control. In this context, the latter is of interest. A model of this controller is given in Figure 8.6. The control servo is here represented simply by a time constant T_p. The main servo is represented by an integrator with the time constant T_G. The change of the set value is indicated by $\Delta P_{m_{set}}$ which is set to zero prior to a disturbance.

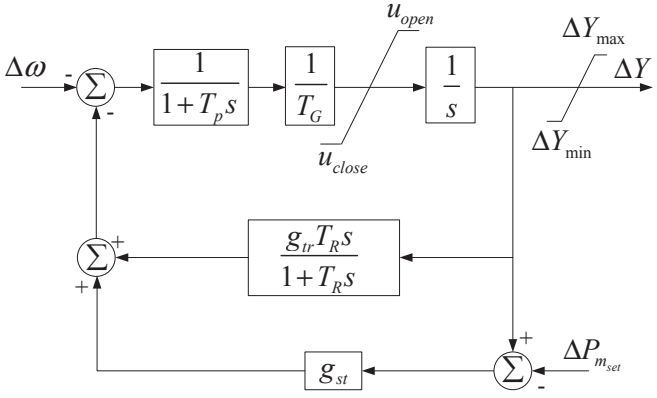

Figure 8.6. Model of governors for hydro turbines.

Typical values for these parameters are given in Table 8.1.

Parameter	Typical values
T_R	2.5 – 7.5 s
T_G	0.2 – 0.4 s
T_p	0.03 – 0.06 s
g_{tr}	0.2 – 1
g_{st}	0.03 – 0.06

Table 8.1. Typical values for some parameters of the turbine controller for hydro power.

The controller has two feedback loops, a transient feedback loop and a static feedback loop. The transient feedback loop has the gain g_{tr} for high frequencies, and the static feedback loop has the gain g_{st}. Thus, the total feedback gain after a frequency change is $-(g_{tr} + g_{st})$. The transient feedback is needed since the water turbine is a non–minimum phase system. If the transient feedback is left out or made too small, the system can become unstable. The transient feedback causes the system to be slower; the transient frequency deviations become considerably larger since the initial total feedback can be about ten times larger than the static feedback.

Setting $T_p = 0$, and neglecting the limiters, the dynamic of the hydro governor of the k-th generator may be (approximately) described by the following transfer function [5]

$$\Delta Y_k = -\frac{1}{g_{st_k}} \frac{1 + T_R\, s}{(1 + T_{g1}\, s)(1 + T_{g2}\, s)} \Delta\omega \tag{8.25}$$

where,

$$T_{g1} \approx \frac{T_R\, T_G}{T_G + T_R(g_{st_k} + g_{tr})} \quad \text{and} \quad T_{g2} = \frac{T_G + T_R(g_{st_k} + g_{tr})}{g_{st_k}} \tag{8.26}$$

Usually $T_{g2} \gg T_{g1}$, therefore it has been assumed $T_{g2} + T_{g1} \approx T_{g2}$.

Figure 8.7 shows the block diagram of the mechanical part of a hydraulic unit which contributes to the control of the system frequency.

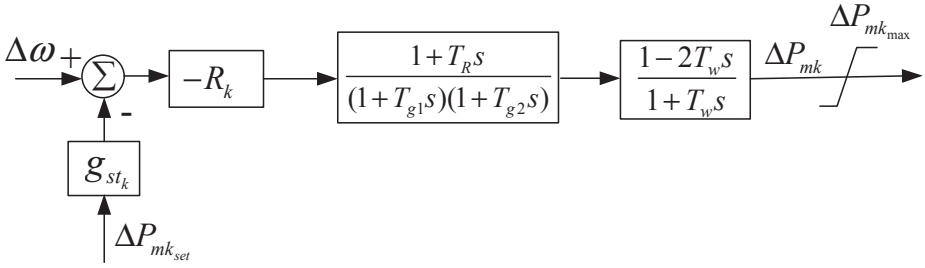

Figure 8.7. Block diagram of the mechanical part of a hydraulic unit.

In the steady-state (see equation (8.25)), the ratio between the frequency deviation and the change in the control gate is given by

$$\Delta Y_k = -\frac{1}{g_{st_k}} \Delta\omega \tag{8.27}$$

Using equation (8.24), the stationary change of power is obtained as

$$\Delta P_{mk} = -\frac{1}{g_{st_k}}\Delta\omega = -R_k\,\Delta\omega \tag{8.28}$$

Summing equation (8.28) for all generators, we have

$$\begin{aligned}\Delta P_m &= \sum_{k=1}^{n_g}\Delta P_{mk} = -\sum_{k=1}^{n_g}\frac{1}{g_{st_k}}\Delta\omega = -\sum_{k=1}^{n_g}R_k\,\Delta\omega \\ &= -\frac{1}{g_{st}}\,\Delta\omega = -R\,\Delta\omega\end{aligned} \tag{8.29}$$

where,

$$\frac{1}{g_{st}} = \sum_{k=1}^{n_g}\frac{1}{g_{st_k}} \quad , \quad R = \sum_{k=1}^{n_g}R_k \quad \text{and} \quad R = \frac{1}{g_{st}} \tag{8.30}$$

- g_{st} is termed the speed-droop (or the droop), and can be interpreted as the percentage change in frequency required to move the gate from fully closed to fully opened. The droop expressed in the nominal value has the unit $(\frac{Hz}{MW})$.
- R $(\frac{MW}{Hz})$ is termed the total gain of the governing systems.

Moreover by virtue of equations (8.4) and (8.29), the steady-state frequency deviation (SSFD) for a load change in a system with governing systems is given by

$$0 = \Delta P_m - \Delta P_L - D\,\Delta\omega \quad \Rightarrow \quad \Delta\omega = -\frac{\Delta P_L}{R+D} \tag{8.31}$$

where, $R + D$ is referred to as the stiffness.

Example 8.1 *Consider the system shown in Figure 8.8 where a hydraulic unit and an infinite bus feed a load. Let the active load be modeled as* $P_L = P_{L0} + D\,\Delta\,\omega$.

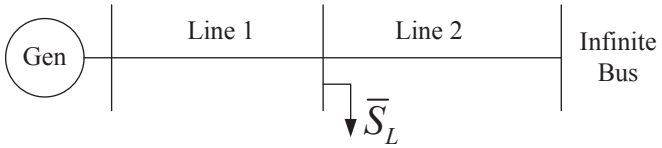

Figure 8.8. An SMIB system.

The system data are given as follows

- $S_{base} = 1000$ *(MVA),* $f_s = 50$ *(Hz)*
- $P_m = 900$ *(MW),* $P_{m_{max}} = 1100$ *(MW)* , $H = 5$ *(s),* $S_{ng} = 1200$ *(MVA)*

- $P_{L0} = 1000$ *(MW),* $D = 20$ *(MW/Hz)*

Assume that due to a disturbance line 2 is disconnected at time $t = 5$ *(s). Assume also that there is no frequency control in this isolated system, i.e.* $\Delta P_m = 0$. *Calculate the steady-state frequency deviation (SSFD) of the isolated system in (Hz).*

For frequency control study, the system may be represented by the block diagram shown in Figure 8.9 where all values are expressed in (pu).

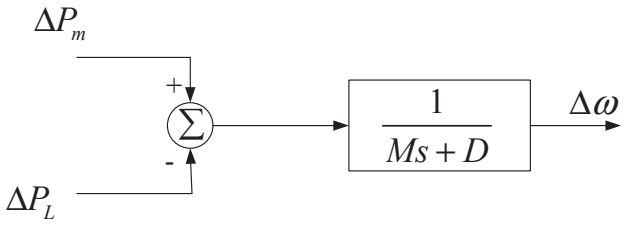

Figure 8.9. Block diagram representation .

We have

$$\Delta P_m = 0 \quad , \quad M = 2\,H\frac{S_{ng}}{S_{base}} = 12 \quad , \quad \Delta P_L = \frac{100}{S_{base}} = 0.1 \quad \text{and} \quad D = 20\,\frac{f_s}{S_{base}} = 1$$

where ΔP_L represents the lost power from the infinite bus to the load. Note also that $\Delta\omega = \Delta f$ since $\Delta\omega$ is expressed in (pu). The SSFD of the isolated system is given by

$$\Delta f = \frac{\Delta P_m - \Delta P_L}{D}\, f_s = \frac{0 - 0.1}{1}\, 50 = -5\,(\text{Hz})$$

Figure 8.10 shows the system frequency response to the disturbance.

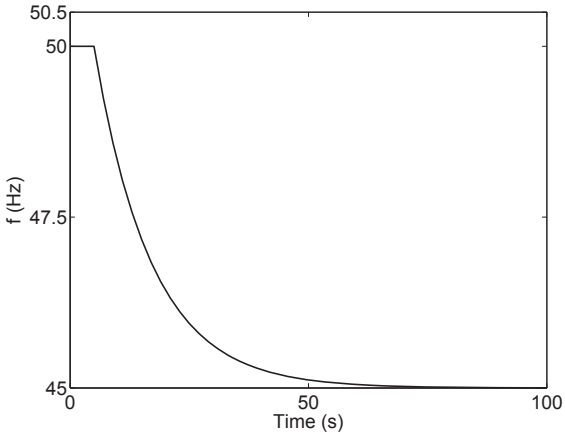

Figure 8.10. System frequency response to the disturbance.

Example 8.2 *Assume that the isolated system has a frequency control function, and the available FCR are used fully at* $f = 49.5$ *(Hz). For the same disturbance, calculate the SSFD of the isolated system in (Hz), and analyze the response of the FCR process.*

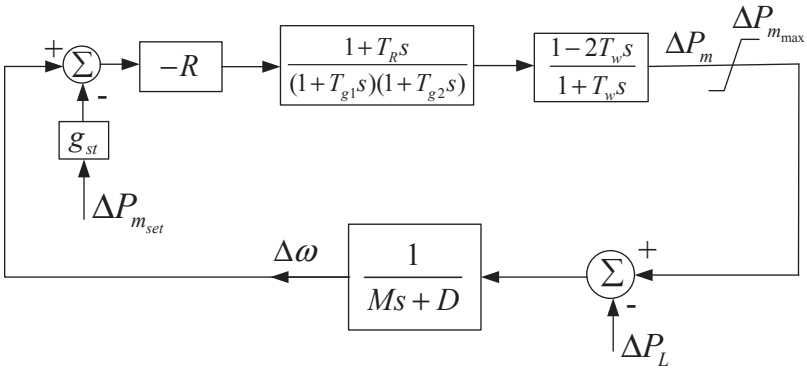

Figure 8.11. Block diagram representation.

Now, we are dealing with the system shown in Figure 8.11.

The SSFD is given by (8.31). The available FCR are given by $P_{m_{max}} - P_m = 200$ (MW). To fulfill the frequency deviation requirement, the total system gain R is then

$$R = \frac{200}{0.5} = 400\ (\text{MW/Hz}) \quad \text{or} \quad R = 400\,\frac{f_s}{S_{base}} = 20\,(\text{pu/pu}) \quad \text{and} \quad g_{st} = \frac{1}{R} = 0.05\,(\text{pu/pu})$$

The stiffness is given by $R + D = 21$, and the SSFD is given by

$$\Delta f = \frac{-\Delta P_L}{R+D}\,f_s = \frac{-0.1}{21}\,50 = -0.2381\,(\text{Hz})$$

Figure 8.12 shows the system frequency response to the disturbance, with $T_G = 0.2$, $T_R = 7$, $g_{tr} = 0.8$ and $T_W = 2$. From equation (8.26), T_{g1} and T_{g2} can be determined.

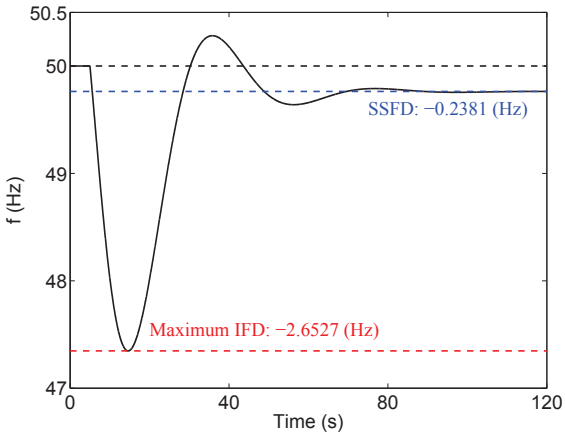

Figure 8.12. The response of FCR to the disturbance.

During transient the frequency drops to $f = 47.3473$ (Hz), i.e. the maximum instantaneous frequency deviation (IFD) is $\Delta f = -2.6527$ (Hz) for this disturbance, however it eventually settles to $f = 49.7619$ (Hz), i.e. the SSFD is $\Delta f = -0.2381$ (Hz) which was determined by the stiffness $R + D$.

Figure 8.13 shows the generation and load characteristics of the isolated power system. In the figure, the characteristic of the load is given by $P_L = P_{L0} + D\Delta f$ whose slope is determined by $\frac{1}{D}$, and the characteristic of the generation of the isolated system is given by $P_m = P_{m0} - R\Delta f$ whose slope is determined by $-g_{st}$. Prior to the disturbance, the system settles at the equilibrium point indicated with "$*$", where $\Delta f = 0$, and $P_m + 100 = P_L = 1000$ (MW). Note that the P_m characteristic shown in the figure is for the isolated system, i.e. the post-disturbance system. (How does the P_m characteristic look like in the pre-disturbance system?)

When the disturbance occurs the system moves from point "$*$" to point p_1 at which $P_m = 900$. However, the frequency initially reminds unchanged (why?). At point p_1, the power difference is $P_m - P_L = -100$ (MW) (which corresponds the lost power from the infinite bus), therefore the frequency starts to drop. When the frequency drops, the governing system should increase the generator output. However, as shown in the figure, the power output first decreases before starting to compensate the lost power. The reason to that is the unpleasant dynamical property of the hydro turbine (i.e. non-minimum phase property), and that is the reason (compared to the steam units) why the system with frequency control based on hydraulic units has larger transient frequency deviation, and needs longer time to reach the new equilibrium point.

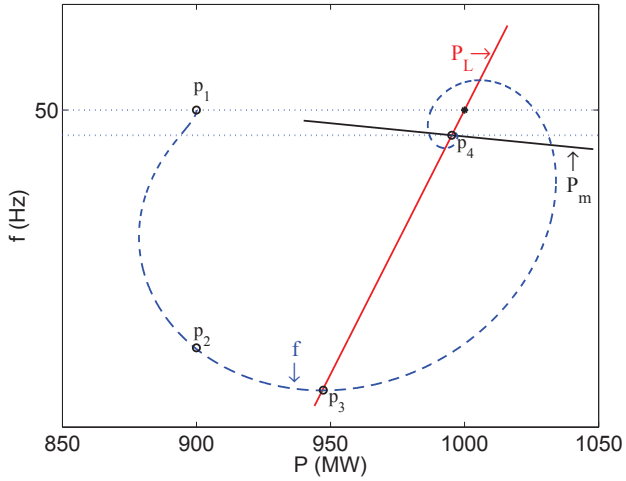

Figure 8.13. Generation and load characteristics of the isolated power system.

When the trajectory intersects the P_L characteristic at point p_3, the output power P_m is equal to P_L (which has decreased due to its frequency dependency), and the frequency reaches a local minimum of $f = 47.3473$ (Hz) (see Figure 8.12). Since p_3 is not an e.p, the trajectory does not stay at this point, but passes it. Then $P_m > P_L$, and therefore the system frequency starts to increase. When the trajectory intersects again the P_L characteristic, the frequency reaches a local maximum. When the trajectory passes the intersection point, P_m becomes less than P_L, and therefore the system frequency starts to decrease. Eventually, the trajectory reaches its new equilibrium point p_4.

Figure 8.14 shows the effects of the governing system and the frequency dependency of the load on the system frequency change. The disturbance ΔP_L results in a generation

increase of ΔP_m, and a load reduction of $D\Delta f$.

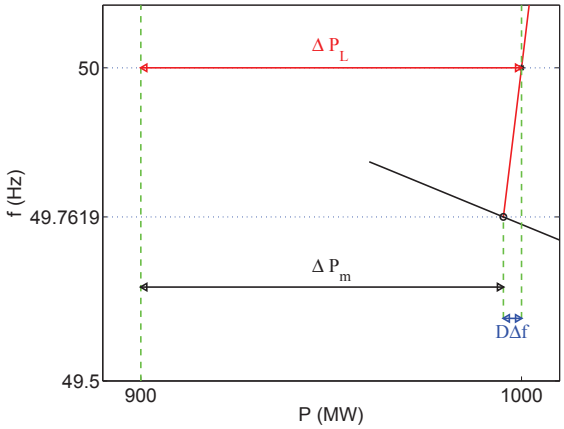

Figure 8.14. The impact of the frequency dependency of the load.

Example 8.3 *Apply the FRR process to restore the system frequency and the load. Also explain the impact of the inertia constant H on the system frequency response.*

In order to restore the system frequency and the load, the generation characteristic must be shifted to a point close to the nominal frequency. Such a shift can be performed in different ways. Since the frequency deviation and the system gain after the disturbance are known, $\Delta P_m = -R\Delta f$ can be calculated. Having known ΔP_m, the generation characteristic can be shifted either by changing the set value of the generator (i.e. $\Delta P_{m_{set}}$) to ΔP_m, or starting a new generator whose power output should be equal to ΔP_m. Another way is to add a supplementary control loop (an integrator) to the governing system with Δf as the input signal as shown in Figure 8.15.

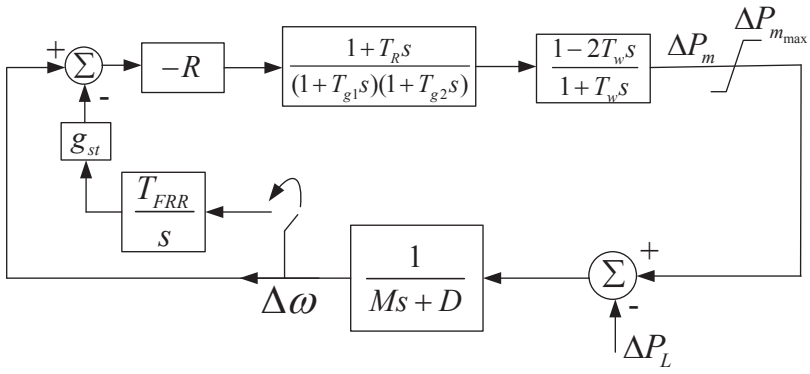

Figure 8.15. Block diagram representation with automatic FRR.

Figure 8.16 shows the system frequency response to FCR process (in blue) and the FRR process (in red). In the figure on the left hand side, the FRR was performed at $t = 120$ (s) by a step change of the set point to $\Delta P_{m_{set}} = -R\Delta f$, where R and Δf were calculated in Example 8.2. However, in the figure on the right hand side, the FRR was performed at $t = 120$ (s) by activating the supplementary control loop shown in Figure 8.15.

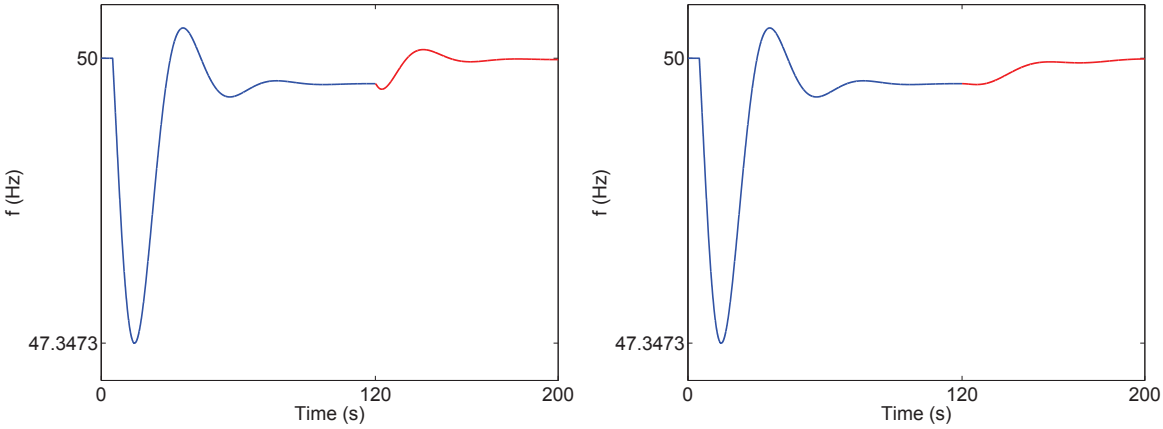

Figure 8.16. System frequency response to the FCR process and the FRR process.

In the first few seconds following the loss of a power plant (in this example the infinite bus), the system frequency starts to drop. Initially, the dynamical behavior of the system frequency is dominated by the inertial response of the generators that are synchronously connected to the system (in this example there is only one generator). This response is known as Inertial Frequency Response (IFR) which is an inertia-based inherent response due to the total stored kinetic energy in the rotating masses (mainly from synchronous generators). The IFR provides a counter response to resist a fast frequency deviation after a disturbance. A low system inertia results in a faster and greater frequency deviation. A large and fast frequency deviation can trigger protection system which may result in system separation, loss of load and costumer outages. Therefore, keeping a minimum level of system inertia is a necessity for having a secure system operation.

Figure 8.17 shows the variations of the rate of change of frequency (RoCoF) after the loss of the infinite bus. In the figure on the right, the region around the minimum of RoCoF is enlarged.

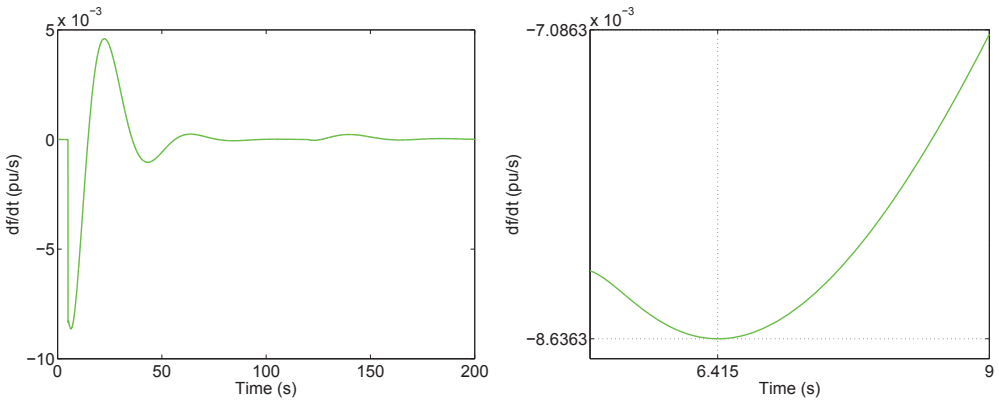

Figure 8.17. Variations of the RoCoF after the loss of the infinite bus.

In a real power system, after loss of a power plant it normally takes some time before the governor control action (i.e. the FCR process) will be activated. Therefore, during the first second(s) following the disturbance, the stored kinetic energy in the rotor and the

frequency dependency of the load are the only counter response to resist the frequency drop (i.e. the IFR). Thus, from Example 8.2 and Example 8.3 we may conclude that as shown in Figure 8.18 following a disturbance the system frequency response may be classified into three different categories, namely the inertial frequency response (in green), the response due to the FCR process (in blue) and the response due to the FRR process (in red).

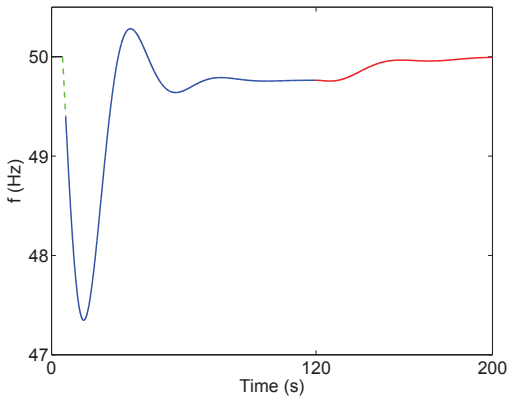

Figure 8.18. Different categories of frequency response.

Figure 8.19 shows the system frequency response for $H = 3$ (in red), $H = 5$ (in green) and $H = 7$ (in blue).

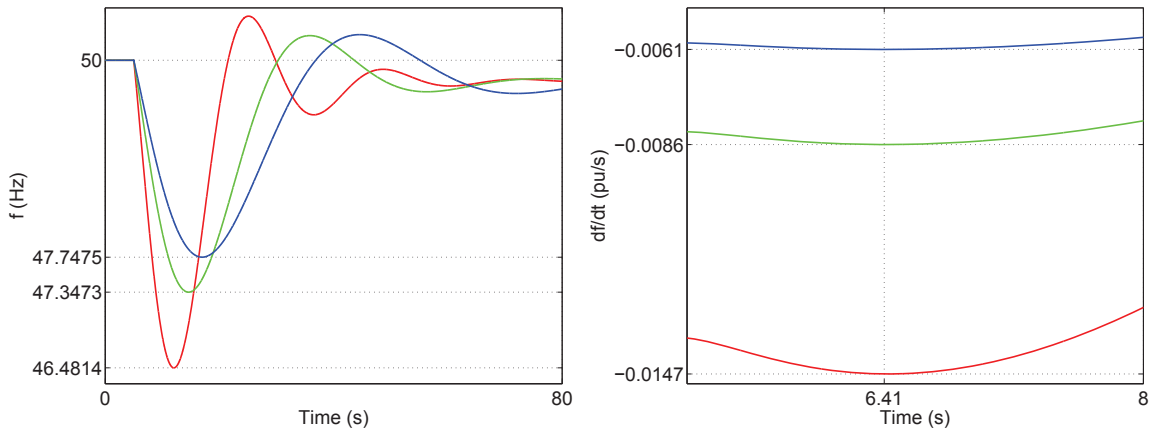

Figure 8.19. System frequency response for $H = 3$, $H = 5$ and $H = 7$.

As shown in the figure, the system inertia has a significant impact on the IFD and the RoCoF. A lower H results in a greater IFD and RoCoF. The settings of some protection systems are based on the frequency deviation and the RoCoF. For example, the steam turbines are very sensitive for a too low frequency, and they must be disconnected by their protection systems when the frequency drop is $\Delta f = \alpha > 0$ (Hz) to avoid damaging of these generators. One of the preventive actions to avoid the frequency reaches $f = f_s - \alpha$ (Hz) is that to disconnect some pre-defined loads (i.e. under-frequency load-shedding) when the frequency drop is $\Delta f = \beta < \alpha$ (Hz). There are also protection systems which will be triggered to disconnect some power

system components if $|df/dt| > \gamma > 0$ (Hz/s). This action may result in jeopardizing the system stability. Therefore, the system must be operated in such a way to fulfill $N-1$ criterion with the frequency nadir greater than $f = f_s - \beta$ (Hz) and the RoCoF less than γ.

Example 8.4 *Consider again the system in Example 5.1. The generators are represented by the classical model with ω_k in (pu), see equation* (3.18)*. The loads are represented by the exponential model expressed in equation* (5.2)*. Let the disturbance be a step increase of the load at BUS 4 with 10%. Let also the load frequency dependency be represented by the damping constants of the generators, i.e. D_k.*

a) *Let $mp = mq = 0$ and assume that no generator has governor control, i.e. P_{mk} is constant. Find a value for each D_k such that the frequency drop is $\Delta f = 5$ (Hz) for this disturbance. Plot also Δf (Hz) in the COI reference frame.*

b) *Re-do* **a)**, *but with*

$$mp = 0 \text{ and } mq = 2 \quad , \quad mp = 2 \text{ and } mq = 0 \quad , \quad mp = 2 \text{ and } mq = 2$$

c) *Let $mp = mq = 0$, and D_k be the same as in task* **a)**. *Let also Gen 1 and Gen 2 be equipped with the governor control shown in Figure 8.15, but without the supplementary control loop, i.e. $T_{FRR} = 0$. Assume that the available FCR used fully at $f = 49.5$ (Hz). Analyze the system frequency response for this disturbance.*

d) *Re-do* **c)**, *but with the supplementary control loop, i.e. $T_{FRR} \neq 0$, from $t \geq 120$ (s).*

a-b) Based on the required frequency drop, we firstly find D_{COI} which is given by

$$D_{COI} = -\frac{\Delta P_L}{\Delta f}\frac{f_s}{S_{base}} = 1.5000 \text{ (pu/pu)}$$

Next, from equations (3.18) and (8.1)-(8.4) we find that $D_1 = 0.0020$, $D_2 = 0.0016$ and $D_3 = 0.0012$.

To run the simulation, the system dynamic described in task **a)** of Example 5.1 with the generator dynamic expressed in equation (3.18) are used. Figure 8.20 shows the system frequency response (in the COI reference frame) to the disturbance with different mp and mq. Why does the system have different settling frequency?

c-d) Based on the given data and the frequency drop requirements, we find that $R_1 = 20$ and $R_2 = 6$ (pu/pu). Next, based on equation (8.31) the SSFD can be obtained which is $\Delta f = 49.7273 - 50 = -0.2727$ (Hz).

To run the simulation, we need to derive a set of differential equation to describe the dynamics of the governor and turbine shown in Figure 8.15. To do that, we use the equivalent model shown in Figure 8.21 from which the following set of differential

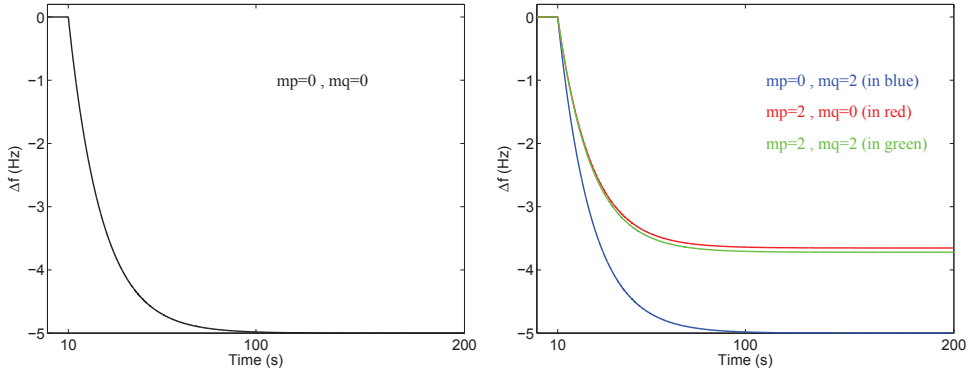

Figure 8.20. System frequency response to the disturbance with different values for mp and mq.

equations can be obtained.

$$\begin{aligned}
\dot{S}_{1k} &= \frac{-1}{T_{g1k}}\left(c_{1k}\, R_k + S_{1k}\right) \\
\dot{S}_{2k} &= \frac{1}{T_{g2k}}\left(c_{2k} - S_{2k}\right) \\
\dot{S}_{3k} &= \frac{1}{T_{Wk}}\left(c_{4k} - S_{3k}\right) \\
\Delta\dot{P}_{m_{setk}} &= \omega_k\, T_{FRRk}
\end{aligned} \tag{8.32}$$

where,

$$\begin{aligned}
c_{1k} &= \omega_k - g_{stk}\, \Delta P_{m_{setk}} \\
c_{2k} &= S_{1k}\left(1 - \frac{T_{Rk}}{T_{g2k}}\right) \\
c_{3k} &= \frac{S_{1k}\, T_{Rk}}{T_{g2k}} + S_{2k} \\
c_{4k} &= 3\, c_{3k}
\end{aligned} \tag{8.33}$$

and finally

$$\Delta P_{mk} = -2\, c_{3k} + S_{3k} \tag{8.34}$$

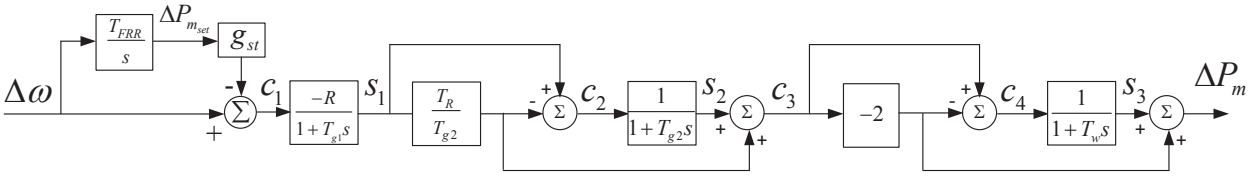

Figure 8.21. The equivalent model of the system shown in Figure 8.15.

Figure 8.22 shows the system frequency response (on the left hand side) and the variations of the mechanical and electrical powers (on the right hand side) to the disturbance.

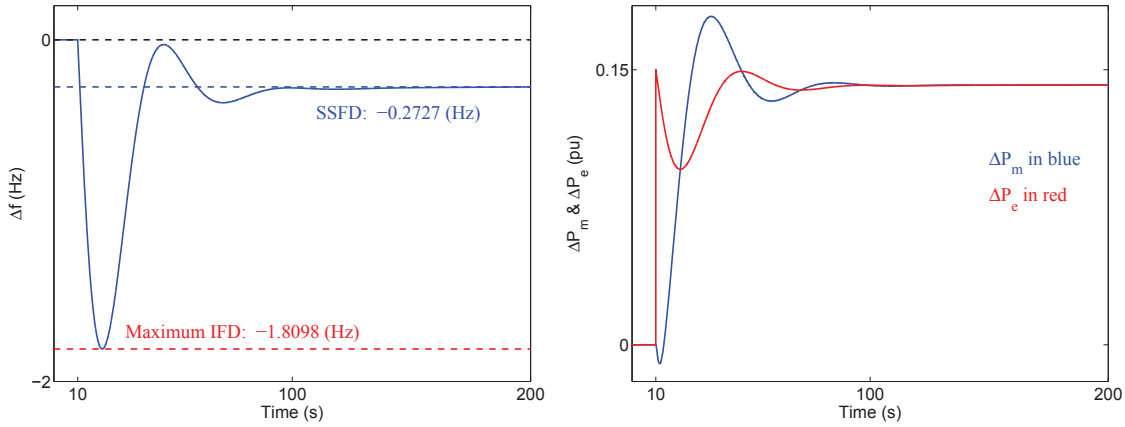

Figure 8.22. System frequency response and the variations of the mechanical and electrical powers with FCR.

As shown in the figure on the left hand side, the frequency nadir is $f = 48.1902$ (Hz), and the settling frequency is $f = 49.7273$ (Hz) (as was expected). When the load is suddenly increased with $\Delta P_L = 0.15$, initially the frequency is unchanged and the load frequency dependency will therefore be unaffected. According to Kirchhoff's current (power) law, $\Delta P_e = \Delta P_{e1} + \Delta P_{e2} + \Delta P_{e3} = \Delta P_L$ at any instant of time. As shown in the figure on the right hand side, immediately after the disturbance $\Delta P_e = 0.15$ (pu), but $\Delta P_m = 0$. Where is this additional power coming from? Moreover, as shown in the figure, the total increased of the load is not entirely compensated, i.e. $\Delta P_m = \Delta P_e \neq 0.15$ (pu). This is due to the load frequency dependency, since $\Delta f \neq 0$. By applying the FRR process, i.e. by activating the supplementary control loop with $T_{FRR} = -0.5$ for Gen 1 and Gen 2, both the frequency and the total new load are restored as shown in Figure 8.23.

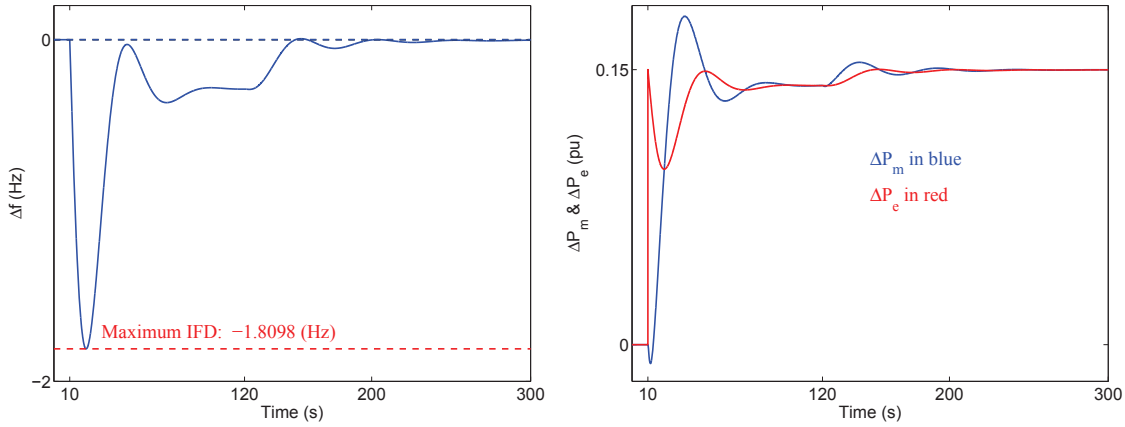

Figure 8.23. System frequency response and the variations of the mechanical and electrical powers with FCR and FRR.

Example 8.5 *Let synchronous generator Gen 3 be replaced by a wind power plant with identical P_g and Q_g to obtain the same load flow results. Re-do task* **c)** *of Example 8.4.*

From the load flow calculations we find that $P_{g3} = 0.2000$ and $Q_{g3} = 0.1579$ which will be used at BUS 3 as power generation at that bus. Then BUS 3 is considered as a pq-bus and the simulation is performed. Figure 8.24 shows some of the simulation results. Due to the fast power electronic based controller in the modern wind power

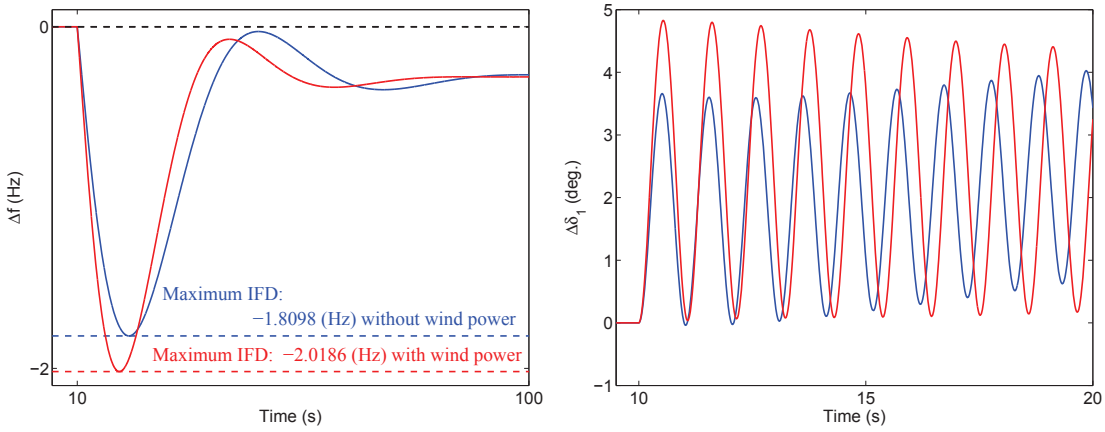

Figure 8.24. System frequency response and the variations of $\Delta\delta_1$ with (red) and without(blue) wind power.

plants, the power system "sees" constant power generations from these wind power plants (which are also termed as non-synchronous generation). This implies that these wind power plants (or in general non-synchronous generations) are not able inherently to be involved in IFR. Today's power systems have been designed and developed based on synchronously connected power plants. To operate a power system in a reliable and cost-effective manner, a mixture of three types of resources has been applied, namely energy, capacity (i.e. power) and flexibility (i.e. controllability). All of conventional power plants (i.e. those which are synchronously connected to the system) imply an important contribution to "capacity". Moreover, they provide synchronizing power (or torque) and inertia which have crucial roles on power system dynamical response, on setting of rotor angle, voltage and frequency stability limits, and also on setting of protection systems. The non-synchronous generation does not however contribute in providing synchronizing power and inertia. Replacing some of the conventional power plants with the non-synchronous generation (due to environmental and economical concerns), it even results in less system inertia and synchronizing power. The high penetration of non-synchronous generation (mostly wind power, but it can also include solar power and other renewable energy) can therefore result in new challenges to operate the system in a secure and cost-effective manner.

As shown in Figure 8.24, the IFD of the system becomes greater when the conventional Gen 3 is replaced by a wind power plant. This means that the system has less inertia compared to the system with three conventional generators. The lower inertia and synchronizing power result also in the system oscillations with higher amplitude as shown in the figure on the right hand side. A low inertia and synchronizing power can jeopardize the system stability in case of large disturbances.

Appendix A

Load flow calculations based on Newton-Raphson method

A.1 Theory

The Newton-Raphson method may be applied to solve for $y_1, y_2, \cdots, y_n$ of the following non-linear equations,

$$\begin{aligned} g_1(y_1, y_2, \cdots, y_n) &= \Upsilon_1(y_1, y_2, \cdots, y_n) - b_1 = 0 \\ g_2(y_1, y_2, \cdots, y_n) &= \Upsilon_2(y_1, y_2, \cdots, y_n) - b_2 = 0 \\ &\vdots \\ g_n(y_1, y_2, \cdots, y_n) &= \Upsilon_n(y_1, y_2, \cdots, y_n) - b_n = 0 \end{aligned} \tag{A.1}$$

or in the vector form

$$g(y) = \Upsilon(y) - b = 0 \tag{A.2}$$

where

$$y = \begin{bmatrix} y_1 \\ y_2 \\ \vdots \\ y_n \end{bmatrix} \quad , \quad g(y) = \begin{bmatrix} g_1(y) \\ g_2(y) \\ \vdots \\ g_n(y) \end{bmatrix} \quad , \quad \Upsilon(y) = \begin{bmatrix} \Upsilon_1(y) \\ \Upsilon_2(y) \\ \vdots \\ \Upsilon_n(y) \end{bmatrix} \quad , \quad b = \begin{bmatrix} b_1 \\ b_2 \\ \vdots \\ b_n \end{bmatrix}$$

y is an $n \times 1$ vector which contains variables, b is an $n \times 1$ vector which contains constants, and $f(y)$ is an $n \times 1$ vector-valued function.

Taylor's series expansion of (A.2) is the basis for the Newton-Raphson method of solving (A.2) in an iterative manner. From an initial estimate (or guess) $y^{(0)}$, a sequence of gradually better estimates $y^{(1)}$, $y^{(2)}$, $y^{(3)}$, $\cdots$ will be made that hopefully will converge to the solution y^*.

Let y^* be the solution of (A.2), i.e. $g(y^*) = 0$, and $y^{(i)}$ be an estimate of y^*. Let also $\Delta y^{(i)} = y^* - y^{(i)}$. Equation (A.2) can now be written as

$$g(y^*) = g(y^{(i)} + \Delta y^{(i)}) = 0 \tag{A.3}$$

Taylor's series expansion of (A.3) gives

$$g(y^{(i)} + \Delta y^{(i)}) = g(y^{(i)}) + JAC^{(y^{(i)})} \Delta y^{(i)} = 0 \tag{A.4}$$

where

$$JAC^{(y^{(i)})} = \left[\frac{\partial g(y)}{\partial y}\right]_{y=y^{(i)}} = \begin{bmatrix} \frac{\partial g_1(y)}{\partial y_1} & \cdots & \frac{\partial g_1(y)}{\partial y_n} \\ \vdots & \ddots & \vdots \\ \frac{\partial g_n(y)}{\partial y_1} & \cdots & \frac{\partial g_n(y)}{\partial y_n} \end{bmatrix}_{y=y^{(i)}} \tag{A.5}$$

where, JAC ia called the jacobian of g.

From (A.4), $\Delta y^{(i)}$ can be calculated as follows

$$\begin{aligned} JAC^{(y^{(i)})}\Delta y^{(i)} &= 0 - g(y^{(i)}) = \Delta g(y^{(i)}) \quad \Rightarrow & \text{(A.6)} \\ \Delta y^{(i)} &= \left[JAC^{(y^{(i)})}\right]^{-1} \Delta g(y^{(i)}) & \text{(A.7)} \end{aligned}$$

Since $g(y^{(i)}) = \Upsilon(y^{(i)}) - b$, $\Delta g(y^{(i)})$ is given by

$$\Delta g(y^{(i)}) = b - \Upsilon(y^{(i)}) = -g(y^{(i)}) \tag{A.8}$$

Furthermore, since b is constant, $JAC^{(y^{(i)})}$ is given by

$$JAC^{(y^{(i)})} = \left[\frac{\partial g(y)}{\partial y}\right]_{y=y^{(i)}} = \left[\frac{\partial \Upsilon(y)}{\partial y}\right]_{y=y^{(i)}} = \begin{bmatrix} \frac{\partial \Upsilon_1(y)}{\partial y_1} & \cdots & \frac{\partial \Upsilon_1(y)}{\partial y_n} \\ \vdots & \ddots & \vdots \\ \frac{\partial \Upsilon_n(y)}{\partial y_1} & \cdots & \frac{\partial \Upsilon_n(y)}{\partial y_n} \end{bmatrix}_{y=y^{(i)}} \tag{A.9}$$

Therefore, $\Delta y^{(i)}$ can be calculated as follows

$$\Delta y^{(i)} = \begin{bmatrix} \Delta y_1^{(i)} \\ \vdots \\ \Delta y_n^{(i)} \end{bmatrix} = \begin{bmatrix} \frac{\partial \Upsilon_1(y)}{\partial y_1} & \cdots & \frac{\partial \Upsilon_1(y)}{\partial y_n} \\ \vdots & \ddots & \vdots \\ \frac{\partial \Upsilon_n(y)}{\partial y_1} & \cdots & \frac{\partial \Upsilon_n(y)}{\partial y_n} \end{bmatrix}^{-1}_{y=y^{(i)}} \begin{bmatrix} b_1 - \Upsilon_1(y_1^{(i)}, \cdots, y_n^{(i)}) \\ \vdots \\ b_n - \Upsilon_n(y_1^{(i)}, \cdots, y_n^{(i)}) \end{bmatrix} \tag{A.10}$$

Finally, the following is obtained

$$\begin{aligned} i &= i + 1 \\ y^{(i)} &= y^{(i-1)} + \Delta y^{(i-1)} \end{aligned}$$

The intention is that $y^{(1)}$ will estimate the solution y^* better than what $y^{(0)}$ does. In the same manner, $y^{(2)}$, $y^{(3)}$, $\cdots$ can be determined until a specified condition is satisfied. Thus, we obtain an iterative method according to the flowchart in Figure A.1.

Example A.1 *Using the Newton-Raphson method, solve for y of the equation*

$$g(y) = k_1\, y + k_2\, \cos(y - k_3) - k_4 = 0$$

Let $k_1 = -0.2$, $k_2 = 1.2$, $k_3 = -0.07$, $k_4 = 0.4$ and $\epsilon = 10^{-4}$.

This equation is of the form given by (A.2), with $\Upsilon(y) = k_1\, y + k_2\, \cos(y - k_3)$ and $b = k_4$.

Step 1

Set $i = 0$ and $y^{(i)} = y^{(0)} = 0.0524$ (radians), i.e. 3 (degrees).

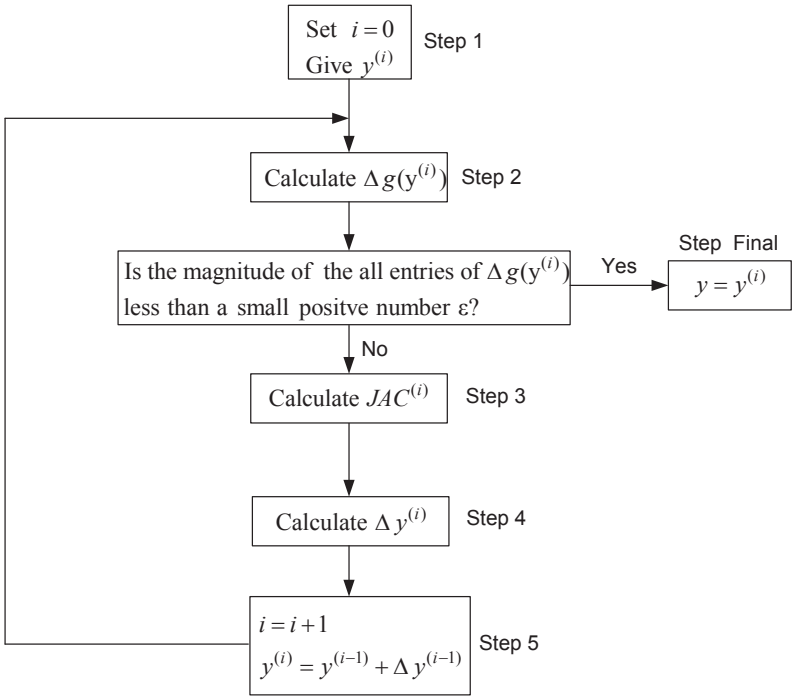

Figure A.1. Flowchart for the Newton-Raphson method.

Step 2

$\Delta g(y^{(i)}) = b - \Upsilon(y^{(i)}) = 0.4 - [(-0.2 * 0.0524) + 1.2\ \cos(0.0524 + 0.07)] = -0.7806$

Go to **Step 3** since $|\Delta g(y^{(i)})| > \epsilon$

Step 3

$JAC^{(y^{(i)})} = \left[\frac{\partial \Upsilon}{\partial y}\right]_{y=y^{(i)}} = -0.2 - 1.2\ \sin(0.0524 + 0.07) = -0.3465$

Step 4

$\Delta y^{(i)} = \left[JAC^{(y^{(i)})}\right]^{-1} \Delta g(y^{(i)}) = \frac{-0.7806}{-0.3465} = 2.2529$

Step 5

$i = i + 1 = 0 + 1 = 1$
$y^{(i)} = y^{(i-1)} + \Delta y^{(i-1)} = 0.0524 + 2.2529 = 2.3053$. Go to **Step 2**

After 5 iterations, i.e. $i = 5$, it was found that $|\Delta g(y^{(i)})| < \epsilon$ for $y^{(5)} = 0.9809$ (rad.). Therefore, the solution becomes $y = 0.9809$ (rad.) or $y = 56.2000$ (deg.).

Analysis of Example A.1

Figure A.2 shows variations of $g(y)$ versus y. The figure shows that the system (or equation) has only three solutions, i.e. the points at which $g(y) = 0$. Due to practical issues, y^* indicted with (O) in the figure is the interesting solution.

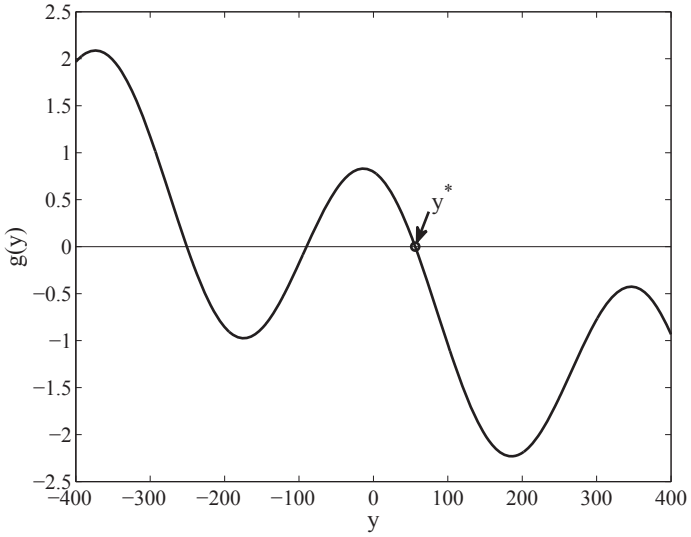

Figure A.2. Variations of $g(y)$ vs. y.

Figure A.3 shows how the equation is solved by the Newton-Raphson method.

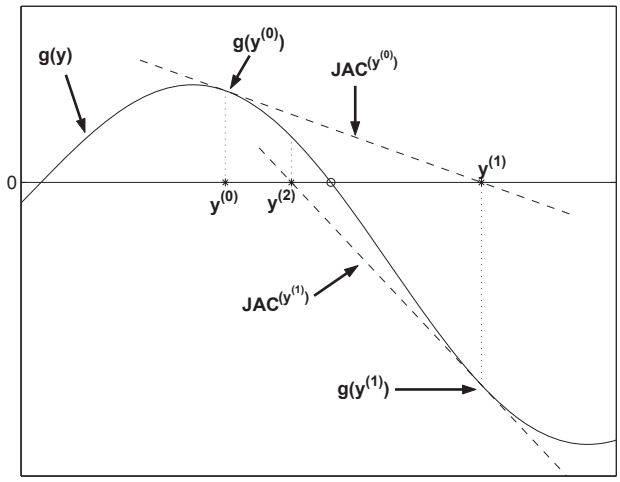

Figure A.3. Variations of $g(y)$ vs. y.

We first guess the initial estimate $y^{(0)}$. In this case $y^{(0)} = 0.0524$ (rad.), i.e 3 (deg.). The tangent to $g(y)$ through the point $\left(y^{(0)}\,,\, g(y^{(0)})\right)$, i.e. $g'(y^{(0)}) = \left[\frac{dg(y)}{dy}\right]_{y=y^{(0)}} = JAC^{(y^{(0)})}$, intersects the x–axis at point $y^{(1)}$. The equation for this tangent is given by

$$\mathcal{G} - g(y^{(0)}) = g'(y^{(0)}) * (y - y^{(0)})$$

The intersection point $y^{(1)}$ is obtained by setting $\mathcal{G} = 0$, i.e.

$$\begin{aligned} y^{(1)} &= y^{(0)} - \frac{g(y^{(0)})}{g'(y^{(0)})} = y^{(0)} - \left(g'(y^{(0)})\right)^{-1} g(y^{(0)}) \\ \Delta y^{(0)} &= y^{(1)} - y^{(0)} = -\left(g'(y^{(0)})\right)^{-1} g(y^{(0)}) = \left[JAC^{(y^{(0)})}\right]^{-1} \Delta g(y^{(0)}) \end{aligned}$$

In a similar manner, $y^{(2)}$ can be obtained which is hopefully a better estimate than $y^{(1)}$. As shown in the figure, from $y^{(2)}$ we obtain $y^{(3)}$ which is a better estimate of y^* than what $y^{(2)}$ does. This iterative method will be continued until $|\Delta g(y)| < \epsilon$.

Example A.2 *Solve for x in Example A.1, but let* $y^{(0)} = 0.0174$ *(rad.), i.e. 1 (deg.).*

D.I.Y, (i.e., Do It Yourself)

A.2 Application to power systems

Consider a symmetrical power system with N buses. The aim is to determine the voltage at all buses in the system by applying the Newton-Raphson method. **All variables are expressed in (pu)**.

Figure A.4 schematically shows connection of the system components to bus k.

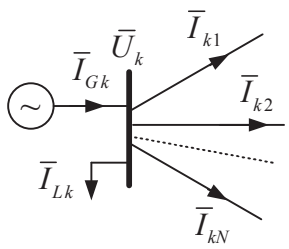

Figure A.4. Notation of bus k in a network.

The generator generates the current $\bar{I}_{Gk}$, the load at the bus draws the current $\bar{I}_{Lk}$, and $\bar{I}_{kj}$ is the currents from bus k to the neighboring buses. According to Kirchhoff's current law, the sum of all currents injected into bus k must be zero, i.e.

$$\bar{I}_{Gk} - \bar{I}_{Lk} = \sum_{j=1}^{N} \bar{I}_{kj} \tag{A.11}$$

By taking the conjugate of equation (A.11) and multiply the equation with the bus voltage, the following holds

$$\bar{U}_k \bar{I}^*_{Gk} - \bar{U}_k \bar{I}^*_{Lk} = \sum_{j=1}^{N} \bar{U}_k \bar{I}^*_{kj} \tag{A.12}$$

This can be rewritten as an expression for complex power in the per-unit system as

$$\bar{S}_{Gk} - \bar{S}_{Lk} = \sum_{j=1}^{N} \bar{S}_{kj} \tag{A.13}$$

where

$\bar{S}_{Gk} = P_{Gk} + jQ_{Gk}$ is the generated complex power at bus k,

$\bar{S}_{Lk} = P_{Lk} + jQ_{Lk}$ is the consumed complex power (the load) at bus k,

$\bar{S}_{kj} = P_{kj} + jQ_{kj}$ is the complex power flow from bus k to bus j.

The power balance at the bus according to equation (A.13) must hold both for the active and for the reactive part of the expression. By using P_{Sk} and Q_{Sk} as notation for the specified active and reactive power (or net generation of active and reactive power) at bus k, respectively, the following expression holds

$$P_{Sk} = P_{Gk} - P_{Lk} \;=\; \sum_{j=1}^{N} P_{kj} \tag{A.14}$$

$$Q_{Sk} = Q_{Gk} - Q_{Lk} \;=\; \sum_{j=1}^{N} Q_{kj} \tag{A.15}$$

i.e. for any bus k in the system, the power balance must hold for both active and reactive power.

Now, consider the π-equivalent model of a line shown in Figure A.5, where all variables expressed in per-unit.

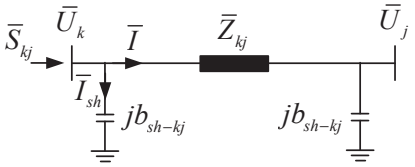

Figure A.5. π-equivalent model of a line.

Let

$$\begin{aligned} \bar{U}_k &= U_k e^{j\theta_k} \quad , \quad \bar{U}_j = U_j e^{j\theta_j} \\ \bar{Z} &= R + jX \quad , \quad Z = \sqrt{R^2 + Y^2} \\ \theta_{kj} &= \theta_k - \theta_j \end{aligned} \tag{A.16}$$

The power $\bar{S}_{kj}$ in the sending end k is given by

$$\begin{aligned} \bar{S}_{kj} &= \bar{U}_k \left(\bar{I}^*_{sh} + \bar{I}^*\right) = \bar{U}_k \left(\left(j\, b_{sh-kj}\, \bar{U}_k\right)^* + \frac{\bar{U}^*_k - \bar{U}^*_j}{\bar{Z}^*_{kj}} \right) = \\ &= -j\, b_{sh-kj}\, U_k^2 + \frac{U_k^2}{R - jX} - \frac{U_k U_j}{R - jX} e^{j(\theta_k - \theta_j)} = \\ &= -j\, b_{sh-kj}\, U_k^2 + \frac{U_k^2}{Y^2}(R + jX) - \frac{U_k U_j}{Y^2}(R + jX)\left(\cos\theta_{kj} + j \sin\theta_{kj}\right) \end{aligned} \tag{A.17}$$

By dividing equation (A.17) into a real and an imaginary part, expressions for the active and reactive power can be obtained, respectively, as

$$\begin{aligned} P_{kj} &= \frac{R}{Z^2}\,U_k^2 + \frac{U_k\,U_j}{Z^2}\,(X\sin\theta_{kj} - R\cos\theta_{kj}) \\ &= \frac{R}{Z^2}\,U_k^2 + \frac{U_k\,U_j}{Z}\,\sin\left(\theta_{kj} - \arctan\left(\frac{R}{X}\right)\right) \end{aligned} \tag{A.18}$$

$$\begin{aligned} Q_{kj} &= -b_{sh-kj}\,U_k^2 + \frac{X}{Z^2}\,U_k^2 - \frac{U_k U_j}{Z^2}\,(R\sin\theta_{kj} + X\cos\theta_{kj}) \\ &= \left(-b_{sh-kj} + \frac{X}{Z^2}\right)\,U_k^2 - \frac{U_k\,U_j}{Z}\,\cos\left(\theta_{kj} - \arctan\left(\frac{R}{X}\right)\right) \end{aligned} \tag{A.19}$$

From equations (A.18) and (A.19), it can be concluded that if the phasor voltages (i.e. the voltage magnitude and phase angle) at both ends of the line are known, the power flow can be uniquely determined. This implies that if the phasor voltages of all buses in a system are known, the power flows in the whole system are known, i.e the phasor voltages define the system state.

Consider again Figure A.5. Let

$$\begin{aligned} g_{kj} + j\,b_{kj} &= \frac{1}{\bar{Z}_{kj}} = \frac{1}{R + j\,X} = \frac{R}{Z^2} + j\,\frac{-X}{Z^2} \quad \Rightarrow \\ g_{kj} &= \frac{R}{Z^2} \\ b_{kj} &= -\frac{X}{Z^2} \end{aligned} \tag{A.20}$$

Based on (A.20), we rewrite (A.18) and (A.19) as follows

$$P_{kj} = g_{kj}\,U_k^2 - U_k\,U_j\,[g_{kj}\cos(\theta_{kj}) + b_{kj}\sin(\theta_{kj})] \tag{A.21}$$

$$Q_{kj} = U_k^2(-b_{sh-kj} - b_{kj}) - U_k\,U_j\,[g_{kj}\sin(\theta_{kj}) - b_{kj}\cos(\theta_{kj})] \tag{A.22}$$

The current through the line, and the active power losses in the line can be calculated by

$$\bar{I}_{kj} = \frac{P_{kj} - j\,Q_{kj}}{\bar{U}_k^*} \tag{A.23}$$

$$P_{loss_{kj}} = P_{kj} + P_{jk} \tag{A.24}$$

Consider again Figure A.4. Let $Y = G + jB$ denote the admittance matrix of the system (or Y-matrix), where Y is an $N \times N$ matrix, i.e. the system has N buses. The relation between the injected currents into the buses and the voltages at the buses is given by $I = Y\,U$. Therefore, the injected current into bus k is given by $\bar{I}_k = \sum_{j=1}^{N} \bar{Y}_{kj}\,\bar{U}_j$.

The injected complex power into bus k can now be calculated by

$$\bar{S}_k = \bar{U}_k\,\bar{I}_k^* = \bar{U}_k \sum_{j=1}^{N} \bar{Y}_{kj}^*\bar{U}_j^* = U_k \sum_{j=1}^{N} (G_{kj} - jB_{kj})\,U_j(\cos(\theta_{kj}) + j\sin(\theta_{kj}))$$

$$= \left(U_k \sum_{j=1}^{N} U_j \left[G_{kj} \cos(\theta_{kj}) + B_{kj} \sin(\theta_{kj}) \right] \right) + j \left(U_k \sum_{j=1}^{N} U_j \left[G_{kj} \sin(\theta_{kj}) - B_{kj} \cos(\theta_{kj}) \right] \right)$$

Let P_k denote the real part of $\bar{S}_k$, i.e. the injected active power, and Q_k denote the imaginary part of $\bar{S}_k$, i.e. the injected reactive power, as follows:

$$\begin{aligned} P_k &= U_k \sum_{j=1}^{N} U_j \left[G_{kj} \cos(\theta_{kj}) + B_{kj} \sin(\theta_{kj}) \right] \\ Q_k &= U_k \sum_{j=1}^{N} U_j \left[G_{kj} \sin(\theta_{kj}) - B_{kj} \cos(\theta_{kj}) \right] \end{aligned} \tag{A.25}$$

Note that $G_{kj} = -g_{kj}$ and $B_{kj} = -b_{kj}$ for $k \neq j$. Furthermore,

$$\begin{aligned} P_k &= \sum_{j=1}^{N} P_{kj} \\ Q_k &= \sum_{j=1}^{N} Q_{kj} \end{aligned}$$

Equations (A.14) and (A.15) can now be rewritten as

$$\begin{aligned} P_k - P_{Sk} &= 0 \\ Q_k - Q_{Sk} &= 0 \end{aligned} \tag{A.26}$$

which are of the form given in equation (A.2), where

$$y = \begin{bmatrix} \theta \\ U \end{bmatrix} = \begin{bmatrix} \theta_1 \\ \vdots \\ \theta_N \\ U_1 \\ \vdots \\ U_N \end{bmatrix}, \ \Upsilon(\theta, U) = \begin{bmatrix} \Upsilon_P(\theta, U) \\ \Upsilon_Q(\theta, U) \end{bmatrix} = \begin{bmatrix} P_1 \\ \vdots \\ P_N \\ Q_1 \\ \vdots \\ Q_N \end{bmatrix}, \ b = \begin{bmatrix} b_P \\ b_Q \end{bmatrix} = \begin{bmatrix} P_{S1} \\ \vdots \\ P_{SN} \\ Q_{S1} \\ \vdots \\ Q_{SN} \end{bmatrix} \tag{A.27}$$

The aim is to determine $y = [\theta \quad U]^T$ by applying the Newton-Raphson method.

Assume that there are 1 slack bus and M PU-buses in the system. Therefore, θ becomes an $(N-1) \times 1$ vector and U becomes an $(N-1-M) \times 1$ vector, why?

Based on (A.8), we define the following:

$$\begin{aligned} \Delta P_k &= P_{Sk} - P_k \quad k \neq \text{slack bus} \\ \Delta Q_k &= Q_{Sk} - Q_k \quad k \neq \text{slack bus and PU-bus} \end{aligned} \tag{A.28}$$

Based on (A.9), the jacobian matrix is given by

$$JAC = \begin{bmatrix} \frac{\partial \Upsilon_P(\theta,U)}{\partial \theta} & \frac{\partial \Upsilon_P(\theta,U)}{\partial U} \\ \frac{\partial \Upsilon_Q(\theta,U)}{\partial \theta} & \frac{\partial \Upsilon_Q(\theta,U)}{\partial U} \end{bmatrix} = \begin{bmatrix} H & N' \\ J & L' \end{bmatrix} \tag{A.29}$$

where,

H	is an	$(N-1)\times(N-1)$	matrix
N'	is an	$(N-1)\times(N-M-1)$	matrix
J	is an	$(N-M-1)\times(N-1)$	matrix
L'	is an	$(N-M-1)\times(N-M-1)$	matrix

The entries of these matrices are given by:

$H_{kj} = \frac{\partial P_k}{\partial \theta_j}$ $\quad k \neq$ slack bus $\quad j \neq$ slack bus

$N'_{kj} = \frac{\partial P_k}{\partial U_j}$ $\quad k \neq$ slack bus $\quad j \neq$ slack bus and PU-bus

$J_{kj} = \frac{\partial Q_k}{\partial \theta_j}$ $\quad k \neq$ slack bus and PU-bus $\quad j \neq$ slack bus

$L'_{kj} = \frac{\partial Q_k}{\partial U_j}$ $\quad k \neq$ slack bus and PU-bus $\quad j \neq$ slack bus and PU-bus

Based on (A.6), (A.28) and (A.29), the following is obtained

$$\begin{bmatrix} H & N' \\ J & L' \end{bmatrix} \begin{bmatrix} \Delta\theta \\ \Delta U \end{bmatrix} = \begin{bmatrix} \Delta P \\ \Delta Q \end{bmatrix} \tag{A.30}$$

To simplify the entries of the matrices N' and L', these matrices are multiplied with U. Then, (A.30) can be rewritten as

$$\begin{bmatrix} H & N \\ J & L \end{bmatrix} \begin{bmatrix} \Delta\theta \\ \frac{\Delta U}{U} \end{bmatrix} = \begin{bmatrix} \Delta P \\ \Delta Q \end{bmatrix} \tag{A.31}$$

where,
for $k \neq j$

$$\begin{aligned} H_{kj} &= \frac{\partial P_k}{\partial \theta_j} &&= U_k\, U_j\, [G_{kj}\sin(\theta_{kj}) - B_{kj}\cos(\theta_{kj})] \\ N_{kj} &= U_j\, N'_{kj} = U_j \frac{\partial P_k}{\partial U_j} &&= U_k\, U_j\, [G_{kj}\cos(\theta_{kj}) + B_{kj}\sin(\theta_{kj})] \\ J_{kj} &= \frac{\partial Q_k}{\partial \theta_j} &&= -U_k\, U_j\, [G_{kj}\cos(\theta_{kj}) + B_{kj}\sin(\theta_{kj})] \\ L_{kj} &= U_j\, L'_{kj} = U_j \frac{\partial Q_k}{\partial U_j} &&= U_k\, U_j\, [G_{kj}\sin(\theta_{kj}) - B_{kj}\cos(\theta_{kj})] \end{aligned} \tag{A.32}$$

and for $k = j$

$$\begin{aligned} H_{kk} &= \frac{\partial P_k}{\partial \theta_k} &&= -Q_k - B_{kk}U_k^2 \\ N_{kk} &= U_k \frac{\partial P_k}{\partial U_k} &&= P_k + G_{kk}U_k^2 \\ J_{kk} &= \frac{\partial Q_k}{\partial \theta_k} &&= P_k - G_{kk}U_k^2 \\ L_{kj} &= U_k \frac{\partial Q_k}{\partial U_k} &&= Q_k - B_{kk}U_k^2 \end{aligned} \tag{A.33}$$

Now based on (A.10), the following is obtained:

$$\begin{bmatrix} \Delta\theta \\ \frac{\Delta U}{U} \end{bmatrix} = \begin{bmatrix} H & N \\ J & L \end{bmatrix}^{-1} \begin{bmatrix} \Delta P \\ \Delta Q \end{bmatrix} \tag{A.34}$$

Finally, U and θ will be updated as follows:

$$\begin{array}{ll} \theta_k = \theta_k + \Delta\theta_k & k \neq \text{slack bus} \\ U_k = U_k \left(1 + \frac{\Delta U_k}{U_k}\right) & k \neq \text{slack bus and PU-bus} \end{array} \tag{A.35}$$

A.2.1 Newton-Raphson method for solving power flow equations

Newton-Raphson method can be applied to non-linear power flow equations as follows:

- **Step 1**

  1a) Read bus and line data. Identify slack bus, PU-buses and PQ-buses.

  1b) Develop the Y-matrix and calculate the specified powers, i.e. $P_S = P_G - P_L$ and $Q_S = Q_G - Q_L$.

  1c) Give the initial estimate of the unknown variables, i.e. U for PQ-buses and θ for PU- and PQ-buses. It is very common to set $U = U_{slack}$ and $\theta = \theta_{slack}$. However, the flat initial estimate may also be applied, i.e. $U = 1$ and $\theta = 0$.

  1d) Go to **Step 2**.

- **Step 2**

  2a) Calculate the injected power into each bus by equation (A.25).

  2b) Calculate the difference between the net production and the injected power for each bus, i.e. ΔP and ΔQ by equation (A.28).

  2c) Is the magnitude of all entries of $[\Delta P \quad \Delta Q]^T$ less than a specified small positive constant ϵ ?

  * If yes, go to **Step Final**.
  * if no, go to **Step 3**.

- **Step 3**

  3a) Calculate the jacobian by equations (A.32) and (A.33).

  3b) Go to **Step 4**.

- **Step 4**

  4a) Calculate $\left[\Delta\theta \quad \frac{\Delta U}{U}\right]^T$ by equation (A.34).

  4b) Go to **Step 5**.

- **Step 5**

  5a) Update U and θ by equation (A.35).

  5b) Go till **Step 2**.

- **Step Final**

  – Calculate the generated powers, i.e. P_G (MW) and Q_G (MVAr) in the slack bus, and Q_G (MVAr) in the PU-buses by using equation (A.26).

  – Calculate the power flows (MW, MVAr) by using equations (A.21) and (A.22).

  – Calculate active power losses (MW) by using equation (A.24).

  – Give all the voltage magnitudes (kV) and the voltage phase angles (degrees).

  – Print out the results.

A.3 The system data of the 3-generator system

```
NS=0;
Pg2=0.3;
Pg3=0.2;
PL01=0.0;  QL01=PL01*0.1;
PL02=0.0;  QL02=PL02*0.1;;
PL03=0.0;  QL03=PL03*0.1;
PL04=1.5;  QL04=PL04*0.1;

%%%%%%%%%%
% Bus Data
%%%%%%%%%%

% NS means "not specified"
% Type=1 means slack-bus, Type=2 means PU-bus, Type=3 means PQ-bus

BUSDATA=[
%          1     2     3     4       5       6    7    8      9      10
%        BUS  Type  Pgen  Qgen   Pload   Qload   YL  Ysh      V   Angle
           1     1    NS    NS    PL01    QL01    0    0   1.00       0
           2     2   Pg2    NS    PL02    QL02    0    0   1.00       0
           3     2   Pg3    NS    PL03    QL03    0    0   1.00       0
           4     3     0     0    PL04    QL04    0    0   1.00       0];

%%%%%%%%%%
% Line Data
%%%%%%%%%%
```

```
LINEDATA = [
% Line  from  to  R    X   B
     1     1   4  0  0.5   0
     2     2   4  0  0.2   0
     3     3   4  0  0.3   0];

%%%%%%%%%%%%%%%%%%%%%%%%%%%%
%% Generator data
%%%%%%%%%%%%%%%%%%%%%%%%%%%%

% GENDATA will be used in the examples of Chapter 4 and Chapter 6
%            1    2     3    4  5  6    7    8    9 10 11 12 13  14   15
%          Gen   xt   xdp   xd  H  D  Tdop  Te   KA T1 T2 T3 T4  Tw KPSS
GENDATA = [  1  0.1  0.10  0.8  5  0   6   0.01 100  1  1  1  1  10    0
             2  0.1  0.10  0.7  4  0   6   0.01 100  1  1  1  1  10    0
             3  0.1  0.10  0.6  3  0   6   0.01 100  1  1  1  1  10    0];


% GOVDATA will be used in the examples of Chapter 8
%            1     2    3     4  5          6           7   8
%          Gen  TWAT   TG  G_tr TR    dPm_max     dPm_min GOV
GOVDATA = [  1   1.0  0.4   1.0  5  0.2*PG(1)  -0.5*PG(1)   1
             2   1.0  0.4   1.0  5  0.2*PG(2)  -0.5*PG(2)   1
             3   1.0  0.4   1.0  5  0.2*PG(3)  -0.5*PG(3)   0];

% TWAT is the water time constant TW
GOV=1 means the generator is equipped with a governor system
```

Appendix B

B.1 Estimation of the stability region

The estimation of the stability region of this system can be obtained by solving the following optimization problem

$$\min \mathcal{V}(x) \quad \text{subject to } \dot{\mathcal{V}}(x) = 0$$

First we define Lagrangian function by

$$\mathcal{L}(x, \gamma) = \mathcal{V}(x) - \gamma \dot{\mathcal{V}}(x)$$

where, γ is called a Lagrange multiplier. The necessary conditions for the optimization problem are

$$\begin{aligned} \frac{\partial \mathcal{L}(x,\gamma)}{\partial x} &= 0 \\ \dot{\mathcal{V}}(x) &= 0 \end{aligned}$$

Based on the above conditions, it can easily be obtained that $x_1^2 = 7.5$ and $x_2^2 = 5$ which imply that $\mathcal{V}(x) = c = 12.5$.

B.2 The Jacobian matrices of the linearized system

Let

- N be the number of network buses
- n_g be the number of generators
- n_s be the number of state variables for each generator.
- $n_x = n_s \times n_g$ be the number of all system state variables
- $n_y = 2 \times N$ be the number of all system algebraic variables
- the loads be modeled as

$$P_L(U) = P_{L0} \left(\frac{U}{U_0}\right)^{mp} \qquad \text{and} \qquad Q_L(U) = Q_{L0} \left(\frac{U}{U_0}\right)^{mq}$$

Assume that the generators are represented by one-axis model. i.e. $n_s = 3$. Then, the dynamic of the system is given by

$$\begin{aligned} \dot{x} &= f(x, y) \\ 0 &= g(x, y) = \begin{bmatrix} g_P(x, y) \\ g_Q(x, y) \end{bmatrix} \end{aligned}$$

The structure of $f(x,y)$ and $g(x,y)$ is given in Example 5.1.

The Jacobian matrix f_x is of order $n_x \times n_x$, and has the form

$$f_x = f_x^{1axis} = \begin{bmatrix} f_{\dot{\delta}}^{\delta} & f_{\dot{\delta}}^{\omega} & f_{\dot{\delta}}^{E'_q} \\ f_{\dot{\omega}}^{\delta} & f_{\dot{\omega}}^{\omega} & f_{\dot{\omega}}^{E'_q} \\ f_{\dot{E}'_q}^{\delta} & f_{\dot{E}'_q}^{\omega} & f_{\dot{E}'_q}^{E'_q} \end{bmatrix} \tag{B.1}$$

All submatrices in (B.1) are of order $n_g \times n_g$ with the following nonzero elements for $k = 1 \cdots n_g$

$$\begin{aligned} f_{\dot{\delta}}^{\omega}(k,k) &= 1 \\ f_{\dot{\omega}}^{\delta}(k,k) &= -\frac{1}{M_k}\, b_{dk}\, E'_{qk_0}\, U_{k_0} \cos(\delta_{k_0} - \theta_{k_0}) \\ f_{\dot{\omega}}^{E'_q}(k,k) &= -\frac{1}{M_k}\, b_{dk}\, U_{k_0} \sin(\delta_{k_0} - \theta_{k_0}) \\ f_{\dot{E}'_q}^{\delta}(k,k) &= -\frac{x_{dk} - x'_{dk}}{T'_{dok}\, x'_{dk}}\, U_{k_0} \sin(\delta_{k_0} - \theta_{k_0}) \\ f_{\dot{E}'_q}^{E'_q}(k,k) &= -\frac{x_{dk}}{T'_{dok}\, x'_{dk}} \end{aligned}$$

The Jacobian matrix f_y is of order $n_x \times n_y$, and has the form

$$f_y = f_y^{1axis} = \begin{bmatrix} f_{\dot{\delta}}^{\theta} & f_{\dot{\delta}}^{U} \\ f_{\dot{\omega}}^{\theta} & f_{\dot{\omega}}^{U} \\ f_{\dot{E}'_q}^{\theta} & f_{\dot{E}'_q}^{U} \end{bmatrix} \tag{B.2}$$

All submatrices in (B.2) are of order $n_g \times N$ with the following nonzero elements for $k = 1 \cdots n_g$

$$\begin{aligned} f_{\dot{\omega}}^{\theta}(k,k) &= \frac{1}{M_k}\, b_{dk}\, E'_{qk_0}\, U_{k_0} \cos(\delta_{k_0} - \theta_{k_0}) \\ f_{\dot{\omega}}^{U}(k,k) &= -\frac{1}{M_k}\, b_{dk}\, E'_{qk_0} \sin(\delta_{k_0} - \theta_{k_0}) \\ f_{\dot{E}'_q}^{\theta}(k,k) &= \frac{x_{dk} - x'_{dk}}{T'_{dok}\, x'_{dk}}\, U_{k_0} \sin(\delta_{k_0} - \theta_{k_0}) \\ f_{\dot{E}'_q}^{U}(k,k) &= \frac{x_{dk} - x'_{dk}}{T'_{dok}\, x'_{dk}} \cos(\delta_{k_0} - \theta_{k_0}) \end{aligned}$$

The Jacobian matrix g_x is of order $n_y \times n_x$, and has the form

$$g_x = g_x^{1axis} = \begin{bmatrix} g_P^{\delta} & g_P^{\omega} & g_P^{E'_q} \\ g_Q^{\delta} & g_Q^{\omega} & g_Q^{E'_q} \end{bmatrix} \tag{B.3}$$

All submatrices in (B.3) are of order $N \times n_g$ with the following nonzero elements (see equations (5.8) and (5.10))

for $k = 1 \cdots n_g$

$$\begin{aligned} g_P^{\delta}(k,k) &= -b_{dk}\, E'_{qk_0}\, U_{k_0} \cos(\theta_{k_0} - \delta_{k_0}) \\ g_P^{E'_q}(k,k) &= b_{dk}\, U_{k_0} \sin(\theta_{k_0} - \delta_{k_0}) \\ g_Q^{\delta}(k,k) &= -b_{dk}\, E'_{qk_0}\, U_{k_0} \sin(\theta_{k_0} - \delta_{k_0}) \\ g_Q^{E'_q}(k,k) &= -b_{dk}\, U_{k_0} \cos(\theta_{k_0} - \delta_{k_0}) \end{aligned}$$

The Jacobian matrix g_y is of order $n_y \times n_y$, and has the form

$$g_y = \begin{bmatrix} g_P^{\theta} & g_P^{U} \\ g_Q^{\theta} & g_Q^{U} \end{bmatrix} \tag{B.4}$$

All submatrices in (B.4) are of order $N \times N$, and given by

$$\begin{aligned} g_P^{\theta} &= H + \begin{bmatrix} \frac{\partial P_g}{\partial \theta} & 0_1 \\ 0_2 & 0_3 \end{bmatrix} \quad , \quad g_P^{U} = N' + \begin{bmatrix} \frac{\partial P_g}{\partial U} & 0_1 \\ 0_2 & 0_3 \end{bmatrix} + \frac{\partial P_L}{\partial U} \\ g_Q^{\theta} &= J + \begin{bmatrix} \frac{\partial Q_g}{\partial \theta} & 0_1 \\ 0_2 & 0_3 \end{bmatrix} \quad , \quad g_Q^{U} = L' + \begin{bmatrix} \frac{\partial Q_g}{\partial U} & 0_1 \\ 0_2 & 0_3 \end{bmatrix} + \frac{\partial Q_L}{\partial U} \end{aligned}$$

where,

- H, N', J and L' are the submatrices of the Jacobian matrix defined in (A.29). Note that all these submatrices are of order $N \times N$ that is all elements associated with slack and PU-buses are included.

- 0_1 is a zero matrix of order $n_g \times (N - n_g)$, $0_2 = (0_1)^T$ and 0_3 is a zero matrix of order $(N - n_g) \times (N - n_g)$.

- $\frac{\partial P_g}{\partial \theta}$, $\frac{\partial P_g}{\partial U}$, $\frac{\partial Q_g}{\partial \theta}$ and $\frac{\partial Q_g}{\partial U}$ are diagonal matrices of order $n_g \times n_g$ whose diagonal elements are

  for $k = 1 \cdots n_g$

$$\begin{aligned} \frac{\partial P_g}{\partial \theta}(k,k) &= b_{dk}\, E'_{qk_0}\, U_{k_0} \cos(\theta_{k_0} - \delta_{k_0}) \\ \frac{\partial P_g}{\partial U}(k,k) &= b_{dk}\, E'_{qk_0} \sin(\theta_{k_0} - \delta_{k_0}) \\ \frac{\partial Q_g}{\partial \theta}(k,k) &= b_{dk}\, E'_{qk_0}\, U_{k_0} \sin(\theta_{k_0} - \delta_{k_0}) \\ \frac{\partial Q_g}{\partial U}(k,k) &= b_{dk} \left(2\, U_{k_0} - E'_{qk_0} \cos(\theta_{k_0} - \delta_{k_0})\right) \end{aligned}$$

- $\dfrac{\partial P_L}{\partial U}$ and $\dfrac{\partial Q_L}{\partial U}$ are diagonal matrices of order $N \times N$ whose diagonal elements are for $k = 1 \cdots N$

$$\begin{aligned} \frac{\partial P_L}{\partial U}(k,k) &= \frac{mp_k\, P_{L0k}}{U_{k_0}} \\ \frac{\partial Q_L}{\partial U}(k,k) &= \frac{mq_k\, Q_{L0k}}{U_{k_0}} \end{aligned}$$

Finally,

$$\Delta\dot{x} = \left(f_x - f_y (g_y)^{-1} g_x\right) \Delta x = A_s\, \Delta x$$

AVR:

If generators are also equipped with AVR whose dynamic is given by (3.101), then $n_s = 4$. Therefore, f_x, f_y and g_x are modified as follows

$$\begin{aligned} f_x = f_x^{avr} &= \begin{bmatrix} f_{\dot\delta}^{\delta} & f_{\dot\delta}^{\omega} & f_{\dot\delta}^{E'_q} & f_{\dot\delta}^{E_f} \\ f_{\dot\omega}^{\delta} & f_{\dot\omega}^{\omega} & f_{\dot\omega}^{E'_q} & f_{\dot\omega}^{E_f} \\ f_{\dot{E}'_q}^{\delta} & f_{\dot{E}'_q}^{\omega} & f_{\dot{E}'_q}^{E'_q} & f_{\dot{E}'_q}^{E_f} \\ f_{\dot{E}_f}^{\delta} & f_{\dot{E}_f}^{\omega} & f_{\dot{E}_f}^{E'_q} & f_{\dot{E}_f}^{E_f} \end{bmatrix} = \begin{bmatrix} f_{\dot\delta}^{\delta} & f_{\dot\delta}^{\omega} & f_{\dot\delta}^{E'_q} & 0 \\ f_{\dot\omega}^{\delta} & f_{\dot\omega}^{\omega} & f_{\dot\omega}^{E'_q} & 0 \\ f_{\dot{E}'_q}^{\delta} & f_{\dot{E}'_q}^{\omega} & f_{\dot{E}'_q}^{E'_q} & f_{\dot{E}'_q}^{E_f} \\ 0 & 0 & 0 & f_{\dot{E}_f}^{E_f} \end{bmatrix} \\ f_y = f_y^{avr} &= \begin{bmatrix} f_{\dot\delta}^{\theta} & f_{\dot\delta}^{U} \\ f_{\dot\omega}^{\theta} & f_{\dot\omega}^{U} \\ f_{\dot{E}'_q}^{\theta} & f_{\dot{E}'_q}^{U} \\ f_{\dot{E}_f}^{\theta} & f_{\dot{E}_f}^{U} \end{bmatrix} = \begin{bmatrix} f_{\dot\delta}^{\theta} & f_{\dot\delta}^{U} \\ f_{\dot\omega}^{\theta} & f_{\dot\omega}^{U} \\ f_{\dot{E}'_q}^{\theta} & f_{\dot{E}'_q}^{U} \\ 0 & f_{\dot{E}_f}^{U} \end{bmatrix} \\ g_x = g_x^{avr} &= \begin{bmatrix} g_P^{\delta} & g_P^{\omega} & g_P^{E'_q} & g_P^{E_f} \\ g_Q^{\delta} & g_Q^{\omega} & g_Q^{E'_q} & g_Q^{E_f} \end{bmatrix} = \begin{bmatrix} g_P^{\delta} & g_P^{\omega} & g_P^{E'_q} & 0 \\ g_Q^{\delta} & g_Q^{\omega} & g_Q^{E'_q} & 0 \end{bmatrix} \end{aligned} \tag{B.5}$$

where, the additional nonzero elements are

for $k = 1 \cdots n_g$

$$\begin{aligned} f_{\dot{E}'_q}^{E_f}(k,k) &= \frac{1}{T'_{dok}} \\ f_{\dot{E}_f}^{E_f}(k,k) &= -\frac{1}{T_{ek}} \\ f_{\dot{E}_f}^{U}(k,k) &= -\frac{K_{Ak}}{T_{ek}} \end{aligned}$$

PSS:

If only a PSS with $nf = 2$ is used in the system (assume that it is installed in the generator k), then $n_x = n_x^{avr} + 3$.

Therefore, f_x, f_y and g_x are modified as follows (see equation (3.112))

$$
\begin{aligned}
f_x = f_x^{1pss} = &\begin{bmatrix}
f_{\dot\delta}^{\delta} & f_{\dot\delta}^{\omega} & f_{\dot\delta}^{E'_q} & f_{\dot\delta}^{E_f} & f_{\dot\delta}^{S_{1k}} & f_{\dot\delta}^{S_{2k}} & f_{\dot\delta}^{S_{3k}} \\
f_{\dot\omega}^{\delta} & f_{\dot\omega}^{\omega} & f_{\dot\omega}^{E'_q} & f_{\dot\omega}^{E_f} & f_{\dot\omega}^{S_{1k}} & f_{\dot\omega}^{S_{2k}} & f_{\dot\omega}^{S_{3k}} \\
f_{\dot E'_q}^{\delta} & f_{\dot E'_q}^{\omega} & f_{\dot E'_q}^{E'_q} & f_{\dot E'_q}^{E_f} & f_{\dot E'_q}^{S_{1k}} & f_{\dot E'_q}^{S_{2k}} & f_{\dot E'_q}^{S_{3k}} \\
f_{\dot E_f}^{\delta} & f_{\dot E_f}^{\omega} & f_{\dot E_f}^{E'_q} & f_{\dot E_f}^{E_f} & f_{\dot E_f}^{S_{1k}} & f_{\dot E_f}^{S_{2k}} & f_{\dot E_f}^{S_{3k}} \\
f_{\dot S_{1k}}^{\delta} & f_{\dot S_{1k}}^{\omega} & f_{\dot S_{1k}}^{E'_q} & f_{\dot S_{1k}}^{E_f} & f_{\dot S_{1k}}^{S_{1k}} & f_{\dot S_{1k}}^{S_{2k}} & f_{\dot S_{1k}}^{S_{3k}} \\
f_{\dot S_{2k}}^{\delta} & f_{\dot S_{2k}}^{\omega} & f_{\dot S_{2k}}^{E'_q} & f_{\dot S_{2k}}^{E_f} & f_{\dot S_{2k}}^{S_{1k}} & f_{\dot S_{2k}}^{S_{2k}} & f_{\dot S_{2k}}^{S_{3k}} \\
f_{\dot S_{3k}}^{\delta} & f_{\dot S_{3k}}^{\omega} & f_{\dot S_{3k}}^{E'_q} & f_{\dot S_{3k}}^{E_f} & f_{\dot S_{3k}}^{S_{1k}} & f_{\dot S_{3k}}^{S_{2k}} & f_{\dot S_{3k}}^{S_{3k}}
\end{bmatrix} \\
f_y = f_y^{1pss} = &\begin{bmatrix}
f_{\dot\delta}^{\theta} & f_{\dot\delta}^{U} \\
f_{\dot\omega}^{\theta} & f_{\dot\omega}^{U} \\
f_{\dot E'_q}^{\theta} & f_{\dot E'_q}^{U} \\
f_{\dot E_f}^{\theta} & f_{\dot E_f}^{U} \\
f_{\dot S_{1k}}^{\theta} & f_{\dot S_{1k}}^{U} \\
f_{\dot S_{2k}}^{\theta} & f_{\dot S_{2k}}^{U} \\
f_{\dot S_{3k}}^{\theta} & f_{\dot S_{3k}}^{U}
\end{bmatrix} \\
g_x = g_x^{1pss} = &\begin{bmatrix}
g_P^{\delta} & g_P^{\omega} & g_P^{E'_q} & g_P^{E_f} & g_P^{S_{1k}} & g_P^{S_{2k}} & g_P^{S_{3k}} \\
g_Q^{\delta} & g_Q^{\omega} & g_Q^{E'_q} & g_Q^{E_f} & g_Q^{S_{1k}} & g_Q^{S_{2k}} & g_Q^{S_{3k}}
\end{bmatrix}
\end{aligned}
\tag{B.6}
$$

Note that $f_{\dot E_f}^{\delta}$, $f_{\dot E_f}^{\omega}$, $f_{\dot E_f}^{E'_q}$, $f_{\dot E_f}^{E_f}$, $f_{\dot E_f}^{\theta}$ and $f_{\dot E_f}^{U}$ are indicated in blue (not red) since the selection of the input signal u_{ink} may affect these submatrices.

Comments:

- If one of the generator terminal buses is considered as an infinite bus, then all rows and columns of f_x, f_y, g_x and g_y associated both to the state variables of the corresponding generator, and the algebraic variables of the generator terminal bus are removed.

- In general, the dynamic of a multi-machine power system may be described by

$$
\begin{aligned}
\dot x &= f(x, y, u) \\
0 &= g(x, y, u)
\end{aligned}
\tag{B.7}
$$

Linearizing the above nonlinear system around its e.p, the following is obtained

$$\begin{aligned} \Delta\dot{x} &= f_x\,\Delta x + f_y\,\Delta y + f_u\,\Delta u && \text{(B.8)} \\ 0 &= g_x\,\Delta x + g_y\,\Delta y + g_u\,\Delta u && \text{(B.9)} \end{aligned}$$

From (B.9),

$$\Delta y = -g_y^{-1}\left[g_x\,\Delta x + g_u\,\Delta u\right] \tag{B.10}$$

Using (B.10) in (B.8), the following is obtained

$$\begin{aligned} \Delta\dot{x} =& \left[f_x - f_y\,g_y^{-1}\,g_x\right]\,\Delta x + \left[f_u - f_y\,g_y^{-1}\,g_u\right]\,\Delta u \\ =& A\,\Delta x + B\,\Delta u \end{aligned} \tag{B.11}$$

Let the output function be given by

$$\mathcal{Y} = \hbar(x, y, u) \tag{B.12}$$

Linearization of this function around the e.p yields

$$\Delta\mathcal{Y} = \hbar_x\,\Delta x + \hbar_y\,\Delta y + \hbar_u\,\Delta u \tag{B.13}$$

Using (B.10) in (B.13), the following is obtained

$$\begin{aligned} \Delta\mathcal{Y} =& \left[\hbar_x - \hbar_y\,g_y^{-1}\,g_x\right]\,\Delta x + \left[\hbar_u - \hbar_y\,g_y^{-1}\,g_u\right]\,\Delta u \\ =& C\,\Delta x + D\,\Delta u \end{aligned} \tag{B.14}$$

Thus, we are dealing with this Linear Time-Invariant system

$$\begin{aligned} \Delta\dot{x} =& A\,\Delta x + B\,\Delta u \\ \Delta\mathcal{Y} =& C\,\Delta x + D\,\Delta u \end{aligned} \tag{B.15}$$

References

[1] IEEE/CIGRE Joint Task Force on Stability Terms and Definitions, *Definition and Classification of Power System Stability*, Power Systems, IEEE Transactions on ,Volume: 19 , Issue: 3 , Aug. 2004.

[2] H. K. Khalil, *Nonlinear Systems (second edition)*, Prentice-Hall, Inc., 1996.

[3] P. M. Andersson and A. A. Fouad, *Power System Control and Stability*, The Iowa State University Press, 1977.

[4] M. Pavella and P.G. Murthy, *Transient Stability of Power Systems, Theory and Practice*, John Wiley & Sons, 1994.

[5] J. Machowski, J. W. Bialek and J. R. Bumby *Power System Dynamics and Stability*, John Wiley & Sons, 1997.

[6] P. Kundur, *Power System Stability and Control*, McGraw-Hill Inc., 1994.

[7] M. A. Pai, *Energy Function Analysis for Power System Stability*, Kluwer Academic Publishers, 1989.

[8] IEEE Task Force on Load Representation for Dynamic performance, *Load Representation for Dynamic Performance Analysis*, IEEE Transactions on Power Systems, Volume: 8 , Issue: 2 , May 1993.

[9] IEEE Task Force on Load Representation for Dynamic performance, *Standard Load Models for Power Flow and Dynamic Performance Simulation*, IEEE Transactions on Power Systems, Volume: 10 , Issue: 3 , August 1995.

[10] IEEE Task Force on Load Representation for Dynamic performance, *Bobliography on Load Models for Power Flow and Dynamic Performance Simulation*, IEEE Transactions on Power Systems, Volume: 10 , Issue: 1 , February 1995.

[11] P. C. Krause, *Analysis of Electric Machinery*, McGraw-Hill, 1986.

[12] M. Pavella, D. Ernst and D. Ruiz-Vega *Power System Transient Stability Analysis and Control*, Kluwer Academic Publishers, 2000.

[13] D. Ruiz-Vega and M. Pavella, *A Comprehensive Approach to Transient Stability Control: (PART I and PART II)*, IEEE Transactions on Power Systems ,Volume: 18 , No: 4 , Nov. 2003.

[14] IEEE Power System Engineering Committee, *Eigenanalysis and frequency domain methods for system dynamic performance*, IEEE Publication 90TH0292-3-PWR, 1989.

[15] I. J. Perez-Arriaga, G. C. Verghese and F. C. Schweppe, *Selective modal analysis with application to electric power systems, PART I: Heuristic introduction*, IEEE Transactions on Power Apparatus and Systems ,Volume: PAS-101 , No: 9 , Sep. 1982.

[16] F. L. Pagola, I. J. Perez-Arriaga , G. C. Verghese, *On Sensitivities, Residues and participation. Application to Oscillatory Stability Analysis and Control*, IEEE Transactions on Power Systems ,Volume: 4 , No: 1 , Feb. 1989.

[17] *The black-out in southern Sweden and eastern Denmark, September 23, 2003*, http://www.svk.se/upload/3813/IEEE_engelskpresentation_jul2003_2230.pdf

[18] *Interim Report of the Investigation Committee on the 28 September 2003 Blackout in Italy*, http://www.ucte.org/pdf/News/20040427_UCTE_IC_Final_report.pdf

[19] T. Van Cutsem and C. Vournas, *Voltage Stability of Electric Power Systems*, Kluwer Academic Publishers, 1998.

[20] C. W. Taylor, *Power System Voltage Stability*, McGraw-Hill Inc., 1994.

[21] G. Andersson, *Dynamic Phenomena in Electric Power Systems*, KTH, March 2000.

[22] *Supporting Document for the Network Code on Load-Frequency Control and Reserves*, https://www.entsoe.eu/major-projects/network-code-development/load-frequency-control-reserves/

[23] *OPERATIONAL RESERVE AD HOC TEAM REPORT FINAL VERSION*, https://www.entsoe.eu/major-projects/network-code-development/load-frequency-control-reserves/